

# **For Reference**

---

**NOT TO BE TAKEN FROM THIS ROOM**

Ex LIBRIS  
UNIVERSITATIS  
ALBERTAENSIS













THE UNIVERSITY OF ALBERTA

RELEASE FORM

NAME OF AUTHOR            ALAIN GUENOT

TITLE OF THESIS           INVESTIGATION   OF   TUNNEL   STABILITY   BY  
MODEL TESTS

DEGREE FOR WHICH THESIS WAS PRESENTED    MASTER OF SCIENCE

YEAR THIS DEGREE GRANTED    FALL, 1979

Permission is hereby granted to THE UNIVERSITY OF ALBERTA LIBRARY to reproduce single copies of this thesis and to lend or sell such copies for private, scholarly or scientific research purposes only.

The author reserves other publication rights, and neither the thesis nor extensive extracts from it may be printed or otherwise reproduced without the author's written permission.



THE UNIVERSITY OF ALBERTA

INVESTIGATION OF TUNNEL STABILITY BY MODEL TESTS

by



ALAIN GUENOT

A THESIS

SUBMITTED TO THE FACULTY OF GRADUATE STUDIES AND RESEARCH

IN PARTIAL FULFILMENT OF THE REQUIREMENTS FOR THE DEGREE

OF MASTER OF SCIENCE

IN

CIVIL ENGINEERING

DEPARTMENT OF CIVIL ENGINEERING

EDMONTON, ALBERTA

FALL, 1979



THE UNIVERSITY OF ALBERTA  
FACULTY OF GRADUATE STUDIES AND RESEARCH

The undersigned certify that they have read, and recommend to the Faculty of Graduate Studies and Research, for acceptance, a thesis entitled INVESTIGATION OF TUNNEL STABILITY BY MODEL TESTS submitted by ALAIN GUENOT in partial fulfilment of the requirements for the degree of MASTER OF SCIENCE in CIVIL ENGINEERING.





" à elles"



## ABSTRACT

This thesis is part of a more general research program investigating the failure process of a tunnel in a brittle jointed material. For this purpose a model testing technique on natural material (coal) is used. Two specimens have been tested for this particular thesis. One of the tests was carried beyond the rupture of the tunnel wall.

The test results and experimental conditions are reported but the analysis is concentrated on the study of the time - independent mechanisms involved in the rupture.

Closed-form solutions for the isotropic elasto-plastic analysis of the tunnel closure measurements have been adapted to the model test conditions. Different hypotheses for the post-failure and volume change behaviour have been considered. Comparisons with experimental data have showed that an isotropic time-independent elasto-plastic analysis cannot explain the failure process in details, even if it is consistent with the elastic and strength properties of the material. It is suggested that an isotropic elastic - anisotropic plastic analysis be used, also taking into account the time-dependent and time -independent anisotropic stress redistribution processes.

The rupture of the tunnel wall in the second test is described and commented. Joints in the material have been proven to play a role in the rupture process by intercepting and shortening the plastic slip lines. The rupture initiation, propagation and eventual stabilization have been



explained by a model taking into account the joint density and the local radius of curvature of the tunnel wall. Local instabilities of the tunnel wall could generate collapse of a tunnel and should be analysed by an anisotropic plastic equilibrium analysis.



## RESUME

Cette thèse est incluse dans un programme de recherche plus général destiné à étudier le processus de ruine d'un tunnel dans une roche fragile et jointive. A ces fins, on utilise des modèles réduits de tunnel dans un matériau naturel(charbon). Deux blocs différents ont été testé pour cette thèse ; l'un d'eux présentant une ruine du tunnel.

Les résultats de ces essais et les conditions dans lesquelles ils ont été effectués sont décrits mais l'analyse concerne essentiellement l'étude des mécanismes indépendants du temps impliqués dans la ruine de l'ouvrage.

La convergence du tunnel a été étudiée par des analyses élasto-plastiques et isotropes, adaptées pour la circonstance aux conditons particulières du modèle réduit. Ces analyses classiques considèrent différentes possibilités pour le comportement de la roche après sa rupture ou en ce qui concerne les variations de volume. Une étude comparative avec les résultats expérimentaux a montré que ce type d'analyse, indépendante du temps, ne peut expliquer complètement les déformations menant à la ruine de l'ouvrage, même si elle peut expliquer individuellement chaque convergence avec des paramètres d'élasticité et de résistance consistents avec les essais de laboratoire. Une analyse isotrope dans le domaine élastique et anisotrope dans le domaine plastique devrait être utilisée pour ce genre d'étude ; elle devrait aussi considérer les processus complexes de redistribution des contraintes qui sont





anisotropes, et qui dépendent ou non du temps.

La rupture de la paroi du tunnel dans le second bloc est décrite et commentée. On a montré comment le jointolement du milieu jouait un rôle important dans cette rupture en interceptant et raccourcissant les lignes de glissement plastiques. L'amorce de cette rupture, sa diffusion et sa stabilisation finale sont expliquées par un modèle dont les principaux paramètres sont la densité du jointolement et le rayon de courbure de la paroi. Des instabilités locales de la paroi peuvent engendrer la ruine de l'ouvrage et doivent être étudiées par une analyse anisotrope de l'équilibre plastique.



## ACKNOWLEDGEMENTS

I would like to express my sincere gratitude to my supervisor Dr N.R. Morgenstern for his guidance and encouragement during the preparation of this thesis.

My gratitude is extended to Dr D. Cruden, Dr M. Dusseault and to my fellow graduate students Sergio da Fontoura, Oldrich Hungr and Fathalla El-Nahhas for valuable discussions.

Financial support provided by the University of Alberta, the Department of Civil Engineering and by the Ministère de l'Équipement of France is appreciated.

The National Research Council and the University of Alberta are responsible for the major funding of this research project, and both Calgary Power Ltd. and Manalta Coal Ltd. at Sundance (Alberta) have supported the sampling program.

I am grateful to Messrs O. Wood, H. Soderberg, D. Fushtey, S. Gamble and R. Gitzel for their competent assistance in the laboratory. I would still be waiting for the measuring devices or others if Messrs A. Muir and T. Brown were not so efficient in the machine shop.

Ray Stewart and Deborah Barnes have had a tremendous task in improving my written English.

The life would have been much harder without the constant friendship of the Konrads, the Léautés, the Simmons', Ray Stewart and all the members of the department. I would like also to thank my friend Jean Marc Deroy, former



graduate student in this department, for bringing Edmonton to my geographical knowledge and for helping me to join this fantastic group.

I would like to express my deep appreciation to Peter Kaiser. He did not only design the testing equipment and procedure, but helped me also to complete this thesis by a constant, patient and friendly assistance.

Without the constant moral support of my family and friends overseas the completion of this thesis would not have been possible. Merci.



## Table of Contents

Chapter		Page
<u>CHAPTER 1</u>		
	<u>INTRODUCTION</u> .....	1
1.1	<u>General</u> .....	1
1.2	<u>Behaviour of the Rock Mass near an Opening in a Brittle Jointed Medium</u> .....	2
1.3	<u>Scope of this Thesis</u> .....	3
<u>CHAPTER 2</u>		
	<u>COAL AS A MODEL MATERIAL</u> .....	6
2.1	<u>Introduction</u> .....	6
2.2	<u>Origin and Structure</u> .....	6
2.2.1	Origin and geology.....	6
2.2.2	Physical Properties.....	7
2.2.3	Alteration of the Physical Properties.....	7
2.2.3.1	Introduction.....	8
2.2.3.2	Changes in moisture content.....	8
2.2.3.3	Oxidation.....	9
2.2.3.4	Precautions to take in storing coal samples.....	9
2.2.3.5	Storage and Handling of the Model Test Blocks.....	10
2.2.3.6	Conclusions.....	10
2.3	<u>Mechanical Properties</u> .....	11
2.3.1	Review of Previous Testing.....	11
2.3.1.1	Strength Properties.....	11
2.3.1.2	Time-dependent properties.....	12
2.3.2	High-Pressure Triaxial Tests.....	13
2.3.2.1	Introduction.....	13
2.3.2.2	Sample Preparation.....	13





2.3.2.3	Testing Procedure.....	13
2.3.2.4	Test Results.....	14
2.4	<u>Description of the Model Test Samples.....</u>	19
2.4.1	Introduction.....	19
2.4.2	Sample MC-3.....	19
2.4.2.1	Sample Without Tunnel.....	19
2.4.2.2	Core Drilled in the Centre of Sample and Tunnel Wall.....	21
2.4.3	Sample MC-4.....	22
2.4.3.1	Sample without Tunnel.....	22
2.4.3.2	Core Drilled in the Centre of the Sample and Tunnel Wall.....	24

### CHAPTER 3

#### DESCRIPTION OF THE MODEL TEST APPARATUS AND PROCEDURE..

3.1	<u>Introduction.....</u>	25
3.1.1	Preliminary Remarks.....	25
3.1.2	Required Specifications of Test Apparatus....	25
3.2	<u>Description of the Testing Equipment.....</u>	26
3.2.1	Compression Machine.....	26
3.2.2	Instrumentation.....	28
3.3	Sample Preparation.....	31
3.4	<u>Loading History.....</u>	32
3.5	<u>Description of the Data Processing System.....</u>	32
3.5.1	Data Processing.....	32
3.5.2	Data Presentation.....	33

### CHAPTER 4

#### DESCRIPTION OF THE TESTS AND EXPERIMENTAL RESULTS.....

4.1	<u>Introduction.....</u>	37
4.2	<u>Sample MC-3 : Loading History.....</u>	39



4.2.1	Introduction.....	39
4.2.2	Loading History.....	39
4.2.3	Comments.....	41
4.3	<u>Sample MC-4 : Loading History</u> .....	42
4.3.1	<u>Introduction</u> .....	42
4.3.2	Loading History.....	42
4.3.3	Comments.....	45
4.4	<u>Time-Dependent Data</u> .....	47
4.4.1	Reliability of the Time - Dependent Data.....	47
4.4.2	Interpretation of the time - dependent data..	47
4.5	<u>Summary and Conclusions</u> .....	51
 <u>CHAPTER 5</u>		
	<u>INTERPRETATION OF STRESS-STRAIN DATA NEAR FAILURE</u> .....	52
5.1	<u>Introduction</u> .....	52
5.1.1	Steps in the Data Interpretation.....	52
5.1.2	Existing Methods.....	52
5.1.3	Outline of the Analysis.....	53
5.2	<u>Determination of Elastic Parameters</u> .....	54
5.2.1	Introduction.....	54
5.2.2	First Method.....	55
5.2.3	Second Method.....	56
5.2.4	Conclusions.....	56
5.3	<u>Elasto-Plastic Models</u> .....	57
5.3.1	Assumptions.....	57
5.3.2	Elastic-Perfectly Plastic Model.....	58
	5.3.2.1 Elastic Behaviour.....	58
	5.3.2.2 Plastic Behaviour.....	58



5.3.2.3	Volume Change.....	61
5.3.2.4	Parametric Study of the Normalized Closure.....	64
5.3.3	Other Elasto-Plastic Models.....	68
5.3.3.1	Introduction.....	68
5.3.3.2	Elastic Brittle Plastic Material.....	68
5.3.3.3	Elastic-Strain Weakening Materials...	70
5.3.4	Factors Influencing Data Interpretation.....	71
5.3.4.1	Influence of the Longitudinal Stress.....	71
5.3.4.2	Influence of the Boundaries.....	72
5.3.4.3	Plane Strain Condition.....	73
5.4	<u>Experimental Results</u> .....	73
5.4.1	Method of Analysis.....	73
5.4.1.1	Theoretical Model Response at a Constant Loading Rate.....	74
5.4.1.2	Theoretical Model Response to Step Loading.....	75
5.4.1.3	Application to Experimental Model Test Responses.....	75
5.4.2	Experimental Measurements.....	77
5.4.3	Limitations of the Method.....	80
5.4.3.1	Linear Elastic Reference Line.....	81
5.4.3.2	Time-Dependent Strength.....	81
5.4.3.3	Uniformity of Loading.....	82
5.4.4	Interpretation of Experimental Results.....	83
5.5	<u>Summary and Conclusions</u> .....	92
<u>CHAPTER 6</u>		
<u>ANALYSIS OF THE RUPTURE PROCESS</u> .....		96
6.1	<u>Introduction</u> .....	96





6.1.1	Scope of the Chapter.....	96
6.1.2	Nomenclature.....	96
6.2	<u>Description of the Observed Ruptures</u> .....	97
6.2.1	Sample MC-3 after Unloading.....	97
6.2.2	Description of the Rupture in Sample MC-4...	102
6.2.2.1	Rupture History.....	102
6.2.2.2	Description of the Rupture as Recorded by the Instruments.....	113
6.3	<u>Interpretation of the Rupture Process</u> .....	116
6.3.1	Effect of Preexisting Discontinuities on the Slip Lines.....	116
6.3.2	Hypotheses for the Rupture Development.....	122
6.3.2.1	Introduction.....	123
6.3.2.2	Rupture initiation.....	123
6.3.2.3	Rupture Development.....	125
6.4	<u>Shape Effect and the Stability of a Tunnel Wall</u> ...	127
6.4.1	Introduction.....	127
6.4.2	Shape Effect on the Strength of the Tunnel Wall.....	127
6.4.3	Time-Dependent Rupture Process.....	129
6.4.4	Model for the Stabilization of the Rupture Process.....	131
6.4.5	Experimental Data on the Rupture.....	134
6.4.6	Discussion on this Model.....	136
6.5	<u>Summary and Conclusions</u> .....	137
CHAPTER 7		
<u>CONCLUSIONS, IMPLICATIONS AND RECOMMENDATIONS</u> .....		140
7.1	<u>Conclusions</u> .....	140
7.2	<u>Implications</u> .....	141
7.3	<u>Recommendations</u> .....	142





List of Tables

Table		Page
2.1	Properties of the Triaxial Test Samples.....	15



## List of Figures

Figure		Page
2.1	Mohr Circle Diagram for Triaxial Compression Test Data.....	17
2.2	Summary of the Stress-Strain Loading Curves for the Triaxial Compression Tests.....	18
2.3	Sketch of the Sample MC-3 before Preparation.....	20
3.1	Typical Creep Curves.....	34
3.2	Typical Strain Rate - Time Curves.....	35
4.1	Creep Curves of Internal Strain Gauges.....	48
4.2	Strain Rate - Time Curves on Log-Log Axes.....	49
4.3	Recovery Curves and a Corresponding Strain Rate - Time Curve.....	50
5.1	Theoretical Tunnel Closure vs. Stress and Average Volume Change.....	63
5.2	Normalized Closure :Sensitivity of the Cohesion Intercept.....	65
5.3	Normalized Closure :Sensitivity of the Friction Angle 66	
5.4	Normalized Closure :Sensitivity of Dilation.....	67
5.5	Closure for other elasto-plastic models.....	69
5.6	Theoretical Model Response for an Elasto-Plastic Linear Visco-Elastic Element.....	76
5.7	Test MC-3 : Experimental Tunnel Closures.....	78
5.8	Test MC-4 : Experimental Tunnel Closures.....	79
5.9	Test MC-3 :Experimental Normalized Closure.....	84
5.10	Test MC-4 :Experimental Normalized Closure.....	85
5.11	Elastic Deformations of an Elliptical Cavity (after Feder(1978)).....	91
6.1	Sample MC-3 after Unloading : Map of the Tunnel Wall. 101	
6.2	Sample MC-4 : Cross-Sections of the Ruptured Tunnel..	



6.3	Sample MC-4 after Unloading :Interpretive Sketch of Plate 6.4.....	108
6.4	Influence of Preexisting Discontinuities on Plastic Slip Lines (1).....	119
6.5	Influence of Preexisting Discontinuities on Plastic Slip Lines (2).....	120
6.6	Rupture Initiation and Propagation.....	124
6.7	Illustration for the Model of Stabilization of the Rupture.....	128
6.8	Size and Shape Effects on the Complete Stress Strain Curve of Marble Samples in Uniaxial Loading (after Hudson <u>et al</u> (1972).....	130
6.9	Model for the Stabilization of the Rupture Process in the Model Test.....	133



## List of Plates

Plate		Page
2.1	Sample MC-4 before Preparation.....	23
3.1	Model Test : Compression Machine and Data Acquisition System.....	27
3.2	Instrumentation : Tunnel Closure Measuring Device and Extensometer.....	29
6.1	Sample MC-3 after unloading :Overall view of the bottom face and close-up of the zone around the tunnel.....	99
6.2	Sample MC-4 after the First Rupture : Ruptured Tunnel Wall and Debris.....	104
6.3	Sample MC-4 after unloading :Overall views of the Sample.....	109
6.4	Sample MC-4 after unloading :Close-up of the tunnel with debris; characteristic piece of debris collected at the back of the excavation....	110
6.5	Sample MC-4 after unloading :Close-up of the tunnel after the debris have been cleaned out.....	111





## CHAPTER 1

### INTRODUCTION

#### 1.1 General

The last fifty years have witnessed tremendous progress in the construction of stable tunnels. The major contributions are known as the New Austrian Tunnelling Method (NATM) and the Observational Tunnelling Method. New technologies such as rock bolting and shotcrete, new construction procedures involving rate and sequences of excavation and subsequent supports with different stiffnesses, monitoring of deformations and loads and subsequent adjustment of the design are the main features of these successful methods.

More recently the availability of advanced computer techniques has permitted theoretical analyses of some of the processes involved in tunnel stability. Although an important contribution, these analyses are now over - sophisticated and need to be supplied with observations on the actual mechanisms involved in the time - dependent and time - independent failure of an opening. For instance stress redistribution due to isotropic or anisotropic creep, or to global or local yielding around a tunnel are rarely taken into account in analyses because the processes involved are not well understood.

Kaiser(1979) initiated a research program at the University of Alberta in order to investigate the time -



dependent deformations around a tunnel in a brittle material. For this purpose he chose to develop model tests rather than to analyse actual case histories (which have the disadvantage of being rarely documented in sufficient details). He used coal as a model material because this natural material was readily available, had suitable structural characteristics and had already been studied by Noonan(1972). Even if it has disadvantages such as lack of control of uniformity, the use of a natural material has the essential advantage of supplying the test with the intrinsic properties of a true scale natural material. Time - dependent rupture mechanisms may thus be controlled, monitored and recorded.

The purpose of the model testing undertaken in this research is not to simulate the behaviour of an actual prototype, but to understand the failure process of a tunnel in natural material. Kaiser(1979) studied in detail the time - dependent deformations of the tunnel before failure occurred. This present thesis analyses the time - independent processes of rupture. Future work will investigate the time - dependence of this rupture process.

## **1.2 Behaviour of the Rock Mass near an Opening in a Brittle Jointed Medium.**

Excavation of a tunnel generates a tangential stress concentration in the vicinity of the wall. Because the creep properties of most rocks are also stress dependent, stress



relaxation occurs near the tunnel where the confinement is the least. This causes a time - dependent redistribution of stresses to zones further from the tunnel wall.

If at any time the stress level exceeds the time - dependent strength of the rock, yielding occurs. These plastic deformations may be global or only local and are another cause for stress redistribution to occur. After larger deformations, the tunnel wall may rupture. This is controlled by the structure of the yielding rock element and it is most likely local. This is a third reason for stress redistribution to occur. The redistribution of stress may be isotropic but it is most likely anisotropic.

Propagation of the plastic zone and propagation of rupture terminate eventually. Where the confinement increases (away from the opening) the material becomes more ductile and the stress redistribution process becomes inhibited. The boundary conditions of rock elements involved in the rupture process become less favourable for a local instability. The recognition of these stress redistribution processes is essential for a proper evaluation of the load on a tunnel support.

### 1.3 Scope of this Thesis

The objective of this thesis is to study the time - independent mechanisms involved in the stability of an opening in a brittle rock mass. This thesis is part of a more general research program and for this reason, the





testing procedure (multiple-stage creep tests) is similar to the one used by Kaiser(1979). The time - dependent data are reported and described but the analysis is concentrated on the rupture mechanisms. Time - dependent aspects of rupture will be analysed in a further study. For the same reason, testing procedure and equipment are only broadly described in this thesis. More details have been already given by Kaiser(1979).

Chapter 2 summarizes the knowledge about the material used in the model tests. This coal has been already studied by Noonan(1972) ,Kaiser(1979) and da Fontoura(1980) . High pressure triaxial tests are reported to constitute the contribution of this thesis to extending our knowledge of this material.

Testing procedure and equipment are described in Chapter 3. More details regarding the development of this equipment are given by Kaiser(1979)

Two coal specimens have been tested during a eight months testing period. They are called MC-3 and MC-4 (MC for Model test on Coal). These tests are described in Chapter 4. The resulting stress - strain curves are given in Appendix B1.

Chapter 5 analyses the data near failure. In order to study the deviation from linearity of the tunnel closure measurements, elasto-plastic analyses with different hypotheses of post-failure and volume change behaviour have been adapted to the model test conditions. Appendices A1 to





A4 give the complete derivations of these methods, a list of symbols and other miscellaneous items. Theoretical and experimental data are compared and the discrepancies analysed. In the same chapter an attempt is made to determine independently elastic parameters of coal from the model test data.

Sample MC-4 experienced a rupture of the tunnel wall. The description of this rupture and of the mechanisms involved in its initiation, propagation and eventual stabilization is the objective of Chapter 6. Time - dependent data of the rupture are described in the same chapter and reported in Appendix B2.

A summary of the conclusions, some implications and recommendations for future research constitute the concluding Chapter 7.



## CHAPTER 2

### COAL AS A MODEL MATERIAL

#### 2.1 Introduction

To use a natural material such as coal as a model material has similar inconveniences to those encountered by any geotechnical engineer in field work. The material is heterogeneous, anisotropic and its properties cannot be controlled but have to be determined.

The purpose of this chapter is to describe briefly the origin, structure and mechanical properties of the coal. Results from several triaxial tests with high confining pressures will be summarized and the structure of two blocks used in the model tests will be described.

This chapter mainly summarizes the work done by Noonan(1972) , Kaiser(1979) and da Fontoura(1980) in the determination of the properties of the coal. Detailed explanations will be found in the above references.

#### 2.2 Origin and Structure

##### 2.2.1 Origin and geology

The coal samples were collected at the Highvale Mine located on the south shore of Wabamun lake, 75 km. west of Edmonton. This strip mine provides coal for the nearby Sundance power plant operated by Calgary Power Ltd.

Large blocks were collected in the mine and samples were trimmed from these blocks for triaxial tests as well as



for model tests (Kaiser(1979)).

Wabamum Lake is located on the boundary between the massive sandstones of the Tertiary Paskapoo Formation to the west and the Upper Cretaceous Edmonton Formation to the east. The coal is in the Scollard member of the upper Ardley coal zone, at the top of the Edmonton formation, which is one of the most promising sources for Albertan coal (Holter et al(1975) ). This coal-bearing stratum overlies different types of bentonitic shales. Pearson(1959)' describes the Wabamum Lake district in detail.

### 2.2.2 Physical Properties

The coal is classified as "Sub-bituminous B" according to the Canadian classification. Its natural moisture content ranges between 21% and 24%. Values for the specific gravity (1.58) and the degree of saturation (70%-100%) have been provided by Noonan(1972).

Most coals are orthotropic in structure ,containing bedding planes and two orthogonal cleat systems (Evans and Pomeroy(1966) , Ko and Gerstle(1976) ). The Highvale mine coal contains horizontal bedding planes, a vertical, discontinuous , closely spaced(0.5-2 cm) first cleat system and a poorly developed, irregular second cleat system. The first cleat system will be called a joint system hereafter.

### 2.2.3 Alteration of the Physical Properties



### 2.2.3.1 Introduction

It will be shown at the end of this chapter that the two blocks used for model test purposes have a different structural aspect. One block contains more micro-fractures than the other. However, they have been collected and handled together in the same manner before being stored. The only difference is in the storage time and in the sample preparation. These observations create a concern to determine the reasons for the alteration of the physical properties of the coal, in order to optimize the storage and sample preparation conditions.

When extracted from its natural environment a coal sample may suffer two major types of alteration :

1. moisture content change
2. oxidation

These processes have been described by Fryer and Szladow(1973) . This section mainly summarizes this work.

### 2.2.3.2 Changes in moisture content

In its natural state, coal is more or less saturated with water. When exposed to air, the moisture content reduces until a new state of equilibrium is reached. If the relative humidity of the environment increases , the coal will reabsorb moisture. This cycle may be repeated many times.

As the moisture transfer is gradual from the surface to the interior of the coal sample, internal stresses are







generated by differential expansion and cause a partial disintegration of the structure. As well as causing this alteration, which is called "decrepitation" or "slacking", absorption of moisture generates heat which accelerates the oxidation process.

#### 2.2.3.3 Oxidation

While losing and absorbing moisture when exposed to air, coal will also "chemisorb" oxygen and so become oxidized. This process may lead to a molecular degradation. It is a function of the exposed surface and the temperature.

#### 2.2.3.4 Precautions to take in storing coal samples

Generally low rank coals will slack much more quickly and extensively than coals of higher ranks. To quantify this phenomenon a slacking index was defined as the proportion of  $-0.265$  in material formed when a  $+1.05$  in coal sample is alternatively air dried and rewetted by immersion in water (Fryer and Slazdow(1973)). This index was statistically correlated to the natural moisture content of the coal. The coal used for the tests, with an average moisture content of 24% , has a slacking index of 50%.

It is important, when storing samples to minimize drying-wetting cycles and oxidation. This can be achieved by storing the samples under conditions of constant humidity or more simply under water, keeping the temperature as low as possible, but above freezing.



#### 2.2.3.5 Storage and Handling of the Model Test Blocks.

The coal samples have been stored in a moisture room with 100% relative humidity and at a temperature of 5°C. To prevent any moisture loss, the model test blocks have been protected after trimming by a latex coating, wrapped in plastic and strapped with plywood sheets. Moisture content determinations on samples stored in such a way for a year have shown that this method prevents any significant alteration.

When in the compression machine, the samples are covered by a 3 mm plaster of Paris layer and a sandwich "wax paper-plaster-wax paper", and the tunnel wall is covered with a double coating of latex. In the room where the experiments are carried out, the relative humidity is unfortunately not kept constant. However, determination of moisture content on the core obtained when drilling the tunnel and on the sample at the end of the test are similar. This shows that the method used to protect the sample is efficient.

The samples will suffer much more during the transient stages of the handling process: the original transfer from the field to the laboratory, the trimming and the preparation.

#### 2.2.3.6 Conclusions

It appears that repetitive drying-wetting cycles have to be avoided in handling coal samples. The best solution is



to keep the original moisture content. Storage conditions in the moisture room are sufficient to achieve this protection against moisture loss for a long period of time. It is essential however to keep the sample protected at all times during the transient stages described above. The most efficient solution is to keep the sample wrapped in plastic sheets and to uncover it for minimum time periods. The practice of "watering" the sample during the preparation, in order to reduce moisture loss, has to be avoided as it may be detrimental for the sample structure. This may have caused the "decrepitation" effect in sample MC-4.

## 2.3 Mechanical Properties

### 2.3.1 Review of Previous Testing

#### 2.3.1.1 Strength Properties

Direct shear tests on both precut and intact samples have been conducted by Noonan(1972)(see also Morgenstern and Noonan(1974) ). The main conclusions can be summarized as follows :

1. For a discontinuously open joint, the angle of friction  $\phi$  associated with the peak strength depends only upon the shearing resistance of the intact material and the cohesion intercept increases with decreasing degree of separation of the joint. The degree of separation is defined as the ratio between the total area of the plane containing a joint and the area of open joint surface.
2. The Young's modulus , back-calculated from direct shear





test results, ranges between 140 and 550 MPa, increasing with normal stress.

3. The ultimate  $\phi$ -value of the strength envelope is  $30^\circ$ .

Kaiser(1979) conducted further direct shear tests with normal stresses between 1 and 4 MPa and concluded that there was a reasonable agreement between his results and Noonan's conclusions. Assuming a linear Coulomb failure envelope and a friction angle of  $30^\circ$ , cohesion intercepts were calculated between 0.87 MPa and 1.9 MPa for the peak strength, and 0.3 MPa and 0.85 MPa for the reversal strength. The higher the value of the strength, the lower is the degree of separation.

A similar approach was used by Kaiser(1979) to analyse the results of several triaxial tests with confining pressures up to 1 MPa. The cohesion intercept ranges between 0.7 and 2.05 MPa at peak strains, and between 0.14 and 0.84 MPa at strains of 3 %. These values are affected by the mode of failure, the confining pressure level and the degree of separation of the joints. The coal was described as a elastic strain-weakening material with a Young's modulus between 850 and 1300 MPa.

#### 2.3.1.2 Time-dependent properties

Kaiser(1979) and da Fontoura(1980) have investigated the time-dependent properties of this coal. Kaiser conducted multiple-stage repeated relaxation tests and concluded that coal, as a brittle rock with time-dependent strength, can be





described as a visco-elastic, visco-plastic, strain-weakening material (Kaiser and Morgenstern(1979) ). From single-stage and multiple-stage creep tests, da Fontoura determined an empirical creep law for the pre-failure range of this coal.

## 2.3.2 High-Pressure Triaxial Tests

### 2.3.2.1 Introduction

In order to understand the behaviour of the coal at high confining pressure, triaxial compression tests were conducted with confining pressures between 3 MPa and 10 MPa. Sample preparation, testing and analysis are described by Kaiser(1979) and only a brief description will be presented here.

### 2.3.2.2 Sample Preparation

Cylindrical samples, 4 cm in diameter and 8 cm in length were drilled from blocks of coal in the laboratory. Water was used as the cutting fluid. The axis of the core barrel was orientated parallel to the bedding planes and at angles of  $30^{\circ}$ ,  $45^{\circ}$  and  $60^{\circ}$  respectively with the major joint set. The samples were cut with an attempt made to keep the major visible joints from intercepting the ends.

### 2.3.2.3 Testing Procedure

The samples were tested in a Wykeham Farrance high-pressure triaxial cell designed for rock specimens up



to 50 mm in diameter with a maximum allowable cell pressure of 10 MPa. The compression machine is a relatively soft testing machine (Wykeham Farrance).

All samples were consolidated and sheared at a constant rate with free drainage. The highest rate was 0.56 mm /hr. The test may be considered as fully drained at this strain-rate(Kaiser(1979)).

#### 2.3.2.4 Test Results

In order to determine the dependence of the strength of a coal mass on the direction of the joints with respect to the principal stress directions, joint orientations of  $30^{\circ}$ ,  $45^{\circ}$  and  $60^{\circ}$  with respect to the sample axis were selected for this study. A  $30^{\circ}$  sample should fail along a joint and a  $60^{\circ}$  sample may be expected to fail through the intact material, with a strength approaching the strength of the intact material.

All the samples exhibited a composite failure plane and the majority of them failed partially along joint surfaces. This is unfortunate as the results will not indicate the maximum strength exhibited by the intact material. The results thus cannot be considered as an upper limit of the strength.

The results of the eight tests are summarized in Table 2.1. The strength envelope is presented on a Mohr circle diagram which is assumed to be linear(Figure 2.1), and the stress-strain curves are plotted together in the Figure 2.2.



Table 2.1 Properties of the Triaxial Test Samples

[illegible]





Two  $30^0$  samples (F and I) failed along joints on a step-like surface. The remaining samples, as indicated before, failed partially through the intact material and along joints. The interpretation is complicated by several other factors :

1. The load cap is not particularly designed to allow lateral deformations and the large deformations after failure will thus be influenced by the apparatus.
2. Subsequent to failure the upper corners of the sample were crushed, which makes the visual observation of the failure zone difficult.
3. As described previously, the axis of the sample is parallel to the bedding plane direction. In some of the samples the composite failure surface included parts of bedding planes in their step-like shape.

Hence some of the stress-strain curves appear peculiar after a first load peak, and before large strains occurred (see Figure 2.2), the analysis will only consider the behaviour of the sample up to the first load peak. The corresponding points are plotted as circles in Figure 2.1 ("Peak values").

Assuming a linear Coulomb failure envelope and a peak friction angle of  $30^0$ , all samples but sample I were found to have a cohesion intercept between 1.9 MPa and 2.4 MPa. Sample I has an unexpectedly high shear strength of 3.6 MPa. This may be explained by the fact that the failure surface intercepted the upper end of the sample.





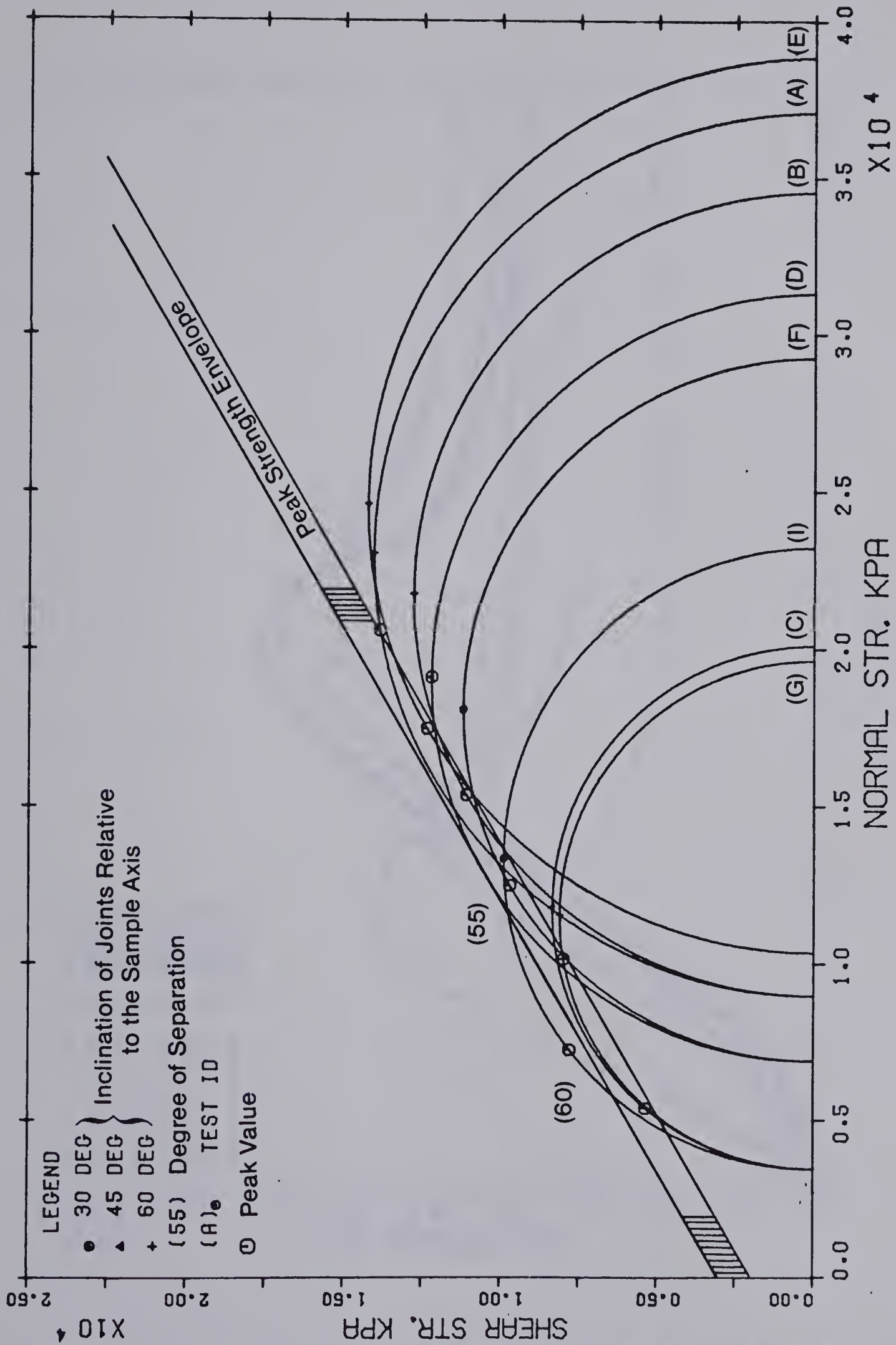


Figure 2.1 Mohr Circle Diagram for Triaxial Compression Test Data



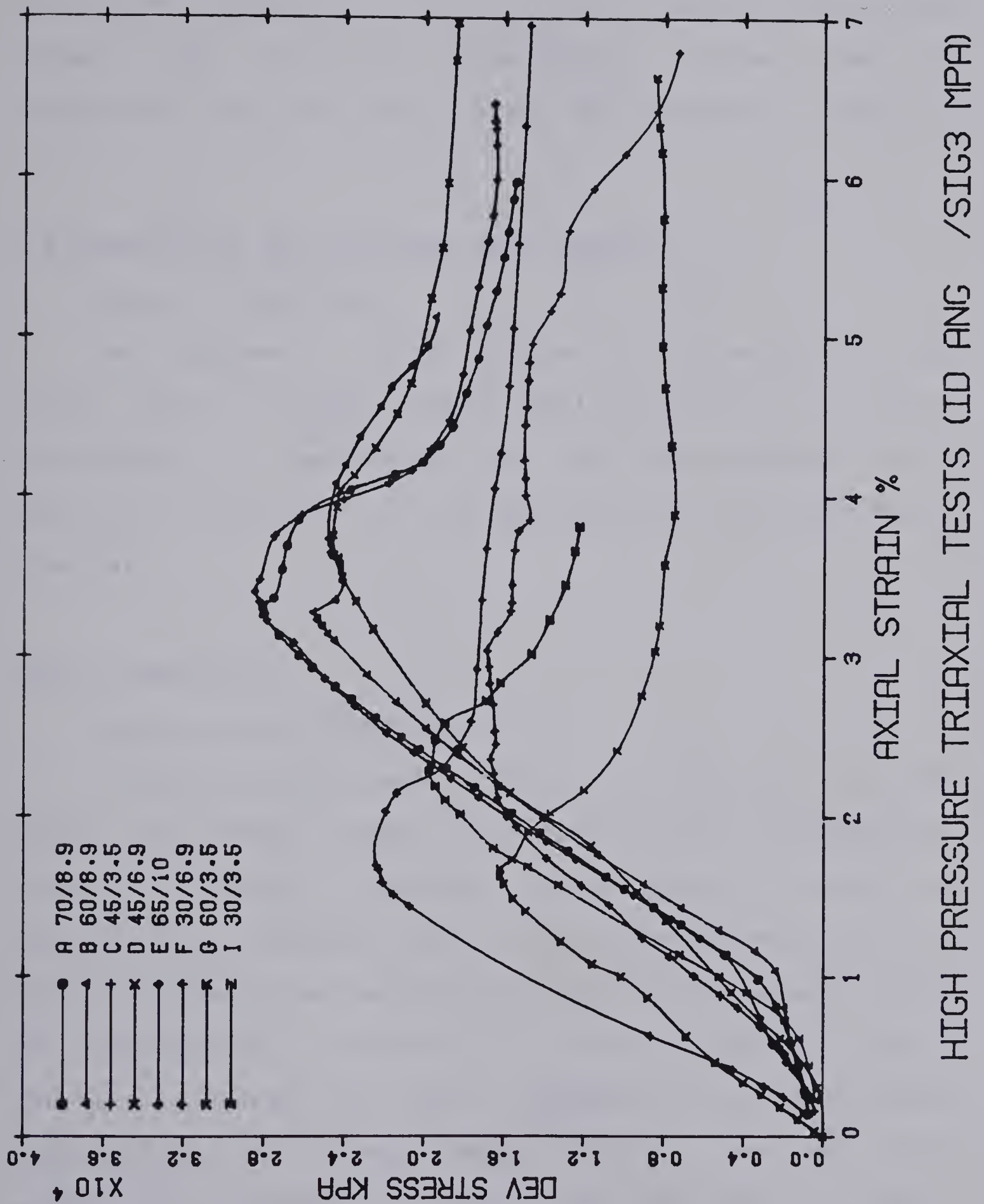


Figure 2.2 Summary of the Stress-Strain Loading Curves for the Triaxial Compression Tests



The general tendency in the volume-change measurements is to show compression prior to failure (0.3% to 0.7% volume change) and dilation subsequently. Since they are incomplete, they will not be presented hereafter in detail.

## 2.4 Description of the Model Test Samples

### 2.4.1 Introduction

The purpose of this section is to describe the coal blocks used in model tests MC-3 and MC-4. A careful description, in particular of the heterogeneity of the samples, is essential for the evaluation of the experimental results.

### 2.4.2 Sample MC-3

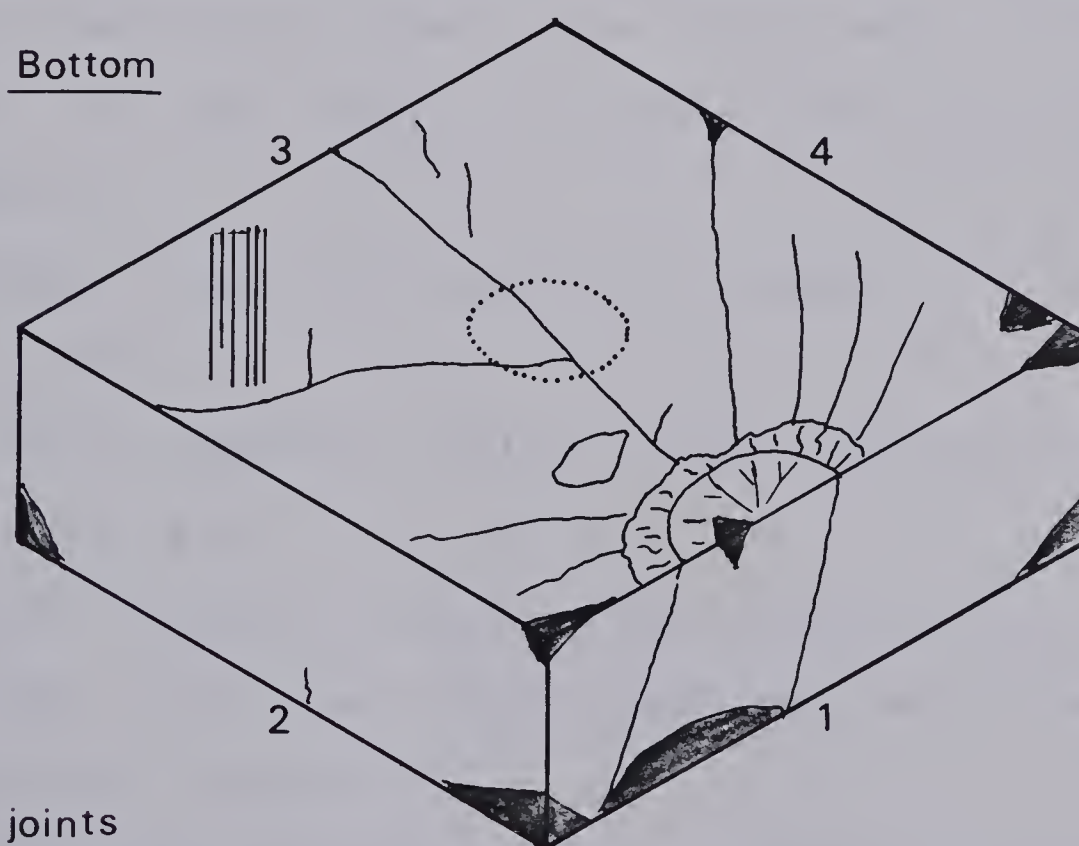
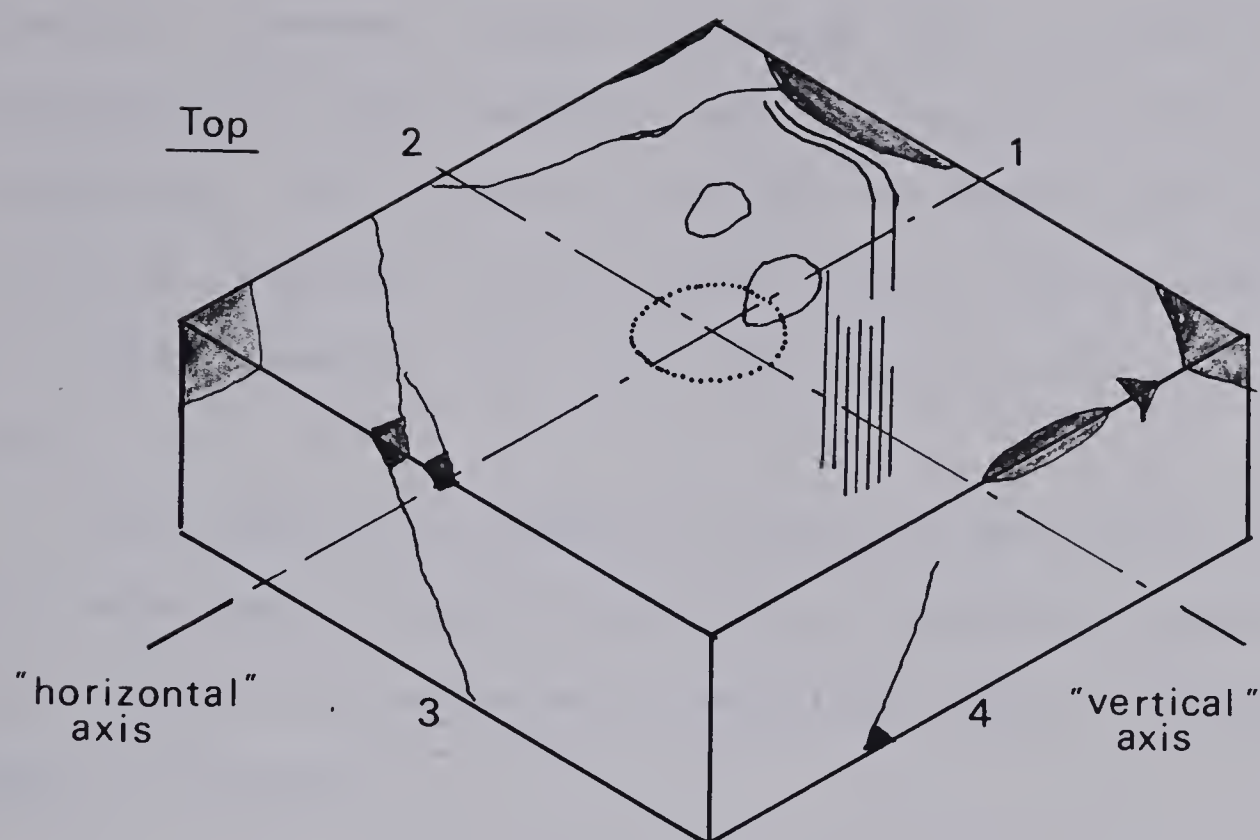
#### 2.4.2.1 Sample Without Tunnel

A sketch of the sample is shown in Figure 2.3. At first sight the sample seems to be particularly heterogeneous. Vegetable remains, apparently from a trunk or a root, were exposed while trimming face 1. The macerals present in this lenticular seems to be harder than the average and as a result of differential stiffness a radial fracture pattern developed centred on these remains. This is particularly apparent on the bottom face. Moreover, the main joint pattern is perturbed by this hard zone from its regular direction, and seems to go round the lenticular.

These features, as interesting they may be from the geological point of view, are obviously not desired in a







- ||| joints
- grouted zone
- fracture

Scale : 1/10

Figure 2.3 Sketch of Sample MC-3 before Preparation





sample for model test, which should be as homogeneous as possible. However, these features are located near the boundaries of the sample and the central part is fairly homogeneous with regular jointing. It appears also that the fractures apparent on the faces are not continuous through the whole sample and thus this block was chosen for test MC-3.

The joints inclination varies between  $40^{\circ}$  and  $45^{\circ}$  from the "horizontal axis" (1-3) and are uniformly spaced (about 1cm). Corner 2-3 exhibits an existing fracture surface which makes it fragile.

#### 2.4.2.2 Core Drilled in the Centre of Sample and Tunnel Wall

The visual observation of the tunnel wall confirmed the structure of the block. It showed three major planes of weaknesses :

1. A major plane of separation crosses the sample at mid-height.
2. The main fracture noticed on the top face dips at  $45^{\circ}$  towards face 4.
3. Another fracture noticed on the bottom face is parallel to the first one. These fractures are not continuous through the sample.

Due to these major discontinuities the core was recovered in five separate pieces. The core was sheared in rotation along the median plane of separation. The moisture content of the core, measured after drilling, was found to be 23.8% on



average, which indicates that the procedure followed to maintain the original moisture of the sample was efficient. After drying, the pieces exhibit a well defined joint pattern with a spacing of about 1 cm and several major bedding planes with an average spacing of about 4 cm.

#### 2.4.3 Sample MC-4

##### 2.4.3.1 Sample without Tunnel

This block does not show any major fracture. The jointing is regular(1-2 cm) and is inclined at  $45^0$ . However the block is heterogeneous :

1. Some inclusions have been exposed by the saw while trimming the block. They have a smoother and harder surface than the other parts of the sample. The jointing does not appear to be continuous through these inclusions. The hard inclusions are located principally near corner 3-4 on the bottom face.
2. The material surrounding the inclusions is more intensively jointed.
3. Some discontinuities may be observed, crossing the side faces 1 and 4 at  $45^0$ . They are thin bands of finer material widening sometimes to accommodate several small inclusions of the same type as the ones described above (1 cm in diameter).
4. All over the sample surface lenses of a dark brown material are visible. It was observed later that this material also filled the discontinuities apparent on the





Plate 2.1 Sample MC-4 before Preparation





side faces. X-rays analyses indicated that the material was mainly composed of kaolinite (85%), montmorillonite (10%) and illite (5% or less), with no organic material).

#### 2.4.3.2 Core Drilled in the Centre of the Sample and Tunnel Wall

The tunnel was drilled by using a core barrel which transmitted lateral vibrations to the material. As a result, there was no recovery from this drilling operation. The core was reduced to small pieces, mainly horizontal flakes, with an average size of 3cm. Some round-edged pieces of coal were recovered. The average moisture content of the recovered material was as low as 18.1%.

This low moisture content indicates that the sample suffered from drying. Even if the mass looks intact and homogeneous, the sample at this stage contains some microfracturing. Actually the sample was left uncovered for 8 hours during the preparation and then heavily watered which may have caused the "slacking" of the structure. However if highly confined, the sample should not be very much affected by this alteration, but the structural alterations may reduce the strength of the material around the tunnel.





## CHAPTER 3

### DESCRIPTION OF THE MODEL TEST APPARATUS AND PROCEDURE

#### 3.1 Introduction

##### 3.1.1 Preliminary Remarks

This geomechanical model study follows that of Kaiser (1979) who designed the test apparatus, based on equipment developed by Heuer and Hendron (1967, 1971). The equipment and the procedure used for this thesis are identical that described by Kaiser (1979) and a complete description of the system will not be repeated here.

##### 3.1.2 Required Specifications of Test Apparatus

The most important aspects of the testing equipment are summarized below.

A block of coal (60cm/60 cm/20 cm) has to be tested under plane strain conditions. Access for instrumentation has to be provided in the middle of each lateral face and at each corner of the sample, and for the tunnel deformations measurements and visual observations through the loading head. A surface pressure of maximum 15 MPa is required on the lateral faces of the sample and will have to be maintained with minor fluctuations during long term creep tests (>5 days). The lateral loading systems have to be independent in order to apply different stress ratios to the model block. A large amount of data is expected and automatic data processing is essential to control the test.



This chapter describes briefly the testing system designed in accordance with the above specifications. The purpose is to introduce the reader to the test apparatus and to make the remainder of this thesis understandable. For a detailed discussion, see Kaiser (1979).

## 3.2 Description of the Testing Equipment

### 3.2.1 Compression Machine

A picture of the compression test machine is presented on Plate 3.1. The sample with the tunnel in the vertical position is seated on a steel base plate. Plane strain is maintained by a rigid loading head which is controlled by four rams (visible on the picture in vertical position). Two rams act on each lateral face. The four rams in each direction are connected to each other and pressurize the sample simultaneously. An upper and a lower reaction head are connected by four rods and constitute the reaction frame in the direction of the tunnel (called hereafter "longitudinal direction"). In the lateral directions (called "horizontal" and "vertical" directions) the reaction frames are cantilevered beams, supporting the rams, and restrained from bending by two upper movable rods. A window is provided in the loading head to make the tunnel accessible during the test. The load is distributed uniformly to the sample sides by a set of triangular prisms in a vertical position. Between the ram piston and the prisms is inserted a load cell (aluminium hollow cylinder with strain gauges glued on





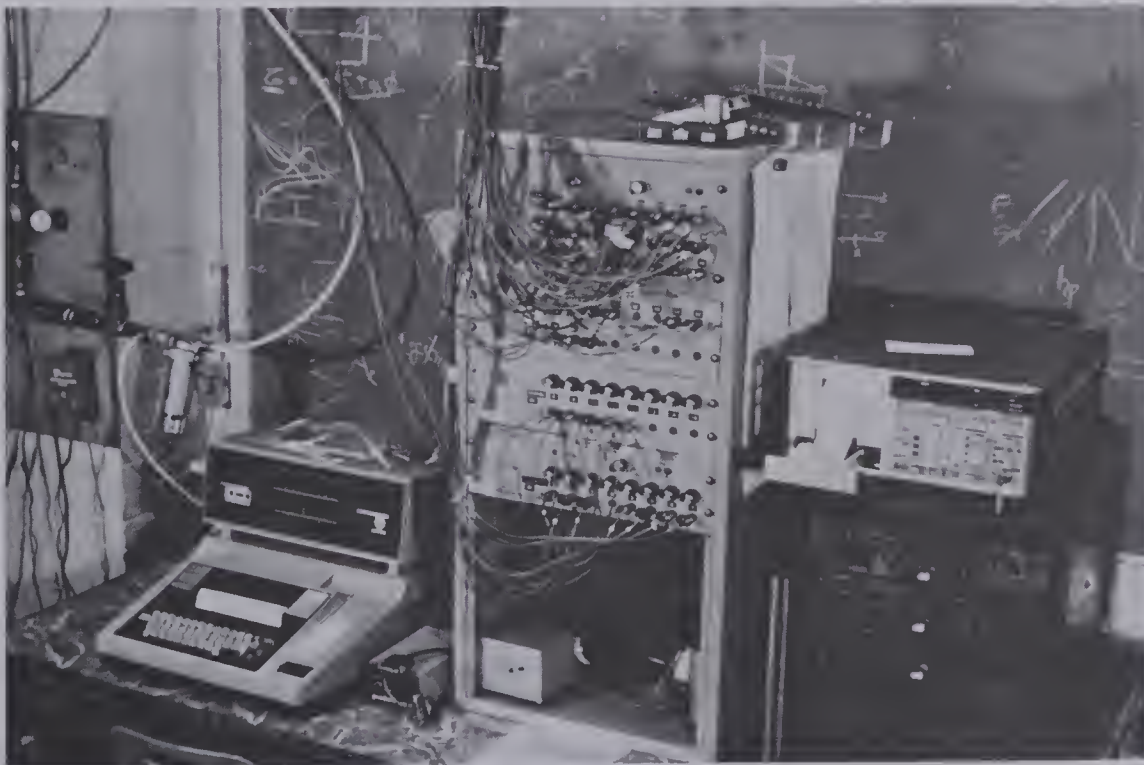
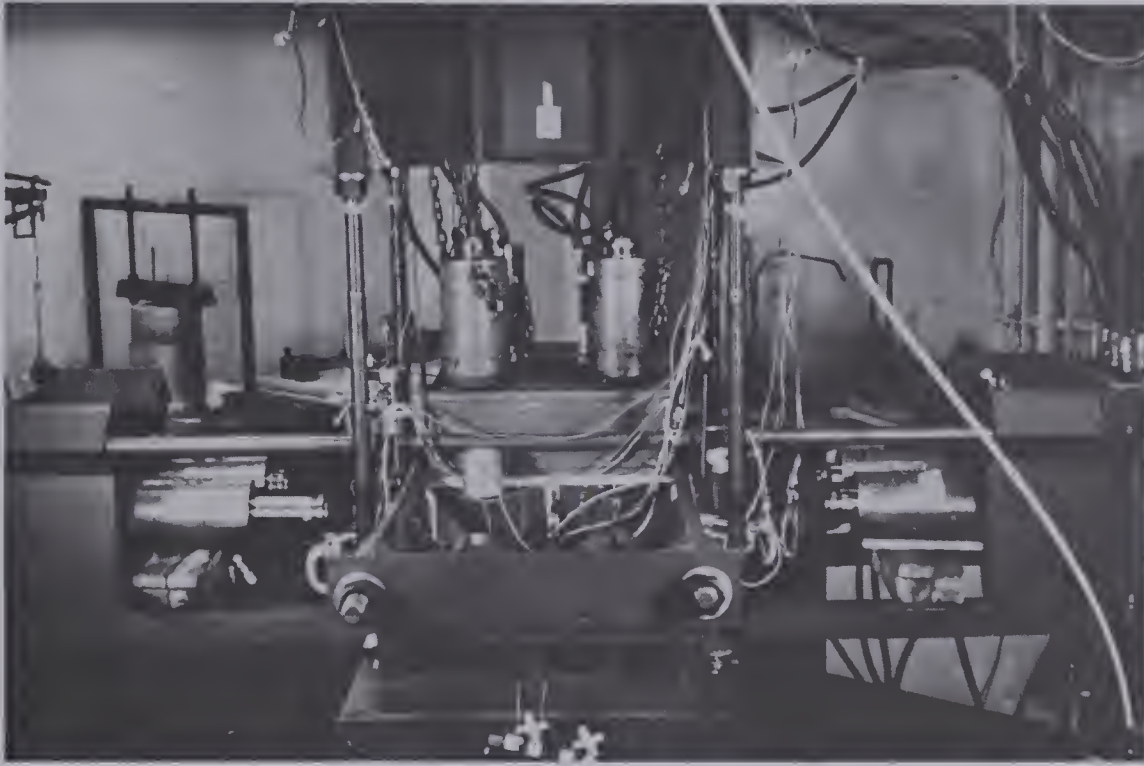


**Plate 3.1 Model Test : Compression Machine and Data Acquisition System**



the inside wall) sitting on a spherical, lubricated seating to avoid the transmission of any bending moment.

The rams are controlled by three independent hydraulic pumps, one for each direction of loading. A maximum surface pressure of 16 MPa can be applied to the sample side and maintained with load fluctuations of less than one percent for days or weeks. This system allows maintenance of plane strain conditions and loading with different ratios of the applied load:

$$N = 5h/5y$$

$5h$  being the load in the "horizontal" direction and  $5y$  the load in the "vertical" direction.

### 3.2.2 Instrumentation

The instrumentation is designed to monitor three different types of displacements :

1. Tunnel deformations in four directions;
2. Internal strains around the tunnel;
3. Overall external deformations of the block.

The deformations are measured by electronic transducers (Linear Voltage-Displacement Transducers or LVDTs).

The device measuring the deformations of the tunnel is presented on Plate 3.2 (upper picture). A vertical stand is fixed on the steel plate below the sample. On each diameter two LVDTs measure the displacements of the tunnel wall giving the closure of the tunnel with an accuracy of  $\pm 2 \cdot 10^{-4}\%$ . The closure of the tunnel is defined as the ratio







**Plate 3.2 Instrumentation : Tunnel Closure Measuring Device  
and Extensometer**



between the change in diameter and the original diameter of the tunnel and is expressed in percent.

The average internal strains are calculated from the measurement of the relative displacements of two points of known original separation within the rock mass. This is achieved in practice by use of the extensometers shown on the lower picture in Plate 3.2. Two coaxial rods are grouted at their ends, in a hole within the sample mass. The inner rod is glued at the end of the hole whereas the outer rod is glued at a known distance from the end of the hole (5 cm). The relative displacement of these points is measured by an LVDT fixed to the other end of the coaxial rods. The third tube shown on the picture is a protective rod. The strains are thus calculated with an accuracy of  $\pm 2 \cdot 10^{-3}$ . Two rings with eight extensometers are installed radially in the direction of the principal stress axes and in the diagonals of the sample. The first ring is set up as close as possible to the tunnel wall (tip at 1 cm from tunnel wall), and the second ring measures the strain further away from the wall (tip at 5 cm from the wall).

The external deformations of the sample are measured in the three directions of loading. Four LVDTs measure the displacements of the four corners of the loading head in order to check the plane strain condition. Four LVDTs mounted on stands fixed on the base plate measure the displacement of each face.

The combination of the readings in each lateral



direction gives the overall strain of the sample.

### 3.3 Sample Preparation

Block of about 1 m<sup>3</sup> are collected from the mine as described by Kaiser (1979). They are trimmed by saw to the shape of a regular parallelepipedon. The joints of the coal are parallel to one of the diagonal plane of the sample and the bedding planes are perpendicular to the tunnel. The faces are carefully mapped and then sanded to create parallel surfaces and to remove any loose material. Small depressions and broken corners are filled in with a stiff grout and sanded until a uniform flat surface is obtained on each face.

The sample is then placed in an aluminium mould with removable sides. Faces and sides of the sample are coated with a 3 mm layer of Plaster of Paris. Two protective sheets of wax paper isolate the plaster layer from the coal surface and from the outside. This surface preparation is necessary to ensure a uniform transmission of load to the sample.

Holes are drilled and the extensometers are installed. Accurate records of the sample dimensions and of the instrument locations are essential for the test result interpretation. The sample is then moved to the testing machine and the loading heads are installed, isolated from the sample by teflon sheets to minimize friction on the sample faces. The LVDTs are mounted and the zero readings of the load cells are taken. The rams are brought into contact





with the loading heads and a zero reading of the LVDTs is taken. The sample is now ready for testing.

### 3.4 Loading History

The intact sample is loaded several times up to 10 MPa, about  $2/3$  of the capacity of the machine. This is done in order to determine the elastic properties of the sample, to compress the plaster layer and to induce crack closure. Sustained load tests are also carried out to study the time-dependent compressibility of the material under hydrostatic compression.

The tunnel is drilled after the loading head has been removed. The tunnel wall is immediately covered with two coatings of latex to prevent it from drying. The sample is reinstalled and loaded by 2 MPa increments, after an original increment of 5 MPa up to the upper limit of the loading range (16 MPa). The load is kept constant at each load stage for a period of one or five days.

If rupture of the tunnel wall does not occur the sample is unloaded and left for recovery. In Chapter 4 the actual loading histories for the two tests are given in detail.

### 3.5 Description of the Data Processing System

#### 3.5.1 Data Processing

A data logger scans automatically the measurements of 44 instruments (36 LVDT and 12 load cells) at regular time





intervals. The data are recorded on a cassette on a computer terminal and can be transferred directly to a file in the main computer of the University. Datalogger, transducers conditioner, and computer terminal are presented on the lower picture in Plate 3.1.

Several computer programs allow one to process the data and produce among other things stress-strain and strain-time plots. These plots may be visualized on a graphic terminal within less than one hour after the last reading has been recorded. This rapid data analysis allows optimal control of the test procedure.

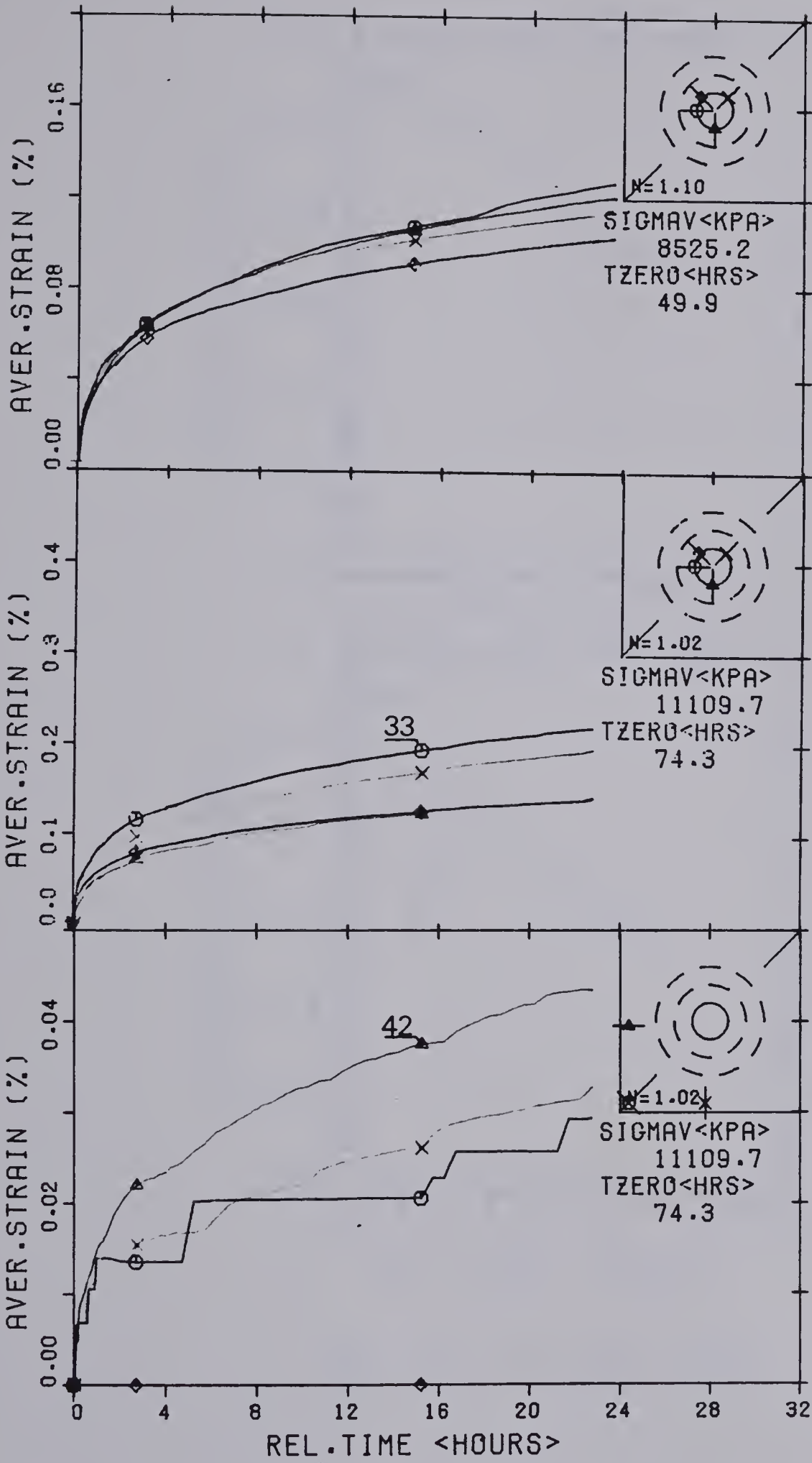
### 3.5.2 Data Presentation

Most data are presented in the following plots:

1. Stress-strain plot (or stress-closure);
2. Strain-time plot (or closure-time);
3. Log strain rate-log time (or closure rate-time).

The first two types of plots have linear axes: there are four curves per diagram, each being identified by a symbol, corresponding to the sketch in the upper right corner of the frame. This sketch represents the sample; two diagonal lines indicate the jointing, the solid circle the tunnel and the dashed circles the two rings of internal extensometers. On each figure the N-value calculated as an average over the data presented on the figure is given. On the strain-time plots, TZERO is the zero time of the sustained load test with respect to the beginning of the test, and SIGMAV is the

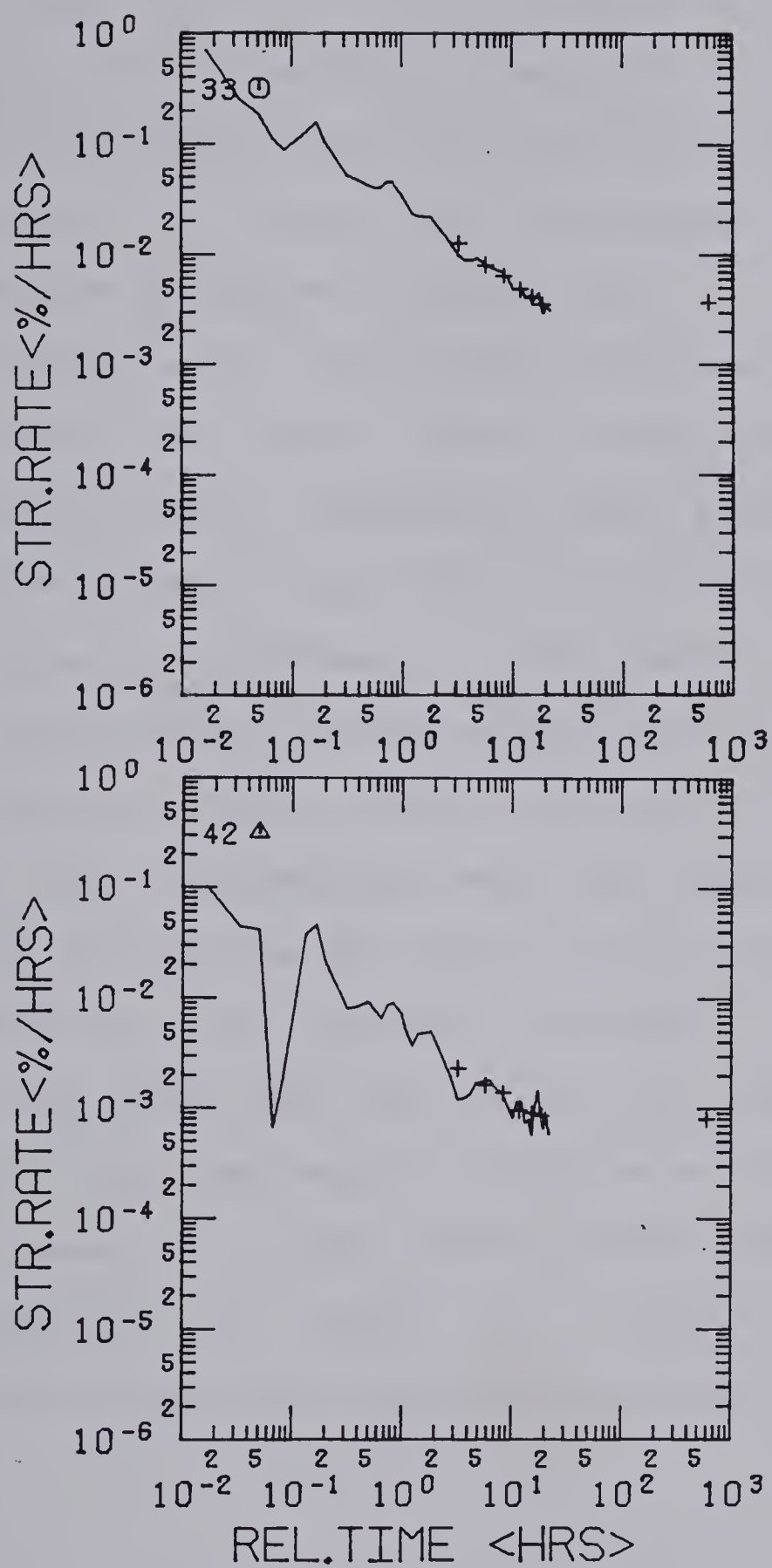




TEST #MC-4.2 WITH TUNNEL 1979

Figure 3.1 Typical Creep Curves





MC 4.2 AT 11000 KPA

Figure 3.2 Typical Strain Rate - Time Curves



average stress in the "vertical" direction. Stress versus strain curves are presented in Appendix B1. Typical creep curves (strain versus time) are presented on Figure 3.1 for the closure of the tunnel and the external deformations. Other curves are presented in Chapter 4.

The strain rate versus time plots are presented on a log-log scale. The strain rate is the slope of the line calculated by linear regression over three points and plotted at the time corresponding to the mid-point. Only the absolute value is plotted. If the rate is positive a straight, solid line is drawn between the points and if the rate is negative, the points are plotted as small solid triangles. After 30 readings have been taken, a "trend" is obtained by calculating the slope of the line between three points separated by 10 readings. The results are plotted as plus for positive rate and crosses inclined at 45 degrees for negative rate. Two typical examples of strain rate time plots are shown in Figure 3.2 and correspond to the creep curves presented in Figure 3.1. Other curves showing negative strain rates are presented in Chapter 4.





## CHAPTER 4

### DESCRIPTION OF THE TESTS AND EXPERIMENTAL RESULTS

#### 4.1 Introduction

Two different specimens were tested in this study (MC-3 and MC-4). Each sample was subjected to a series of sequential loadings (e.g. Tests MC-3.0 to MC-3.2). The actual loading histories are described in Sections 4.2 and 4.3 and are based on the procedure discussed in Section 3.4. They are also presented in graphs in Appendix B1.

Too many data have been acquired to be presented fully here. All data has been summarized in an internal report (1979) of the Geotechnical Section of the Department of Civil Engineering, University of Alberta. Only the stress-strain curves are reported in full in this thesis and are given in Appendix B1. Some representative strain - time and strain rate - time curves are shown in Section 4.4.

Although similar, the two tests differ in several aspects:

1. Diameter of the opening : 12.7 cm for sample MC-3 and 15.2 cm for the sample MC-4.
2. Duration of the creep tests: 5 days for sample MC-3 and 1 day for sample MC-4.
3. Ultimate behaviour: Sample MC-3 collapsed by shearing of a corner, while the tunnel was still intact; Sample MC-4 did not collapse fully but the test was stopped after extended rupture of the tunnel wall.



The interpretation of the experimental data may be subdivided into three parts: elastic properties, strength properties and time - dependent (visco - elastic and visco - plastic) properties.

While the loading of a classical triaxial sample can provide independently an elastic constant (e.g. Young's modulus), the loading of the model test cannot permit the distinction between two elastic parameters which influence simultaneously the measurements (e.g. Young's modulus and Poisson's ratio). An attempt was made to determine these elastic parameters independently (Section 5.2). It led, however, to scattered results. Because of this complexity the elastic deformations will not be analysed in detail. The assumption of a Poisson's ratio of 0.2 leads to values for Young's modulus between 1000 and 1700 MPa. These values are slightly higher than the results of triaxial tests.

The strength properties will be analysed in Chapter 5.

The visco - elastic properties of the material in the pre-failure range of the loading have been analysed in detail by Kaiser(1979) based on the results of previous tests. The time - dependent behaviour of samples MC-3 and MC-4 are in agreement with his conclusions which are summarized in Section 4.4. The analysis of the time - dependent plastic deformations is beyond the scope of this thesis.



## 4.2 Sample MC-3 : Loading History

### 4.2.1 Introduction

Sample MC-3 was collected and trimmed during winter 1976-77 and instrumented in August 1978. It was tested over a three month period between August 30th and December 9th 1978. The intact sample was loaded 4 times and the sample with tunnel was subjected to two loadings: the first one is a multiple-stage creep test and the second one a short term loading test. The complete loading history is presented in the following. The different steps are described for each test. For each step a time is given ( $t=...$ ). It corresponds to the end of the load step and is measured from the beginning of the test. The vertical stress and the N-value are also given.

### 4.2.2 Loading History

Intact sample

\* Test MC-3.0 \* Aug. 30th \* N=0.75

- Loading : 8500 kPa  $t=2h$ .
- Unloading : 1000 kPa  $t=4h$ .
- Reloading : 4500 kPa  $t=7h$ .

\* Test MC-3.01 \* Sept. 1st \* N=1.01

- Loading : 6000 kPa  $t=2h$ .
- Unloading : 0 kPa  $t=2.5h$ .

\* Test MC-3.02 \* Sept. 4th \* N=1.09

- Loading : 9500 kPa  $t=3.5h$ .
- Unloading : 0 kPa  $t=4h$ .





\* Test MC-3.03 \* Sept. 6th \* N=1.01

- Loading : 8500 kPa t=2.5h.
- Creep : 8500 kPa t=20h.
- Unloading : 0 kPa t=20h.
- Recovery : t=45h.

The tunnel was drilled on September 8th 1978. The drilling operation took about 10 minutes . The core was recovered in five major pieces and is described in Section 2.4.2.2.

#### Sample with Tunnel

\* Test MC-3.1 \* Sept. 28th \*

- Loading : 4781 kPa t=2h.
- Creep : N=1.06 t=120h.
- Loading : 6917 kPa t=121h.
- Creep N=1.02 t=238h.
- Loading : 9000 kPa t=240h.
- Creep N=1.00 t=350h.
- Loading : 11117 kPa t=350h.
- Creep N=0.99 t=609h. (double duration)
- Loading : 13336 kPa t=610h.
- Creep N=0.98 t=719h.
- Loading : 15000 kPa t=715h.
- Unloading t=717h
- Recovery t=1067hr

\* Test MC-3.2 \* December 9th

- Loading : 14902 kPa t=3.5h.
- Creep N=0.97 t=6.5h.



- Uncontrolled unloading after the rupture of a corner of the sample

#### 4.2.3 Comments

The complete stress-strain curves are presented on pages B1.1 to B1.12 in Appendix B1. This test was disturbed by several accidents. It happened several times during the tests that a hydraulic ram leaked internally and was temporarily unable to maintain a constant pressure on the sample. This caused a break in the symmetry of the applied pressures and the sample rotated slightly. In the worst cases the sample had to be unloaded and the ram repaired. This happened at the end of test MC-3.1, preventing any creep test during the last load increment. This also accounts for the important time lapses during the loading program. New rams with higher load capacity have now been built to prevent these delays.

The sample failed by shearing of corner 2-3 along a plane parallel to the joints. After being loaded, the sample rotated slightly during the creep test and the rams, no longer perpendicular to the sample faces, created stress conditions which sheared the sample along this plane of weakness. The readings of the strain gauges do not show evidence of the shearing process at the corner. This suggests that the presence of a major plane of weakness parallel to the tunnel axis is not critical for the stability of this opening.



### 4.3 Sample MC-4 : Loading History

#### 4.3.1 Introduction

Sample MC-4 was collected and trimmed during winter 1976-77 and instrumented in January 1979. It was tested over a 2 month period between February 3rd and March 23th 1979. The intact sample was subjected to 7 loadings and the sample with tunnel to two multiple-stage creep tests.

Because the previous samples did not show any significant rupture of the tunnel wall, it was decided to increase the tunnel diameter by 2.3 cm . As the behaviour of the sample in the prefailure range has been investigated and because most of the creep occurs in the first day, the creep test duration was reduced to 1 day.

#### 4.3.2 Loading History

Intact sample

\* Test MC-4.0 \* Feb. 3rd \*  $N=1.04$

- Loading : 10000 kPa  $t=1.2\text{hr}$  (test MC-4.01)
- Creep  $t=2.2\text{h}$ .
- Unloading : 0 kPa  $t=3.5\text{h}$ .
- Time laps  $t=5\text{h}$ .
- Reloading : 10000 kPa  $t=6.2\text{h}$ . (test MC-4.02)
- Unloading : 0 kPa  $t=7.4\text{h}$ .

\* Test MC-4.03 \* Feb. 4th

- Loading : 4985 kPa  $t=0.9\text{h}$ .
- Creep  $N=1.08$   $t=24\text{h}$ .
- Loading : 7004 kPa  $t=25\text{h}$ .



- Creep  $N=1.07$   $t=48h$ .
- Loading : 9294 kPa  $t=49h$ .
- Creep  $N=1.00$   $t=71h$ .
- Loading : 11356 kPa  $t=73h$ .
- Creep  $N=1.00$   $t=95h$ .
- Unloading : 0 kPa  $t=99hr$ .
- Recovery  $t=119h$ .

\* Test MC-4.04 \* Feb. 10th

- Loading : 9168 kPa  $t=1.8h$ .
- Creep  $N=1.00$   $t=24h$ .
- Unloading : 0 kPa  $t=26h$ .
- Recovery  $t=42h$ .

\* Test MC-4.11 \* Feb 22nd

- Loading : 5008 kPa  $t=0.8h$ .
- Creep  $N=1.07$   $t=5.5h$ .
- Unloading : 0 kPa  $t=6.5h$ .
- Recovery  $t=22h$ .

\* Test MC 4.13 \* Feb 23rd

- Loading : 4995 kPa  $t=1.2h$ .
- Creep  $N=1.02$   $t=24h$ .
- Loading : 7166 kPa  $t=25h$ .
- Creep  $N=1.02$   $t=49h$ .
- Loading : 9419 kPa  $t=49.3h$ .
- Creep  $N=1.00$   $t=73h$ .
- Loading : 1535 kPa  $t=74h$ .
- Creep  $N=1.00$   $t=97.5h$ .
- Unloading : 0 kPa  $t=105h$ .





- Recovery  $t=182h$ .

The tunnel was drilled on March 5th in about 10 minutes. The core was recovered in small pieces and is described in Section 2.4 .

#### Sample with tunnel

##### \* Test MC-4.2 \* March 8th

- Loading : 4499 kPa  $t=0.7h$ .
- Creep  $N=1.11$   $t=24h$ .
- Loading : 6469 kPa  $t=25h$ .
- Creep  $N=1.13$   $t=49h$ .
- Loading : 8525 kPa  $t=50h$ .
- Creep  $N=1.10$   $t=73h$ .
- Loading : 11109 kPa  $t=74h$ .
- Creep  $N=1.02$   $t=97.3h$ .
- Loading : 13354 kPa  $t=98h$ .
- Creep  $N=0.98$   $t=123h$ . (first rupture of the tunnel)
- Loading : 15967 kPa  $t=128h$ .
- Creep  $N=0.95$   $t=152h$ .
- Unloading : 0 kPa  $t=153h$ .
- Recovery  $t=238h$ .

##### \* Test MC-4.3 \* March 21th

- Loading : 7129 kPa  $t=1.1h$ .
- Creep  $N=0.99$   $t=24h$ .
- Loading : 9361 kPa  $t=25h$ .
- Creep  $N=0.98$   $t=48h$ .
- Loading : 11753 kPa  $t=49h$ .



- Creep  $N=0.95$   $t=73h$ .
- Loading : 14109 kPa  $t=74h$ .
- Creep  $N=0.94$   $t=98h$ .
- Loading : 15018 kPa  $t=99h$ .
- Creep  $N=0.95$   $t=115h$ .
- Loading : 15216 kPa  $t=115h$ .
- Creep  $N=0.95$   $t=142h$ .
- Loading : 16628 kPa  $t=143h$ .
- Creep  $N=0.90$   $t=169h$ .
- Unloading : 0 kPa  $t=171h$ .
- Recovery  $t=421h$ .

#### 4.3.3 Comments

The stress - strain curves are presented in Appendix B1 (pages B1.13 to B1.30). This test is characterized by the rupture of the tunnel wall during the 5th increment in test MC-4.2. The rupture is described in detail in Chapter 6.

During the first sustained load test in test MC-4.01, the intact sample exhibited high time - dependent deformations (0.12% in 30 minutes). At the same time water was expelled from the sample as drops forming along the coaxial strain gauges. This water had previously been introduced into the sample cracks by a heavy watering of the sample during the preparation. Consequently, the inner rods of the extensometers rusted. This explains the peculiar results of tests MC-4.03 and MC-4.04 during which an



unsuccessful attempt was made to clean the extensometers.

The gauges were changed at the end of test MC-4.04 and results improve the change. Only one instrument could not be changed and it was not monitored further (lower right corner 3-4, second ring of extensometers). The available LVDT was installed to monitor the displacements of the triangles applying the pressure on the sample face. This was done in order to compare the measurements of the external displacements of the sample given by the usual method (see Chapter 3) to the displacements of the triangles. This measurement is given in the figures presented in Appendix B1 and the corresponding symbol is in the right position on the reference sketch.

The data for test MC-4.2 are presented twice in Appendix B1: the first series shows the data for loading only and the scale allows the analysis of the small deformations; the second series presents the data for the whole test where the large deformations require a larger scale.

A safety system protects the testing system from excessive displacements of the rams. Micro-switches are installed close to the loading heads of the rams during creep tests. These switches control electro - valves which stop the air pressure supply if large displacements of the ram occur. In test MC-4.3 this line was accidentally switched off for 30 minutes in the first creep test at 1500 kPa. The load in the rams dropped anisotropically which





explains the particular aspect of the stress - strain curve for this test. The sample was reloaded for a second creep test at an equivalent stress level.

#### 4.4 Time-Dependent Data

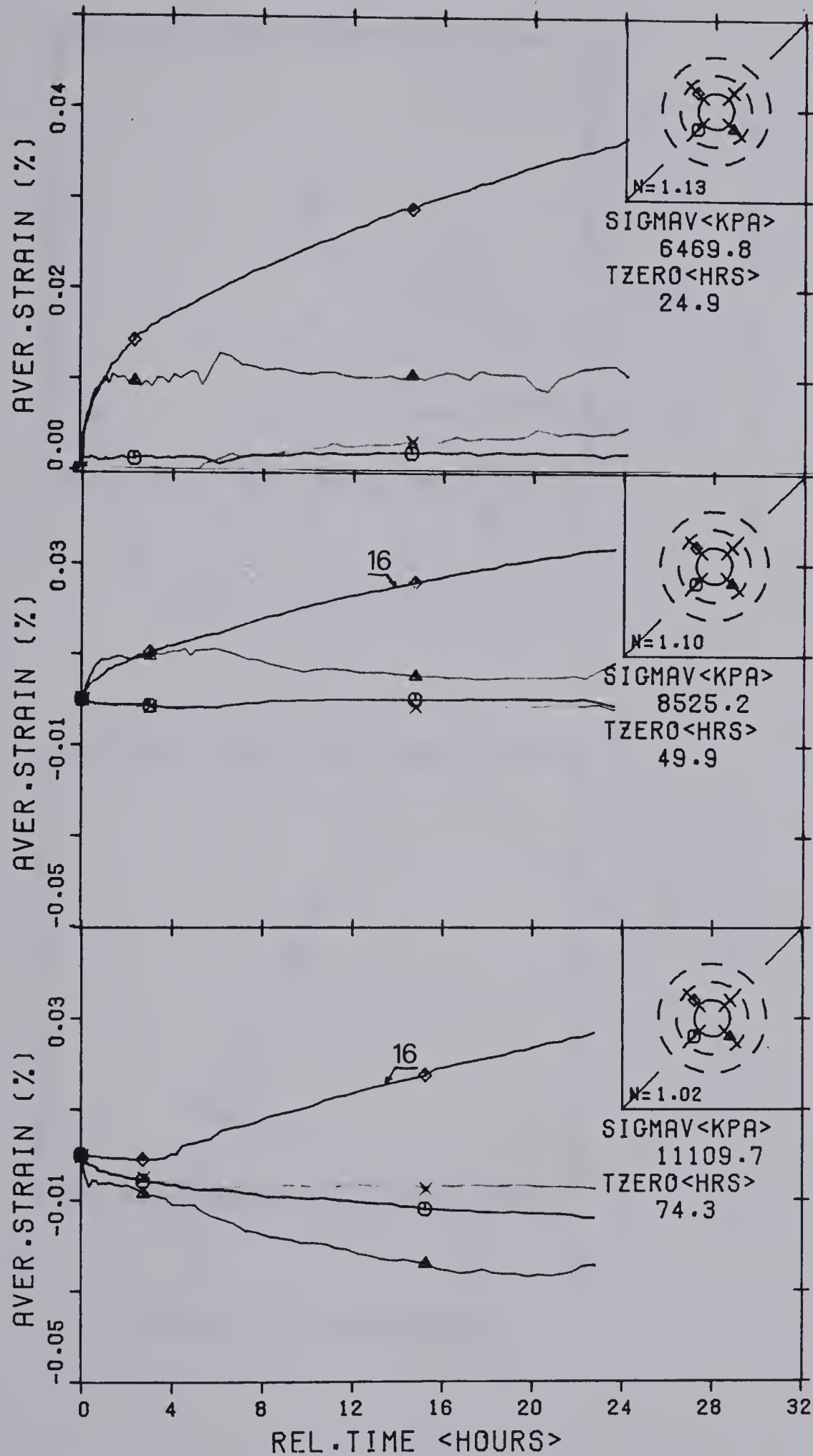
##### 4.4.1 Reliability of the Time - Dependent Data

The testing equipment and procedure are satisfactory to study the time - dependent deformations around the tunnel. Responses of an instrument in a sustained load test are very accurate in particular in a recovery test. Typical curves are given on Figures 4.1 and 4.3. Responses of the closure measuring device have already been shown in Chapter 3. The procedure to calculate the strain rates seems successful : most of the data show a linear relationship between log strain rate and log time. The slope of this line is negative and is more or less constant throughout a test. This corresponds to the response of a rheological model composed of a series of Kelvin models with a particular retardation spectrum. This model has been proposed to explain the time - dependent behaviour of coal (Terry(1956) ) Typical strain rate - time curves are shown in Figure 4.2 and correspond to some of the strain - time curves presented on Figure 4.1

##### 4.4.2 Interpretation of the time - dependent data

Similar time - dependent data in the pre - failure range have been analysed by Kaiser(1979). He explained the time - dependent process by a non - linear bulk modulus at





TEST #MC-4.2 WITH TUNNEL 1979

Figure 4.1 Creep Curves of Internal Strain Gauges



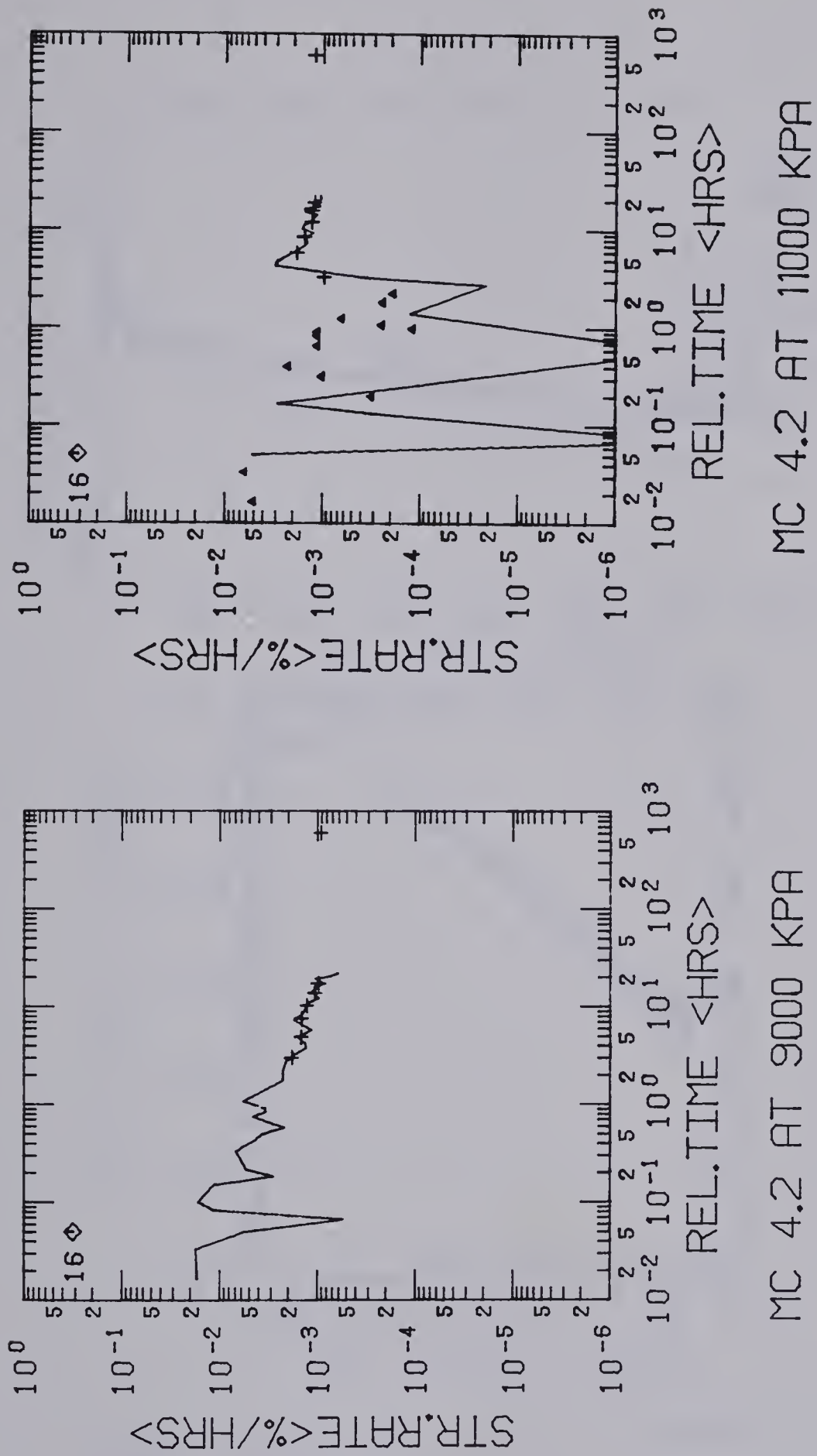
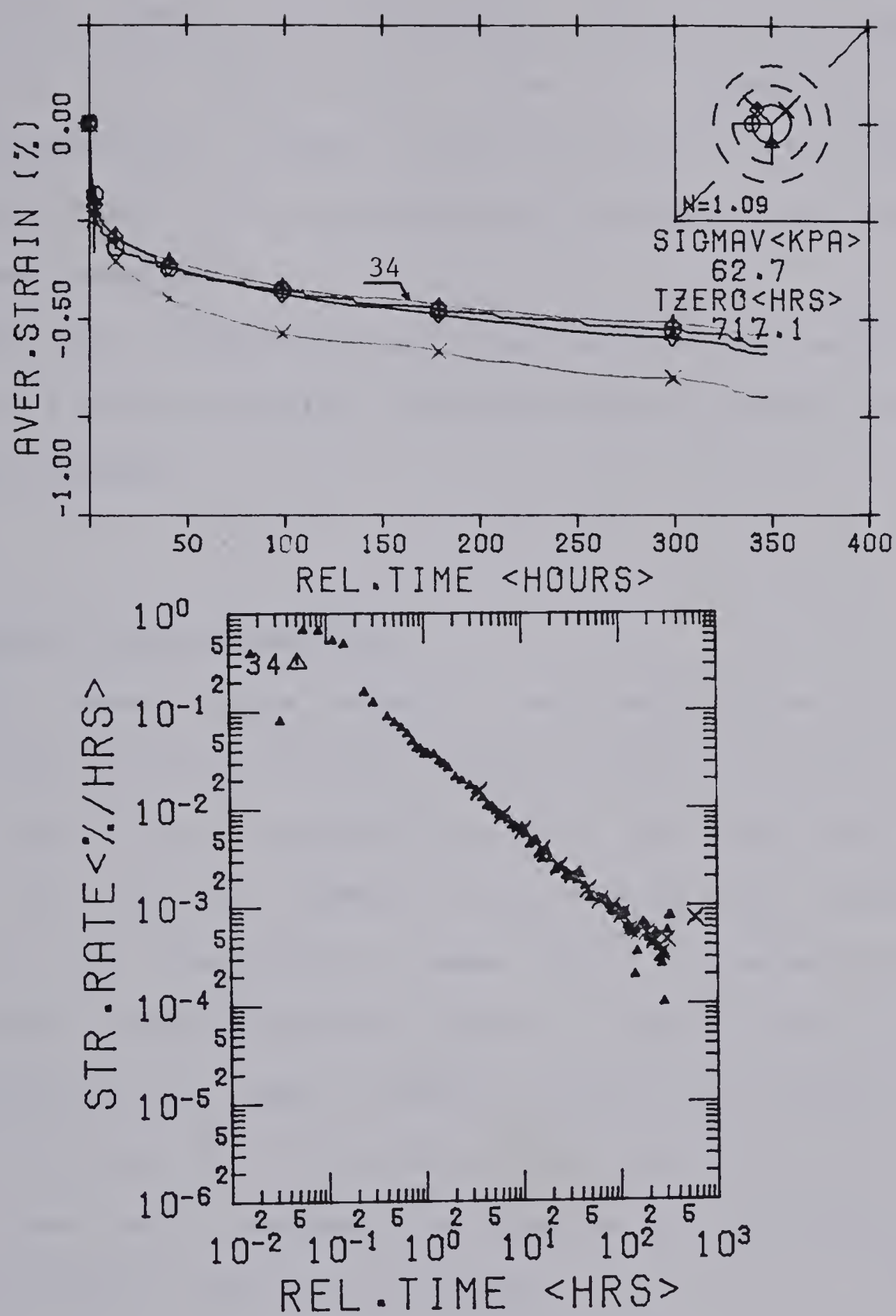


Figure 4.2 Strain Rate - Time Curves on Log-Log Axes





TEST #MC-3.1 WITH TUNNEL 1978

RECOVERY

Figure 4.3 Recovery Curves and a Corresponding Strain Rate - Time Curve





low stress level, superposition of hydrostatic and deviatoric creep at intermediate stress levels and by an isotropic or anisotropic time - dependent stress redistribution at higher stress levels. He also mentioned the importance of the anisotropic character of the time - dependent process.

The time - dependent data near failure are described in Chapter 6 but a detailed interpretation is beyond the scope of this thesis.

#### 4.5 Summary and Conclusions

Two model tests samples have been tested during the eight months of the testing program for this thesis. For the first time in this research program a test was carried out beyond the initial rupture of the tunnel wall. Because the data in the pre-failure range are in agreement with the conclusions of Kaiser(1979) based on similar data, the test interpretation has been oriented towards the analysis of the rupture process. The different ultimate behaviour of the two tests deserves a comparative study of the failure process. This is given in Chapters 5 and 6.



## CHAPTER 5

### INTERPRETATION OF STRESS-STRAIN DATA NEAR FAILURE

#### 5.1 Introduction

##### 5.1.1 Steps in the Data Interpretation

Visual observations on both tests indicate that plastic deformations occur before the completion of the loading program. Since this initiates on the tunnel wall, therefore only the tunnel closure measurements will be analysed in detail. The internal extensometers measurements are perturbed by local effects. Therefore their interpretation is more difficult and it will not be undertaken here. The behaviour of the sample near failure will be studied by comparison of the experimental data with the response of a theoretical elasto-plastic model.

##### 5.1.2 Existing Methods

Numerous methods employing elasto-plastic analyses are available to evaluate the stability of an opening. Daemen(1975) reports the most important methods and gives his own contribution, the use of particular strain-weakening models. Egger(1973) was one of the first to investigate the effect of the post-failure behaviour of the material. Descœudres(1977) gives a detailed derivation of the solution which employs an elastic perfectly plastic and elastic perfectly brittle material model. Florence and Schwer(1978) point out the importance of the intermediate principal



stress. Borsetto and Ribacchi(1979) studied the influence of a strain-weakening behaviour after strength failure. A ring of "weakening" material between the remaining elastic and the "residual" material provides an apparent support pressure.

Most of these authors analyse the unloading of a prestressed rock mass due to tunnel advance. They also take into account an internal support pressure provided either by the nearby tunnel face or by an artificial support. The aim of these theoretical methods is to evaluate criteria for the design of underground cavities.

Model tests have the same stress and strain distributions as encountered in an actual tunnel, but do not have the same displacement field. At an infinite distance from the tunnel the displacement in the model test has a finite value. The test behaviour results from the simultaneous loading of a finite intact plate and unloading of an infinite medium due to a cavity. As a consequence, particular solutions for the model test have to be adapted.

### 5.1.3 Outline of the Analysis

When testing a nonhomogeneous material with time - dependent properties, it appears reasonable at the outset to try and explain the observations by simple methods, preferably with closed-form solutions. This allows identification of the processes, the dominant parameters and provides a basis for more advanced calculations.





Closed-form solutions for the model test are developed in the second section of this chapter. These solutions facilitate the analysis of the influence of different elasto-plastic models on the deformations of an opening near failure, as a function of material properties. They require very restrictive assumptions, such as homogeneous and time-independent characteristics of the material and axisymmetric stress conditions. Experimental results permit the validity of the solutions and the importance of the assumptions to be evaluated. This analysis is presented in the third section. A first section presents a method for evaluation of the elastic parameters of the material by use of the experimental data.

## 5.2 Determination of Elastic Parameters

### 5.2.1 Introduction

It will be shown in the next sections that one limitation in the analysis of the experimental data is due to non-linearity of the elastic response of the system. It is therefore of interest to know the variation of the elastic constants with stress level.

The slope of the response of any instruments measuring the deformations in the model test is always a function of two elastic constants, and one curve is not enough to know the variation of each parameter independently. It is possible to get this variation by comparing the responses of two different instruments. Two methods have been derived and



are explained in detail in Appendix A4. Both are based on elasticity and are only valid before the yield point.

#### 5.2.2 First Method

The first method consists of comparing the responses of an internal strain gauge before and after excavation of the tunnel. It assumes that the elastic constants are not affected by the loading history and that the rate of loading is the same in the two different tests. For each model test the method has been applied to the deformations of the 16 internal gauges. This study is valid because the rates of loading are similar, and because the effect of the loading history was not important any more, as the sample had been loaded several times before the studied tests. The results are presented in Appendix A4. They are extremely scattered. The values of Poisson's ratio are between 0 and 0.2 and of Young's modulus between 1300 and 2300 MPa.

It can be seen from the expressions given in Appendix A4 that the accuracy of the values of Poisson's ratio is a function of the distance of the gauge from the tunnel wall. In other words the further the gauge is from the tunnel, the less is the effect of the presence of an opening. Thus the results are totally erratic for the furthest row of gauges from the tunnel wall. The results for the other instruments are affected by the inaccuracy in determining the exact position of the gauge and by the heterogeneity of the sample.



### 5.2.3 Second Method

The second method deals with one test only, in comparing the response of a tunnel diameter and of the external deformation of the block in the same direction. The limitations encountered in the first method by using two different tests with different loading histories are thus overcome but only two values (instead of 16) are now obtained in each model test (one for each of the vertical and horizontal directions). The results are presented in Appendix A4. They show a tendency for the Poisson's ratio to increase from a value near 0 to a value near 0.2. The corresponding values for Young's modulus range between 1300 and 2300 MPa.

The value of Poisson's ratio appears to be lower than the values published for coal (Labasse(1949) , Ko and Gerstle(1976) ), which are around 0.4. However, the high density of jointing, the presence of bedding planes and the state of fracturation make that the overall value of Poisson's ratio for the rock mass to be lower than this published value. While 0.4 is a value of Poisson's ratio for coal as a mineral, 0.2 or less is the value to be input in any theoretical analysis of the behaviour of the coal mass.

### 5.2.4 Conclusions

The methods used to calculate the elastic constants do not give accurate results, but indicate a trend. They could be used to characterize the variation of stiffness in the





sample on a qualitative basis. Similar methods, but assuming an orthotropic structure for the material, must be considered in further work (see Ko and Gerstle(1976) for the study of an orthotropic coal).

### 5.3 Elasto-Plastic Models

#### 5.3.1 Assumptions

In the following the assumptions used throughout the theoretical analyses are given. It is assumed that the material is homogeneous, isotropic, and linear elastic before the yield point. Plastic and strength failures are assumed to occur simultaneously when the Mohr circle touches a linear Mohr-Coulomb failure envelope, characterized by a cohesion intercept  $C$  and a friction angle  $\phi$ . After failure the stresses in the material obey a "plastic criterion". For a perfectly plastic material only, this criterion coincides with the failure criterion. This criterion is different for materials with a different post-failure behaviour, and is strain-dependent for a strain-weakening material.

The model test block is considered as a plate with a circular hole (radius  $a$ ) under plane strain conditions. The hydrostatic loading conditions ( $N=1$ ) make the stress field axisymmetric.

Cylindrical coordinates are used and the longitudinal stress is the intermediate principal stress. No support pressure is applied to the tunnel wall. The radial stress therefore increases continuously from zero to the applied





field stress.

The material properties are time-independent.

### 5.3.2 Elastic-Perfectly Plastic Model

Only the logic of the solution is presented here. The complete derivation is given in appendix A2.

#### 5.3.2.1 Elastic Behaviour

The elastic analysis of a cavity in an infinite medium was originally attributed to Kirsch. The derivation of the stress distribution by use of Airy's stress functions is found in numerous textbooks (i.e. Obert and Duvall(1967) ). Hooke's law will be used to obtain the strain distribution. The integration of the strain-displacement relationships, with the appropriate boundary conditions, will give the displacement field. The elastic closure of the tunnel, defined as the ratio between the change in diameter and the original diameter, is equal to

$$u/a = 5q(1-\nu^2)/E$$

where  $u$  is the displacement at the tunnel wall,  $a$  the radius of the opening,  $5q$  the external stress,  $\nu$  is the Poisson's ratio and  $E$  the appropriate modulus of elasticity.

#### 5.3.2.2 Plastic Behaviour

If the tangential stress at the tunnel wall exceeds the unconfined compressive strength of the material, failure occurs uniformly around the tunnel. An annular zone of



yielding material develops and propagates into the rock mass as the load is increased. For a given value of external stress, the stress, strain, and displacement fields and the radius  $R$  of the plastic zone are determined in the following manner.

The combination of the equilibrium equation and the failure criterion gives the stress distribution in the plastic zone. By assuming continuity of the radial stresses, the radius of the plastic zone can be determined. If the boundary between the plastic and elastic zones is known, the radial stress at this level is given and may be considered as a support pressure for the remaining elastic zone. Therefore the stress, strain, and displacement fields can be determined in the elastic zone.

Strains in the plastic zone are assumed to be the sum of elastic and plastic components. It is further assumed that Hooke's law applies for the elastic part of the strain in the plastic zone, with the same elastic constants as in the elastic zone. As the stresses in the plastic zone are known, the elastic part of the strain can then be determined by applying Hooke's law.

In order to obtain the plastic part of the strain, a flow rule must be postulated. The following relationship between the radial and tangential plastic strains was chosen (Egger, 1973).

$$\epsilon_r^p + \alpha \epsilon_\theta^p = 0$$

The parameter  $\alpha$  is a measure of the dilation associated with



the plastic flow. If  $\alpha$  is equal to one, the plastic volumetric strain is equal to zero since the longitudinal strain is considered to be zero during plane strain loading. It can be shown that the strain increments are then normal to the Von Mises criterion failure surface (Salençon(1969)). The associated flow rule together with the Coulomb failure criterion will lead to a similar relationship between principal plastic strains, with the boundary conditions stated. This relationship is equivalent to the above expression where  $\alpha$  is replaced by  $m$ , coefficient of failure earth pressure and also coefficient of the Coulomb failure criterion. The parameter  $\alpha$  will then be between 1 and  $m$ .

The combination of the compatibility equation and this relationship will give the plastic strain and the displacement field. The closure of the tunnel under these conditions is as follows :

$$\frac{u}{a} = \frac{\sigma_c (1-\nu^2)}{E} \left(1 + \frac{m+1}{m+\alpha} \left[\left(\frac{R}{a}\right)^{m+\alpha} - 1\right]\right)$$

The normalized closure has been introduced as the ratio between the closure given by the above expression and the closure of a tunnel in a linear elastic material. This ratio is one up to the yield point and increases for higher stresses as a function of the strength parameters  $C$  and  $\phi$ , and of the dilation characteristics of the material. It is independent of the elastic properties of the material. If the strength parameters are time independent, the normalized





closure is independent of the rate of loading. It is valid, however, only if the loading is hydrostatic and if no stress redistribution occurs within the sample.

#### 5.3.2.3 Volume Change

The dilation parameter  $\alpha$  has been introduced and the sensitivity of the closure to this value will be studied. The amount of volume change induced by using a particular value of this parameter and the variation in volume change for different values of  $\alpha$  will be given. Such a detailed study was not found in the literature because most of the authors are concerned with real tunnels where volume change does not present any particular interest. This is not true for the model test where the volume of material is finite.

The volumetric strain is the sum of the values of the principal strains. It is determined at each point as soon as the strain field is known. The volumetric strain is also defined as the change in volume of a unit volume surrounding the point. The volume change of a body is the integral over the entire volume of the body of this unit volume change. It can be shown that if the volumetric strain is constant throughout a body, the corresponding volume change of the body is equal to this constant value.

The volumetric strain is constant in the elastic region and varies in the plastic region by becoming more dilatant. In reality, this constant value is zero and only dilation occurs in the plastic zone. However in the model, this



constant value is compression due to the displacement of the external boundaries and this compression is superposed on the dilation in the plastic zone.

The volumetric strain in the plastic zone is the sum of an elastic and a plastic component. If the dilation parameter increases, the elastic part remains constant in the plastic zone as it is a function only of the stress distribution. The total volume change is only equal to the elastic volume change if the dilation parameter is 1. If the dilation parameter increases, the plastic part of the volumetric strain changes and becomes more dilatant.

The integration of the varying values of the total volumetric strain, through the plastic zone, gives a constant average value which will be called hereafter the "average volume change" (Ladanyi(1974) )

Figure 5.1 shows typical closure stress curves and the corresponding average volume change versus closure curves. The strain due to the compression of the plate only is given as a reference. The behaviour of the model test is shown for a purely elastic material and for an elastic-perfectly plastic material with different values of the dilation coefficient. The elastic and strength parameters are typical for the behaviour of the actual model. The friction angle is 30 degrees; the corresponding value of the passive earth pressure coefficient  $m$  is 3, which is the highest value for the dilation parameter on the figure (associated flow rule). The values 1 and 2 correspond respectively to no volume



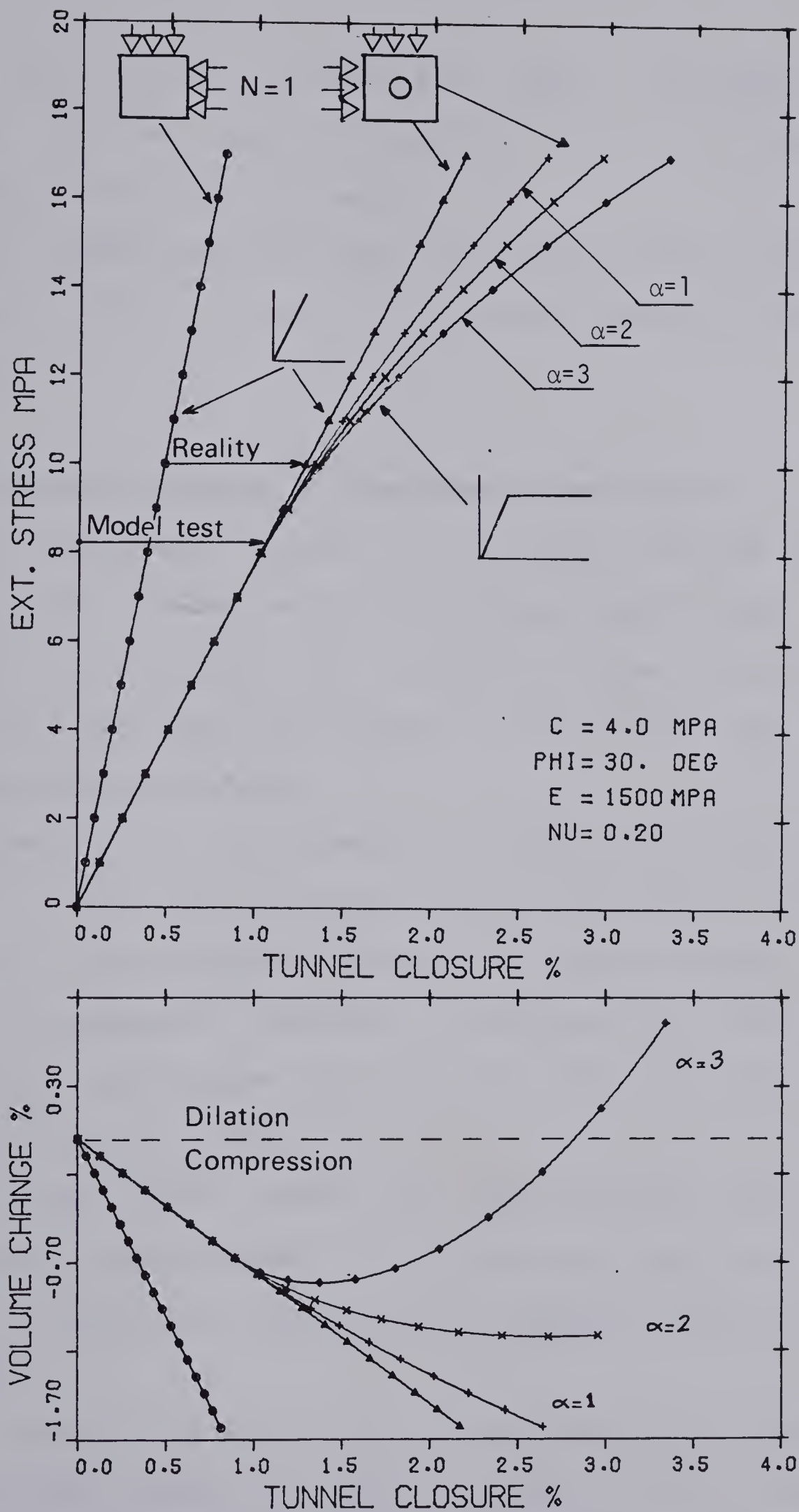


Figure 5.1 Theoretical Tunnel Closure vs. Stress and Average Volume Change





change and to an intermediate stage. Throughout the remainder of the chapter these values of the dilation parameters (1,2,3) will be used.

The figure shows how much the average volume change is affected by the use of a different value of dilation parameter.

#### 5.3.2.4 Parametric Study of the Normalized Closure

The normalized closure as previously defined depends only on three parameters:  $C$ ,  $\phi$  (strength parameters), and  $\alpha$  (dilation coefficient). The purpose of this section is to evaluate the influence of changes in these parameters on the normalized closure values.

Figures 5.2 to 5.4 present the results of a sensitivity analysis in the form of normalized closure versus external stress plots. The following conclusions can be shown:

1. The normalized closure increases with decreasing cohesion and angle of friction and with increasing dilation coefficient.
2. The yield point where the curve deviates from 1, is directly proportional to the cohesion intercept  $C$ , but it is relatively insensitive to changes in the friction angle.
3. In Figures 5.2 and 5.3 the curves have similar shapes. Therefore several groups of values ( $C$ ,  $\phi$ ) could fit given experimental data. However figure 5.2 shows that the cohesion is clearly determined by the yield point





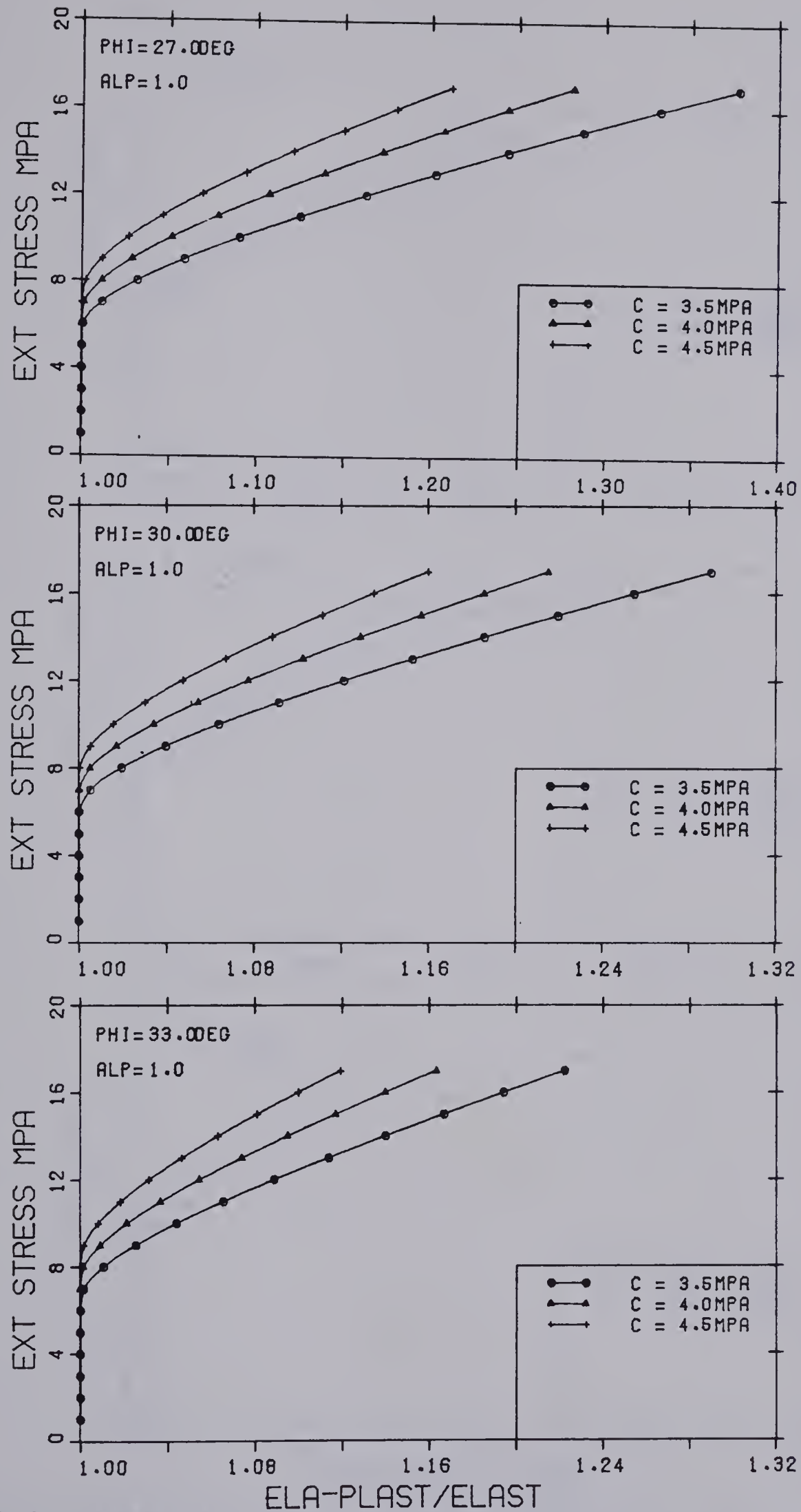


Figure 5.2 Normalized Closure :Sensitivity of the Cohesion Intercept



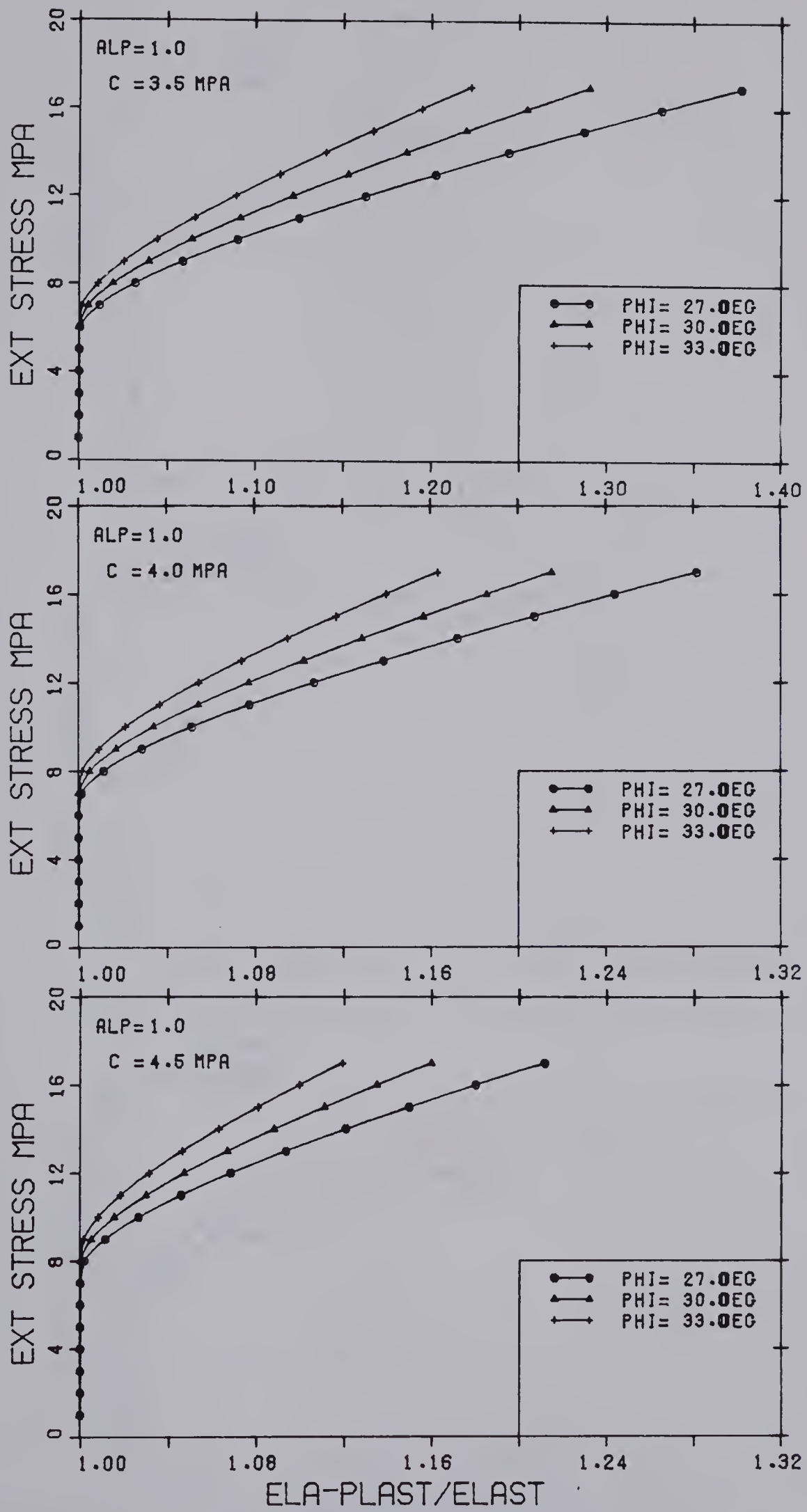


Figure 5.3 Normalized Closure :Sensitivity of the Friction Angle



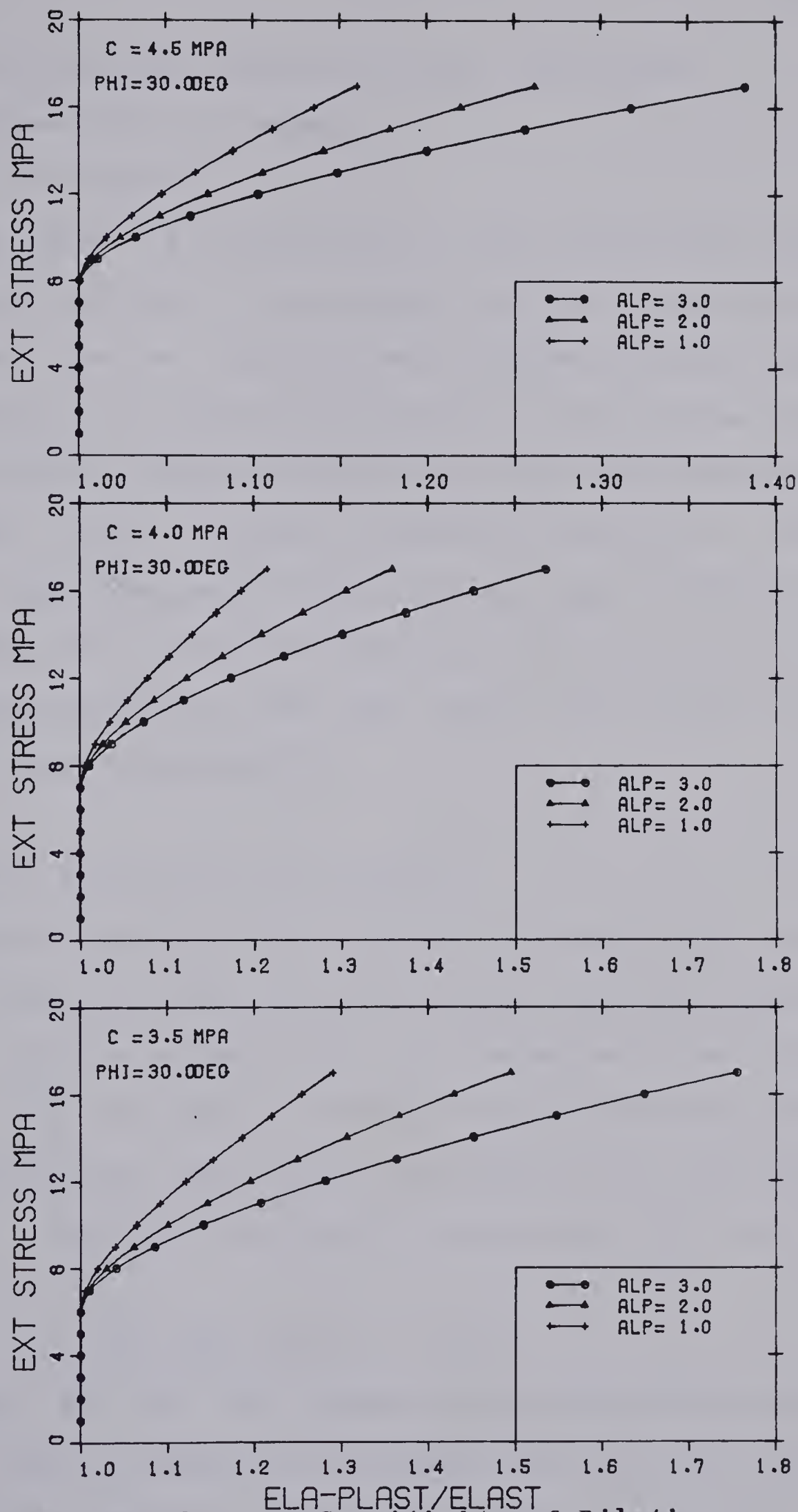


Figure 5.4 Normalized Closure : Sensitivity of Dilation





where the normalized closure deviates from unity.

### 5.3.3 Other Elasto-Plastic Models

#### 5.3.3.1 Introduction

Two other types of elasto-plastic models have been used to explain the behaviour of an opening: an elastic perfectly brittle model and an elastic-strain-weakening model. The first one leads to a closed form solution of the problem and the latter requires numerical treatment. Only the perfectly brittle model will be used to derive a solution for the model test case. Published results on the strain-weakening material indicate a particular shape for the closure curve, which is characteristic for this model (see curve 4 on Figure 5.5A, after Egger(1973)).

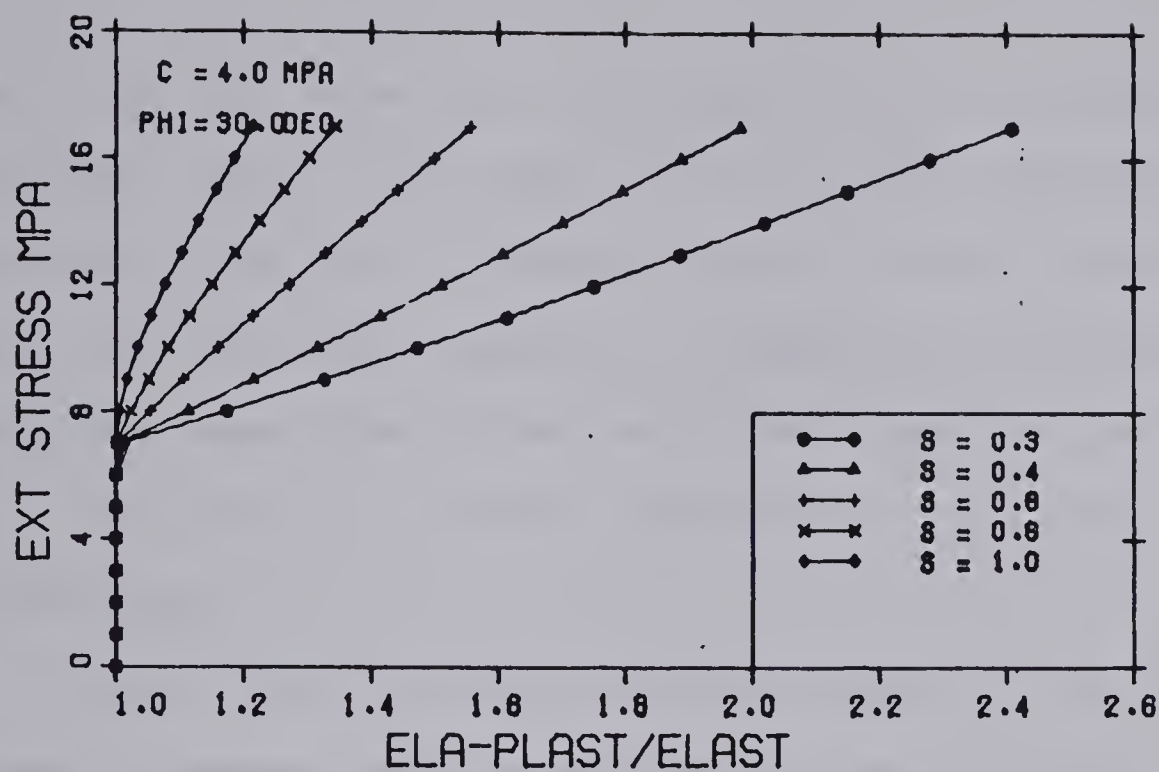
#### 5.3.3.2 Elastic Brittle Plastic Material

This model has been used to derive expressions for the normalized closure in the case of the model test and typical results are shown on figure 5.5A. The derivation, presented in Appendix A2 (Section 4), does not differ significantly from the previous one. The failure criterion is the same but the plastic criterion relating the stresses in the plastic zone is :

$$\sigma_t = m\sigma_r + s\sigma_c \dots 0 < s < 1$$

where  $\sigma_t$  and  $\sigma_r$  are the maximum and minimum principal stresses,  $m$  the coefficient of passive earth pressure,  $\sigma_c$  the unconfined compressive strength and  $s$  a parameter to evaluate the strength drop after brittle failure. If  $s$  is





## NORMALIZED CLOSURE VS STRESS

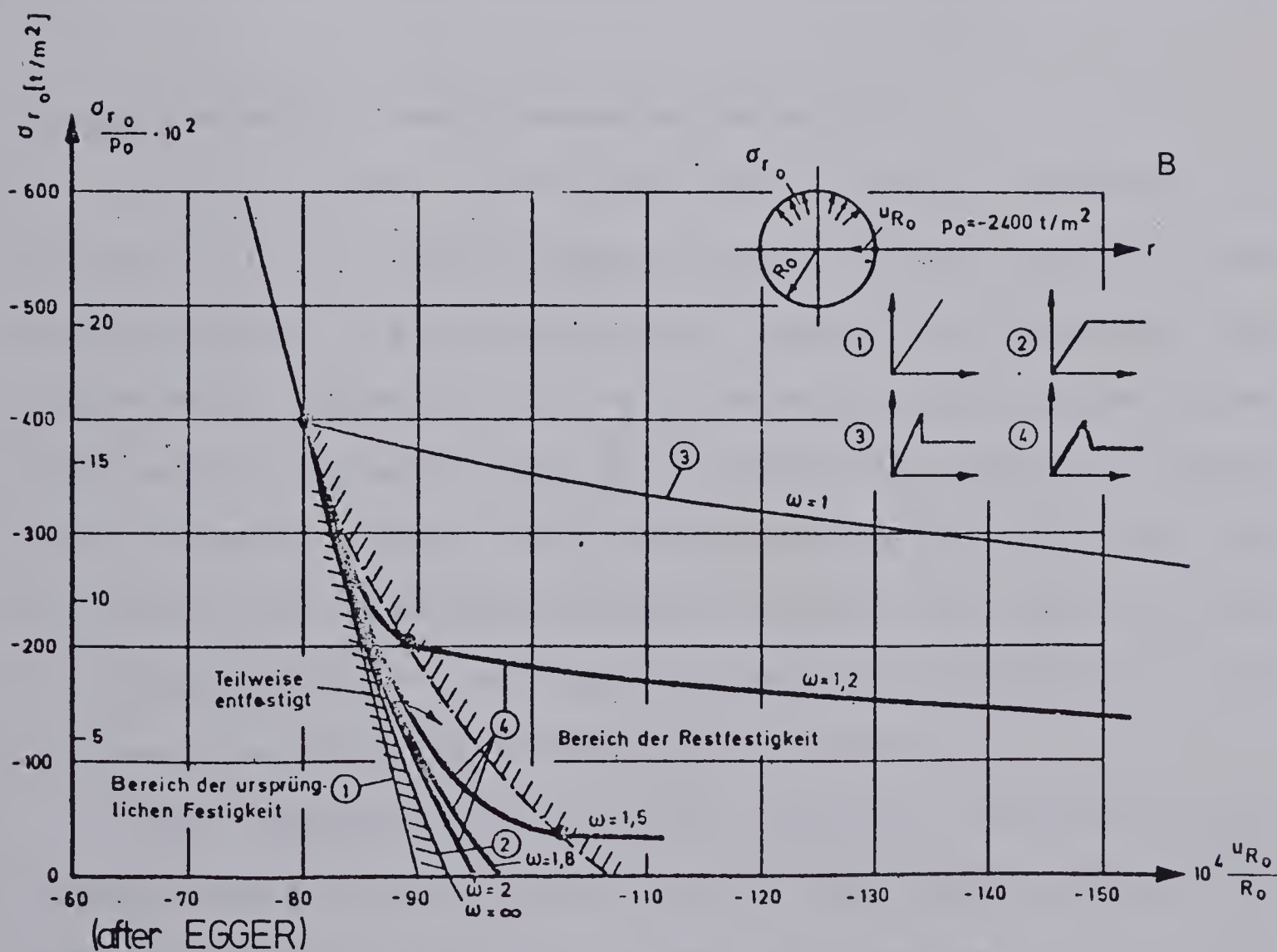


Figure 5.5 A : Normalized Closure : Elastic Perfectly Brittle Material

B : Theoretical Ground Reaction Curves for Different Materials (after Egger(1973))



equal to 1, this is equivalent to a perfectly plastic material. If  $s$  is equal to 0, the material is purely frictional in its ultimate state. In the latter case the stability of the opening is impossible without a support pressure, and the tunnel collapses immediately. This model has been used to study rockbursts in deep tunnels by Panet(1976) .

Figure 5.5A shows a discontinuity in the slope of the stress closure curve immediately after yielding. This slope after yielding decreases with decreasing ultimate strength towards zero where the ultimate state is purely frictional.

#### 5.3.3.3 Elastic-Strain Weakening Materials

Figure 5.5B indicates the results obtained by Egger(1973) in using different elasto-plastic models. They are presented as ground reaction curves resulting from the progressive unloading of a rock mass. The closure curves obtained in the model test by progressively loading a tunnel have a similar shape. The elastic response is different, but as far as the normalized closure is valid, the results shown in figure 5.5B may be used as a qualitative description of the response of a strain-weakening material.

Four material models are presented in Figure 5.5B, characterized by the sketch in the upper right corner. The strain-weakening material has a response intermediate between the perfectly plastic and the perfectly brittle materials. There is no discontinuity in the slope of the





response curve after yielding, but this slope decreases quickly to become equal to the slope of a perfectly brittle material response.

The response of a strain-weakening material, as described here, requires a numerical treatment. However, the closure-stress curves have the characteristic shape described above and this will be recognized if evident on experimental data. If necessary, a numerical analysis could then be carried out.

#### 5.3.4 Factors Influencing Data Interpretation

##### 5.3.4.1 Influence of the Longitudinal Stress

Throughout the derivation it has been assumed that the longitudinal principal stress is the intermediate principal stress and that the Coulomb failure criterion holds in terms of the tangential and radial stresses. It is reasonable to assume, as did Florence and Schwer(1978), that at a certain distance from the tunnel the longitudinal principal stress becomes equal to the radial stress which increases. Further the longitudinal stress will become the minimum principal stress. In the latter case, the failure criterion is to be taken between the tangential and the longitudinal stress. In the intermediate zone where the two smaller stresses are equal the stresses have to satisfy simultaneously both above-mentioned failure criteria. The failure surface changes from the original position, parallel to the longitudinal axis.





The analysis of this problem is reported in Appendix A3.2. It shows that a value of Poisson's ratio higher than 0.15 is required to avoid a change in failure surface, at the upper limit of the loading range of the machine. The value of Poisson's ratio measured in the longitudinal direction and based on the assumptions of isotropic material properties is about 0.1 (measured as a ratio of the applied loads).

The problem will be more significant if a support pressure is applied on the tunnel wall. As there is no experimental evidence of a change in failure direction, this effect has been neglected in the present study.

#### 5.3.4.2 Influence of the Boundaries

The sample block used in the previous analysis was assumed to be infinitely large with respect to the size of the opening. However its size is finite and the ratio of the width of the sample to the tunnel diameter is 4.80 and 4.0 for the tests MC-3 and MC-4, respectively. Theoretically the analysis should be corrected by assuming that the external stress is multiplied by a coefficient:

$$\sigma_q = \sigma_q \times b^2 / (b^2 - a^2)$$

where  $\sigma_q$  is the external stress,  $a$  the radius of the opening, and  $b$  the distance from the center of the tunnel to the boundary of the sample.

However, this only means an increase in the true external stress of 6.7% and 4.5% for the test MC-4 and MC-3,



respectively. This error is not significant and is neglected.

#### 5.3.4.3 Plane Strain Condition

The expressions for the normalized closure have been established by use of an elastic relationship valid only for plane strain conditions. The experimental data would differ from the theory if this plane strain condition was violated. As explained in chapter 3, the loading head is rigid and controlled by four independent rams which allow control of the displacements in the longitudinal direction (Heuer and Hendron (1969)). It can be shown that the minor longitudinal displacements occurring during the test cause an insignificant error. This is partly due to the low value of Poisson's ratio.

It is important that the operator maintain plane strain conditions within reasonable limits during the whole test.

### 5.4 Experimental Results

From the experimental measurements of the tunnel closure in four directions inclined at  $45^0$  to each other, the normalized closure has been determined for the two different tests and related to the external stress.

#### 5.4.1 Method of Analysis

The sample was loaded in increments to stages where it was allowed to creep for a constant period of time (5 days



for test MC-3, 1 day for test MC-4). In order to get the normalized closure from the experimental stress-strain curves, some assumptions about the time - dependent behaviour of the sample have to be made. The following approach has been adopted as a result of analyses undertaken by Kaiser(1979) on the time-dependent behaviour in the pre-failure zone.

#### 5.4.1.1 Theoretical Model Response at a Constant Loading Rate

The modulus of elasticity of rock is time-dependent and varies between two extreme limits: the upper limit corresponds to instantaneous loading (short-term stiffness), whereas the lower limit corresponds to infinitely slow loading (long-term stiffness). If a rock sample is loaded at a finite rate to a given stress level and left under a constant load, it will creep until the accumulated strain reaches the value which would have been obtained during infinitely slow loading of the sample. This is achieved theoretically after an infinitely long period of time, but in practice, most of the creep strain occurs within the first day. The amount of creep strain is a function of the rate of loading and of the stress increase during the latter loading (comparable to a visco-elastic material).

Assuming limits for the modulus of elasticity and a value of Poisson's ratio, the corresponding limiting curves for the closure can be determined. This has been done in





Figure 5.6. From the elastic curves, which are assumed to be linear (dashed lines), the corresponding elasto-plastic limits have been obtained by multiplying the elastic closure by the value of the normalized closure at a given stress level. Reasonable elastic and strength parameters, as indicated on Figure 5.6, have been assumed.

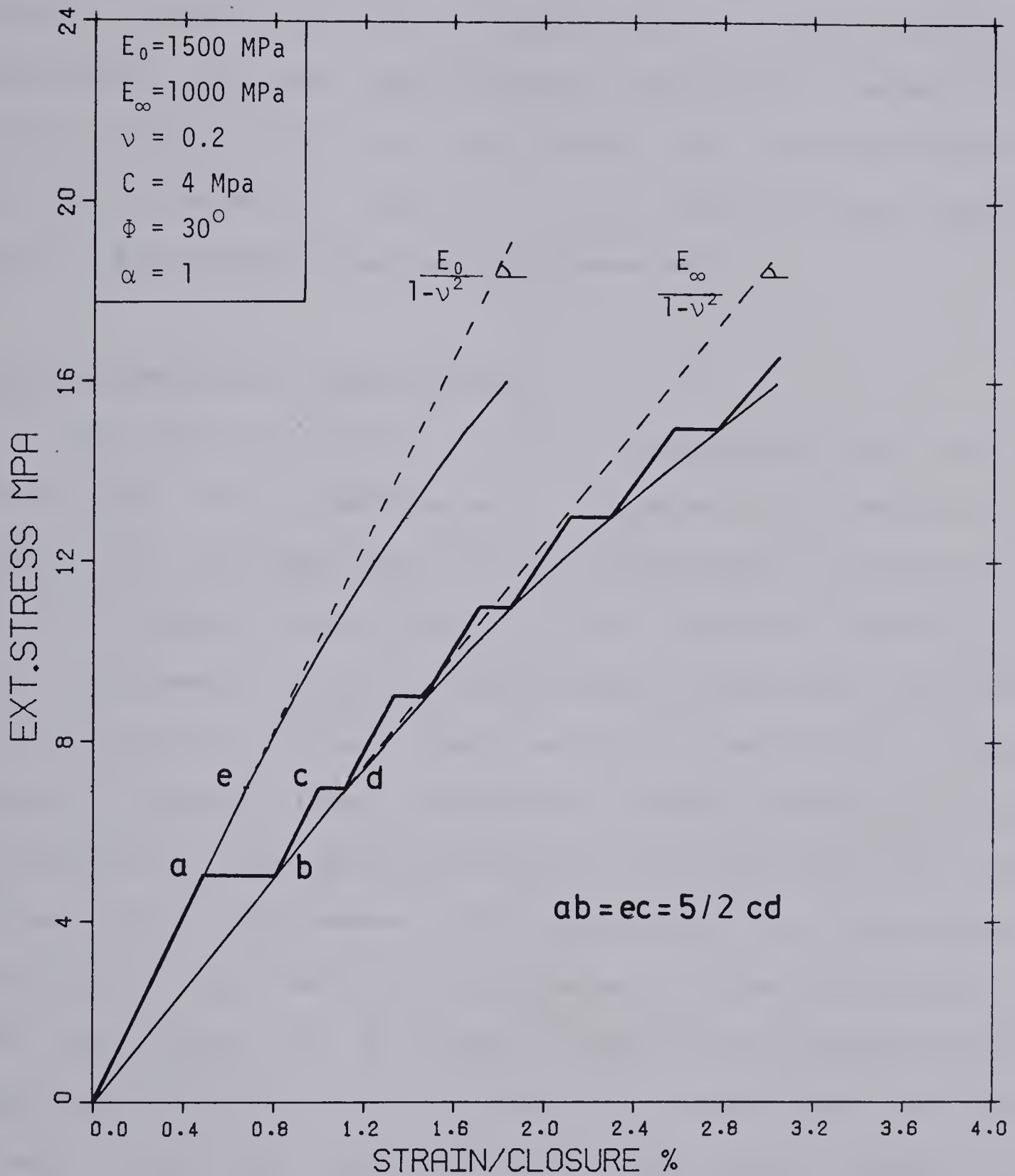
#### 5.4.1.2 Theoretical Model Response to Step Loading

A theoretical closure curve for the stress history of the model test may be plotted within this framework. The sample is loaded up to the first increment along a constant-rate loading curve. In order to simplify the explanations, this rate of loading is assumed to be the instantaneous loading. Then the sample creeps along a horizontal line until it reaches the long-term loading curve. It is reloaded to the next increment following a line parallel to the instantaneous elasto-plastic loading curve and this cycle repeats up to the upper limit of the loading range. It can be further assumed that the material behaves as a linear visco-elastic material and then the amount of the creep deformation at any stage is proportional to the previous stress increment.

#### 5.4.1.3 Application to Experimental Model Test Responses

As a consequence of the above analysis, it is assumed that the curve which is obtained by joining the points corresponding to the ends of the creep tests is the





### TUNNEL CLOSURE VS EXT. STRESS

**Figure 5.6 Theoretical Model Response for an Elasto-Plastic Linear Visco-Elastic Element.**



elasto-plastic long-term loading curve. A straight line drawn through the initial portion of this curve is the linear elastic long-term loading curve. This enables a calculation of the experimental normalized closure (see later Figures 5.7, 5.8 and 5.9). By assuming that the reloading curve is parallel to the instantaneous loading curve, this latter line can be determined.

#### 5.4.2 Experimental Measurements

The original tunnel closure measurements for the two tests have been reproduced in Figures 5.7 and 5.8. The sketch in the upper right corner indicates the orientation of the joints(line portions) and the relative direction of the instrument. From this experimental step-like curve the elasto-plastic (axis line) and the constructed linear elastic (dashed line) long-term loading curves have been determined in the manner explained in the last section. This latter line intersects the abscissa at a strain which corresponds to the strain necessary to close the cracks in the rock mass and to allow some initial seating of the instruments. This crack closure is deducted from the total strain values to calculate the normalized closure, by dividing the reduced value of the elasto-plastic closure by the reduced value of the elastic closure at each stress level (see section 5.3.4).

The second solid line on each plot corresponds to the constructed instantaneous loading curve. Its shape confirms



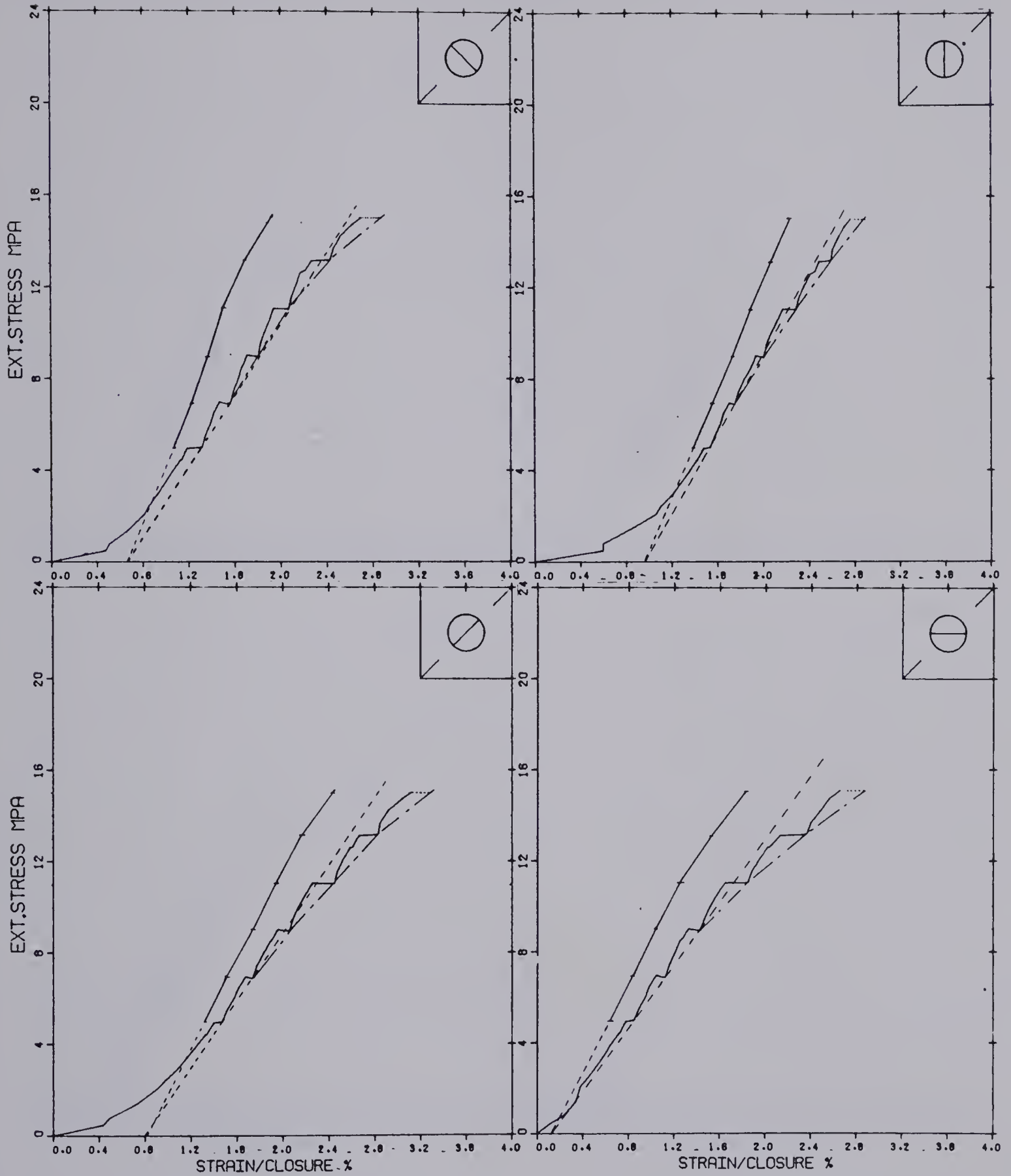


Figure 5.7 Test MC-3 : Experimental Tunnel Closures





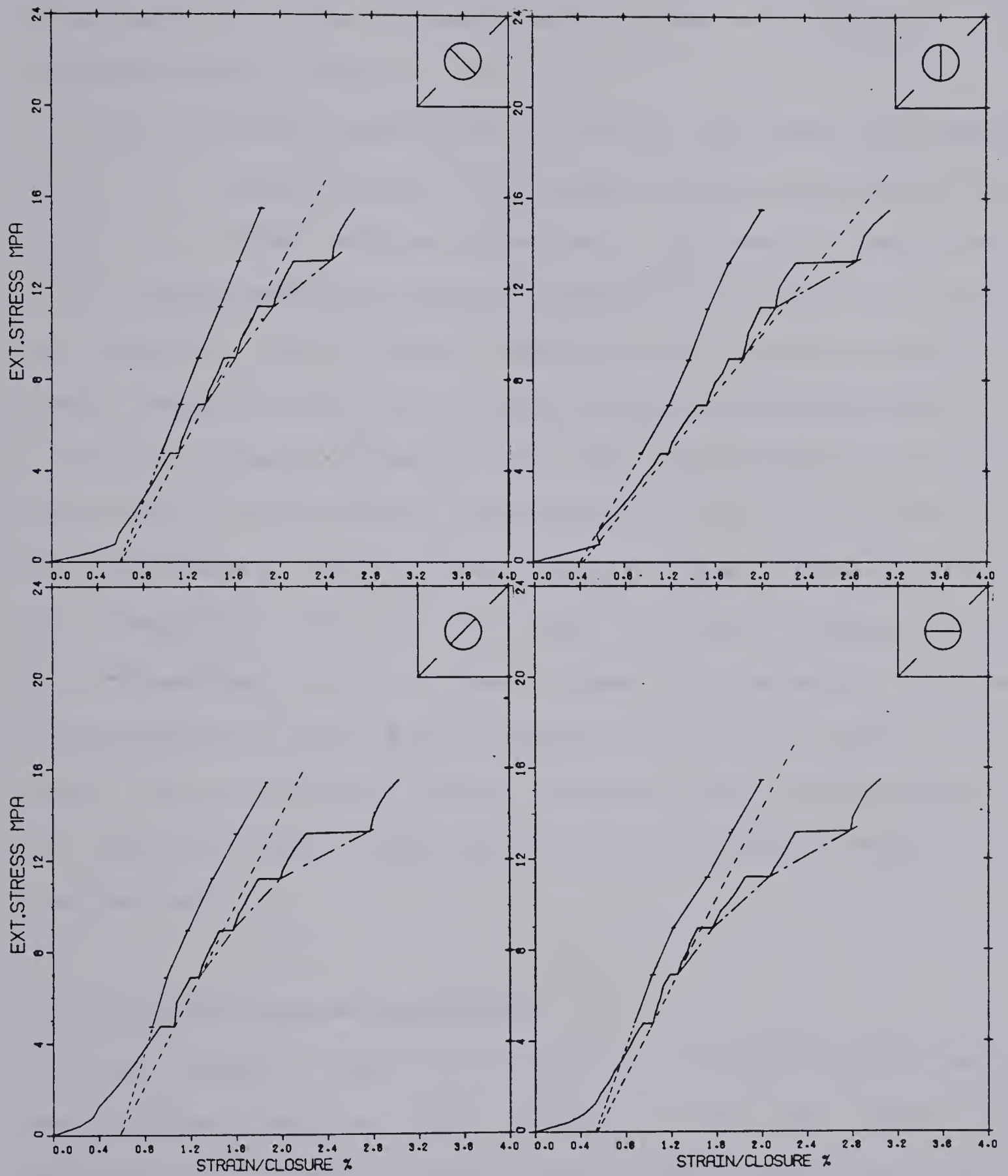


Figure 5.8 Test MC-4 : Experimental Tunnel Closures



the validity of the method of analysis. It has been constructed in the following manner (the references in the brackets refer to figure 5.6).

For a linear visco-elastic material the amount of creep strain is proportional to the latter stress increment. The amount of creep strain occurring in the second creep test (cd) corresponds to a stress increment of 2 MPa. It is used to calculate what should theoretically be the amount of creep strain in the first stage of loading corresponding to a 5 MPa stress increase (ab). The first point (a) of the short-term loading curve is determined. It is not a point of the experimental curve as some creep already occurred before the completion of the first load increment. Assuming that the reloading curve between stages is parallel to the elasto-plastic short-term loading curve (in other words  $ab=ec$ ) the next point (e) of this curve may be determined. The same process is repeated to get the complete short-term loading curve.

#### 5.4.3 Limitations of the Method

The actual shape of the estimated loading curves show some inconsistencies which indicate that the method of analysis is limited by several restrictive assumptions, such as linear elasticity, linear visco-elasticity, and uniformity of loading.



#### 5.4.3.1 Linear Elastic Reference Line

A linear elastic reference line was assumed in order to calculate the normalized closure. However, it is evident from the loading tests on the sample without the tunnel that this assumption is not completely satisfied. The elastic properties of the material tend to change with increasing stress in such a way that the coal becomes less compressible. A linear elastic reference line leads to an overestimation of the elastic closure and an underestimation of the normalized closure. Linearity is not a criterion for elasticity; a straight line could be interpreted as the yielding line of a non-linear stiffening elastic line.

On the other hand, the elastic line is based on the first two creep tests where the material is assumed to behave elastically. If this is true for the first stress stage, this assumption may be questionable for the second creep test at 7 MPa.

#### 5.4.3.2 Time-Dependent Strength

The method supposes that the normalized closure is time-independent and that the strength parameters are constant throughout the test. However, coal has a visco-plastic behaviour (Kaiser and Morgenstern, 1979); the strength parameters and particularly the cohesion intercept  $C$  decrease with time, and as explained in the sensitivity analysis, the normalized closure increases for a given stress level. The experimental normalized closure has been





calculated from long-term loading curves where the strength parameters have their lower but constant values. The analysis of the data should give a lower bound of the strength parameters.

#### 5.4.3.3 Uniformity of Loading

The solution is based on the assumption of isotropic loading conditions. However, if the  $N$ -value is kept sensibly constant during each load stage, it is difficult to reproduce the same  $N$ -value at different load stages and also to get the  $N$ -value exactly equal to unity. This analysis of the data appears to be extremely sensitive to a change in  $N$ -value at different load-stages. The elastic reference line used to calculate the normalized closure is no longer linear as the elastic response is a function of  $N$ . The upper right plot on Figure 5.8 is a good example of this feature. The linear elastic line crosses the "plastic" line which is impossible.

If  $N$  differs from 1, the concept of normalized closure, independent of the elastic constants, is no longer of value. But as the variation of  $N$  from unity is small, values of the normalized closure, corrected for a change in  $N$ -value at different load stages have been calculated. The method is explained in detail in Appendix A3.1. It is assumed again that the first two points of the experimental closure curve are in the elastic range. Their secant moduli result from the multiplication of a function  $A$  of the elastic constants



by a function of  $N$  depending on the relative orientation of the gauge and the maximum applied stress. To close the cracks an original "closure strain"  $\epsilon_{cl}$  is necessary. The secant moduli are calculated by assuming a translation of the origin of value  $\epsilon_{cl}$  as in the conventional method. The knowledge of the  $N$ -value at the first two load stages will permit the calculation of the values of the unknown  $A$  and  $\epsilon_{cl}$  for each curve. Knowing these values and knowing  $N$  at each subsequent stress stage, it is possible to calculate a reference elastic closure for each stress level and then to calculate the normalized closure. The application of this method to the experimental data (lower plot on Figure 5.9 and 5.10) proved to be successful in reducing the scatter of the results.

#### 5.4.4 Interpretation of Experimental Results

Figures 5.9 and 5.10 present the experimental results as dashed lines for the tests MC-3 and MC-4 respectively. The upper plots correspond to data directly interpreted from Figures 5.7 and 5.8. Only three measurements are given; in each case one of the diameters shows a normalized closure smaller than 1 and is not represented on the figure. The lower plots show the data corrected for a varying  $N$ -value according to the method noted in the previous section. The curves are smoother and the results become more consistent.

The comparison between the experimental data and the results of the theoretical analysis given in section 5.3.2,



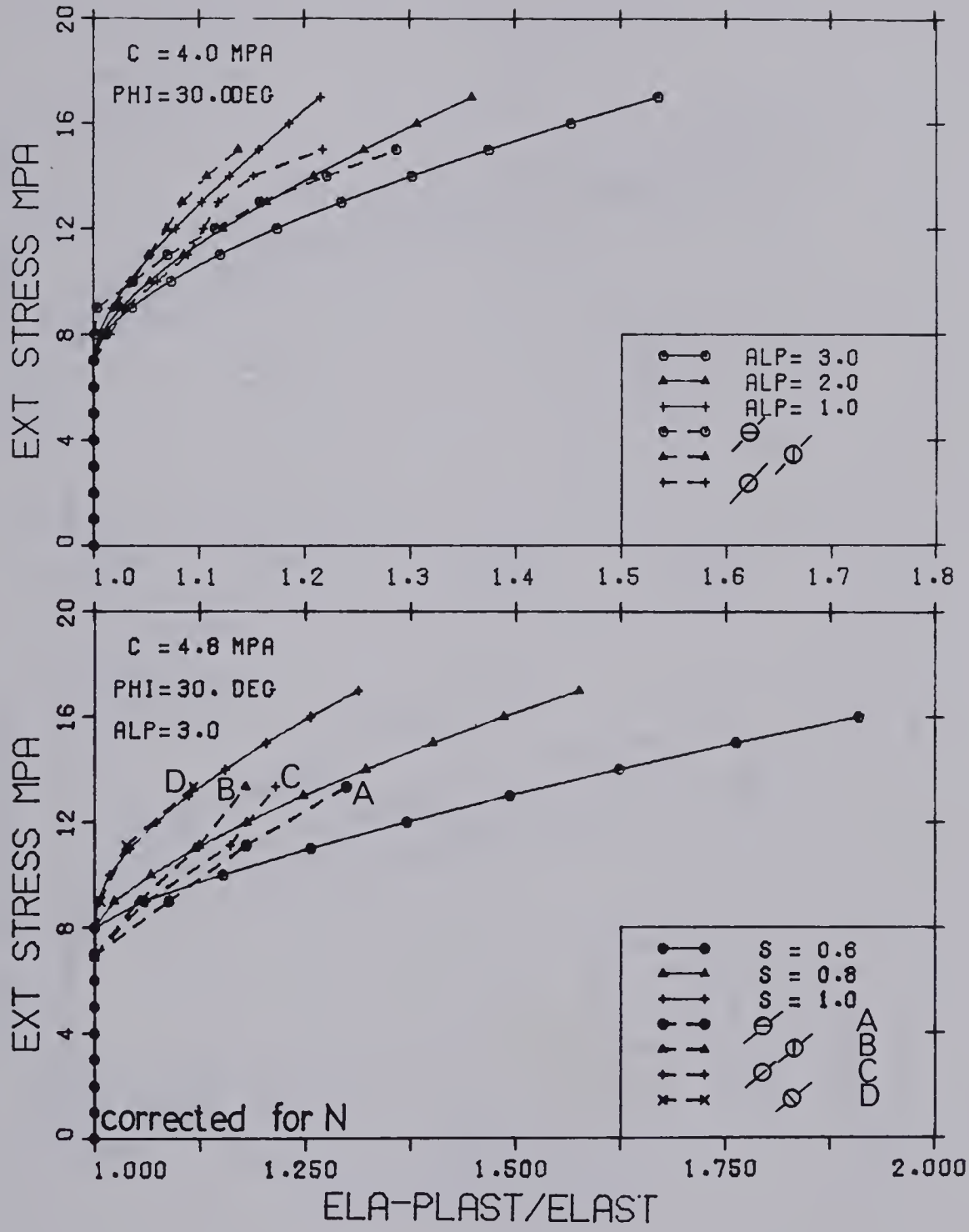


Figure 5.9 Test MC-3 :Experimental Normalized Closure



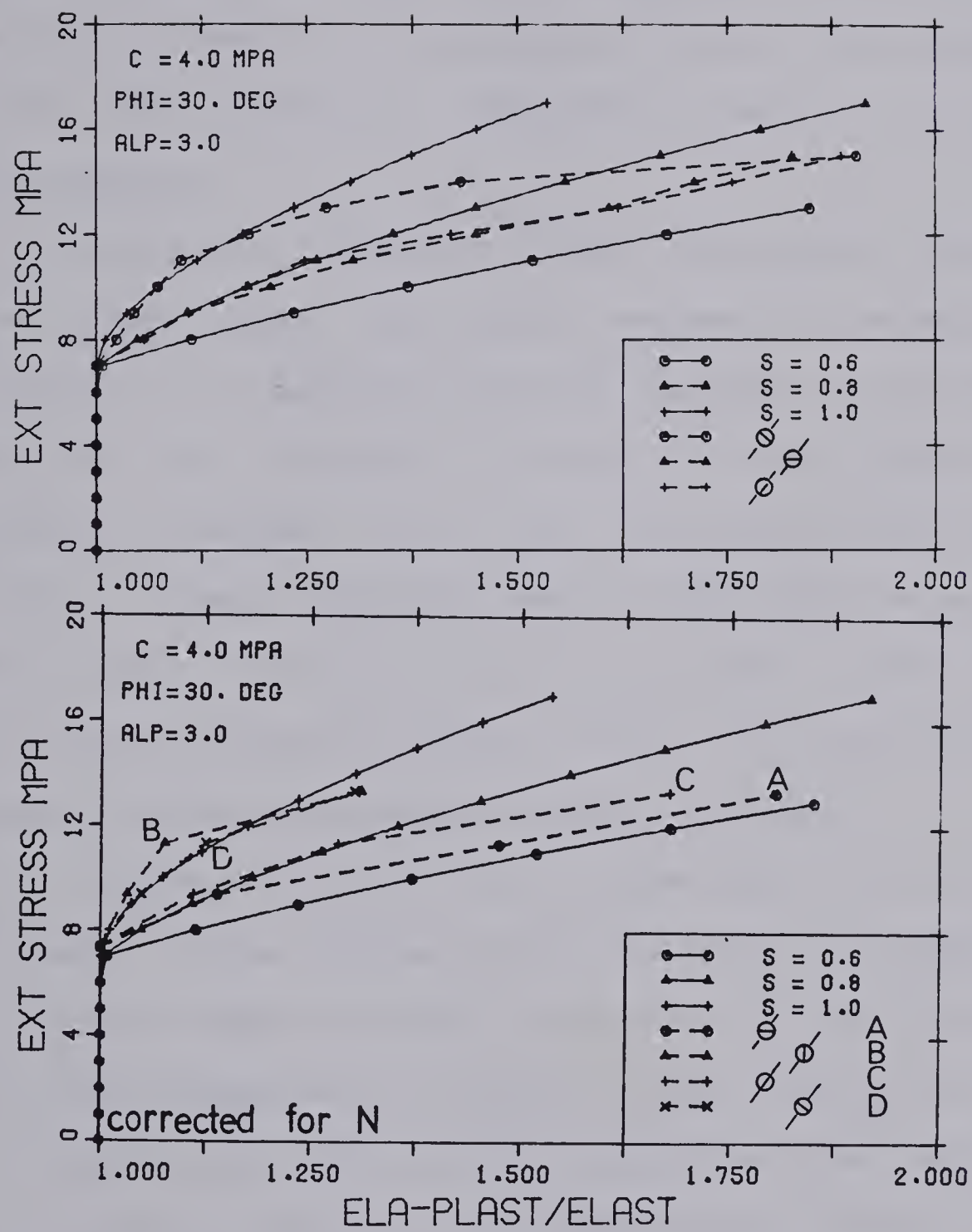


Figure 5.10 Test MC-4 :Experimental Normalized Closure





has been undertaken in the following manner.

1. A computer code permits the visualization on a graphic terminal of theoretical elasto-plastic responses of the model with any set of parameters  $C$ ,  $\emptyset$ ,  $\alpha$ ,  $s$ . The analysis consists of comparing plots of the experimental data with different theoretical curves for changes in parameters.
2. The cohesion intercept  $C$  will vary around 4 MPa, as it has been shown that the response is sensitive to a change in  $C$ . Moreover, as the analysis has to take into account the relative orientation of the joints in the failing element,  $C$  is an appropriate parameter with which to study variation due to structural anisotropy.
3. The angle of friction  $\emptyset$  is kept equal to  $30^\circ$ , which is the value given by triaxial tests, as it does not affect substantially the elasto-plastic response.
4. The dilation parameter  $\alpha$  is taken equal to 1 (no volume change) or to 3 (associated flow rule if  $\emptyset$  equal to  $30^\circ$ ). This is done in order to account for the theory found in the literature, by which one may expect the material to dilate according to the associated flow rule only to a limited portion of the post-failure strains and then to maintain a constant volume. (Ladanyi, 1974)
5. The strength loss parameter  $s$  is given the values 1, 0.8 and 0.6. The three curves then obtained will give an indication of what would be the response of a strain-weakening material with a progressive strength



loss.

This analysis leads to the following conclusions about the elasto-plastic closure of an opening. These conclusions are in accordance with the generally accepted practice in the interpretation of field data. Right after the onset of yielding the material dilates according to the associated flow rule. This effect is dominant but tends to decrease when yielding proceeds, until the material no longer shows volume change. This reduction in volume change may be explained by some arching after dilation has taken place. This would explain why the curves B and C on Figure 5.9 show a change in curvature and tend to exhibit less closure. At the same time, as the plastic strains increase, the strain-weakening material loses progressively its strength and more deformations occur. The strain-weakening effect become progressively more dominant.

This scheme explains individually every curve on Figures 5.9 and 5.10 and the following conclusions can be drawn :

1. Test MC-4 results (where the tunnel ruptured) are more dominated by the strain-weakening character of the material than test MC-3 results.
2. The D-curves presenting the closure in the direction perpendicular to the joints are much more affected by the strain-weakening effect than the other measurements.
3. The anisotropy in structure and in strength may be argued to explain the different behaviour of the four



gauges in the same test.

4. The strength parameters found to fit the experimental curves are in accordance with our knowledge of the coal. The cohesion intercept may be considered as high with respect to the values obtained in triaxial tests. This can be explained as an effect of the size of the rupturing element which is much smaller in the tunnel wall than in a triaxial test.
5. This size or shape effect which influences also the post-failure behaviour (see Chapter 6 Fig. 6.8) may explain why the test MC-4 with a bigger opening and a larger rupturing element may exhibit a larger strength loss for the same value of the strain than the test MC-3. (See Chapter 6 for more details about the shape effect on the stability )

However, this interpretation does not explain a major inconsistency. In both tests, the diameter C parallel to the joints shows much more closure than the diameter D perpendicular to the joints. The above interpretation indicated an effect of the anisotropy. But if this was true, the cohesion intercept would have to be much lower along the C-diameter (where the joints are perpendicular to the maximum principal stress) than along the D-diameter. According to common knowledge about the anisotropic strength of a jointed mass, this cannot be true. Moreover visual observations on the samples show that in particular on sample MC-4, the tunnel wall was intact in the C-direction





after unloading and the large closure cannot be attributed to yielding only. This serious inconsistency occurs in both tests, showing that some assumptions on which the theory is based are not valid.

Because of the heterogeneous and time-dependent characteristics of the material, it is reasonable to assume that the discrepancy between the data and elasto-plastic theory is due to non-axisymmetrical yielding conditions and to an anisotropic time-dependent stress redistribution. Simplifying assumptions were essential in order to derive closed-form solutions to analyse this problem and only numerical analyses, which are beyond the scope of this thesis, will give a quantitative answer to the problem with this increased complexity.

Kaiser (1979) analysed the results of a similar test and studied in detail the time-dependent pre-failure behaviour. He was able to explain the time-independent and time-dependent behaviour by stress-redistribution due to non-linear creep properties, non-isotropic creep properties or local yielding and argued that an "equivalent opening" approach can be used to describe the observed non linearity of the closure-stress curves. This work, in connection with the conclusions from this chapter, leads to the following interpretation of the failure process in the model test:

1. elastic deformations (more or less isotropic) ,
2. anisotropic stress redistribution (creep),
3. anisotropic stress redistribution (yielding),



#### 4. anisotropic rupture.

Each of the last three phenomena makes the tunnel behave like an elliptical opening. In the cases 2 and 3 the elliptical opening is only apparent while in case 4 the opening actually become elliptical.

In the light of this interpretation a simple analysis of the experimental data was carried out by use of charts given by Feder (1978) for the elastic deformations of an elliptical opening (Figure 5.11). The particular expressions for the closure of the model test are indicated on the Figure 5.11. These charts provide only the closure of the cavity in the direction of the axes of the ellipse and the experimental measurements are not necessarily along the axes of the "apparent" ellipse. The application of these charts shows that the curves C and A on Figure 5.9 and 5.10 may be interpreted as the elastic closure of an elliptical cavity along its small axis, while an isotropic elasto-plastic analysis interprets them as substantially influenced by a plastic behaviour. The curves B, and in particular D, correspond to the minor deformations along the long axis of a similar elliptical cavity, under uniform loading conditions ( $N=1$ ). They are influenced by yielding effects.

It appears then that the deviation from linearity of the tunnel closure measurement curves are not essentially due to the yielding of the material but may be due to other effects associated with the anisotropic character of the material. As shown above, the interpretation of closure data



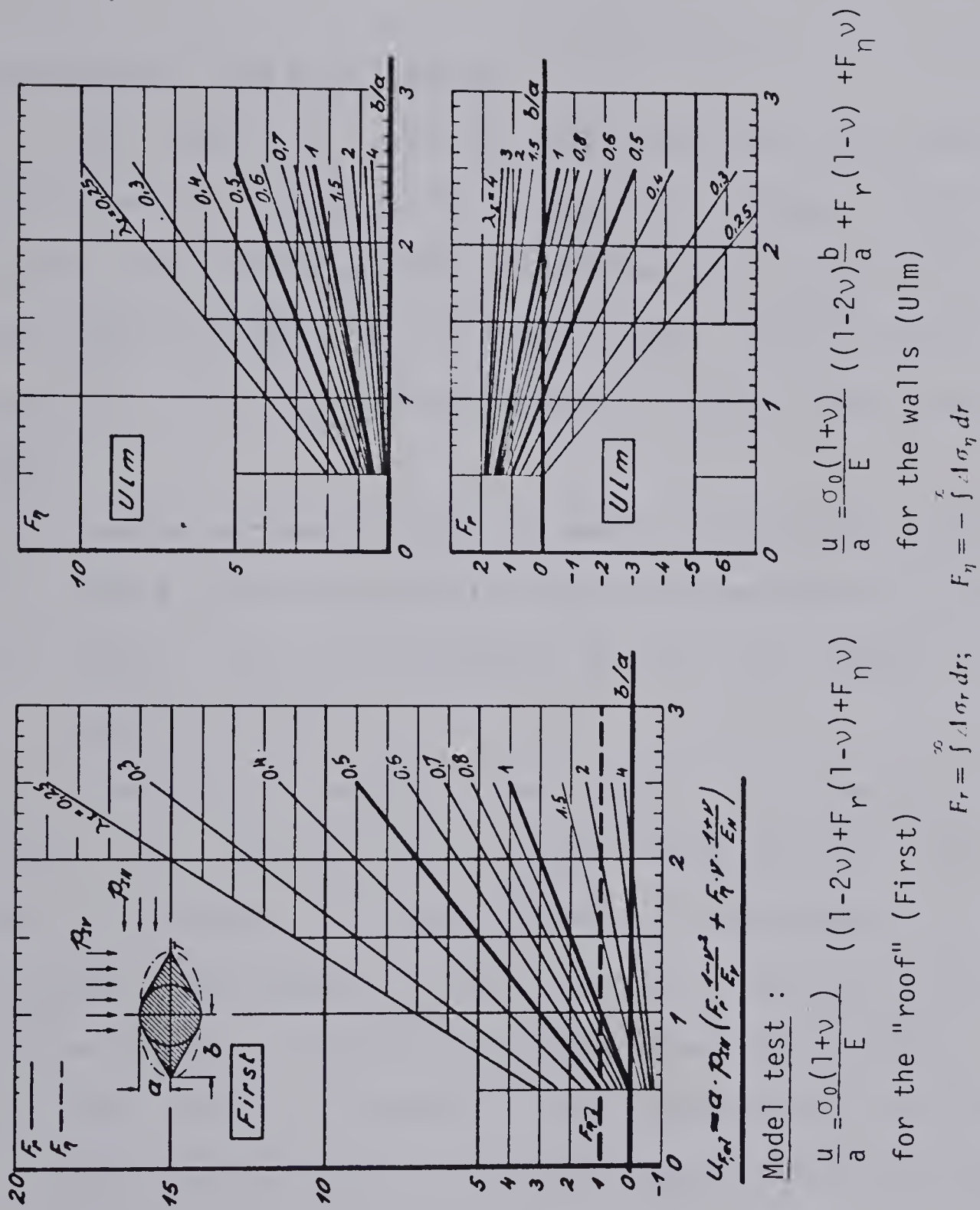


Figure 5.11 Elastic Deformations of an Elliptical Cavity  
(after Feder(1978))





by mean of elasto-plastic methods is apparently possible but may lead to incorrect conclusions.

### 5.5 Summary and Conclusions

In order to explain the non-linear behaviour in the experimental closure-stress curves, several elasto-plastic models have been adapted to derive the theoretical value of the tunnel closure in the model tests. These models are used commonly in the interpretation of field measurements. They are:

1. elastic perfectly plastic model (closed-form solution)
2. elastic brittle-plastic model (closed-form solution)
3. elastic strain-weakening model (after Egger (1973) and Borsetto (1979)).

For isotropic loading, the concept of normalized closure (ratio of elasto-plastic over purely elastic closure) has been introduced and the analysis of the sensitivity of the strength parameters  $C$  and  $\phi$  and the dilation coefficient  $\alpha$  on the closure, leads to the following conclusions :

1. The closure increases when decreasing the cohesion  $C$ , when decreasing the friction angle  $\phi$  and when increasing the dilation parameter  $\alpha$ .
2. The yield stress where the closure-stress curve deviates from linearity is proportional to the cohesion  $C$  but is not particularly affected by the other parameters.
3. The use of the perfectly brittle model causes the curve to present a discontinuity in the slope right after the





onset of yielding.

4. A strain-weakening model shows an intermediate response between a perfectly plastic model and a perfectly brittle model and may be recognized in this manner.
5. The influence of several factors such as plane strain conditions, isotropic loading, and sample boundaries has been recognized and their effect has been either neglected or taken into account in the analysis.

The interpretation of the experimental data after this theoretical elasto-plastic analysis leads to the following conclusions:

1. The closure of a tunnel seems to be dominated by two superposed effects : right after failure by a volume change following the associated flow rule and whose importance decreases with increasing plastic strains and by a strain-weakening post-failure behaviour which is sensitive after some plastic strains occur.
2. The influence of the strain-weakening is more sensible in test MC-4 where the diameter of the opening is larger. This may be explained by the size effect of the rupturing element on the strength and on the post-failure behaviour of this element.
3. In the light of this interpretation each individual normalized closure curve may be fitted by a theoretical curve with values of the parameters  $C$  and  $\theta$  in agreement with our knowledge of the coal ( $30^\circ$  for the friction angle and values varying around 4MPa for the cohesion



intercept).

4. However the group of four measurements in the tunnel cannot be consistently interpreted in such a manner, and the discrepancy is too important to be attributed to some error in the experimental procedures or in the data analysis. In particular the measurements of the closure along the diameters parallel to the joints show a major deviation from linearity as visual observations indicate an intact material. Even if it appears so, the closure of the tunnel cannot be completely explained by an isotropic elasto-plastic analysis.
5. The original assumptions of an isotropic, time-independent material were suspected to be not valid and contribute to the discrepancy between theoretical and experimental closures. These assumptions are, however, essential for the derivation of closed-formed solutions and if they are not valid the solutions require a numerical analysis which has to be developed for this purpose.
6. In connection with the conclusions of this chapter, Kaiser (1979) showed that an "equivalent opening approach" can be used to describe the observed non-linearity in the stress-closure curves. A brief analysis conducted on the experimental data in the light of this hypothesis show reasonable agreement between the data and the closure of an apparent or real elliptical cavity.



The most important conclusion of this chapter is that even if an isotropic elasto-plastic analysis predicts well the deformations of a tunnel, it may lead to incorrect conclusions about the failure process. An anticipation of a global yielding around the cavity leads to an incorrect design of the support if the failure is local and anisotropic. The importance of the different anisotropic stress redistribution processes has to be analysed and evaluated in future work.





## CHAPTER 6

### ANALYSIS OF THE RUPTURE PROCESS

#### 6.1 Introduction

##### 6.1.1 Scope of the Chapter

Chapter 5 concludes that the recognition of the failure mechanisms is essential to develop a design criterion for the support of a tunnel. The advantage of model tests performed on real material over a case history study or a test on artificial material is that it allows us to instrument, control and observe the failure mechanism of an opening, in a real material, under known stress conditions. However the laws of similitude are particularly difficult in the inelastic range of the material, and as explained in Chapter 3, they have to be carefully investigated before the conclusions obtained on the model could be applied to real cavities .

In this chapter, the tunnel failures observed during the tests are described. In particular, the actual slip lines are described in the context of a plastic equilibrium analysis. An hypothesis on the rupture initiation and propagation is given and the role of preexisting discontinuities is emphasized.

##### 6.1.2 Nomenclature

In accordance with Bieniawski(1967) , the following nomenclature will be used. The material is linear elastic up



to the yield point. As the stresses increase further, irreversible deformations occur. Strength failure is characterized by a loss of resistance to the load ("peak"). Rupture is a failure which corresponds to the separation of the rock element in several pieces. Experiments have shown that the behaviour of a rock sample between strength failure and rupture may be controlled, if the loading frame is stiff enough. In a rock mass subjected to differential stress conditions, intact elements surrounding a rupturing element play the role of the loading frame and may control the rupture. Rupture depends on the structure of the rock mass.

## 6.2 Description of the Observed Ruptures

### 6.2.1 Sample MC-3 after Unloading

As noted in the test history (Chapter 4), this test was interrupted when a corner of the sample sheared off. No rupture was apparent on the tunnel wall during the test. The block was taken out of the compression machine. Plate 6.1 shows the crack pattern on the bottom face of the sample. The sheared-off corner indicates the direction of the joints as the sample failed along a steplike plane parallel to the joints.

If the stresses are released, a tensile crack pattern develops in the plaster layer covering the sample. The cracks are theoretically perpendicular to the direction of the maximum principal stress. This is due to a difference in plastic behaviour between coal and plaster. Irreversible



plastic strains are created in the plaster by loading, and they cause tensile stresses during unloading as the coal imposes the displacements.

The crack pattern is randomly distributed near the boundaries and is radial around the tunnel. The assumption of a uniform radial stress field is therefore supported. The extent of the cracks is a function of the state of stress reached in underlying coal elements. If stress redistribution occurs during the test, the stress level increases first and decreases subsequently on each element around the tunnel. The plaster layer will "memorize" this stress increase as an irreversible strain. A circular crack pattern will indicate a uniform stress distribution, and an elliptical zone will show a non-uniform stress redistribution, and will give the preferential direction of this redistribution.

A careful observation of the crack pattern presented in Plate 6.1 indicates a vertical preferential direction for stress redistribution. This corresponds to the behaviour recorded by the instruments and described in the last section of Chapter 5. The other major cracks correspond to preexisting faults described in Chapter 2.

The plaster covering the sample and the latex film which prevented the tunnel wall from drying were removed. Some debris remained attached to this membrane, leaving cavities and cracks on the tunnel wall. Some slip lines opened up, indicating that even if the tunnel did not







Plate 6.1 Sample MC-3 after unloading :Overall view of the bottom face and close-up of the zone around the tunnel





rupture, a small plastic zone existed. When compressed locally by finger, the "intact" tunnel wall has a friable appearance, indicating a high level of microfracturing in the neighbourhood of the tunnel wall.

The second picture in Plate 6.1 is a close-up of the tunnel wall and of the jointed material near it. Some joints are open, and in the direction perpendicular to them, tensile cracks propagate through the sample. It is difficult however to differentiate the preexisting cleat system of the coal and cracks due to overstressing. Inside the tunnel, some features presented in Figure 6.1 are recognizable (near axis 4 of the figure).

Figure 6.1 shows a complete sketch of the tunnel wall; a shaded area indicates a cavity; the curved smooth lines are the traces of preexisting faults; in the middle of the sample, there is the trace of a major bedding plane which was noted in the core description. Most of the depressions in the wall, resulting from rock fall, are located near one of the major discontinuities. This confirms the importance of such discontinuities on the stability of a tunnel, particularly with respect to rock fall.

The shearing of the corner is due to a local change in stress conditions after a slight rotation of the sample. The measurements in the vicinity of the tunnel were not affected by this failure.



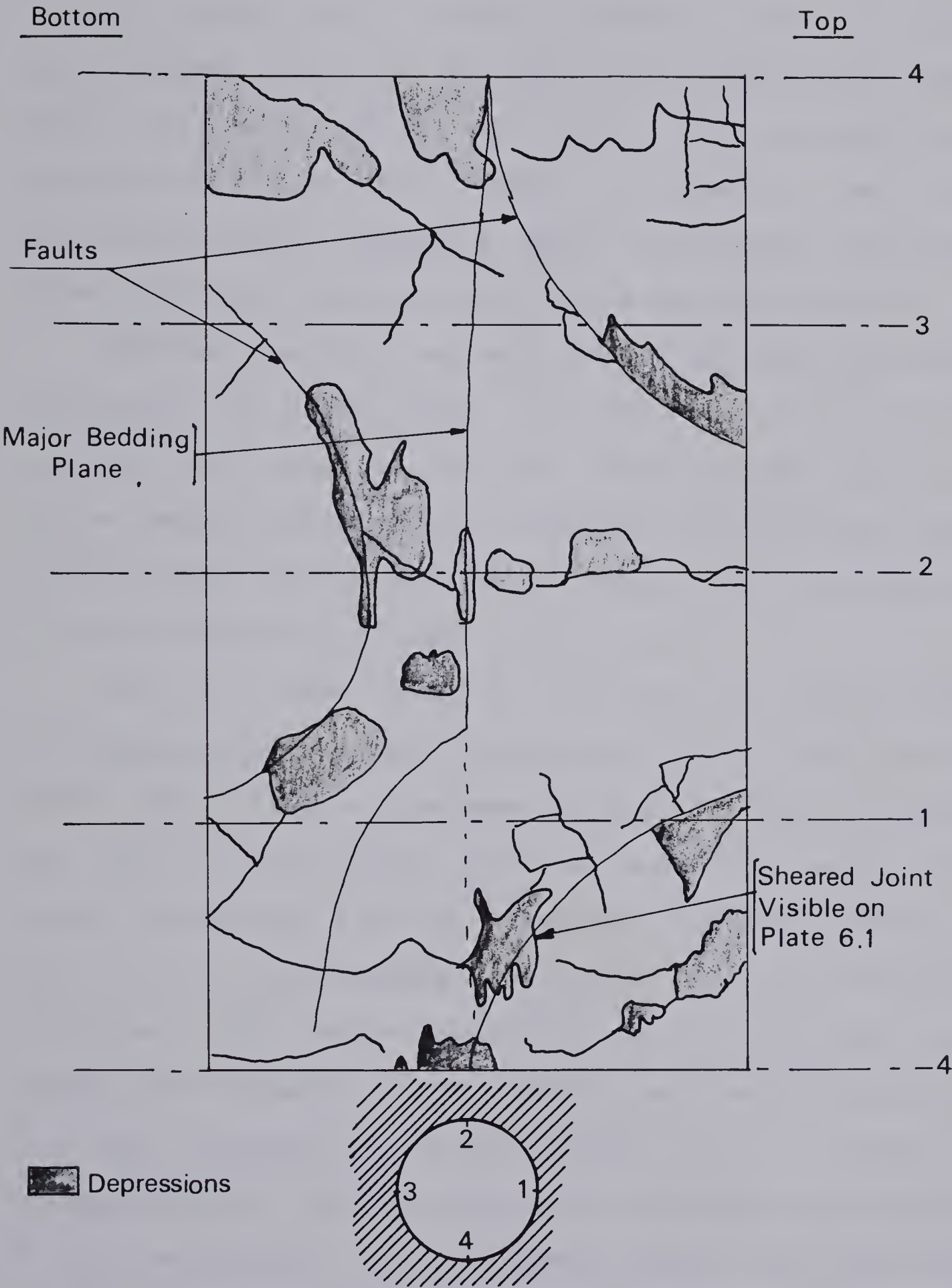


Figure 6.1 Sample MC-3 after Unloading : Map of the Tunnel Wall



## 6.2.2 Description of the Rupture in Sample MC-4

### 6.2.2.1 Rupture History

The sample was loaded in stages as described in the test history (Chapter 4). The rupture initiation occurred about two hours after the sample had been loaded to the increment of 13.3 MPa. Then, as shown on the strain rate-time curves (Appendix B2), the rupture proceeded by waves, until the process stabilized (see next section).

Deformations of the tunnel wall have been observed at mid-height in the tunnel, on both ends of a diameter inclined at about  $40^\circ$  to the vertical axis, close to the points where the joints are tangent to the circular tunnel. A square area (2cm by 2cm) of the tunnel wall is broken with a V-shape, pointing towards the cavity.

After a creep test of 28 hours, the failure became stabilized and the sample was reloaded to the next increment (15.9 MPa). Failure proceeded immediately after loading; it was again characterized by the wave-like aspect of the strain rate-time log-log plots. The ruptures extended not only in the horizontal but also in the longitudinal direction. The debris contained by the latex film was so loose that the points of the LVDT's penetrated into it, and it then occupied a large volume of the cavity. The measurements of the closure in the direction perpendicular to the joints are thereafter questionable, not only because of the crushing of the wall, but also because of the large displacement values, beyond the linear range of the





electronic transducers. After a 24 hour creep test, the sample had to be unloaded because it began to rotate.

After recovery, the sample was uncovered, the debris cleaned out and the measurement device was removed. The sample at this stage is shown on Plate 6.2. On these pictures, several details should be noted :

1. The rupture occurred in a direction between the vertical and a direction inclined at  $45^{\circ}$ . This deviation is most likely due to the error in maintaining isotropic loading at the beginning of the test. The actual value of this angle, measured on the cleaned tunnel, is  $35^{\circ}$  from the vertical direction.
2. The rupture is more apparent on one side of the tunnel; more displacement occurred in this location.
3. The plaster covering the sample followed the displacements of the broken mass and cracked along lines whose shape approaches a logarithmic spiral.
4. The close-up of the failed area shows clearly in the debris broken "bands" of coal. The joints are still parallel, but the whole mass is rotated towards the inside of the cavity.
5. Another remark concerns the crack in the plaster which is, on the picture, the closest to the opening. The edges of the crack are displaced and show evidence of a sliding movement of the underlying rock. This movement is directed towards the bottom of the failed cavity. Feder(1978) proposed a movement in the other direction



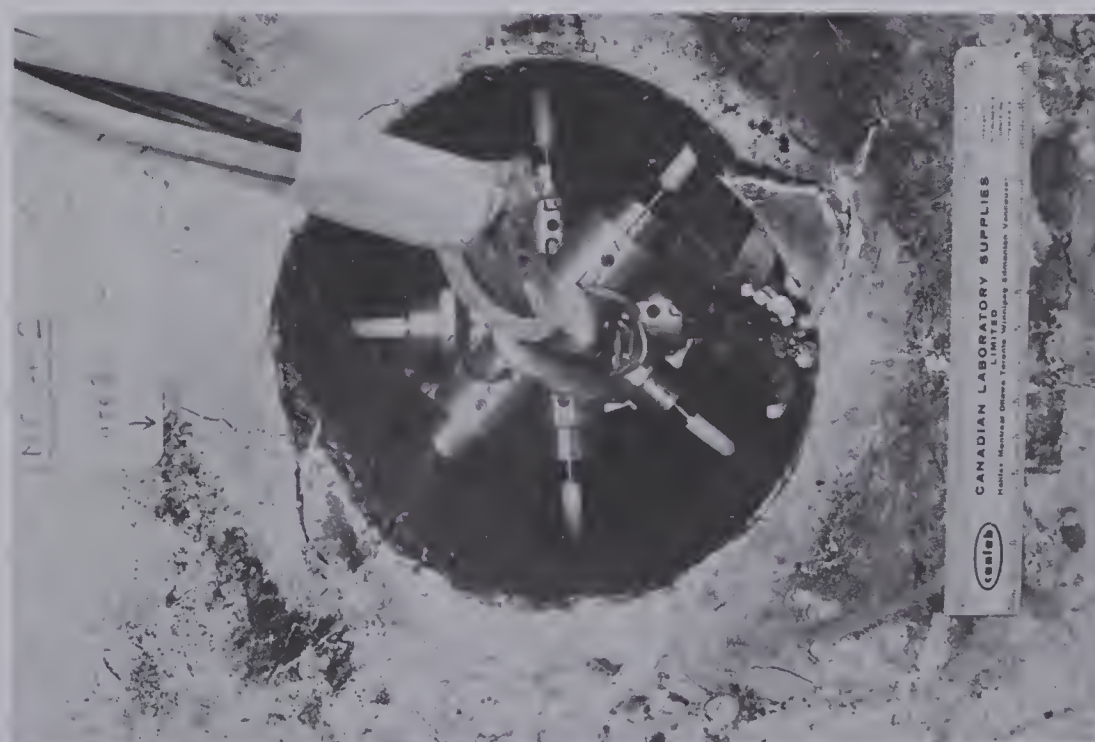
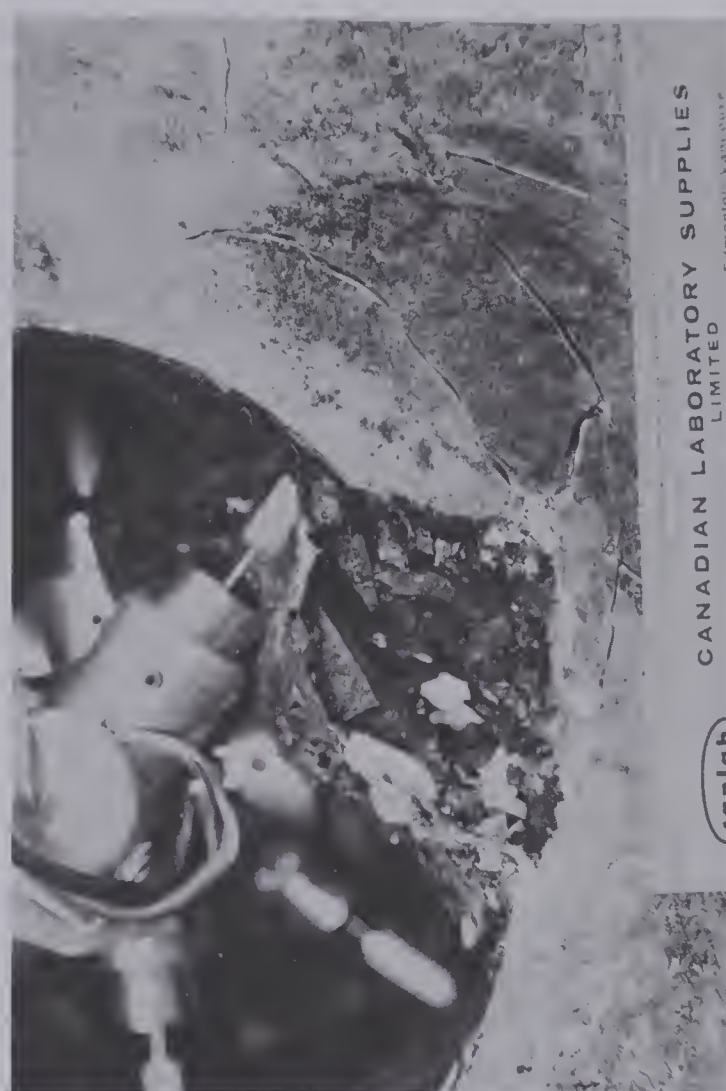
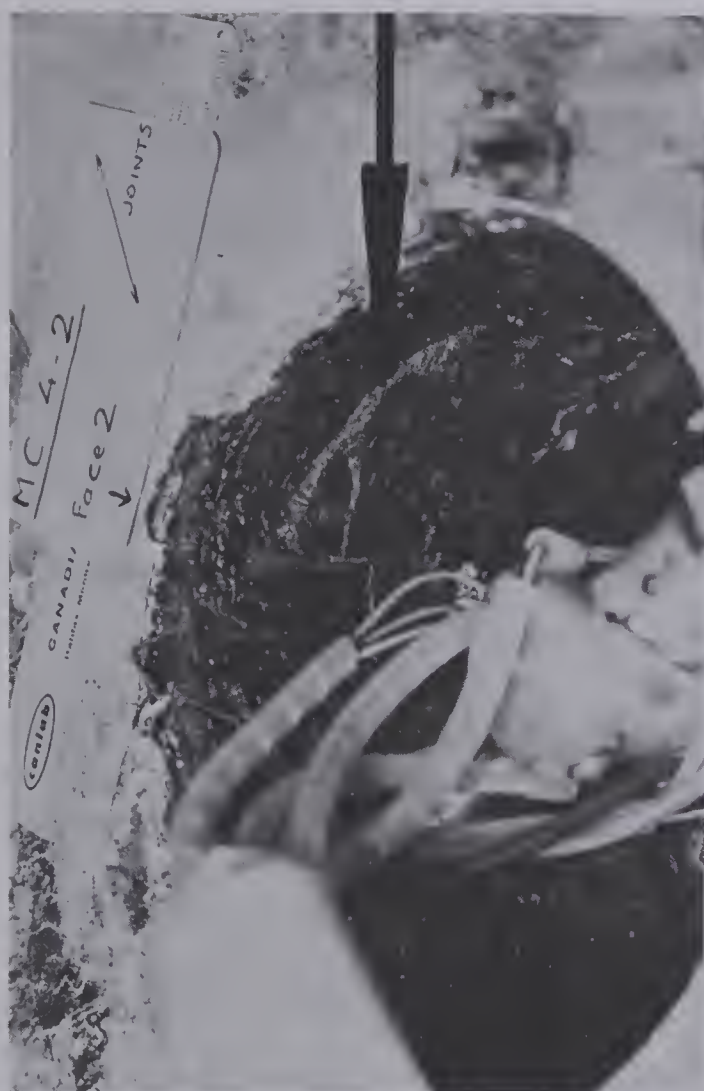


Plate 6.2 Sample MC-4 after the First Rupture : Ruptured Tunnel Wall and Debris





(towards the intact part of the wall) in his analysis of an elliptical failed cavity.

6. Because of this sliding movement, the rupture is not only a splitting phenomenon.

The section of the broken tunnel, presented on Figure 6.2, is more or less elliptical; the ratio between the dimensions of the axes is 1.7. The value of this ratio is in accordance with the estimated value presented in Chapter 5; it is smaller than the calculated ratio for the equivalent opening, but only the material in its ultimate state was removed, leaving a zone of weakened material around the cavity.

The tunnel walls were protected by another latex coating and the sample was loaded by increments of 2 MPa, after an initial increment of 7 MPa. Evidence of failure appeared after loading to 11 MPa; the latex membrane containing the broken material swelled again into the cavity. Loading proceeded by steps up to 16.6 MPa where the rupture process seemed to terminate and the sample was unloaded and left for a recovery test.

The new cross-section of the opening is shown on the Figure 6.2. It seems that the rupture started again from the bottom of the failed zone and created an elliptical cavity propagating radially outward from this point.

Pictures of the sample after the plaster has been removed are shown on Plates 6.3 to 6.5. Plate 6.3 presents the general aspect of the sample after unloading, before and



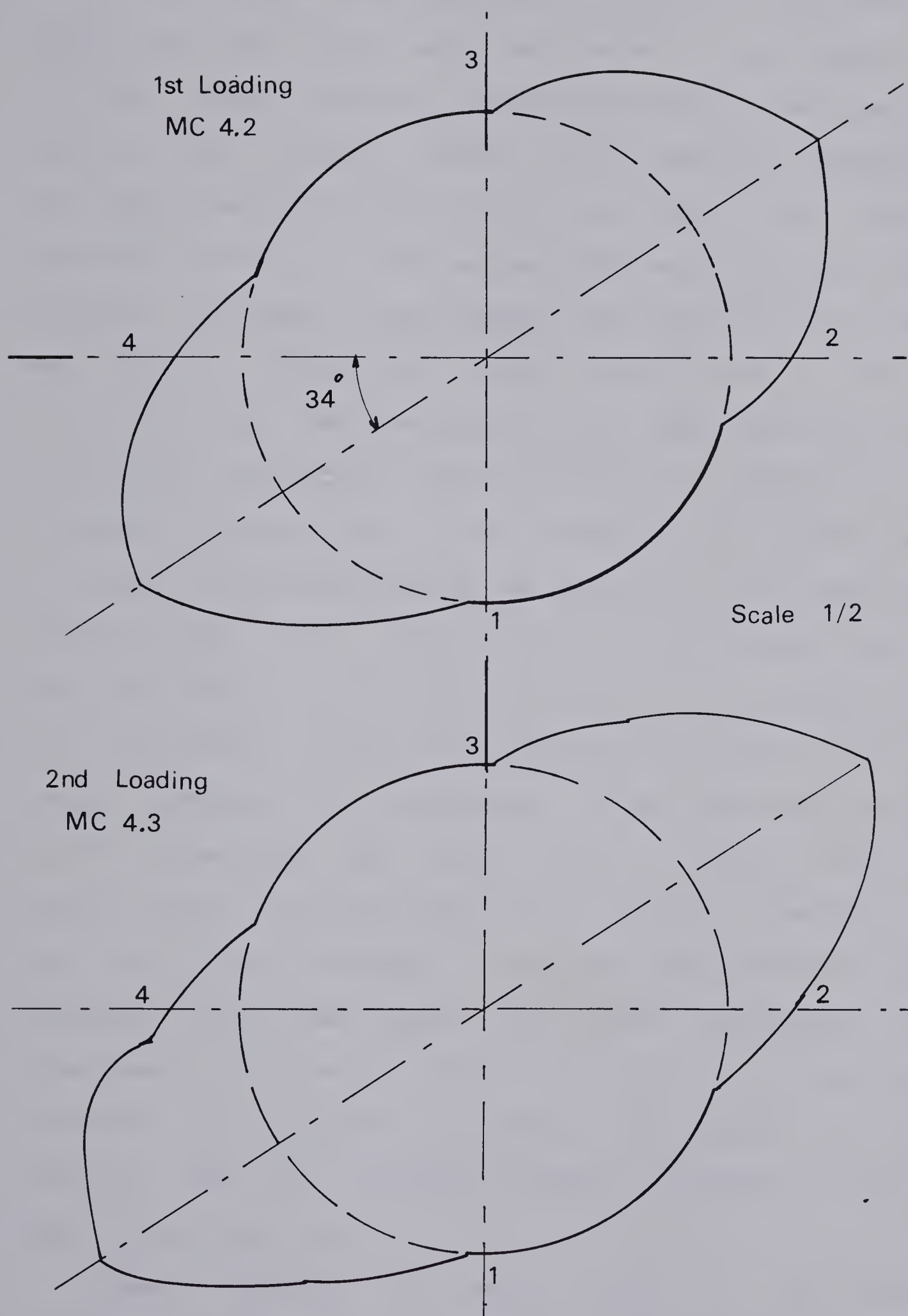


Figure 6.2 Sample MC-4 : Cross-Sections of the Ruptured Tunnel





after the debris was removed. The overall view shows that there are two major sets of cracks, on each side of the ellipse, along joints, proceeding towards the upper left corner. The sample would have finally collapse by "through-stamping" of the cavity roof. Feder(1978) conducted similar tests on artificial material and described such an ultimate collapse of the sample. The internal strain gauges now visible inside the broken tunnel are in the  $45^0$  direction, and the deviation of the major axis of the new elliptical section from this direction is apparent. On both pictures of Plate 6.3, the set of slip lines and the manner in which it is affected by the joints is also apparent(see further Fig. 6.6A). The following explanations refer not only to Plate 6.3 but also to Plate 6.4 and Figure 6.3. A set of tensile cracks approximately parallel to the free tunnel surface can be observed. On one side the debris is highly crushed; on the other side, a whole broken lump remains intact. Actually this block failed by shearing along the slip line, apparent in the remaining material, and by breaking along the other side. This difference in the consistency of debris could be due to a variation in structure and strength throughout the sample. It is also apparent that the rupture is more pronounced on one side than on the other side.

These features are more visible on the close-up presented on Plate 6.4 and on the interpretive sketch of Figure 6.3 :



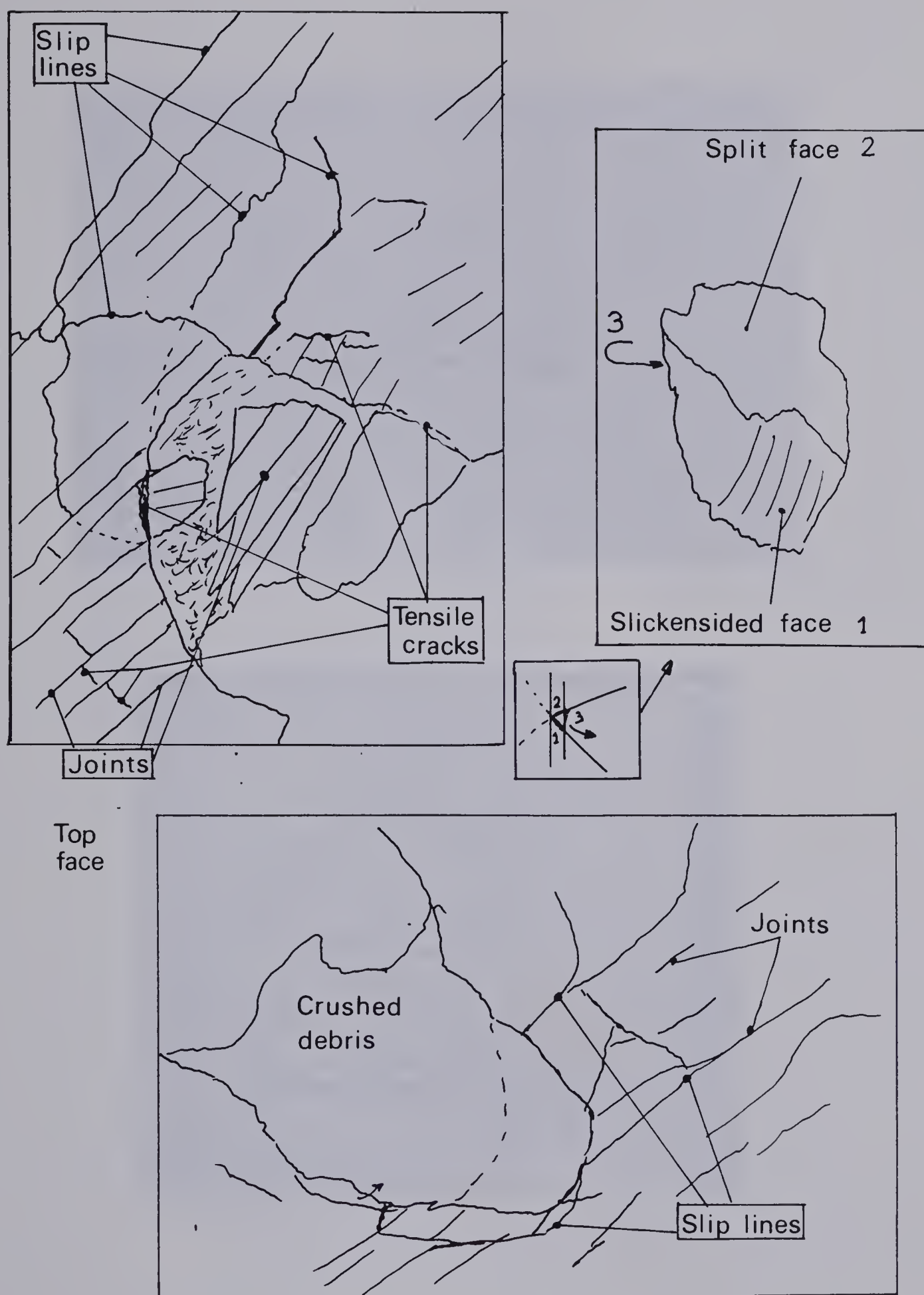


Figure 6.3 Sample MC-4 after Unloading : Interpretive Sketch of Plate 6.4





Plate 6.3 Sample MC-4 after unloading :Overall views of the Sample







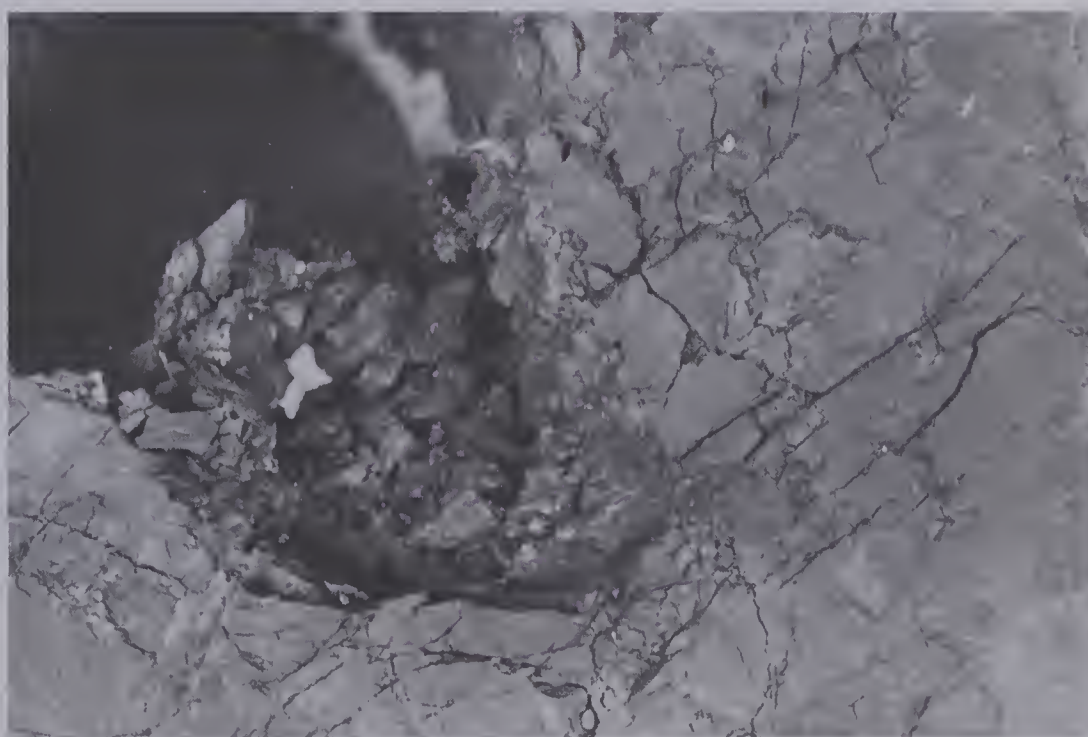
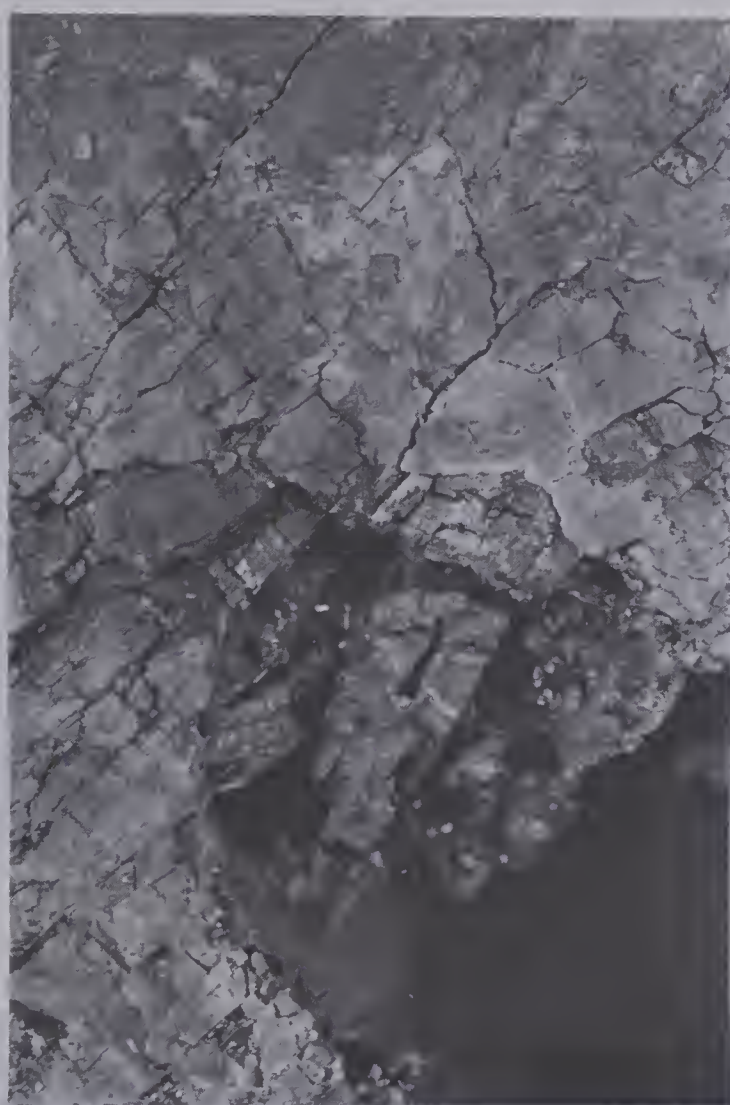


Plate 6.4 Sample MC-4 after unloading :Close-up of the tunnel with debris; characteristic piece of debris collected at the back of the excavation



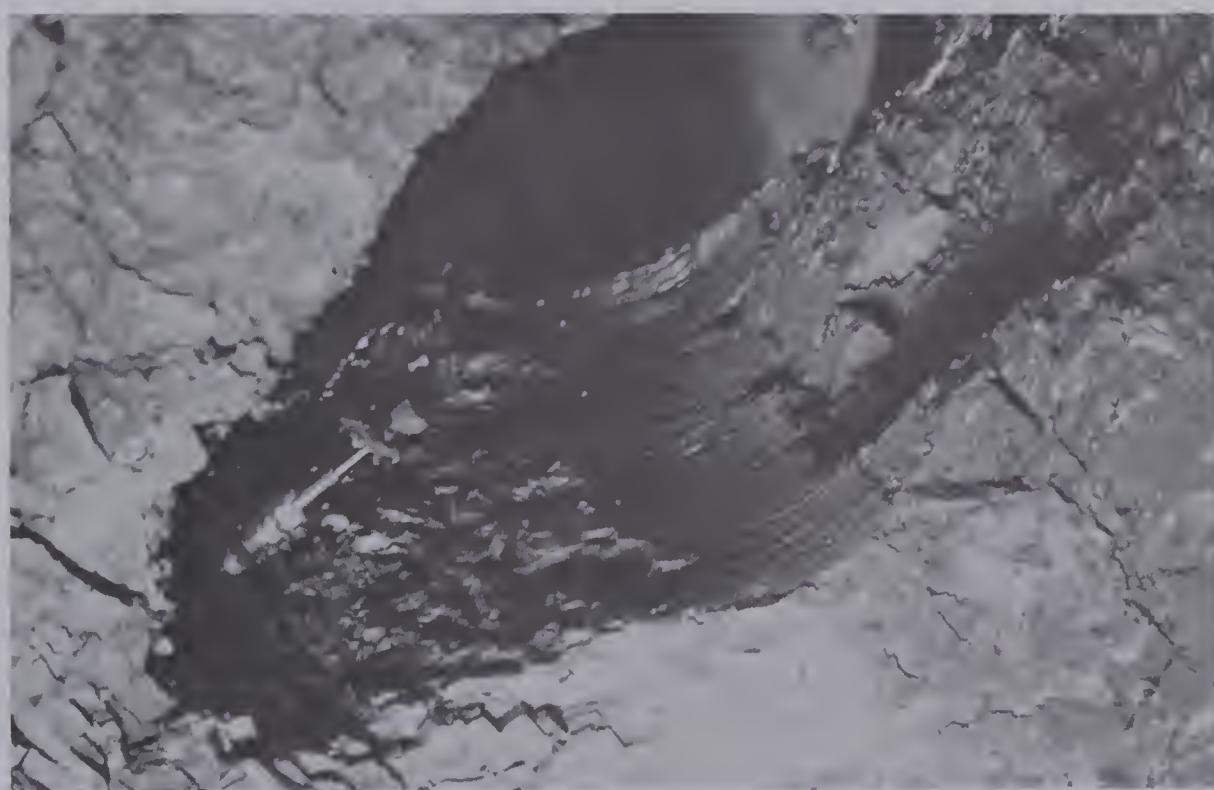


Plate 6.5 Sample MC-4 after unloading :Close-up of the  
tunnel after the debris has been cleaned out.





1. propagation of a logarithmic spiral slip line through the joints.
2. the shortening of these slip lines due to a joint
3. tensile cracks
4. compact failed blocks.

A small piece of debris found at the bottom of the failed opening shows clearly two failure faces: one of them is slickensided and results from a shear whereas the other one is irregular and may result from tensile failure. The third hidden part of this block is a slip line parallel to the joints.

Plate 6.5 shows the tunnel after the debris has been removed. A strain gauge is now visible. The picture shows the wall inside the tunnel, the granular aspect of the broken section, and the intact section in the direction of the joints. A crack developed at the limit of this intact section. It may be due to tension in the "roof" of the elliptical cavity. The material is highly jointed as is apparent on the second picture in Plate 6.5. Near the end of the excavation, the material is more dislocated than near the sides. Slip lines start from the acute end in both directions, sometimes using joints and cross-cleats, or shearing the material. At the bottom of the same picture, a crack crosses the joints. The corresponding block will have failed by splitting of this crack and shear along a joint. A similar mechanism caused the cavity visible on the tunnel wall at the bottom of the first picture.



The preceeding describes only one test. The interpretation of the failure and of the role played by different cracks has to be confirmed by other tests, carried up to this state of fracture prpagation. The following conclusions can be drawn from the observations:

1. A local instability generates the rupture which then propagates in giving to the cavity an elliptical shape.
2. This propagation did not mean collapse in this test, as the opening reached a stable condition at each step after propagation stopped.
3. The preexisting discontinuities, mainly the joints, play an important role in the rupture process, by intercepting and shortening the slip lines (see further Figure 6.5).
4. Each failed lump is separated from the mass along two crossing slip lines; the displacement occurs by sliding on the line subparallel to the joints and splitting on the other line (see Figure 6.3).

#### 6.2.2.2 Description of the Rupture as Recorded by the Instruments

In this section the measurements recorded during the rupture process will be presented. They will only be described and commented on briefly.

The stress-strain curves of the tests MC-4.2 and MC-4.3 up to failure are given in Appendix B1 and described in Chapter 4. The strain-time curves and the strain rate-time curves are presented in Appendix B2 for the last two load





steps of test MC-4.2. Test MC-4.3 has a similar behaviour, and will not be presented in detail here. As explained in Chapter 4 all the experimental results are summarized in an Internal Report of the Department of Civil Engineering.

Appendix B2 contains creep curves for the extensometers and the corresponding strain rate-time curves on a log-log scale for the first and the second loading steps. The tunnel closures and the external displacements as a function of time are also presented for both load steps. In each step the curves are numbered from 9 to 36. Each page of Log strain rate vs. Log time diagrams presents four different curves corresponding to the four curves grouped on a single plot of the creep curves. Numbers and symbols correspond.

In the first load step presented (13.3 MPa) there is evidence of failure on the curves 10, 11, 14, 18 and 19 (page B2.1 of the appendix). The corresponding instruments are all located in one zone near the tunnel where failure seems to occur first. As a reference, this side of the failure, corresponding to the lower right corner on the sketch representing the sample, is the one where failure is of lesser importance in the upper picture on Plate 6.3 (right side of the picture).

Large deformations occur for gauge 14 in extension and 22 in compression (page B2.1). This may be explained by stress redistribution due to rupture of the wall. The response of the curves 18 and 19 is delayed, corresponding to a further propagation of the ruptured zone.



The strain rate-time curves give an accurate picture of the rupture. Unlike the creep curve, they indicate that all the instruments respond to the rupture. Curve 14 (page B2.3) is typical for the rupture process. It shows successive acceleration of strain up to a peak, corresponding to different rupture stages. Instruments 12 and 16 should show the fracture visually observed in this region, but their response is not obvious. The first sign of rupture occurred on curve 10 (page B2.2) by an acceleration in compression about 5 minutes after the time zero of the creep test, and it is followed by the extension of the instrument 14 (page B2.3), 3 minutes after. The other instruments then responded to a variable extent.

The creep curves for the next load step are different (page B2.7). They are characterized by extremely large deformations, and the corresponding scale does not allow the analysis of smaller deformations. The strain rate-time plots are once more useful. Most of the curves present a plateau at the beginning, corresponding to a higher value of the strain rate than in the previous load step. The rapid succession of ruptures cause the wave-like aspect of the plots to be suppressed; only peak values remain. The instruments monitoring the behaviour of the "upper left" side of the tunnel respond now and the measurements correspond to the large deformations visually observed. The curves 13 to 16 (page B2.9) are typical; the instruments 14 and 16 in the failure zone show a constant high value of the



strain rate, and instruments 13 and 15 show a constant decrease in extension rate. If the long axis of the intact elliptical cavity increases regularly, the influence on the elastic closure in the direction of the small axis decreases regularly.

The closures of the tunnel also reflect the rupture (page B2.13). They are, however, difficult to interpret as the fractured material disturbs the readings of the instruments. The external displacements are also affected by the rupture of the tunnel wall. Large strain rates required a change in the strain-axis scale which has to be noted. The discontinuities in strain visible on some curves (page B2.13) result from technical problems generated by the large deformations.

### 6.3 Interpretation of the Rupture Process

The purpose of this section is to explain the rupture mechanism in the model test. More tests are required to confirm the hypotheses presented here, and to apply them to real openings. However, the recognition of some phenomena is relevant as it may help in the interpretation of other rupture cases.

#### 6.3.1 Effect of Preexisting Discontinuities on the Slip Lines

The theory of plastic equilibrium shows that the slip lines around a failing circular opening have the shape of







logarithmic spirals for a Coulomb material. In other words, they make everywhere within the plastic zone, the same angle with the principal directions of stress. This angle is the friction angle of the material (used in the Coulomb failure criterion) with respect to the maximum principal stress direction. Jaeger (1960) was one of the first to explain in detail the anisotropic character of the strength in a jointed rock mass. Patton (1966) presented the concept of multiple mode of shear failure in rock : Depending on the relative orientation of the joints with respect to the direction of principal stress, the rock mass is sheared either along a joint or through the intact material.

The above phenomenon has been observed in the sample. The slip lines shear the material along a joint if the angle of incidence is large enough. Otherwise they follow the encountered joint. A joint constitutes a "shortcut" for a slip line.

A qualitative interpretation of the influence of joints on the slip lines around a tunnel is presented in Figures 6.4 and 6.5. This method was already suggested by Rechsteiner and Lombardi (1974) . On a Mohr circle diagram three different circles are represented, corresponding to the state of stress at three different points along a slip line. As the slip line is within the plastic zone, the circles are tangent to the intact rock failure envelope, corresponding to the failure criterion. Because of the assumed axisymmetrical conditions all the points located in



the rock mass on a circle concentric with the tunnel have the same stress level. Hence each Mohr circle on Figure 6.3 represents the state of stress for every point on one of these concentric circles. The set of three Mohr circles are then available for the study of any slip line around the tunnel.

Circle 1 has a minimum principal stress equal to zero. It represents the state of stress on the tunnel wall. Mohr circles 2 and 3 correspond to particular circles concentric with the tunnel. For the points on a particular logarithmic spiral slip line, the principal directions of stress will rotate with increasing the radial distance of the point. This particular slip line is intercepted by circles 1, 2 and 3 at points A<sub>1</sub>, A<sub>2</sub> and A<sub>3</sub>. Circle 2 will be characterized by the rotation in the principal directions between A<sub>1</sub> and A<sub>2</sub>, circle 3 between A<sub>1</sub> and A<sub>3</sub>. These angles are 20° and 40° for the circles 2 and 3 respectively. The relevance of such an unusual characterization is that it makes the determination of the traces of a discontinuity on the Mohr circle easier.

Four couples of slip lines are chosen arbitrarily for this study; points A, B, C and D are the intersections of these slip lines with the tunnel wall (Figure 6.5). The Mohr diagram is symmetrical with respect to the abscissa axis. From each of the four points a pair of slip lines are then initiated within the rock mass, symmetrical with respect to the radial direction. Along one slip line the shear stress is positive and the failure corresponds to the envelope P in



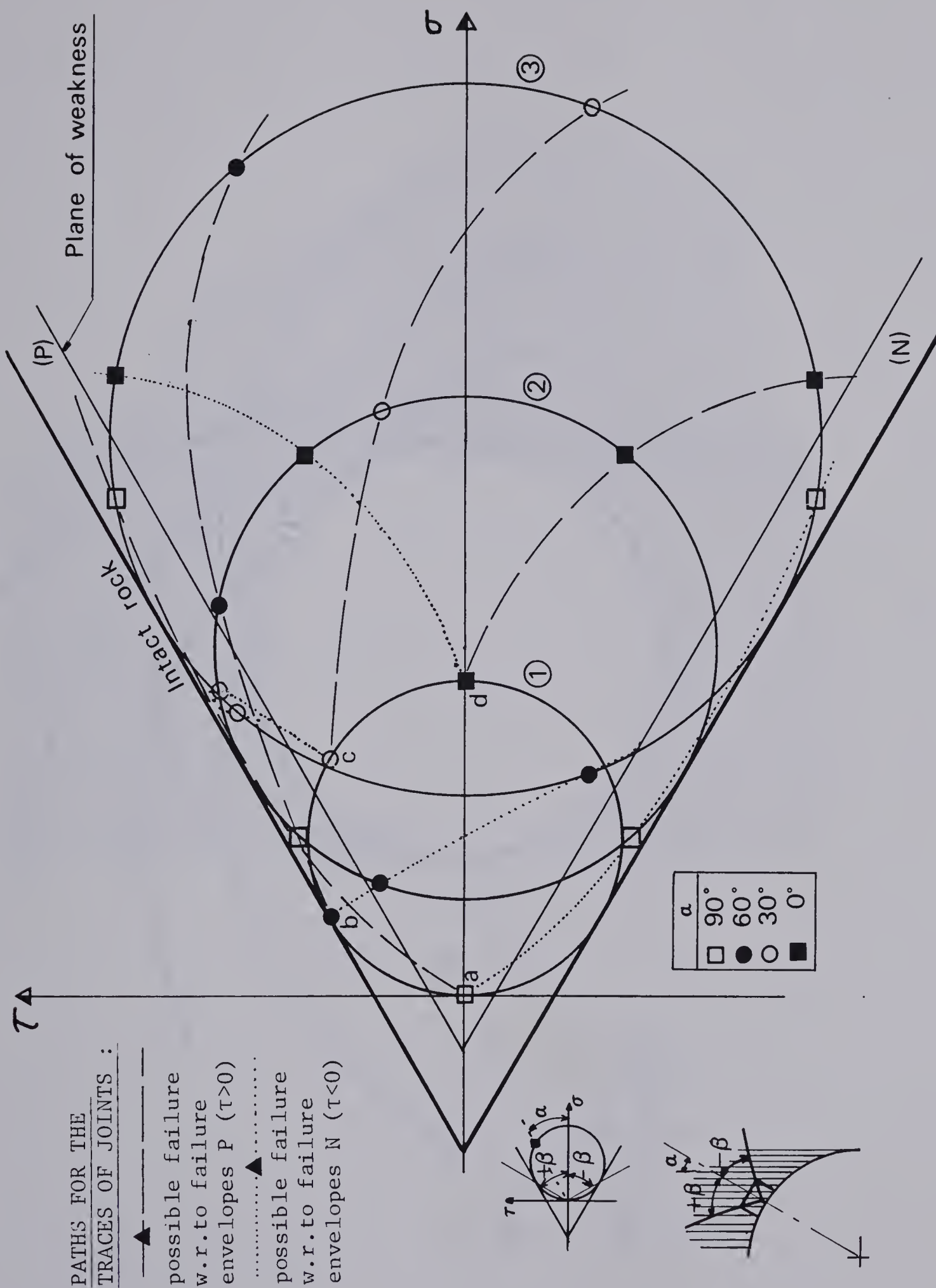


Figure 6.4 Influence of Preexisting Discontinuities on Plastic Slip Lines (1)





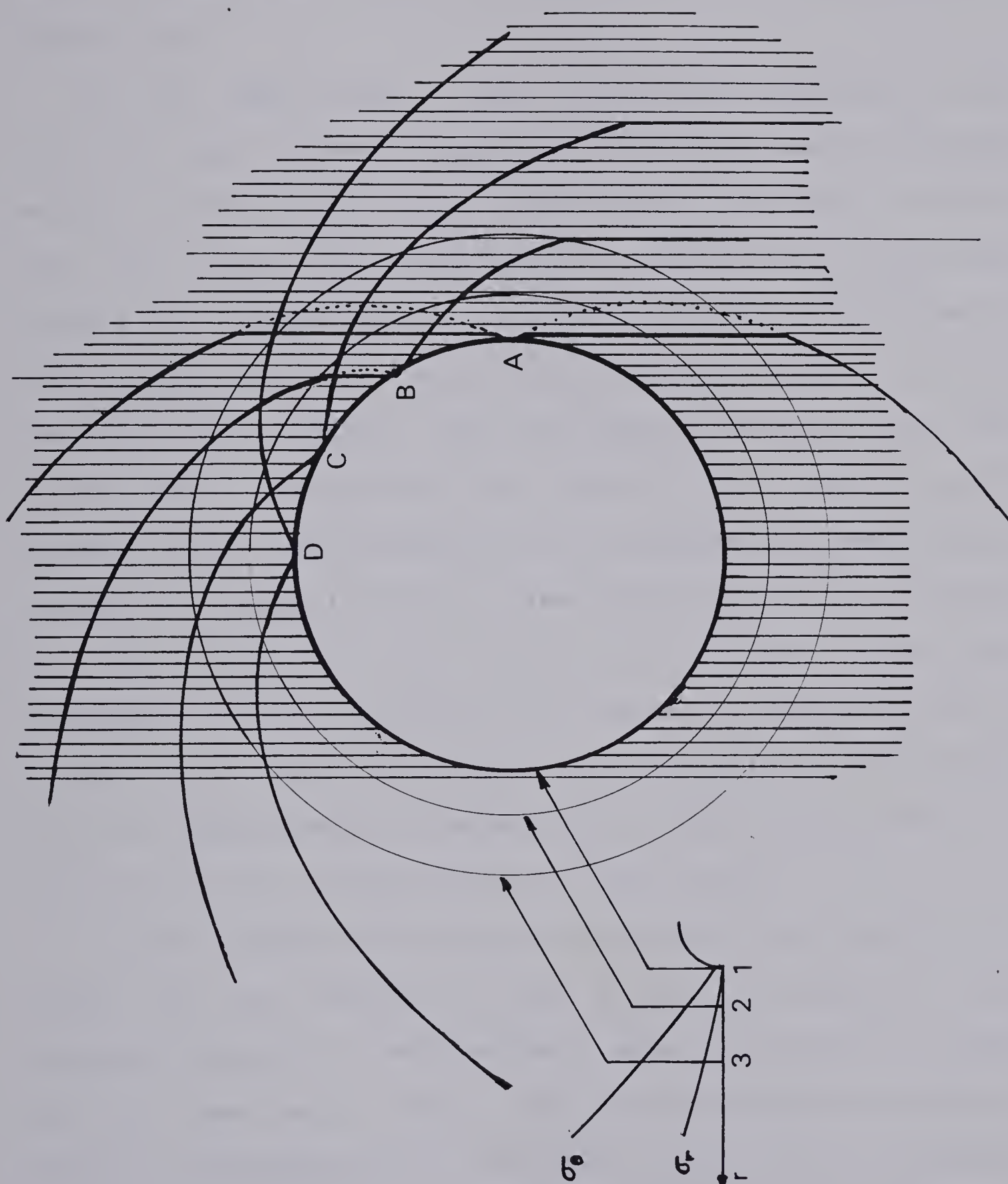


Figure 6.5 Influence of Preexisting Discontinuities on Plastic Slip Lines (2)





Figure 6.4. Along the other slip line the shear stress is negative and the failure corresponds to the envelope N in Figure 6.4.

Up to this point, the anisotropic character of the material has not been considered. A double linear envelope for the failure along a plane of weakness is given in Figure 6.4. The trace of the joints will be plotted in the Mohr circles as indicated on the sketch in the left corner of Figure 6.4. If the trace of the joints is above the joint envelope the material will be sheared along a joint. The joints make respectively an angle of 0, 30, 60 and 90 degrees with the direction of the maximum principal stress (tangential stress). If on a given Mohr circle (i. e. circle 1) the traces of the joints are plotted, they will correspond to the points a, b, c and d as indicated on the circle 1 in Figure 6.4. Actually, the principal directions are rotating giving four superposable Mohr circles which are represented by a unique circle on the figure.

These conventions being established, the traces of the joints on the circles 2 and 3 will be plotted in the following manner. To move along a slip line from the tunnel wall to the point where the state of stress is given by circle 2, corresponds to a rotation of  $\pm 20^\circ$  of the principal directions of stress. The traces of the joints on the circle 2 are given by a rotation of  $\pm 20^\circ$  on this Mohr circle with respect to the former radial position on circle 1. The same procedure is used on circle 3.



Initiated at each point a, b, c and d a double path corresponding to a particular couple of slip lines may be established in such a manner. The dashed lines correspond to a positive rotation along the Mohr circle and to a failure with respect to the envelope P, the dotted lines to a negative rotation and to a failure with respect to the envelope N. If a point of the trajectory is over the joint envelope, the corresponding slip line will shear the rock along the joint. Otherwise, the line will shear across the intact material. Corresponding slip lines initiated on the tunnel wall at A, B, C and D are shown in Figure 6.3.

The anisotropic redistribution of stress resulting from the failure along a joint has not been taken into account. A more sophisticated anisotropic plastic equilibrium analysis will be necessary to explain the complete phenomenon.

The actual slip line net is affected by the non-axisymmetric characteristics of the material. Only lines near A or B will develop. This simple analysis neglects the effect of the other discontinuities like the cross-cleat joints and existing faults which have been proven to affect the mechanism.

The recognition of the influence of the joints is, however, important near point A, as it is one of the reasons for a rupture mechanism to be initiated.

### 6.3.2 Hypotheses for the Rupture Development



#### 6.3.2.1 Introduction

Test MC-3 did not show any rupture but test MC-4 was conducted beyond the rupture of the tunnel wall. The nature and the properties of the material are similar for both tests and the stress history is comparable. It is assumed that the difference in structure between the samples described in the section 2.4 will not interfere with the rupture process. The only difference is a change in the tunnel diameter. It has been shown in section 5.3 ("Influence of the Boundaries") that this diameter change does not induce a significant change in the stress level around the tunnel. A different shape of the viscoelastic stress redistribution could also influence the stresses but it is assumed that it is not significant enough to cause this difference in rupture behaviour. Actually sample MC-3 was finally loaded to the maximum capacity of the compression machine with a high loading rate (this should partly overcome the eventual problem of the influence of the stress redistribution), but the tunnel wall did not rupture. It seems that the rupture mechanism is influenced by the local radius of curvature.

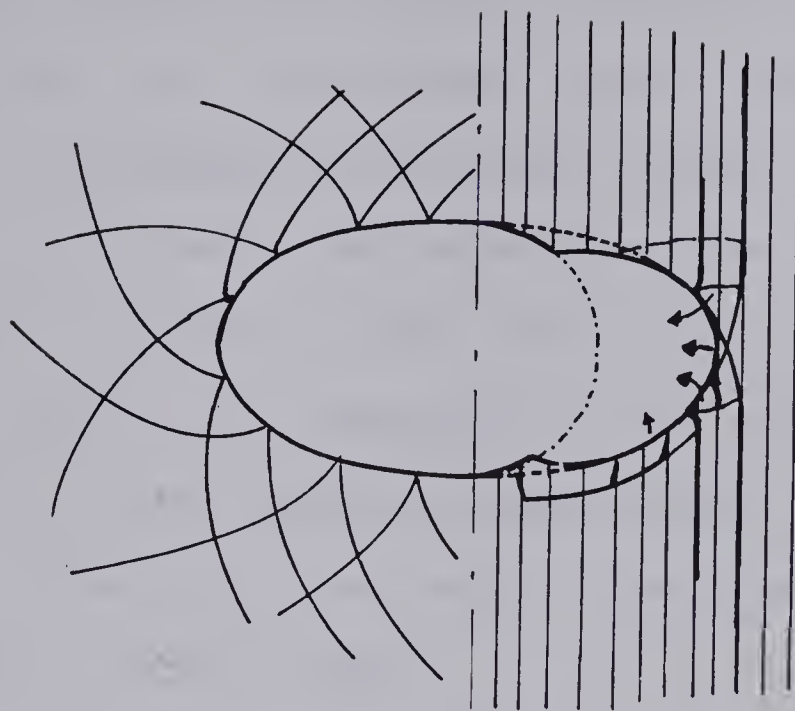
#### 6.3.2.2 Rupture initiation

Three types of rupture initiation may be recognized. They are shown on the Figure 6.6 B and are as follows :

1. Splitting : A column of material is isolated by two slip lines and a joint parallel to the tangent to the tunnel







Possible Shape For a Slip Lines Net

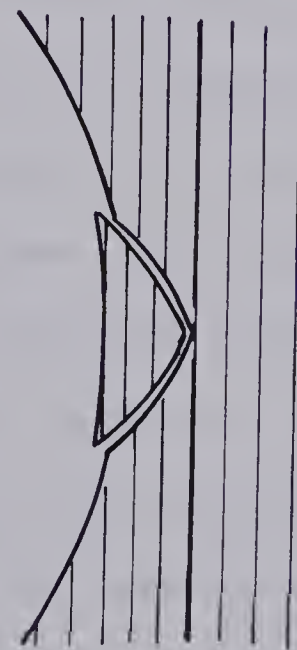
Observed Fractures



Buckling



Sliding



"Cherrystone"

Figure 6.6 A : Possible Slip Lines around an Elliptical Cavity and Observed Fractures.

B : Different Types of Initiation for the Rupture of the Tunnel Wall



surface. It is subjected to compression by the maximum principal stress and fails by buckling. The width of the column and the slenderness ratio are influenced for geometrical reasons by the local radius of curvature.

2. Sliding : A pair of slip lines are initiated at the point A of Figure 6.5. They isolate two symmetrical blocks which are subjected to the same compression as the block in the previous description. The blocks slide on one side and are split along their bases on the second set of slip lines.

3. Kirschkern ("Cherrystone") : This phenomenon is described by Feder (1978). It is the expulsion of a block out of the wall by sliding on both sides.

These effects result from local instabilities. They are three-dimensional and depend on the degrees of freedom in the longitudinal direction. It is difficult to make a distinction between the three mechanisms by visual observations. The arrow-like aspect of the observed rupture may indicate either buckling or sliding. The important fact is that the three mechanisms are dependent on the radius of curvature of the opening. A smaller radius will decrease the area involved in any of the rupture process and cause the "apparent strength" of the tunnel wall to be higher.

#### 6.3.2.3 Rupture Development

A rupture initiation gives a preferential direction for the progression of this phenomenon. The opening takes an



elliptical shape. The stress concentration increases at the ends of the growing long axis of the ellipse, and rupture proceeds by one of the described mechanisms. The blocks tend to slide and rotate towards the long axis of the ellipse.

Figure 6.6A shows on an elliptical cavity a possible slip line net without the influence of discontinuities and, on the other half, the main features observed on the actual opening. As rupture proceeds, new slip lines corresponding to the elliptical opening are generated. The shearing process on the sides of the opening is complex as it involves these new lines as well as the lines generated when the opening was circular. This particularity is illustrated on Figure 6.3.

As the ellipse propagates, and if the stress stays constant, the tunnel would collapse immediately and completely if the strength was constant. However, the rupture process was slower after some hours of creep in test MC-4.2 and stable in test MC-4.3 (reloading of the broken tunnel). In order to achieve that stabilization, the apparent strength must increase. Actually the radius of curvature tends to decrease continuously if the long axis of the elliptical cavity grows. At the same time, and because of this decrease in the radius of curvature, the rupture of the wall becomes more difficult. This could be generalized in saying that the apparent strength of the wall increases.

The rupture mechanism has been recognized to be curvature-dependent and this relates to the stabilization of





the phenomenon. This concept will be visualized in association with the size effect on the strength of a jointed material.

#### 6.4 Shape Effect and the Stability of a Tunnel Wall

##### 6.4.1 Introduction

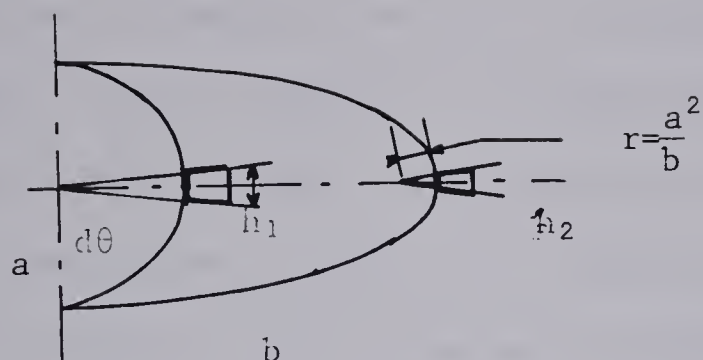
The rupture initiation and propagation have been described in the previous section. The actual physical processes were described. It is of interest to introduce a macro - analysis of this rupture phenomenon. For this purpose the "apparent strength" is introduced as the stress required to initiate a rupture on the intact or already damaged tunnel wall. In this section the change in apparent strength with propagating the rupturing opening, will be discussed in order to study the stabilization of the rupture process.

##### 6.4.2 Shape Effect on the Strength of the Tunnel Wall

The curvature of the opening, or in other words the shape of the element involved in a failure process, has been shown to affect the rupture mechanism. The element of the tunnel wall involved in a rupture will be assumed to be limited by an elementary solid angle  $d\alpha$ , its width being constant as a function of the joint spacing. This is illustrated on the upper sketch in Figure 6.7. If the radius of curvature is larger, the element will be longer. Hudson et al(1972) have shown the influence of the shape of the







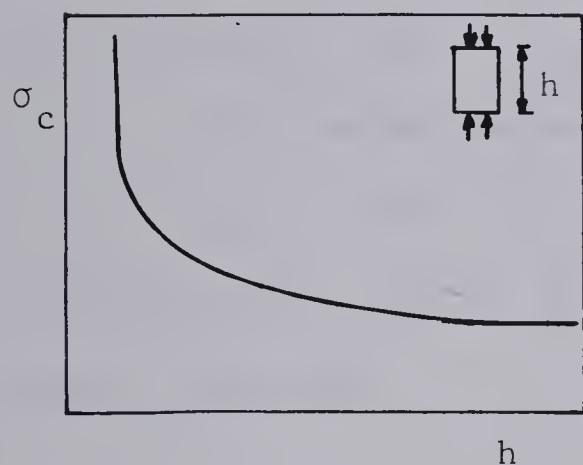
### Size of a Failing Element

$h_1 = a d\theta$  : circular opening

$h_2 = a^2 d\theta / b$  elliptical "

normalized size :

$$0 < h_2/h_1 = a/b < 1$$



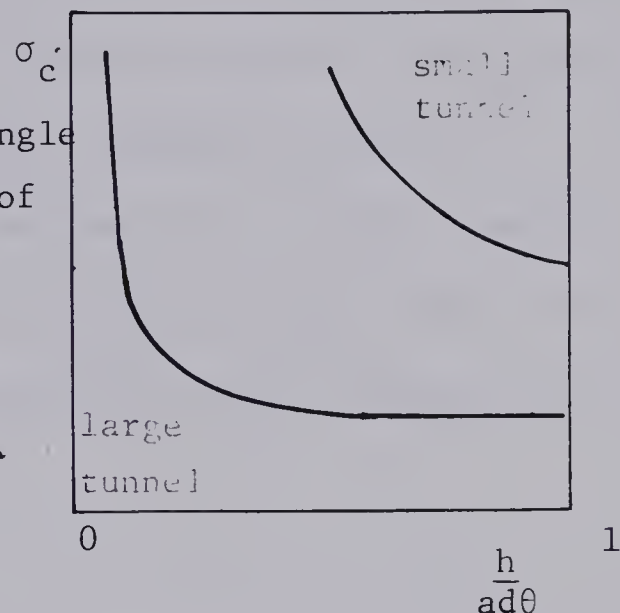
Unconfined compressive strength vs. Size of the failing element :

Intrinsic curve for the material

Given :

- $d\theta$  solid angle
- $a$  radius of opening

$$h \rightarrow \frac{h}{a d\theta}$$



Curves 1 :

depend on :

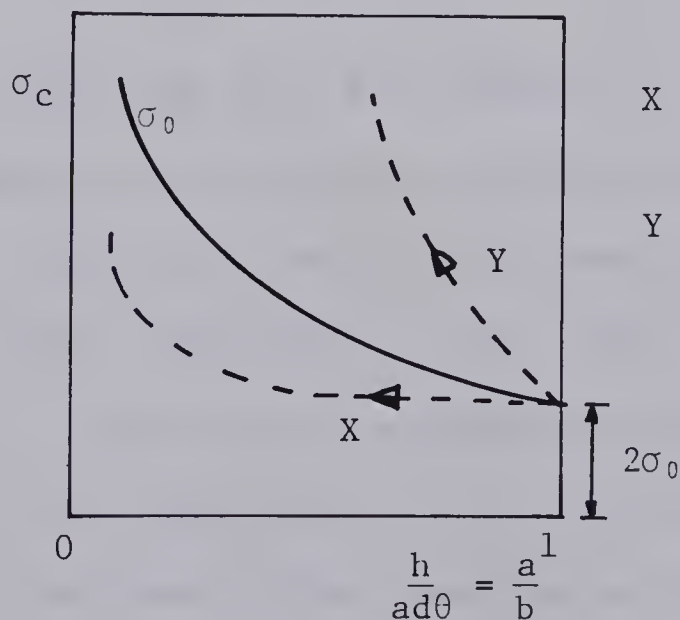
- Size of the original tunnel
- Size-dependent Strength

Curves 2 :

$$\sigma_c = 2 \frac{b}{a} \sigma_0 = 2 \sigma_0 \frac{1}{a/b}$$

depend on :

- Opening Shape  $a/b$
- Stress Conditions  $\sigma_0$



X Opening collapses

Y Opening stable

Figure 6.7 Illustration for the Model of Stabilization of the Rupture



tested element on the complete stress strain curve of a rock. The results obtained for marble samples in uniaxial compression are reproduced in Figure 6.8 and are given for illustration only. It can be seen on these plots that the shape of the rock element affects not only the peak strength but also the post-peak behaviour. A longer element will have lower strength and a steeper post-peak strength curve.

A similar behaviour may be expected for a rock element on a tunnel wall even if the boundary conditions are different. This will be used to qualitatively analyse the rupture process.

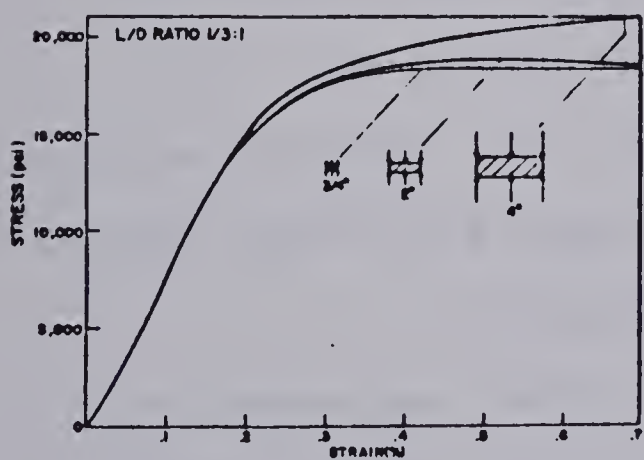
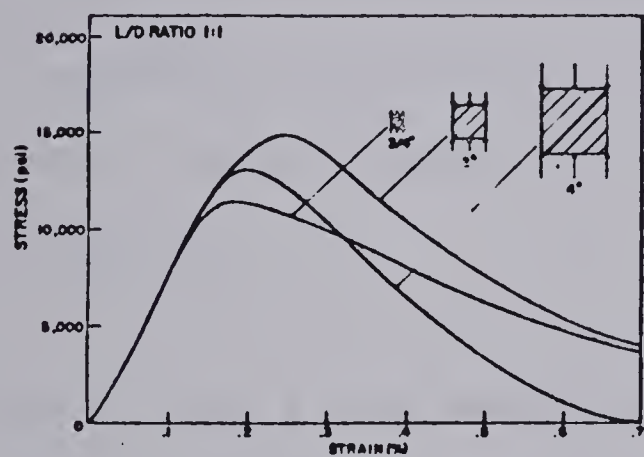
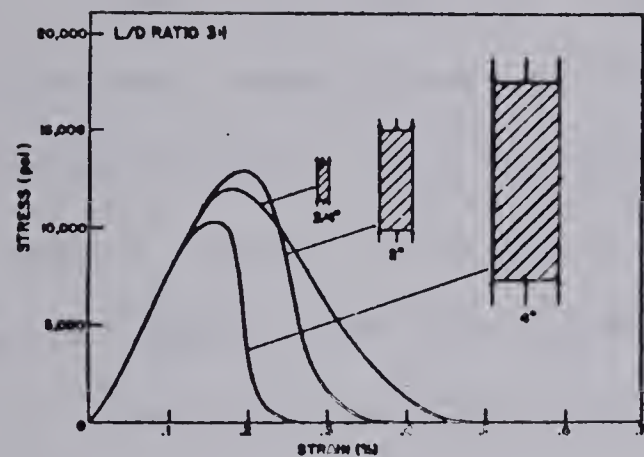
#### 6.4.3 Time-Dependent Rupture Process

After the sample has been loaded near rupture, the elements near the tunnel wall experience a strength failure either immediately or after some creep. Rupture subsequently occurs, creating a new elliptical opening. Elements initially further from the wall are suddenly at the surface of the new opening. As the stress concentration increases, they support more load. The radius of curvature decreases, the apparent strength increases, and the new cavity may support the load. If the stress increases more rapidly than the strength, the new opening will collapse. This process goes on until the curvature of the opening provides a higher strength than the stress level and the rupture is stabilized.

This repetitive process explains the wave-like aspect



## SIZE EFFECT



## SHAPE EFFECT

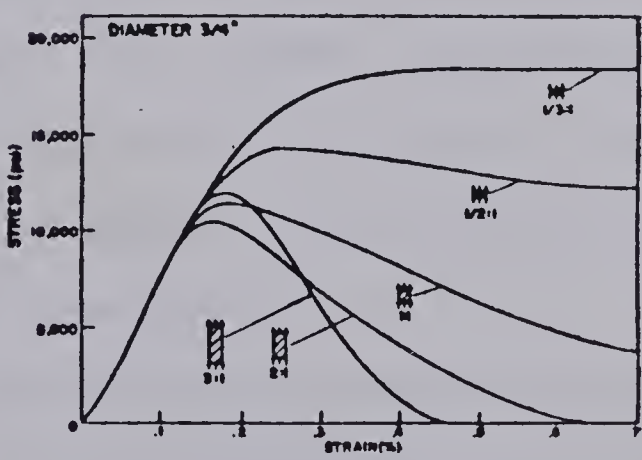
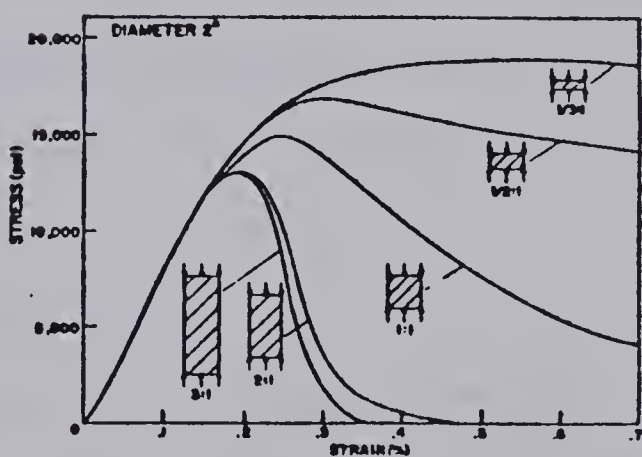
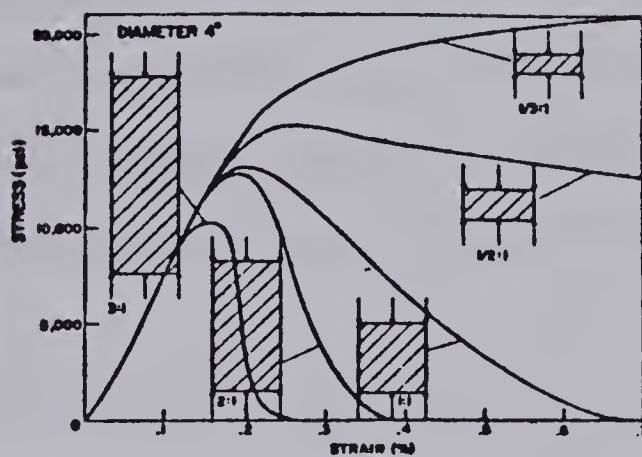


Figure 6.8 Size and Shape Effects on the Complete Stress Strain Curve of Marble Samples in Uniaxial Loading (after Hudson et al (1972))





of the instrument response described in the second section of this chapter.

#### 6.4.4 Model for the Stabilization of the Rupture Process

The stabilization of the rupture process depends on the relative importance of the stress increase due a change in opening shape and the strength increase due to a change in element shape. This has been recognized to a certain extent by Fairhurst and Cook(1966)

The model description is illustrated on Figure 6.7. The height  $h$  of a rupturing element is equal to the local radius of curvature multiplied by the elementary solid angle  $d\alpha$ . The radius of curvature at the end of the long axis of an ellipse is:

$$r=a^2/b$$

where  $a$  and  $b$  are respectively half the lengths of the small and the long axis. The normalized size of the element, defined as the ratio between the length of the actual rupturing element to the initial rupturing element length (circular cavity) is equal to the ratio of the ellipse axes:

$$h/ada\alpha=a^2d\alpha/b \quad a \quad d\alpha =a/b$$

If the behaviour of the material is time-independent, the tangential stress at the wall in the direction of the long axis is :

$$\sigma=2\sigma_0*b/a$$

if  $\sigma_0$  is the external stress.

Then, for the opening to be stable, the unconfined



compressive strength has to be at least equal to this value of the tangential stress which will be called here "required strength". A relation is found between the required strength for an opening to be stable and the normalized size of the rupturing element. This curve is called curve 2 in Figure 6.7. Figure 6.9 shows the corresponding family of hyperbolas for different values of the external stress (solid lines, curves 2).

These curves are a function of the stress level in the rock mass and show the evolution of the required strength as the elliptical cavity propagates.

The influence of the shape of tested coal samples on its strength has been shown by several authors. Bieniawski(1968) or Hustrulid(1975) gave relationships for this variation. They found a unique curve relating the strength of the sample to the size of the element. It is assumed thereafter that a similar curve exists to relate the size  $h$  of a rupturing element on the tunnel wall to the strength of the material. This curve is unique and intrinsic for the material. Given this curve of the strength as a function of the size of the sample, given the radius  $a$  of the opening and assuming a value for the solid angle  $d\alpha$ , a curve expressing the variation of the strength as a function of the normalized size may be obtained from the intrinsic strength curve by an axial affinity parallel to the abscissa axis and whose ratio is  $1/a d\alpha$ : This process is illustrated on Figure 6.7. A point of Curve 1 is obtained from a point



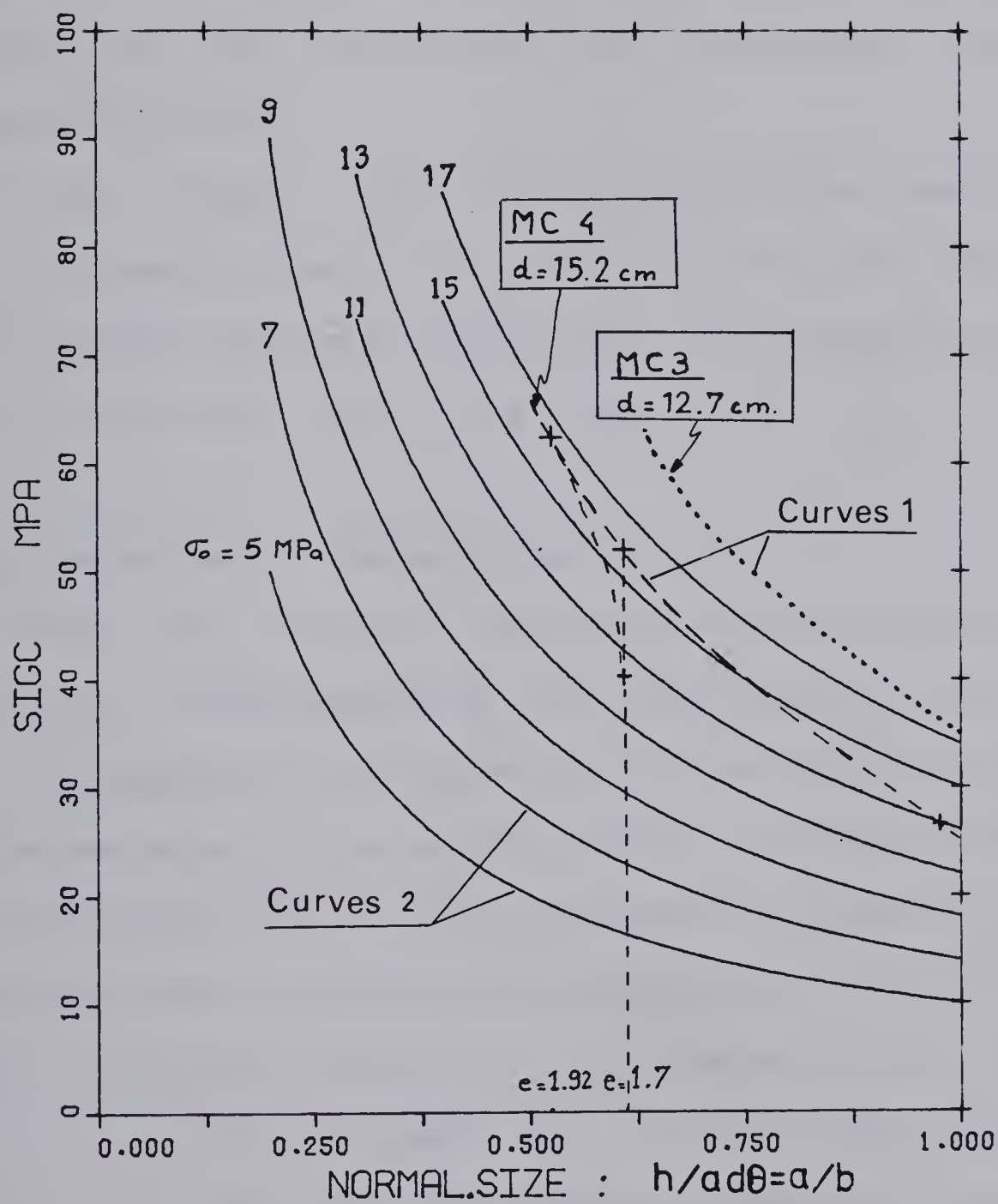


Figure 6.9 Model for the Stabilization of the Rupture Process in the Model Test





of the intrinsic curve by keeping the ordinate constant and multiplying the abscissa by the ratio  $1/ada$ . The curves 1 depend on the material properties and on the size of the opening. Different opening sizes define another family of curves in the strength versus normalized size axes. These curves show the variation of the provided strength when rupture proceeds.

The stress , material and geometrical conditions will give a curve of each of the two families. The comparison of the provided strength and the required strength will give an idea of the stability of the tunnel wall.

#### 6.4.5 Experimental Data on the Rupture

From the load and rupture history of sample MC-4, and from the measurements of the tunnel section after rupture, it is possible to get experimental points in the previously described axes. These points are on the experimental curve 1 corresponding to a 15.2 cm. tunnel in Sundance coal. This has been done in Figure 6.9 (dashed line). Failure initiates for an external stress of 13 MPa; the sample was then loaded up to 16 MPa, unloaded and reloaded. The corresponding values of the axes ratio give the abscissa (the normalized size has been shown to be equal to the axes ratio of the ellipse). When the sample is reloaded after the debris has been removed, the new rupture initiates for values of the external stress between 11 MPa and 13 MPa. This shows that the debris provides a small support pressure which is not





taken into account here, but seems to have an important effect.

From this experimental curve an intrinsic curve for the strength of the material as a function of size may be obtained. Furthermore a back calculated curve 1 may be obtained for sample MC-3. An horizontal affinity with ratio  $a_4 d\alpha$  will transform the experimental curve for test MC-4 to the intrinsic strength vs. size curve for Sundance coal, if  $a_4$  is the radius of the MC-4 tunnel. The curve 1 for test MC-3 results from a further transformation of the intrinsic curve by an horizontal affinity with ratio  $1/a_3 d\alpha$ , where  $a_3$  is the radius of the MC-3 tunnel. In other words the curve 1 for sample MC-3 may be calculated from the curve 1 for sample MC-4 by keeping at each point the ordinate constant and by multiplying the abscissa by the ratio  $a_4/a_3$ . The results of this transformation are presented on Figure 6.9 as a dotted line. According to this curve it is normal that the sample MC-3 did not rupture, but it is also reasonable to assume that plastic yielding already occurred, in agreement with the plastic lines observed when the sample was unloaded from 17MPa. The intrinsic curve relating for Sundance coal strength and size of the rupturing element is not presented here but it is in agreement with an extrapolation of published results to small size, even if these published curves relate strength and size of a free sample.



#### 6.4.6 Discussion on this Model

This model explains the behaviour of the model test samples with respect to the rupture. It is based on simplified hypotheses and needs to be extended to include for instance time-dependency or strain-softening effects in order to be applicable to the reality. However, some basic conclusions may be drawn.

1. For the same material, a smaller tunnel will have a strength versus normalized size curve higher than that for a larger tunnel. Thus for a given density of joints a small tunnel is more stable than a larger one. This corresponds to real observations described, for instance, by Talobre(1957) (p. 318).
2. The stability of an opening will depend on the relative slopes of the provided strength (Curve 1) and required strength (Curve 2) curves. The lower graph on Figure 6.7 illustrates that if curve 1 tends to be above curve 2 the tunnel is stable, otherwise the rupture will propagate. A material for which strength does not depend on element size will exhibit collapse and a complete rupture as the provided strength curve is flat and the required strength curve remains unchanged.
3. The same conclusion is valid for a large opening in a dense material as the provided strength curve is also relatively flat.
4. The rupture of a tunnel is scale-dependent and a study of the laws of similitude applicable to this case will



be necessary to show under which conditions the same type of controlled failure may occur in reality.

### 6.5 Summary and Conclusions

The following conclusions may be drawn from the observations and analysis of the rupture process :

1. The observation of the plaster covering the sample indicates that the stress distribution in the model test is radial around the opening. An elliptical crack pattern observed on one of the samples indicates an anisotropic stress redistribution .
2. Even if the tunnel wall does not rupture, a small plastic zone develops around the tunnel, allowing some blocks to be separated from the rock mass ;this rock fall phenomenon is influenced by preexisting faults on the tunnel wall.
3. Rupture of the tunnel wall is triggered by a mechanism involving the joints of the rock mass. It initiates in the direction perpendicular to the joints, and is caused either by a sliding or a buckling of a "band" of coal (between two joints) towards the cavity.
4. The joints influence the rupture mechanism by intercepting plastic slip lines and in this way shortening the length of their resistant section.
5. The rupture mechanism depends on the radius of curvature of the surface to be broken. A surface with a smaller radius of curvature has a higher resistance against such a rupture mechanism.







6. The rupture propagates in the direction perpendicular to the joints, creating a new elliptical opening.
7. The rupture is better recorded by strain gauges inside the rock mass than by closure measurements. The time-dependency of the rupture is well recorded on a log strain rate versus log time representation of the internal strain gauges measurements. These curves have a characteristic wave-like aspect.
8. The rupture process stabilizes in the model test. A simple model taking into account the shape-dependent strength of a rupturing element has been developed. It compares the strength provided to an element on the tunnel wall by its shape with the strength required to keep an opening stable, if this opening, involved in a rupture process, changes its shape from circular to elliptical.
9. This model explains the stabilization of the rupture in the test MC-4, and why the sample MC-3 stayed intact. It shows also that for a given jointed material, a small tunnel is more stable than a larger tunnel.

It appears from these observations that an elastic - anisotropic plastic analysis should be undertaken to analyse the stability of a tunnel in a jointed brittle rock mass. The importance of the shape of the excavation with respect to the orientation and the density of the joints has to be recognized in order to control a local rupture. A local instability could initiate a complete collapse of the



cavity.



## CHAPTER 7

### CONCLUSIONS, IMPLICATIONS AND RECOMMENDATIONS

#### 7.1 Conclusions

An extensive testing program of eight months duration on two different model test samples was conducted. Rupture of the tunnel was obtained only in the second sample and the different ultimate behaviour permits a comparison between the two samples.

Material, testing equipment and procedure are sufficiently developed to study the time - dependent failure process of a model test of a tunnel in a natural material. The testing technology is now improved and will allow more rapid collection of relevant additional data in future tests.

In the pre-failure range the elastic and visco-elastic deformations of the sample are in agreement with the results of previous experiments on model test and triaxial samples. Because of the ultimate behaviour of the second sample the interpretation of the test data has been orientated towards the analysis of the near - failure behaviour of the tunnel. An isotropic elasto-plastic analysis of the model deformations has been conducted with different hypotheses of post - failure behaviour. The experimental data are consistent with the results of this theoretical analysis; the corresponding values of the strength parameters are reasonable for coal and the volume change and post failure



behaviour agree with the generally accepted practice in the interpretation of field data.

However, the conclusions obtained from this analysis and the visual observations of the failure mechanism are not compatible. Direct observations indicate that this isotropic elasto-plastic analysis is not appropriate to study the failure mechanism of a tunnel in a jointed brittle material. It is suspected that the hypotheses of axi-symmetry and time-independence of the stress field lead to important discrepancies.

Rupture was initiated by a local instability of the tunnel wall. This occurred in zones where the joints are tangent to the tunnel wall and it was influenced by the density of jointing in the material and by the local radius of curvature of the cavity. Initial rupture may lead to a complete collapse of the tunnel or to a stabilizing process. A simple model explains that this ultimate behaviour is influenced by the structure - dependent character of the rupture of a brittle rock. For the same jointed material a small tunnel will be stable, a larger tunnel will experience a stabilizing local failure and a larger tunnel a collapsing process.

## 7.2 Implications

Even if the laws of similitude in the inelastic range do not allow at the present time a direct application of the model test results to reality, this thesis has some





implications in the practice of tunnel design.

For a tunnel in brittle jointed material the interpretation of field data should no longer be undertaken by use of isotropic elasto-plastic analysis only. It is advised that analytical models be developed taking into account the anisotropic character of the strength, the time-dependent and time - independent stress redistribution processes and the implications of local instability.

The evaluation of rock characteristics as well as the stress conditions inferred from a pilot tunnel could be misleading if stress redistribution and scale effects are not taken into account.

### 7.3 Recommendations

The continuing research program should take advantage of the experience gained in the previous tests in order to conduct further experiments with maximum efficiency.

The detrimental effect of excessive drying - wetting cycles on the structure and the strength of a sample has been recognized. This practice is to be avoided by always protecting the sample. It was assumed that the rupture process itself was not controlled by the change in structure of sample MC-4 resulting from these effects. A complete experimental investigation of the effect of successive changes in moisture content could not be undertaken within the time frame of this thesis. It should be completed if further experiments on model tests prove the importance of



this effect.

Similarity between the model test and the reality would be improved if the tunnel could be drilled through a sample under load. However, under these conditions the tunnel closure will only be measured after the time delay necessary to install the measuring device.

Time - dependent stress redistribution has been proven to be essential in the analysis of tunnel deformations. It is difficult (if not impossible) to monitor this local effect independently in the model test. A separate experiment could be undertaken to study the rate and the amplitude of the stress redistribution process. This might be achieved by pushing an element of coal, cut by two longitudinal sections from a hollow cylinder of coal, against a rigid wedge-shaped frame instrumented with load cells. The major problem for the feasibility of this experiment is the development of a non - frictional contact between the sample and the rigid frame. Other experiments could be designed to study the time - dependent response of a rock sample subjected to non uniform loading.

The responses of the instruments in the model test are sensitive to a change in loading rate and in N-value (ratio between the horizontal and the vertical stress). Uniformity in the loading conditions depends on the ability of the operator. The next step in the improvement of the compression machine should be the design of an automatic and reliable loading system where the N-value could be constantly



monitored. A servo-control for the plane-strain condition could also be included. A system or computer code allowing rapid monitoring of the N-value would be useful for experiments in the near future.

In the stress stages preceeding the rupture there was no clear indication of the future local instability. Therefore the time - dependent aspect of the rupture was not correctly controlled and analysed in test MC-4. This may be the most important point to be studied in further experiments. It is advised for further experiments to keep the same procedure up to 11 MPa field stress. An amount of creep for the tunnel closure in the order of 0.2% during the first day at this stage seems to preceed rupture but does not ensure this type of ultimate behaviour. The next stress increments should only be 1 MPa and the corresponding creep tests should be carried on for a two day period, even after the eventual initiation of rupture. The data should be analysed and termination of the creep or rupture process should be confirmed by viewing the strain rate - time plots, before the next load increment is applied to the sample. The tunnel closure measuring device should be improved to monitor large deformations and adapted to measure the closure of the elliptical cavity after initiation of rupture.







## References

- Bieniawski, Z.T., 1967. "Mechanism of brittle fracture of rock", International Journal of Rock Mechanics and Mining Sciences, Vol.4, pp.395-430.
- Bieniawski, Z.T., 1968. "In situ strength and deformation characteristics of coal", Engineering Geology, Vol.2, n.5, pp.325-340.
- Borsetto, M., and Ribacchi, R., 1979. "Influence of the strain-softening behaviour of rock masses on the stability of a tunnel" Proceedings of the Third International Conference on Numerical Methods in Geomechanics, Aachen, Germany, Vol.2, pp.611-620.
- da Fontoura, S., 1980. Ph.D. Thesis (to be published), Department of Civil Engineering, University of Alberta.
- Daemen, J.J.K., 1975. "Tunnel Support Loading Caused by Rock Failure", Ph.D. thesis in Civil Engineering, University of Minnesota.
- Descœudres, F., 1977. "Mécanique des Roches", 229 pp., Cours de l'Ecole Polytechnique Fédérale de Lausanne, Switzerland.
- Egger, P., 1973. "Einfluss des Post-Failure-Verhaltens von Fels auf den Tunnel Ausbau", Veröffentlichungen des Institutes fuer Bodenmechanik und Felsmechanik, Universitaet Fridericiiana Karlsruhe, Heft 57, pp.1-83.
- Evans, I. and Pomeroy, C.D., 1966. "The Strength, Fracture and Workability of Coal", Pergamon Press.
- Fairhurst, C., and Cook, N.G.W., 1966. "The phenomenon of rock splitting parallel to the direction of maximum compression in the neighbourhood of a surface", Proceedings of the First Congress of the International Society of Rock Mechanics, Lisbon, Portugal, Vol.1, pp.687-690.
- Florence, A.L., and Schwer, L.E., 1978. "Axisymmetric compression of a Mohr-Coulomb medium around a circular hole", International Journal for Numerical Methods in Geomechanics, Vol.2, pp.367-379.
- Fryer, J.F., and Szladow, A.J., 1973. "Storage of Coal Samples", Alberta Research Council, Information Series #66,
- Holter, M.E., Yurko, J.R., Chu, , 1975. "Geology and Coal Reserves of the Ardley Coal Formation -Zone of Central Alberta", Alberta Research Council, Report 75.7,
- Hudson, J.A., Brown, E.T., and Fairhurst, C., 1972. "Shape of the complete stress-strain curve for rock", Proceedings of the Thirteen Symposium on Rock Mechanics, University of Illinois, pp.773-795.
- Hustrulid, W.A., 1975. "A review of coal pillar strength formulas", Rock Mechanics, Vol.8, pp.115-145.
- Jaeger, J., C., 1960. "Shear failure of anisotropic rock" ,



- Geology Magazine, Vol.97, pp.65-72.
- Kaiser, P.K. and Morgenstern, N.R., 1979. "Time-dependent deformation of jointed rock near failure", Proceedings of the Fourth International Congress on Rock Mechanics, Montreux, Switzerland, Vol.1, pp.195-202.
- Kaiser, P.K., 1979. "Time-Dependent Behaviour of Tunnels in Jointed Rock Masses", Ph.D. Thesis, Department of Civil Engineering, University of Alberta,
- Ko, H.Y., and Gerstle, K.H., 1976. "Elastic Properties of Two Coals", International Journal of Rock Mechanics and Mining Sciences, Vol.13, pp.81-90,
- Labasse, H., 1949. "Les pressions des terrains dans les mines de houille", Revue Universelle des Mines (Liege, Belgique), Serie 9, Tome 5, N.1, pp.2-15, pp.78-88,
- Ladanyi, B., 1974. "Use of the long-term strength concept in the determination of ground pressure on tunnel linings", Proceedings of the Third Congress of the International Society of Rock Mechanics, Denver, Colorado, Vol 2B, pp.1150-1156.
- Morgenstern, N.R. and Noonan, D.K.J., 1974. "Fractured coal subjected to direct shear", Proceedings of the Third Congress of the International Society of Rock Mechanics, Denver, Colorado, Vol.2A, pp.282-287.
- Noonan, D.K.J., 1972. "Fractured Rock Subjected to Direct Shear", M.Sc.Thesis, Department of Civil Engineering, University of Alberta, Edmonton.
- Obert, L. and Duvall, W.I., 1967. "Rock Mechanics and the Design of Structures in Rock", John Wiley and Sons, New York, 650pp.
- Panet, M., 1976. "La Mécanique des Roches Appliquée aux Ouvrages de Génie Civil", 235pp., Association amicale des ingénieurs anciens de l'Ecole Nationale des Ponts et Chaussées, Paris,
- Patton, F.D., 1966. "Multiple mode of shear failure in rock", Proceedings of the First Congress of the International Society of Rock Mechanics, Lisbon, Portugal, pp.509-513.
- Pearson, G.R., 1959. "Coal reserves for strip mining, Wabamun Lake District Alberta", Research Council of Alberta, Geology Division, Preliminary Report 59-1, 37pp.
- Rechsteiner, G.F., and Lombardi, G., 1974. "Une méthode de calcul élasto-plastique de l'état de tension et de déformation autour d'une cavité souterraine /Part1", Proceedings of the Third Congress of the International Society of Rock Mechanics, Denver, Colorado, Vol.2B, pp.1043-1054.
- Salençon, J., 1969. "Contraction quasi-statique d'une cavité sphérique ou cylindrique dans un milieu élasto-plastique", Annales des Ponts et Chaussées, N°4, pp231-236.
- Talobre, M.T., 1957. "La Mécanique des Roches", Dunod,



Paris.

Terry, N.B., 1956. "The elastic properties of coal",  
British National Coal Board, Mining Research  
Establishment Report 2080, Part 6.





## APPENDICES

### Table of content

#### Appendix A1 :

Continuum mechanics relationships for plane strain conditions

#### Appendix A2

Elasto - plastic analysis of the model test results

#### Appendix A3

- 1) Correction of data for non-isotropic loading
- 2) Influence of the intermediate principal stress
- 3) Volume change

#### Appendix A4

Determination of elastic parameters in the model test

#### Appendix B1

Stress - strain curves

#### Appendix B2

Creep data near rupture in test MC 4.2





## APPENDIX A1

---

### CONTINUUM MECHANICS RELATIONSHIPS FOR PLANE STRAIN CONDITIONS

---

The equations of solid mechanics under plane strain conditions are summarized as follows.

For plane strain conditions the longitudinal strain is equal to zero and the value of the stress in this direction is given by :

$$\sigma^{33} = \nu(\sigma^{11} + \sigma^{22}) \quad (1)$$

→Equilibrium equation : (2 eq.)

$$\frac{\partial \sigma_{ij}}{\partial j} + F_i = 0 \quad (2)$$

→Strain-displacement (3 eq.)

$$e_{ij} = \frac{1}{2} \left( \frac{\partial u_i}{\partial j} + \frac{\partial u_j}{\partial i} \right) \quad (3)$$

→Hooke's law (3 eq.)

$$\sigma_{ij} = \lambda \delta_{ij} e_{kk} + 2G e_{ij} \quad (4)$$

$\lambda, G$  Lamé constants ,  $\delta_{ij}$  Kronecker delta

These 8 equations are sufficient to calculate the values of the 8 unknown :

$$\sigma_{ij} \quad (3) \quad \epsilon_{ij} \quad (3) \quad u_i \quad (2)$$

For convenience the solution is usually expressed either in terms of displacements or stresses. This will take into account the boundary conditions.

a) Solution in terms of stresses

The compatibility equation is given by :

$$\frac{\partial^2 \epsilon_{ii}}{\partial j^2} + \frac{\partial^2 \epsilon_{jj}}{\partial i^2} = \frac{\partial^2 \epsilon_{ij}}{\partial i \partial j} \quad (5)$$



From equations 2,4 and 5 the following relationship between the stresses and the body forces yields :

$$\nabla^2 \sigma_{ii} = \frac{1}{\nu-1} \frac{\partial F_i}{\partial i} \quad (6)$$

For a two-dimensional problem the Airy's stress function  $\phi$  is introduced as follows :

$$\sigma_{ij} = -\frac{\partial^2 \phi}{\partial i \partial j}$$

The body forces are said to derive from a potential if a function  $V$  may be found such that the following equation be verified :

$$F_i = \frac{\partial V}{\partial i}$$

The substitution of functions  $\phi$  and  $V$  into equation 6 leads to a governing equation for the problem, called biharmonic equation :

$$\nabla^4 \phi = \frac{1-2\nu}{1-\nu} \nabla^2 V \quad (7)$$

#### b) Solution in terms of displacements

From equations 3 and 4 the following relationship between stress and displacement is obtained :

$$\sigma_{ij} = \lambda \delta_{ij} \frac{\partial u_k}{\partial k} + G \left( \frac{\partial u_i}{\partial j} + \frac{\partial u_j}{\partial i} \right)$$

Substitution of  $\sigma_{ij}$  into the equilibrium equations will give Navier's equation :

$$G \nabla^2 u_i + (\lambda + G) \frac{\partial}{\partial i} \left( \frac{\partial u_i}{\partial i} + \frac{\partial u_j}{\partial j} \right) + F_i = 0 \quad (8)$$

#### c) Solution in terms of polar coordinates

The stresses are transformed from polar to cartesian coordinates as follows :

$$\sigma_x = \sigma_r \cos^2 \theta + \sigma_\theta \sin^2 \theta - \tau_{r\theta} \sin 2\theta$$

$$\sigma_y = \sigma_r \sin^2 \theta + \sigma_\theta \cos^2 \theta + \tau_{r\theta} \sin 2\theta$$

$$\tau_{xy} = (\sigma_r - \sigma_\theta) \sin \theta \cos \theta + \tau_{r\theta} (\cos^2 \theta - \sin^2 \theta)$$



The equilibrium equations become :

$$\begin{aligned}\frac{\partial \sigma_r}{\partial r} + \frac{1}{r} \frac{\partial \tau_{r\theta}}{\partial \theta} + \frac{\sigma_r - \sigma_\theta}{r} + F_r &= 0 \\ \frac{1}{r} \frac{\partial \sigma_\theta}{\partial \theta} + \frac{\partial \tau_{r\theta}}{\partial r} + 2 \frac{\sigma_\theta}{r} + F_\theta &= 0\end{aligned}\quad (9)$$

and Hooke's law may be expressed as follows :

$$\begin{aligned}\epsilon_r &= \frac{1-\nu^2}{E} \left( \sigma_r - \left( \frac{\nu}{1-\nu} \right) \sigma_\theta \right) \\ \epsilon_\theta &= \frac{1-\nu^2}{E} \left( \sigma_\theta - \left( \frac{\nu}{1-\nu} \right) \sigma_r \right) \\ \gamma_{r\theta} &= \frac{1}{G} \tau_{r\theta}\end{aligned}\quad (11)$$

The strain-displacement relationships become :

$$\begin{aligned}\epsilon_r &= \frac{\partial u_r}{\partial r} \\ \epsilon_\theta &= \frac{u_r}{r} + \frac{1}{r} \frac{\partial u_\theta}{\partial \theta} \\ \gamma_{r\theta} &= \frac{1}{r} \frac{\partial u_r}{\partial \theta} + \frac{\partial u_\theta}{\partial r} - \frac{u_\theta}{r}\end{aligned}\quad (12)$$

and Navier's equations reduce to :

$$\begin{aligned}(\lambda+2G) \frac{\partial \epsilon}{\partial r} - \frac{2G}{r} \frac{\partial \omega}{\partial \theta} + F_r &= 0 \\ (\lambda+2G) \frac{1}{r} \frac{\partial \epsilon}{\partial \theta} + 2G \frac{\partial \omega}{\partial r} + F_\theta &= 0\end{aligned}\quad (10)$$

where :

$$\begin{aligned}\epsilon &= \epsilon_r + \epsilon_\theta = \frac{1}{r} \frac{\partial (ru_r)}{\partial r} + \frac{1}{r} \frac{\partial u_\theta}{\partial \theta} \\ \omega &= \frac{1}{2r} \left( \frac{\partial (ru_r)}{\partial r} + \frac{\partial u_\theta}{\partial \theta} \right)\end{aligned}$$

Therefore the biharmonic equation becomes :

$$\nabla^4 \phi = \left( \frac{\partial^2}{\partial r^2} + \frac{1}{r} \frac{\partial}{\partial r} + \frac{1}{r^2} \frac{\partial^2}{\partial \theta^2} \right) \left( \frac{\partial^2}{\partial r^2} + \frac{1}{r} \frac{\partial}{\partial r} + \frac{1}{r^2} \frac{\partial^2}{\partial \theta^2} \right) \phi = 0 \quad (13)$$





Stresses in polar coordinates may be derived from the Airy's stress function by the following expressions :

$$\sigma_r = \frac{1}{r} \frac{\partial \phi}{\partial r} + \frac{1}{r^2} \frac{\partial^2 \phi}{\partial \theta^2}$$

$$\sigma_\theta = \frac{\partial^2 \phi}{\partial r^2}$$

$$\tau_{r\theta} = - \frac{\partial}{\partial r} \left( \frac{1}{r} \frac{\partial \phi}{\partial \theta} \right)$$

The general solution of the biharmonic equation in polar coordinates is given by the following expression :

(after Obert and Duval (1967))

$$\begin{aligned} \phi(r, \theta) = & A^0 r^2 + B^0 r^2 \log r + C^0 \log r + D^0 \dots \\ & + (E^0 r^2 + F^0 r^2 \log r + G^0 \log r + H^0) \theta \\ & + (A_1 r + \frac{B_1}{r} + C_1 r^3 + D_1 r \log r) \sin \theta \\ & + (E_1 r + \frac{F_1}{r} + G_1 r^3 + H_1 r \log r) \cos \theta \\ & + (J_1 r + K_1 r \log r) \theta \sin \theta + (L_1 r + M_1 r \log r) \theta \cos \theta \\ & + \sum_2^\infty (A_n r^n + B_n r^{-n} + C_n r^{2-n} + D_n r^{2+n}) \sin n\theta \\ & + \sum_2^\infty (E_n r^n + F_n r^{-n} + G_n r^{2-n} + H_n r^{2+n}) \cos n\theta \end{aligned}$$



## APPENDIX A2

### ELASTO-PLASTIC ANALYSIS OF THE MODEL TEST RESULTS

#### 2.1 ASSUMPTIONS

The stress conditions are isotropic( $N=1$ ) creating an axisymmetric stress field . ( $u_\theta=0$ )

##### List of symbols

$\sigma^0$  external pressure  
 $\sigma_r$  radial stress  
 $\sigma_\theta$  tangential stress  
 $\sigma_c$  unconfined compressive strength

$E$  Young's modulus  
 $\nu$  Poisson's ratio

$\left. \begin{matrix} G \\ \lambda \end{matrix} \right\}$  Lamé constants  $G = \frac{E}{2(1+\nu)}$  ,  $\lambda = \frac{E \nu}{(1+\nu)(1-2\nu)}$

$a$  radius of the tunnel  
 $r$  current radius  
 $R$  radius of the plastic zone

$\left. \begin{matrix} \epsilon_r \\ \epsilon_\theta \end{matrix} \right\}$  radial strain                       $u_r$  radial displacement  
                                                                                                   $u_\theta$  tangential displacement(=0)

$\phi$  angle of internal friction  
 $C$  cohesion intercept  
 $m$  coefficient of passive earth pressure ( $=k_p$ )  
 $\alpha$  dilation coefficient

##### List of Superscripts

$p$  in the plastic zone : plastic part of ...  
 $e$  in the elastic zone : elastic part of ...



## 2.2 Elastic Relationships for the Model Test

### a) Stress distribution

The original derivation of the stress distribution around a circular hole is attributed to Kirsch. The stress field obtained by using Airy's stress functions is found in numerous books (Obert and Duvall 1967).

$$\sigma_r = \sigma^0 \left(1 - \frac{a^2}{r^2}\right) ; \quad \sigma_\theta = \sigma^0 \left(1 + \frac{a^2}{r^2}\right) ; \quad \tau_{r\theta} = 0$$

$$\sigma_r + \sigma_\theta = 2\sigma^0 \quad (14)$$

### b) Strain distribution

The strains are obtained from the stress distribution using Hooke's law (11) :

$$\epsilon_r = \frac{\sigma^0(1+\nu)}{E} \left(1 - 2\nu - \frac{a^2}{r^2}\right) \quad \gamma_{r\theta} = 0$$

$$\epsilon_\theta = \frac{\sigma^0(1+\nu)}{E} \left(1 - 2\nu + \frac{a^2}{r^2}\right) \quad (15)$$

An intact plate would have the following uniform strain distribution if stressed under the same conditions than the model with tunnel :

$$\epsilon = \frac{\sigma^0(1+\nu)}{E} (1 - 2\nu)$$

### c) Displacement field

The displacements are obtained by integrating the strain-displacement relationships (12) :

$$u_\theta = 0 ; \quad u_r = \frac{\sigma^0(1+\nu)}{E} \left( (1 - 2\nu)r + \frac{a^2}{r} \right) \quad (16)$$

### d) Elastic closure of the tunnel

The closure of the tunnel is defined as the ratio between the displacement at the tunnel wall and the original radius of the tunnel. It has the dimension of strain. The closure of the tunnel in the test is given by :

$$\left(\frac{u_r}{r}\right)_{r=a} = \frac{2\sigma^0(1-\nu^2)}{E} \quad (17)$$

The closure of a real tunnel excavated in a prestressed body is :



$$\left(\frac{u}{r}\right) = \frac{2\sigma^0(1+\nu)}{E}$$

Assuming a Poisson's ratio  $\nu=0.25$ , which leads to the so-called Poisson's relation:

$$\lambda = G$$

the relationship between the closure of the tunnel in the model test and the closure of the tunnel in the field is given by :

$$\left(\frac{u}{r}\right)_{\text{model}} = \frac{3}{2} \left(\frac{u}{r}\right)_{\text{reality}}$$

### 2.3 Elastic-Perfectly Plastic Model

#### a) Coulomb failure criterion

The Coulomb failure criterion relates the minimum and maximum principal stresses as follows ;

$$\sigma_1 = m\sigma_3 + \sigma_c$$

where :  $\sigma_1, \sigma_3$  are the maximum and minimum principal stress

$\sigma_c$  is the unconfined compressive strength

$$m = \frac{1+\sin\phi}{1-\sin\phi} \quad \text{and} \quad \sigma_c = 2C \frac{\cos\phi}{1-\sin\phi}$$

In the case of the model test, this criterion is between the radial and the tangential stress.

$$\sigma_\theta = m\sigma_r + \sigma_c$$

$$\text{or} \quad f = \sigma_\theta - m\sigma_r - \sigma_c = 0 \quad (18)$$

#### b) Stress distribution in the Plastic Zone

The combination of the equilibrium equation (9) and the failure criterion(18) gives the following differential equation :

$$r \frac{d\sigma}{dr} = \sigma_r(m-1) + \sigma_c \quad (19)$$

whose solution is :

$$\sigma_r = \frac{1}{r^{1-m}} \left( \frac{\sigma_c}{1-m} r^{1-m} + Cte \right)$$





The boundary conditions give the value of the constant :

$$Cte = a^{1-m} \left( p_i - \frac{\sigma_c}{1-m} \right) = - \frac{a^{1-m} \sigma_c}{1-m}$$

if at  $r=a$   $\sigma_r = p_i = 0$  .

Then the stress distribution in the plastic zone is given by :

$$\begin{aligned} \sigma_r &= \frac{\sigma_c}{m-1} \left( \left( \frac{a}{r} \right)^{1-m} - 1 \right) \\ \sigma_\theta &= \frac{\sigma_c}{m-1} \left( m \left( \frac{a}{r} \right)^{1-m} - 1 \right) \end{aligned} \quad (20)$$

### c) Radius of the Plastic Zone R

In order to estimate the radius R of the boundary between the plastic zone and the elastic zone, the radial stress is assumed to be continuous across this boundary. The value of the stress from the plastic side of the boundary is given by :

$$(\sigma_r)_{r=R} = \frac{\sigma_c}{m-1} \left( \left( \frac{a}{R} \right)^{1-m} - 1 \right)$$

The value of the stress from the elastic side of the boundary is :

$$(\sigma_r)_{r=R} = \frac{1}{m+1} (2\sigma^0 - \sigma_c)$$

The latter equation is obtained after the following relationships :

$$(\sigma_\theta)_{r=R} = m(\sigma_r)_{r=R} + \sigma_c$$

$$(\sigma_\theta)_{el.} + (\sigma_r)_{el.} = 2\sigma^0$$

The radius R is determined from the elimination of  $(\sigma_r)_{r=R}$  between the above equations.

$$\frac{R}{a} = \left( \frac{2}{[m+1]} \frac{\sigma^0(m-1) + \sigma_c}{\sigma_c} \right)^{\frac{1}{m-1}} \quad (21)$$



d) Stresses in the elastic region surrounding the plastic zone

The stress distribution in the elastic region is identical to the one encountered in a body with a R-diameter tunnel, which is supported by a uniform pressure  $\sigma_{rR}$ , under the same field stress conditions.

At the elastic-plastic boundary, the stresses are given by :

$$\sigma_{rR} = \frac{\sigma_c}{m-1} \left( \left( \frac{R}{a} \right)^{m-1} - 1 \right) \quad (22)$$

$$\sigma_{\theta R} = \frac{\sigma_c}{m-1} \left( m \left( \frac{R}{a} \right)^{m-1} - 1 \right)$$

$$\sigma_{\theta R} + \sigma_{rR} = 2\sigma^0 \quad (23)$$

and in the elastic region the stresses are given by :

$$\begin{aligned} \sigma_r &= \sigma^0 \left( 1 - \frac{R^2}{r^2} \right) + \sigma_{rR} \frac{R^2}{r^2} \\ \sigma_\theta &= \sigma^0 \left( 1 + \frac{R^2}{r^2} \right) - \sigma_{rR} \frac{R^2}{r^2} \end{aligned} \quad (24)$$

Hooke's law (11) and the integration of the strain-displacement relationships (12) give the strain and displacement fields.

$$\begin{aligned} \epsilon_r &= \frac{\sigma^0(1+\nu)}{E} \left( 1-2\nu + \left( \frac{\sigma_{rR}}{\sigma^0} - 1 \right) \frac{R^2}{r^2} \right) \\ \epsilon_\theta &= \frac{\sigma^0(1+\nu)}{E} \left( 1-2\nu - \left( \frac{\sigma_{rR}}{\sigma^0} - 1 \right) \frac{R^2}{r^2} \right) \\ u_r &= \frac{\sigma^0(1+\nu)}{E} \left( (1-2\nu)r - \left( \frac{\sigma_{rR}}{\sigma^0} - 1 \right) \frac{R^2}{r} \right) \end{aligned} \quad (25)$$

The substitution of equations (22) into (23) and (25) will give the exact expressions for the stress, strain, displacement fields in the elastic zone.



e) Strains in the plastic zone

The plastic strain increments are obtained by application of the associated flow rule definition:

$$\dot{\epsilon}_r^p = \lambda \frac{\partial f}{\partial \sigma_r} = -\lambda m$$

$$\dot{\epsilon}_\theta^p = \lambda \frac{\partial f}{\partial \sigma_\theta} = \lambda$$

$$\dot{\epsilon}_z^p = \lambda \frac{\partial f}{\partial \sigma_z} = 0$$

where  $f$  is the failure criterion given by equation (18).  
It follows that :

$$\dot{\epsilon}_r^p + m \dot{\epsilon}_\theta^p = 0$$

$$\dot{\epsilon}_z^p = 0$$

The integration of these equations yields :

$$\epsilon_r^p + m \epsilon_\theta^p = g_1(r)$$

$$\epsilon_z^p = g_2(r)$$

Initially the plastic strains are equal to zero

$$g_1(r) = g_2(r) = 0$$

Hence the associated flow rule which causes the plastic increments of strain to be normal to the Coulomb failure surface may be summarized as :

$$\epsilon_r^p + m \epsilon_\theta^p = 0$$

$$\epsilon_z^p = 0$$

In order to control the plastic flow, the following relationship will be used between the plastic strain values;

$$\epsilon_r^p + \alpha \epsilon_\theta^p = 0 \quad \epsilon_z^p = 0 \quad (26)$$

The parameter  $\alpha$  is a measure of the dilation occurring during the plastic flow. If there is no plastic volume change,  $\alpha=1$ ; if  $\alpha=m$ , the flow rule is associated to the Coulomb failure criterion.





The total strain in the plastic zone is the sum of the plastic and elastic strains. Plane strain conditions have to be satisfied in the plastic region. As the plastic longitudinal strain is equal to 0 (see 26), the elastic longitudinal strain has to be equal to 0. Hence the stress  $\sigma_z$  in the longitudinal direction is :

$$\sigma_z = \frac{\nu \sigma_c}{m-1} ((m+1) \left(\frac{a}{r}\right)^{1-m} - 2) \quad (27)$$

The elastic strains in the plastic zone are determined from the combination of Hooke's law (11) and plane strain condition :

$$\begin{aligned} \epsilon_r^e &= \frac{1}{2G} [(1-(m+1)\nu)\sigma_r - \nu\sigma_c] \\ \epsilon_\theta^e &= \frac{1}{2G} [(m-(m+1)\nu)\sigma_r + (1-\nu)\sigma_c] \end{aligned} \quad (28)$$

The compatibility equation for the total strains is :

$$r \frac{d\epsilon_\theta}{dr} + \epsilon_\theta - \epsilon_r = 0 \quad (29)$$

From this relationship the following differential equation is obtained for the plastic strains :

$$r \frac{d\epsilon_\theta^p}{dr} + \epsilon_\theta^p (1+\alpha) = -\frac{\sigma_c}{2G} (1-\nu)(m+1) \left(\frac{r}{a}\right)^{m-1} \quad (30)$$

The solution of this equation is (with  $\epsilon_\theta^p(R)=0$ ) :

$$\begin{aligned} \epsilon_\theta^p &= \frac{1-\nu}{2G} \frac{m+1}{m+\alpha} \sigma_c \left(\frac{r}{a}\right)^{m-1} \left[ \left(\frac{R}{r}\right)^{m+\alpha} - 1 \right] \\ \epsilon_r^p &= -\alpha \epsilon_\theta^p \end{aligned} \quad (31)$$

The total strain distribution in the plastic zone is determined from the combination of equations 31 and 28 :

$$\begin{aligned} \epsilon_\theta &= \frac{\sigma_c}{2G} \left[ \left(\frac{r}{a}\right)^{m-1} \left( \frac{m(1-\nu)-\nu}{m-1} + (1-\nu) \frac{m+1}{m+\alpha} \left(\frac{R}{r}\right)^{m+\alpha} - 1 \right) + \frac{2\nu-1}{m-1} \right] \\ \epsilon_r &= \frac{\sigma_c}{2G} \left[ \left(\frac{r}{a}\right)^{m-1} \left( \frac{1-m\nu-\nu}{m-1} - \alpha(1-\nu) \frac{m+1}{m+\alpha} \left(\frac{R}{r}\right)^{m+\alpha} - 1 \right) + \frac{2\nu-1}{m-1} \right] \end{aligned} \quad (32)$$



It follows from the integration of the strain-displacement relationships(12) :

$$u_r = r\epsilon_\theta$$

The closure at  $r=a$  is given by :

$$\frac{u_a}{a} = \frac{\sigma_c(1-\nu)}{2G} \left[ 1 + \frac{m+1}{m+\alpha} \left( \left( \frac{R}{a} \right)^{m+\alpha} - 1 \right) \right] \quad (33)$$

For  $\alpha=1$  this expression yields :

$$\frac{u_a}{a} = \frac{\sigma_c(1-\nu)}{2G} \left[ \frac{R}{a} \right]^{m+1} \quad (34)$$

f) Comparaison between the elasto-plastic and the elastic closure

The closure may be normalized by dividing the "elasto-plastic" closure by the elastic closure : (34/17)

$$\text{For } \alpha=1 \quad \dots \quad \frac{(u/a)_{e.pl.}}{(u/a)_{el.}} = \frac{\sigma_c}{2\sigma_0} \left( \frac{R}{a} \right)^{m+1} \quad (35)$$

$$\text{For } \alpha \neq 1 \quad \dots \quad \frac{(u/a)_{e.pl.}}{(u/a)_{el.}} = \frac{\sigma_c}{2\sigma_0} \left[ 1 + \frac{m+1}{m+\alpha} \left( \left( \frac{R}{a} \right)^{m+\alpha} - 1 \right) \right] \quad (36)$$

This ratio is independent of the elastic constants.

## 2.4 Elastic-brittle plastic material

### a) Failure criterion

The same Coulomb failure criterion still applies, but now the stresses in the plastic zone are related by the following "plasticity" criterion:

$$\begin{aligned} \sigma_\theta &= m\sigma_r + s\sigma_c \\ 0 &< s < 1 \end{aligned} \quad (37)$$

The parameter  $s$  measure the intensity of the strength loss occuring immediately after the strength failure. The strength after the failure is reduced to  $s$ -times the value it was before failure.



The solution is similar to the one described in the previous section for an elastic perfectly plastic material. Only some equations are affected by the "plasticity" criterion and are given thereafter.

#### b) Stresses in the Plastic Region

The stresses in the plastic region are now given by the following expressions :

$$\begin{aligned}\sigma_r &= \frac{s\sigma_c}{m-1} \left[ \left( \frac{a}{r} \right)^{1-m} - 1 \right] \\ \sigma_\theta &= \frac{s\sigma_c}{m-1} \left[ \left( \frac{a}{r} \right)^{1-m} - 1 \right]\end{aligned}\quad (38)$$

The radial stress is continuous but the tangential stress experiences a stress drop of  $(1-s)\sigma_c$  at the elastic-plastic boundary.

#### c) Radius of the Plastic Region

The radius of the boundary of the plastic region is given by :

$$\frac{R}{a} = \left[ \frac{2}{(m+1)s} \left( \frac{\sigma^0}{\sigma_c} (m-1) + \frac{m(s-1)+1+s}{2} \right) \right]^{\frac{1}{m-1}} \quad (39)$$

If the material loses all its cohesion after failure ( $s=0$ ), this radius increases to infinity and the tunnel collapses. Actually, a tunnel in a purely frictional material would collapse without a support pressure.

#### d) Strains in the Plastic Region

The derivation leads to a differential equation which is identical to equation 30. However, because of the boundary conditions, the solution is different.

The total strains have to be continuous across the elastic-plastic boundary. Because of the brittle character of the material, the stresses in the plastic region, given by equations 38 are smaller than in the case of a perfectly plastic material. Hence the elastic strains which are related to the stresses by Hooke's law are also smaller. Then for the continuity of the total strains the plastic tangential strain has the following finite value at the elastic-plastic boundary :

$$\epsilon_{\theta R}^p = \frac{\sigma_c}{2G} (1-\nu)(1-s) \quad (40)$$



The strain field in the plastic zone is :

$$\begin{aligned}\epsilon_{\theta} &= \frac{\sigma_c}{2G} \left[ s \left( \frac{r}{a} \right)^{m-1} \left( \frac{m(1-\nu)-\nu}{m-1} + (1-\nu) \frac{m+1}{m+\alpha} \left( \left( \frac{R}{r} \right)^{m+\alpha} - 1 \right) \right) + \frac{s(2\nu-1)}{m-1} + \dots \right. \\ &\quad \left. \dots (1-\nu)(1-s) \left( \frac{R}{r} \right)^{\alpha+1} \right] \\ \epsilon_r &= \frac{\sigma_c}{2G} \left[ s \left( \frac{r}{a} \right)^{m-1} \left( \frac{1-m\nu-\nu}{m-1} - \alpha(1-\nu) \frac{m+1}{m+\alpha} \left( \left( \frac{R}{r} \right)^{m+\alpha} - 1 \right) \right) + \frac{s(2\nu-1)}{m-1} \dots \right. \\ &\quad \left. \dots -\alpha(1-\nu)(1-s) \left( \frac{R}{r} \right)^{\alpha+1} \right] \quad (41)\end{aligned}$$

The displacement field in the plastic region is determined from the integration of the following strain-displacement relationships :

$$u_{\theta} = 0 \quad u_r = r\epsilon_{\theta}$$

In this case the closure of the tunnel is :

$$\frac{u_a}{a} = \frac{\sigma_c}{2G} (1-\nu) \left[ s \left( 1 + \frac{m+1}{m+\alpha} \left( \left( \frac{R}{a} \right)^{m+\alpha} - 1 \right) \right) + (1-s) \left( \frac{R}{a} \right)^{\alpha+1} \right] \quad (42)$$

And the corresponding normalized closure is :

$$\frac{u_{e.pl.}}{u_{el.}} = \frac{\sigma_c}{2G} \left[ s \left( 1 + \frac{m+1}{m+\alpha} \left( \left( \frac{R}{a} \right)^{m+\alpha} - 1 \right) \right) + (1-s) \left( \frac{R}{a} \right)^{\alpha+1} \right] \quad (43)$$

## 2.5 Elastic - strain weakening material

This model assumes that the strength loss after peak is strain-dependent. The "plastic" criterion is then strain-dependent ; it is :

$$\sigma_{\theta} = m\sigma_r + \sigma_c \left( 1 - \frac{\epsilon_{\theta} - \epsilon_r}{\gamma} \right) \quad (\epsilon_{\theta} - \epsilon_r) < \gamma < \infty \quad (44)$$

The solution is more complicated but the system is isostatic.

The coefficient  $\gamma$  is a measure of the after peak slope of the stress-strain curve of the strain-weakening model





The constitutive relationships are :

→ equilibrium equation

$$\frac{d\sigma_r}{dr} = \frac{\sigma_\theta - \sigma_r}{r}$$

→ plastic criterion

$$\sigma_\theta = m\sigma_r + \sigma_c \left(1 - \frac{\epsilon_\theta - \epsilon_r}{\gamma}\right)$$

→ Hooke's law

$$\epsilon_\theta^e = \frac{1-\nu^2}{E} \left( \sigma_\theta - \frac{\nu}{1-\nu} \sigma_r \right)$$

$$\epsilon_r^e = \frac{1-\nu^2}{E} \left( \sigma_r - \frac{\nu}{1-\nu} \sigma_\theta \right)$$

→ flow rule

$$\epsilon_r^p + \alpha \epsilon_\theta^p = 0$$

→ total strain

$$\epsilon_\theta = \epsilon_\theta^p + \epsilon_\theta^e \quad ; \quad \epsilon_r = \epsilon_r^p + \epsilon_r^e$$

→ compatibility equation

$$r \frac{d\epsilon_\theta}{dr} + \epsilon_\theta - \epsilon_r = 0$$

This system is isostatic: 8 unknown and 8 equations. However, the solution is difficult as the derivation ends up to a differential equation of the second order with variable coefficients, and needs numerical treatment.



### APPENDIX A3

#### A3.1 Correction of Data for a Non-Isotropic Loading

The method which is described in the following, shows how to find an elastic reference value to calculate the normalized closure if the N-value ( $N = \sigma_h^0 / \sigma_v^0$ ) varies slightly around 1. This method does not overcome the problem of the non-validity of the normalized closure concept if N is different from 1, but permits to get more consistent results for the experimental normalized closure.

The regular method, as described in Chapter 5, takes as a elastic reference line a straight line through the two first points of the long term loading curve. The N-value is assumed to be constant during the test. Actually at each experimental point corresponds a particular value of the parameter N, calculated from the load-cells measurements.

At each point the secant modulus of elasticity is theoretically given by :

$$SL = \frac{2(1-\nu^2)}{E} X_{\alpha} = A X_{\alpha} \quad (1)$$

where  $X_{\alpha}$  is a function of the ratio N only and depends on the direction <sup>$\alpha$</sup>  of the measurement with respect to the external stress axes. If  $\alpha$  is the angle between the direction of the closure measuring gauge and the direction of the maximum external stress,  $X_{\alpha}$  is given by :

$$X^0 = \frac{3N-1}{2} ; X^{135} = X^{45} = \frac{N+1}{2} ; X^{90} = \frac{3-N}{2} \quad (2)$$

Considering the first two points (1&2) of the experimental curve, the knowledge of the corresponding N-values will allow to calculate their appropriate  $X_{\alpha}$ -values ( $X_{\alpha 1}$  &  $X_{\alpha 2}$ ). If SL1 and SL2 are the secant moduli of the curve at points 1 and 2 respectively, they are :

$$SL1 = \frac{2(1-\nu^2)}{E} X_{\alpha 1} ; SL2 = \frac{2(1-\nu^2)}{E} X_{\alpha 2} ; \frac{SL1}{SL2} = \frac{X_{\alpha 1}}{X_{\alpha 2}} \quad (3)$$

If  $\epsilon^1$  and  $\epsilon^2$  are the values of the total abscissa of the points 1 and 2, and if  $\sigma^1$  and  $\sigma^2$  are the values of the stress at points 1 and 2, SL1 and SL2 may be determined as a function of the strain



corresponding to the closure of the cracks  $\epsilon_{c1}$  :

$$SL1 = \frac{\epsilon^1 - \epsilon_{c1}}{\sigma^1} \quad ; \quad SL2 = \frac{\epsilon^2 - \epsilon_{c1}}{\sigma^2} \quad (4)$$

From the equations 3 and 4 it is possible to get the expression for the crack closure strain :

$$\epsilon_{c1} = \frac{\epsilon^1 X_{\alpha 2} \sigma^2 - \epsilon^2 X_{\alpha 1} \sigma^1}{X_{\alpha 2} \sigma^2 - X_{\alpha 1} \sigma^1} \quad (5)$$

The value of the elastic parameter can be also evaluated :

$$A = \frac{2(1-\nu^2)}{E} = \frac{\epsilon^2 - \epsilon^1}{X_{\alpha 2} \sigma^2 - X_{\alpha 1} \sigma^1} \quad (6)$$

For the next points the value of N will give the  $X_{\alpha}$ -value, which will allow to calculate the elastic secant slope  $SL^{\alpha}$  by multiplying by the A-value independent of the N-parameter. :

$$SL = A X_{\alpha}$$

The elastic reference strain is then known. The subtraction from the total experimental elasto-plastic strain of the crack closure strain  $\epsilon_{c1}$  will give the elasto-plastic closure to be used to calculate the normalized closure :

$$\text{norm.clos.} = \frac{\epsilon_t - \epsilon_{c1}}{A X_{\alpha} \sigma} \quad (7)$$





### A 3.2 Influence of the Intermediate Principal Stress

---

In the model test, the longitudinal stress  $\sigma_z$  is assumed to be a function of the other stresses, as the model sample is loaded under plane strain conditions.

$$\sigma_z = \nu(\sigma_r + \sigma_\theta) \quad (1)$$

This relation is also valid in the plastic zone. But in this zone the radial and tangential stress are related by a failure criterion;

$$\sigma_\theta = m\sigma_r + \sigma_c \quad (2)$$

The combination of these equations will give the following expression for the longitudinal stress:

$$\sigma_z = \nu(\sigma_r(1+m) + \sigma_c) \quad (3)$$

When loading proceeds, the elastic-plastic radius  $R$  attains a value  $\tilde{R}$  such that :

$$\begin{aligned} \tilde{\sigma}_{zR} &= \tilde{\sigma}_{rR} \\ \text{or } \tilde{\sigma}_z &= \frac{\nu\sigma_c}{1-\nu(1+m)} \end{aligned} \quad (4)$$

In the elastic zone the relation (1) is equivalent to :

$$\sigma_z = 2\nu\sigma_0 \quad (5)$$

where  $\sigma_0$  is the external stress. In the elastic zone, the longitudinal stress is constant. To the critical value  $\tilde{\sigma}_z$  corresponds by the relation (5) a value of the external stress  $\tilde{\sigma}_0$  :

$$\tilde{\sigma}_0 = \frac{\sigma_c}{2(1-(1+m)\nu)} \quad (6)$$

At the upper limit of the loading range of the compression machine, the external stress is equal approximately to 17 MPa. In order to have the longitudinal stress as the intermediate principal stress, in loading the sample, the Poisson's ratio has to be higher than a critical value given by the relation (6).

Numerical application :  $m=3$  ( $\phi=30^\circ$ ),  $C=4\text{MPa}$ ,  $\sigma_c=13.87\text{ MPa}$  :

$$\tilde{\sigma}_0 = 17\text{ MPa} \rightarrow \tilde{\nu} = 0.148$$

Poisson's ratio may be expected to be bigger than 0.15, and



the failure criterion (2) will be assumed to be valid throughout the test.

This section is based on a paper by Florence and Schwer(1978). The authors explained the formation of three different regions around an opening;right around the cavity,a first annular region obeys the criterion (2);away from the tunnel the longitudinal stress is the minimum principal stress and the failure criterion is then :

$$\sigma_{\theta} = m\sigma_z + \sigma_c \quad (7)$$

The third zone is located between the two other zones,as the longitudinal and the radial stress are equal in this third zone.The stresses obey both failure criteria (2) and (7).These three plastic regions develop one after the other ,and in the model test,it is assumed that only the first zone develops within the loading range of the compression machine.



### A 3.3 Volume Change

The total volume affected by plastic deformations around the tunnel is :

$$V = \pi \left( \left( \frac{R}{a} \right)^2 - 1 \right) \quad (1)$$

At each point of this body under plane strain condition, the volumetric strain  $e(r)$  is given by :

$$e(r) = \epsilon_r + \epsilon_\theta \quad (\epsilon_z = 0) \quad (2)$$

The change in volume is equal to the integration of the volumetric strain over the whole yielding volume.

$$\Delta V = \int_{\theta=0}^{2\pi} \int_{r=a}^R e(r) r d\theta dr \quad (3)$$

In the plastic zone the volumetric strain is given by :

$$e(r) = \underbrace{\epsilon_r^e + \epsilon_\theta^e}_{\text{elastic}} + \underbrace{\epsilon_r^p + \epsilon_\theta^p}_{\text{plastic}} = \epsilon_r + \epsilon_\theta \quad (4)$$

#### Volumetric strain

##### a) Elastic part

Equation 28 in Appendix A2 gives the elastic strain distribution in the plastic zone. From these expressions it follows :

$$e(r)^{el} = \frac{\sigma_c (1-2\nu)}{2G(m-1)} \left[ \left( \frac{r}{a} \right)^{m-1} (m+1) - 2 \right] \quad (5)$$

This expression may also be written as follow :

$$e(r)^{el} = \left( \frac{\Delta V}{V} \right)_{\text{ext}} + \frac{1-2\nu}{2} \frac{\sigma_c}{G} \frac{m+1}{m-1} \left( \frac{R}{a} \right)^{m-1} \left[ \left( \frac{r}{R} \right)^{m-1} - 1 \right] \quad (6)$$

where  $\frac{\Delta V}{V}_{\text{ext}}$  is the constant volumetric strain in the elastic zone and also the external volume change due to the displacement of the external boundaries.

##### b) Plastic part

From the flow rule in the plastic zone (equation 26 - A2), the volumetric strain in the plastic zone is given by :

$$e(r)^p = \epsilon_r^p + \epsilon_\theta^p = (1-\alpha) \epsilon_\theta^p \quad (7)$$

for the plastic part of the strains.



The substitution in equation 7 of the value of  $\epsilon_{\theta}^p$  given by the equation A2-31 gives the following expression :

$$e(r)^p = (1-\alpha) \frac{1-\nu}{2} \frac{\sigma_c}{G} \frac{m+1}{m-\alpha} \left(\frac{r}{a}\right)^{m-1} \left[\left(\frac{R}{r}\right)^{m+\alpha} - 1\right] \quad (8)$$

### Integration of the volumetric strain

The integration of equation 6 and 7 according to the expression given by equation 3 will give the change in volume occurring with plastic deformations. This change in volume may be divided by the volume of the plastic zone ( equation 1 ) to obtain an "average volume change".

In the following, expressions for the average volume change are given (for the elastic and plastic component of the strain). The combination of these expressions will give the total volume change. This is illustrated in Figure 5.1 in Chapter 5.

-elastic :

$$e_e = \left(\frac{\Delta V}{V}\right)_{\text{ext}} \frac{\sigma_{rR}}{\sigma^0} \frac{R^2}{R^2 - a^2} \quad (9)$$

where  $\sigma_{rR}$  is the radial stress at the boundary elasto/plastic (equation A2 - 22) and  $\frac{\Delta V}{V}_{\text{ext}}$  the external volume change given by the following expression:

$$\left(\frac{\Delta V}{V}\right)_{\text{ext}} = \frac{2 \sigma^0 (1+\nu)(1-2\nu)}{E} \quad (10)$$

-plastic :

$$e_p = \frac{1-\nu}{m+\alpha} \frac{\sigma_c}{2G} \frac{1}{\frac{R^2}{a^2} - 1} \left[ (m+\alpha) \left(\frac{R}{a}\right)^{m+1} - (m+1) \left(\frac{R}{a}\right)^{m+\alpha} + 1 - \alpha \right] \quad (11)$$

$$e = e_e + e_p \quad (12)$$





## APPENDIX A4

### DETERMINATION OF ELASTIC PARAMETERS IN THE MODEL TEST

#### Introduction

The purpose of this appendix is to present two methods which have been developed to determine the elastic parameters of the coal specimen used in the model test. As the loading is not uniaxial, the elastic response of the instruments is a function of two elastic parameters. The methods presented hereafter compare the responses of two different instruments in order to eliminate one of these unknown elastic parameters.

#### Instrument responses

##### - Internal Strain Gauge :

$$\epsilon = \frac{\sigma^0(1-2\nu)}{2G} - \frac{\sigma^0}{2G} \frac{a^2}{d^2-e^2} \quad C = \frac{a^2}{d^2-e^2} \quad (1)$$

- where
- $\epsilon$  is the engineering strain resulting from the analysis of the data by the computer codes and appearing on the plots
  - $d$  is the distance from the centre of the tunnel to the middle of the strain gauge
  - $e$  is half the length of the strain gauge
  - $\sigma^0$  is the applied external stress assumed hydrostatic.

In the remainder of this appendix the internal strain gauge will be characterized by a constant  $C$  which is determined with the location of the gauge.

##### - Tunnel closure :

$$\epsilon = \frac{2 \sigma^0(1-\nu^2)}{E} \quad (2)$$

##### - External Displacement :

$$\epsilon = \frac{\sigma^0(1+\nu)}{E} (1-2\nu) + \frac{\sigma^0(1+\nu)}{E} \frac{a^2}{b^2} \quad (3)$$

where  $b$  is the distance from the centre of the tunnel to the boundary where the displacement is measured.



### First method

This method compares the responses of the same internal strain gauge before and after the tunnel is drilled.

#### - Assumptions

- \*  $\epsilon^1$  is the response of the gauge before the tunnel is drilled
- \*  $\epsilon^2$  is the response after the tunnel has been drilled.
- \* the loading rates are similar for the two loadings.
- \* no yielding occurs
- \* the elastic properties are not significantly affected by the loading history after the specimen has experienced several previous loadings.
- \* the specimen is homogeneous

#### - Derivation

If the function  $A(\sigma)$  is supposed to be :

$$A(\sigma) = \frac{\sigma(1+\nu)}{E} \quad (4)$$

the responses  $\epsilon^1$  and  $\epsilon^2$  may be written as follows :

$$\begin{aligned} \epsilon^1 &= A(\sigma^0) (1-2\nu) \\ \epsilon^2 &= A(\sigma^0) (1-2\nu-C) \end{aligned} \quad (5)$$

The elimination of the function  $A(\sigma^0)$  between the two equations 5 leads to an expression of the Poisson's ratio  $\nu$  :

$$\nu = \frac{1}{2} \frac{\epsilon^1(1-C) - \epsilon^2}{\epsilon^1 - \epsilon^2} \quad (6)$$

with  $-1 < \nu < 0.5$

This method is applied to each of the 16 internal strain gauges.

### Second method

This method compares the external deformation to the tunnel closure in the same direction during a loading of the specimen.

#### - Assumptions

The stresses in the model test are equal to the stresses in an infinite medium around a tunnel, multiplied by a coefficient function of the geometry of the specimen used in the model test.

$$\sigma^0 = \sigma^0 \frac{b^2}{b^2 - a^2}$$

where  $b$  is half the width of the specimen.



But as shown in Chapter 5, the change in stress is not significant and is neglected in this analysis.

The restricting assumptions resulting in the first method from the use of responses during two different loadings are overcome. But instead of 16 measurements the actual method gives only 2 measurements, one in the vertical and one in the horizontal direction.

#### - Derivation

The overall deformation of the sample ( $\epsilon^1$ ) is given by equation 3 of this Appendix. The tunnel closure ( $\epsilon^2$ ) is given by equation 4. The elimination of the same function  $A(\sigma^0)$  between these two expressions leads to an expression for Poisson's ratio.

$$\nu = \frac{\epsilon^2 \frac{1}{2} \left(1 + \frac{a^2}{b^2}\right) - \epsilon^1}{\epsilon^2 - \epsilon^1} \quad (7)$$

#### Results

The results are too erratic to be presented here in detail. However, some remarks may be made about them :

- Poisson's ratio is increasing during loading up to a value around 0.2.
- The knowledge of Poisson's ratio and of the instrument responses make possible the determination of any other elastic parameter.
- Young's and Bulk moduli are also increasing during loading up to values around 2200 MPa and 1000 MPa respectively.

#### Conclusion

The only valuable conclusion of this analysis is that it confirmed a value of Poisson's ratio lower or equal to 0.2 in the planes parallel to the bedding planes.



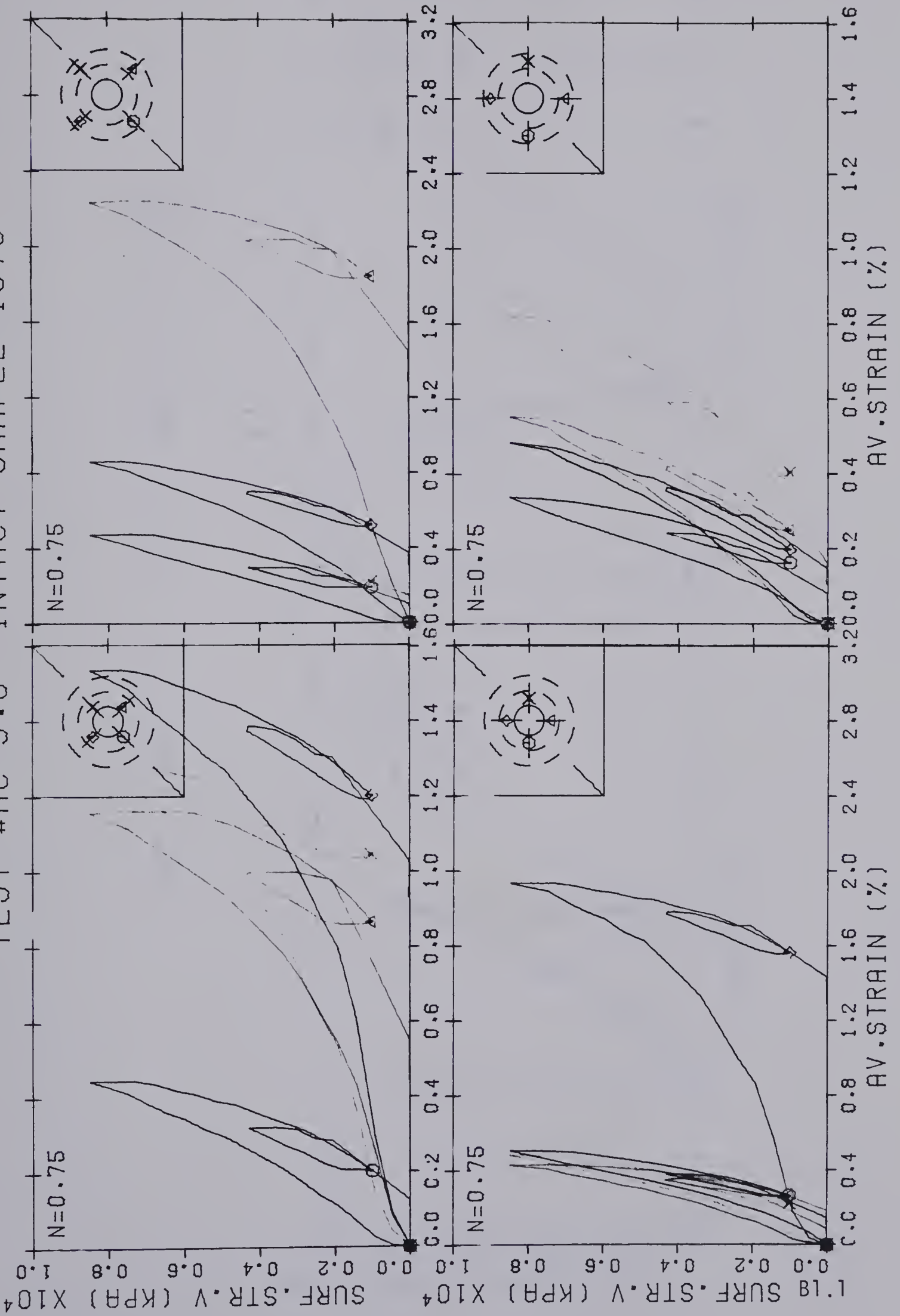


## APPENDIX B1

### STRESS - STRAIN CURVES

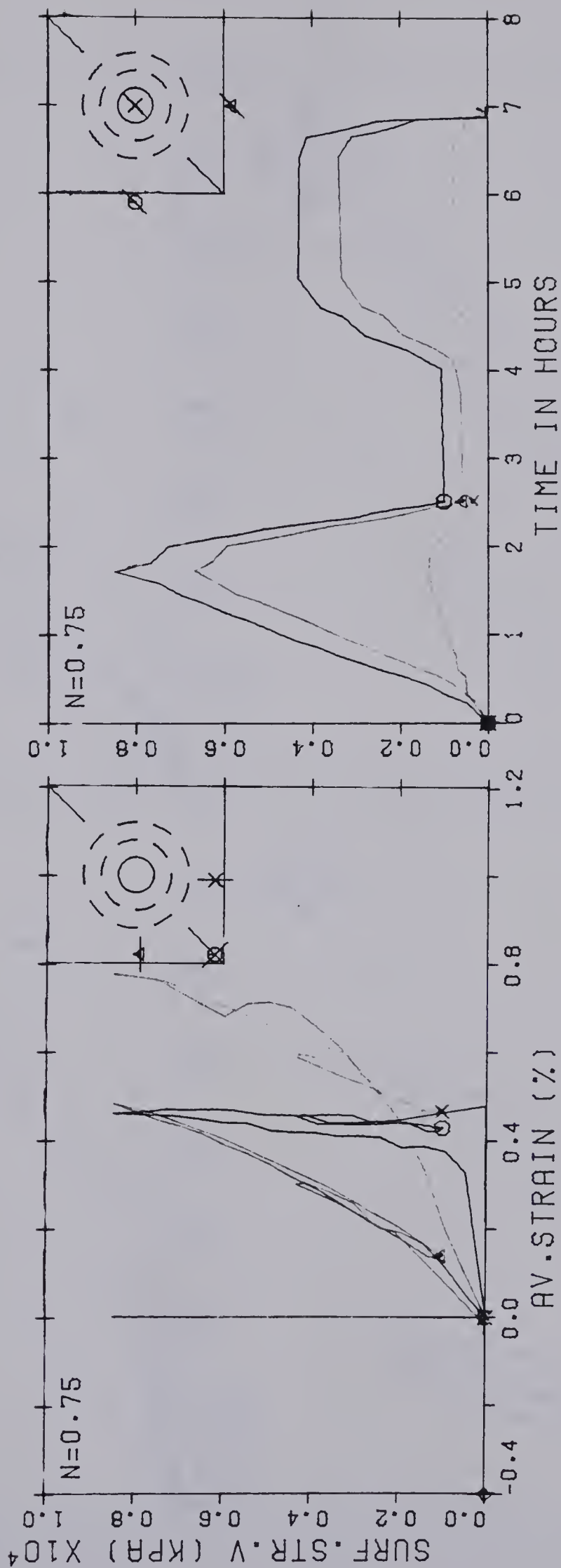


TEST #MC-3.0 INTACT SAMPLE 1978



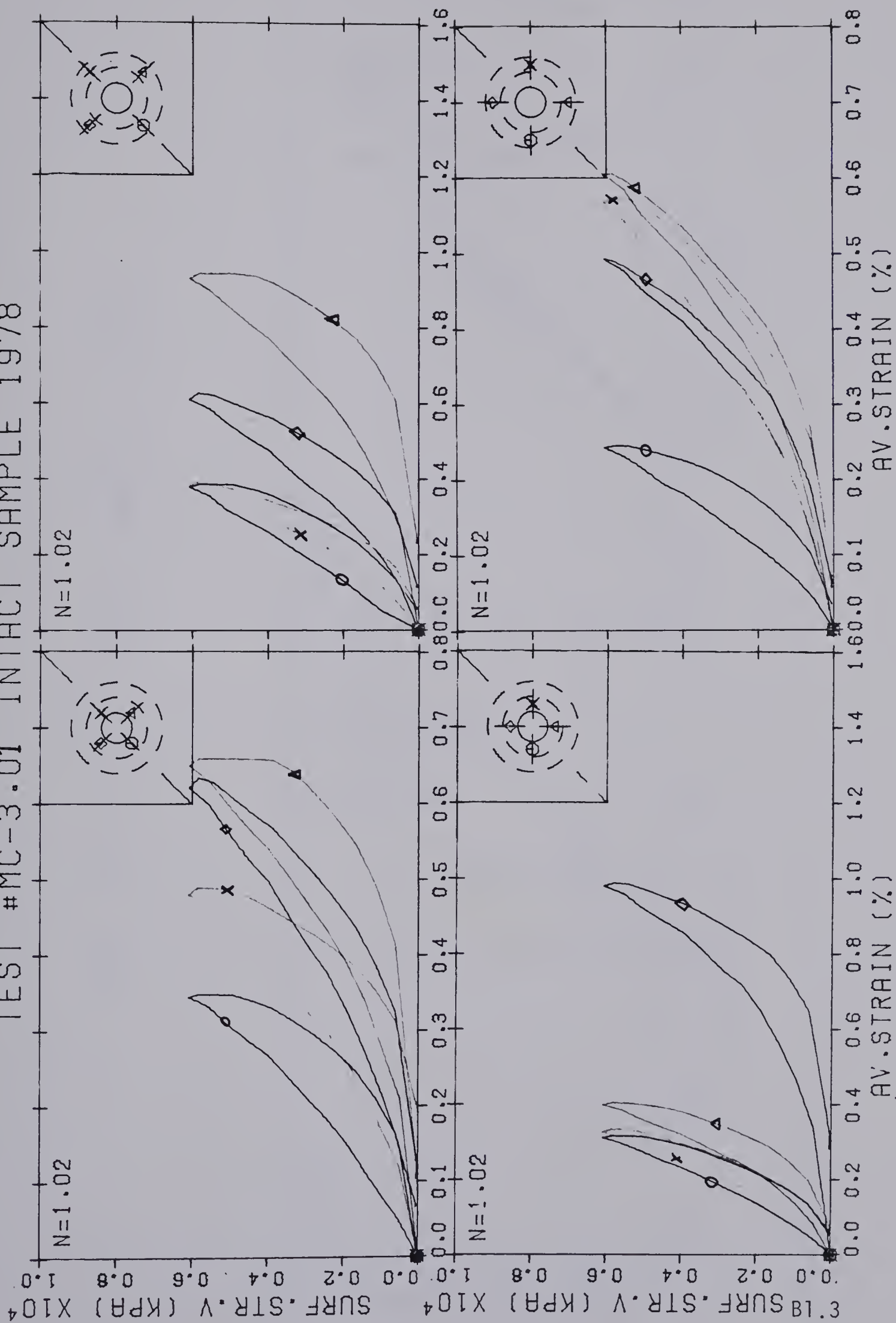


TEST #MC-3.0 INTACT SAMPLE 1978





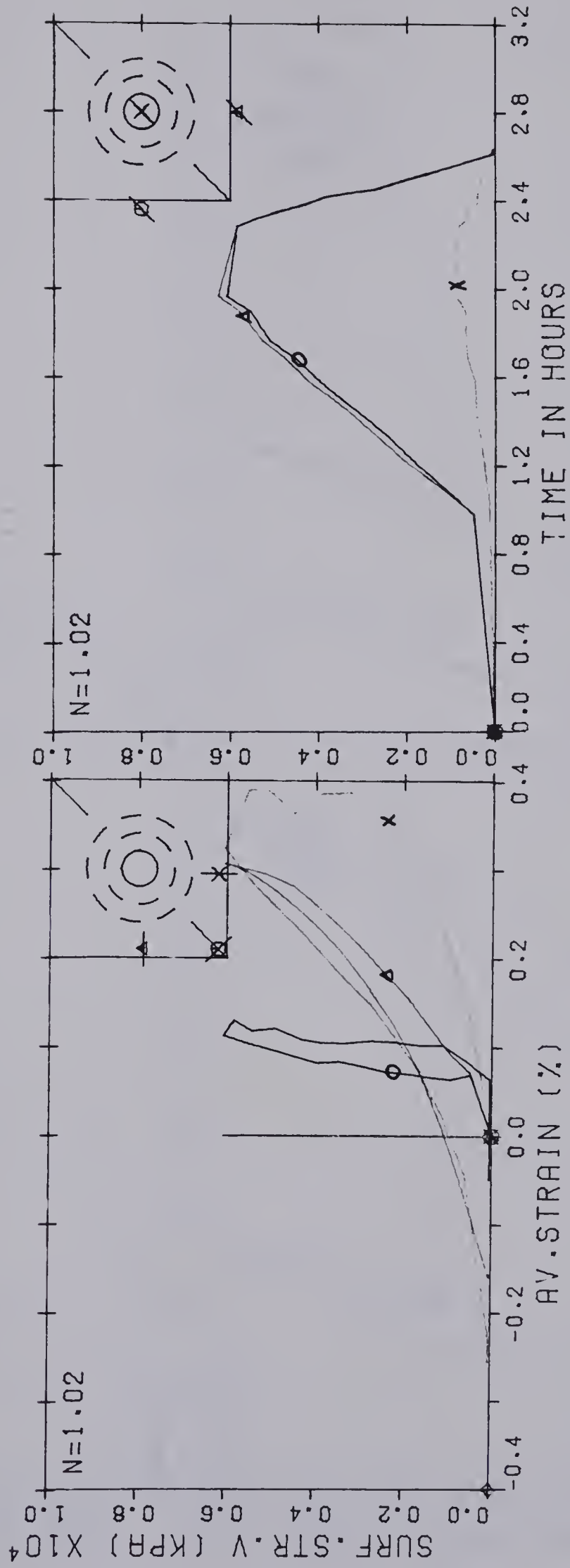
## TEST #MC-3.01 INTACT SAMPLE 1978





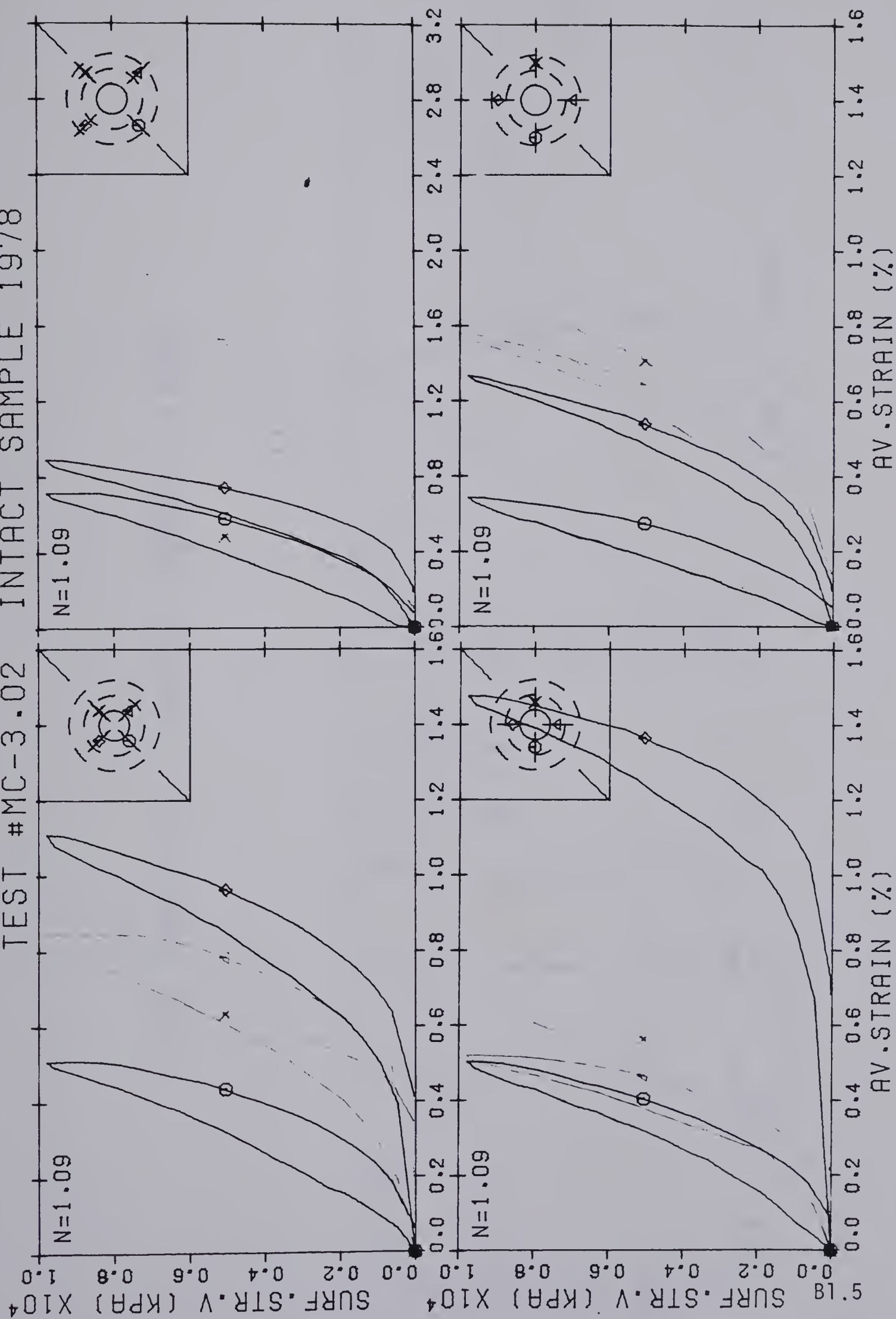


# TEST #MC-3.01 INTACT SAMPLE 1978



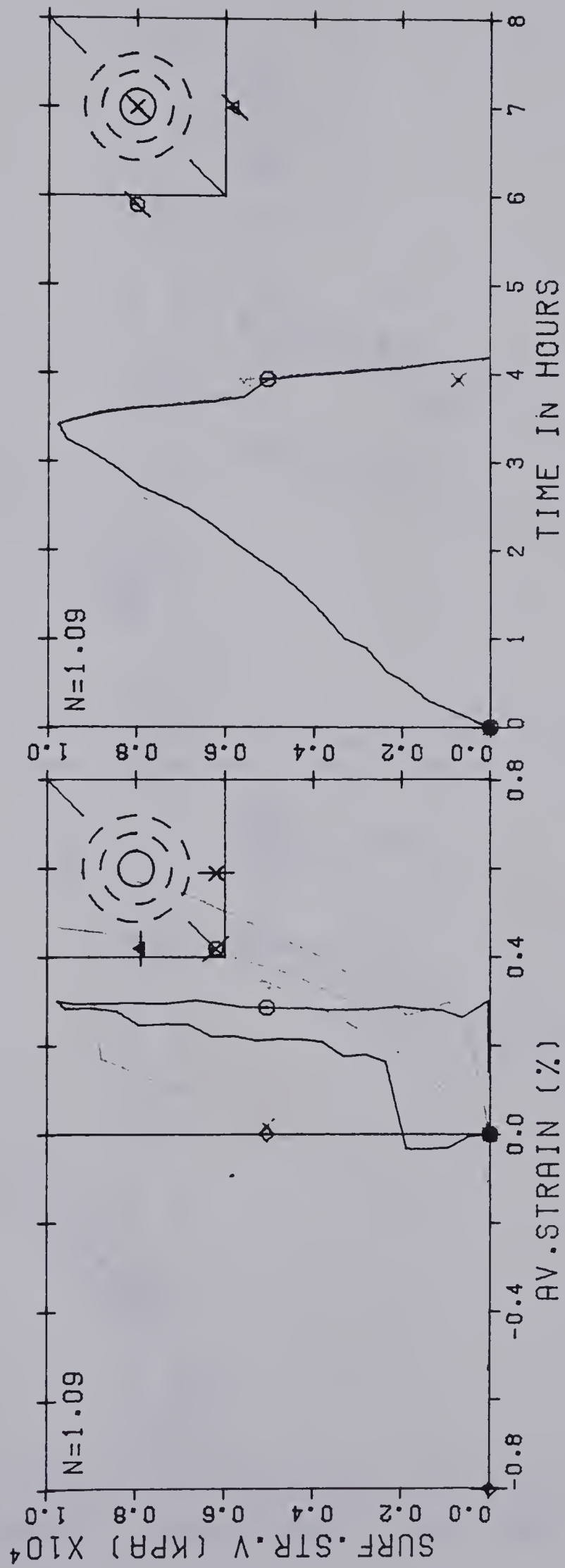


## TEST #MC-3.02 INTACT SAMPLE 1978



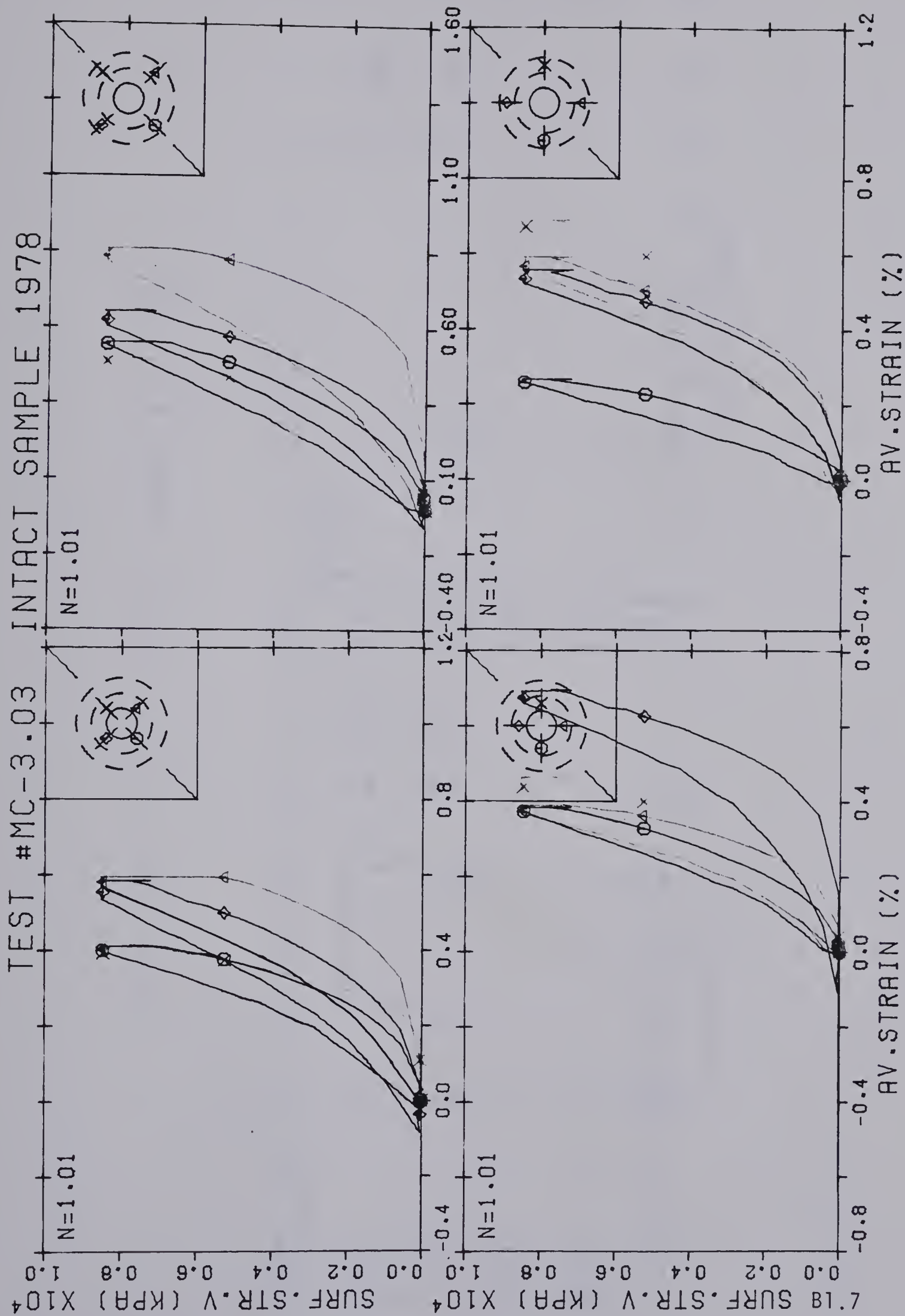


# TEST #MC-3.02 INTACT SAMPLE 1978



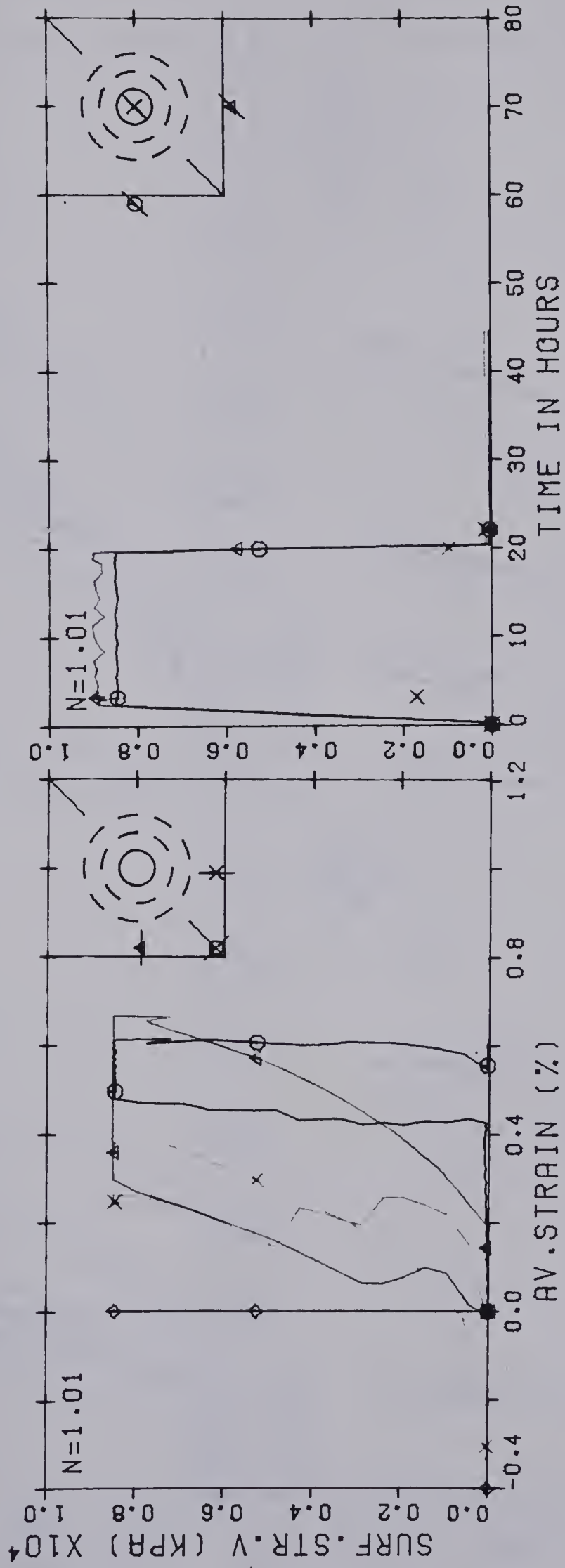




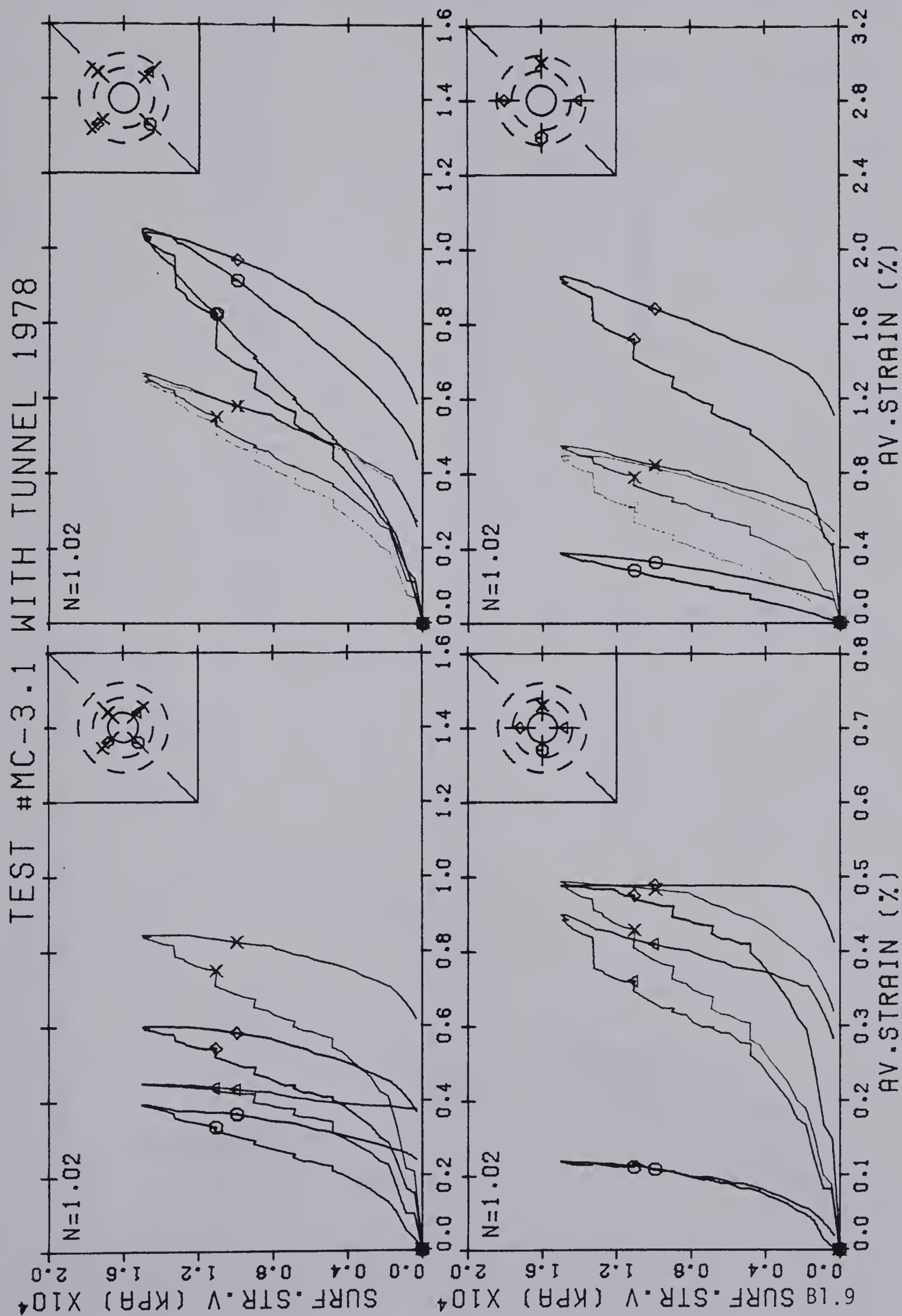




TEST #MC-3.03 INTACT SAMPLE 1978

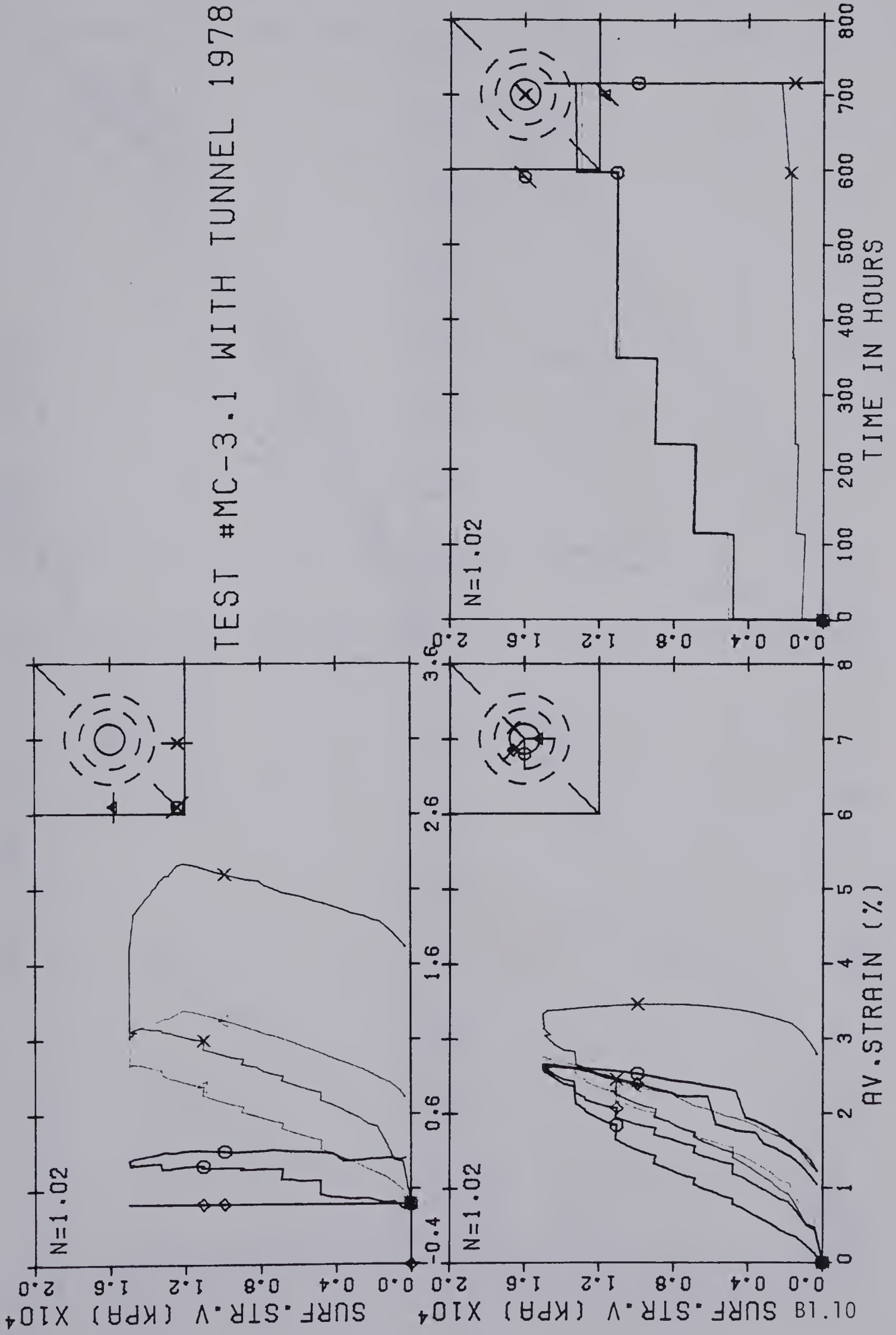








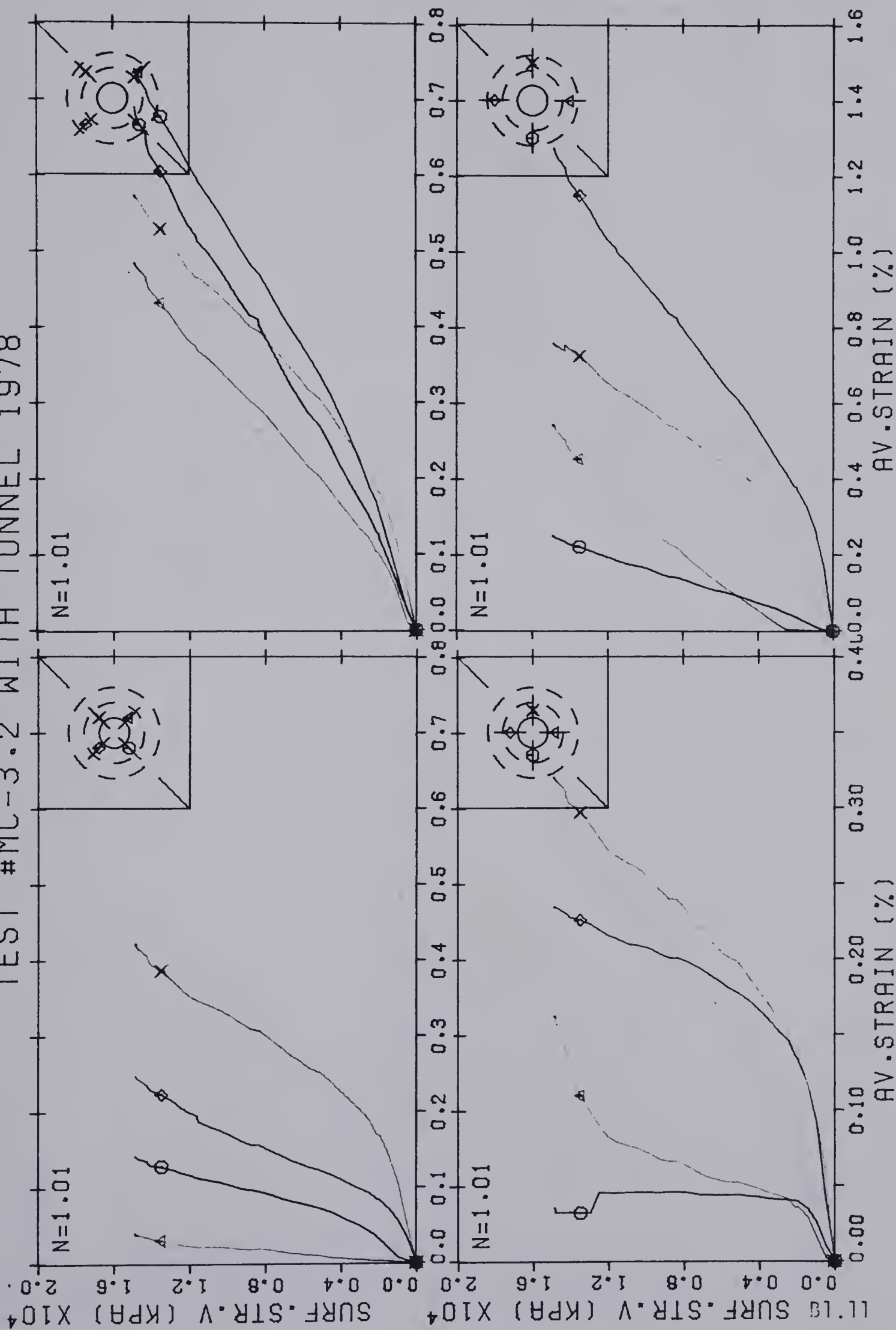
TEST #MC-3.1 WITH TUNNEL 1978





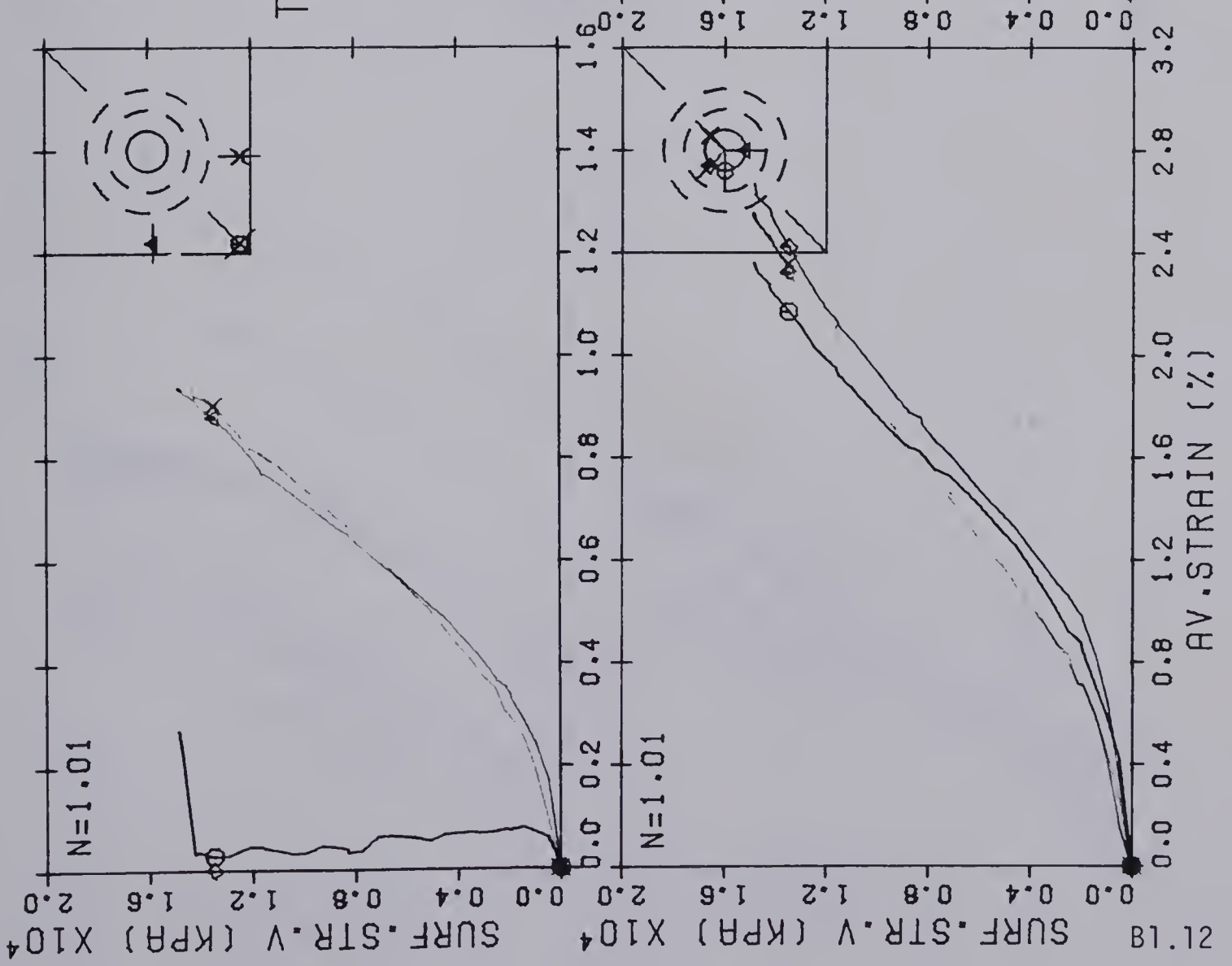


# TEST #MC-3.2 WITH TUNNEL 1978



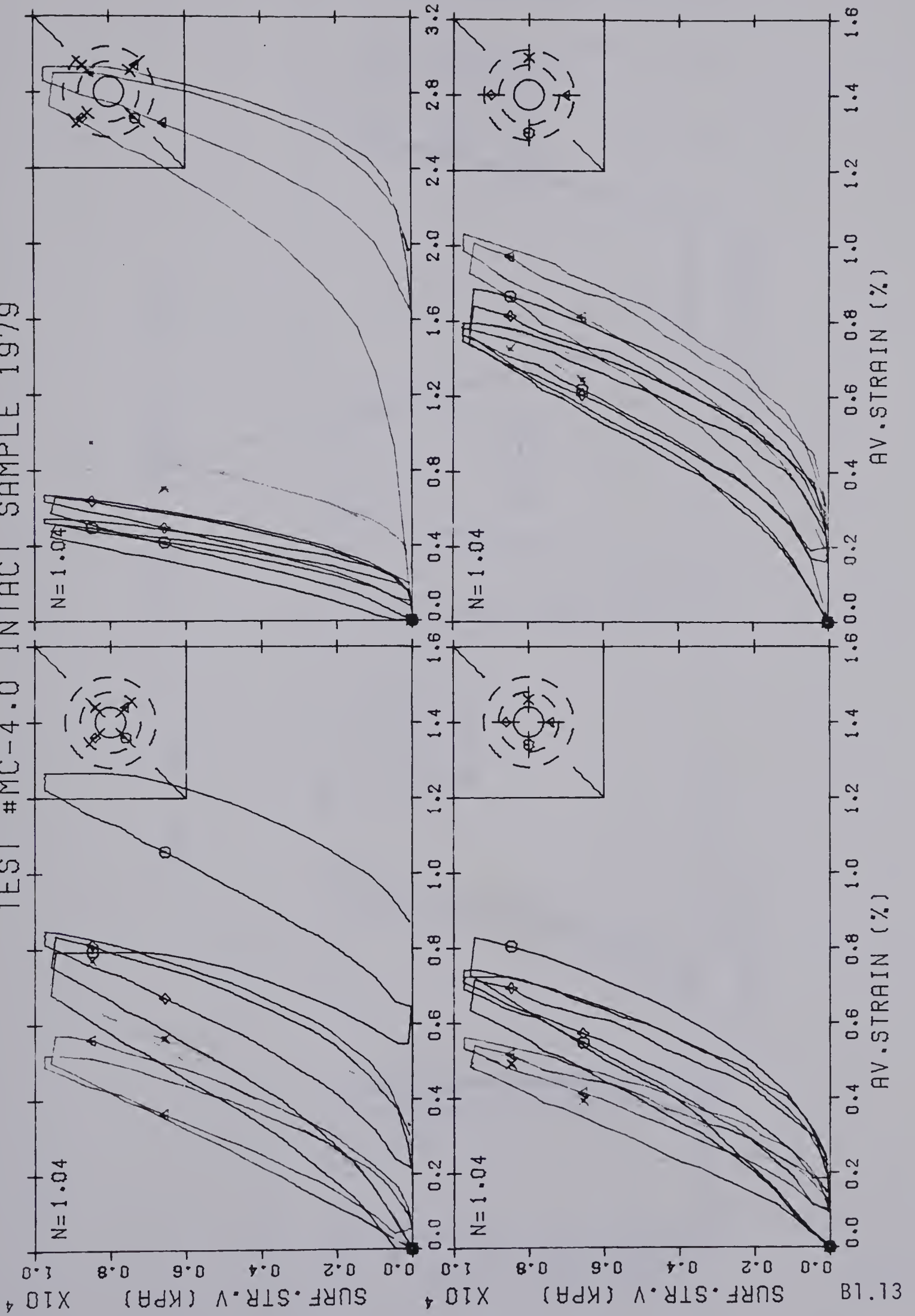


TEST #MC-3.2 WITH TUNNEL 1978





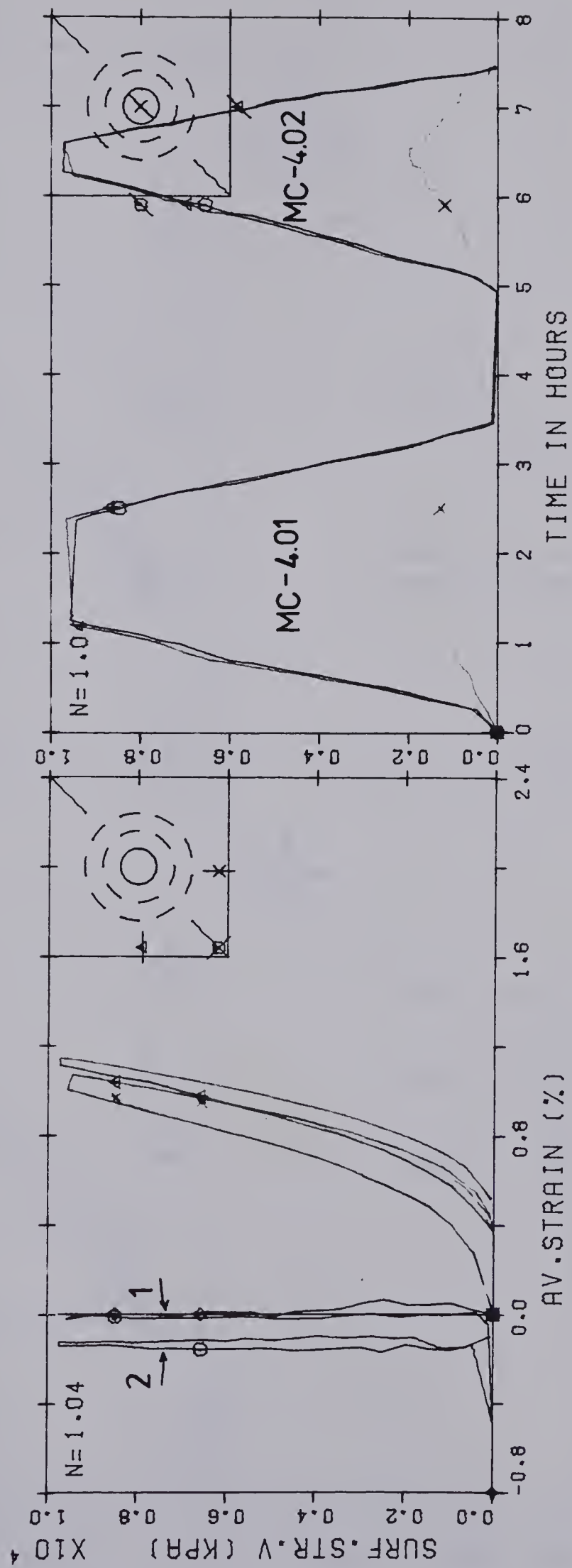
# TEST #MC-4.0 INTACT SAMPLE 1979







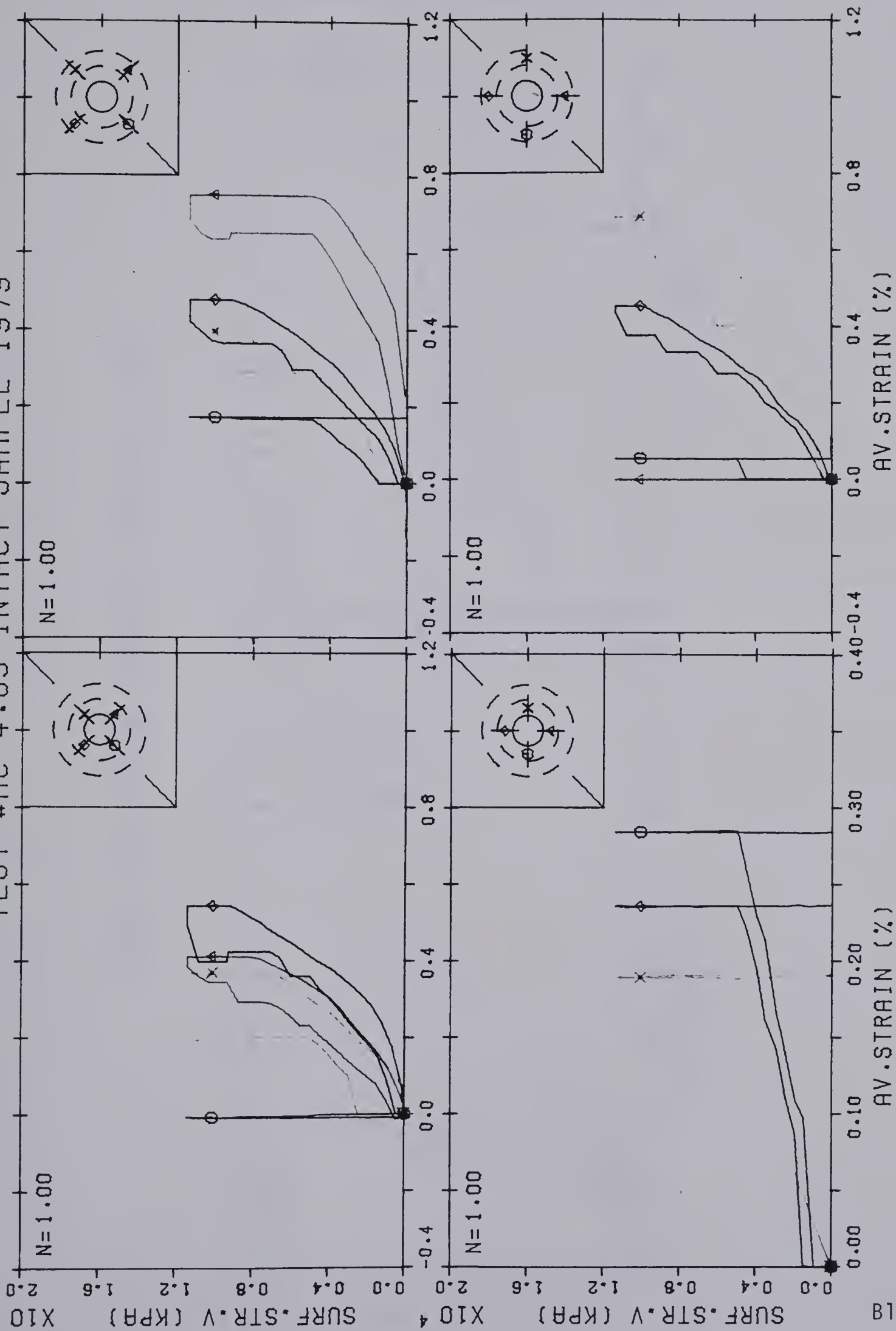
# TEST #MC-4.0 INTACT SAMPLE 1979





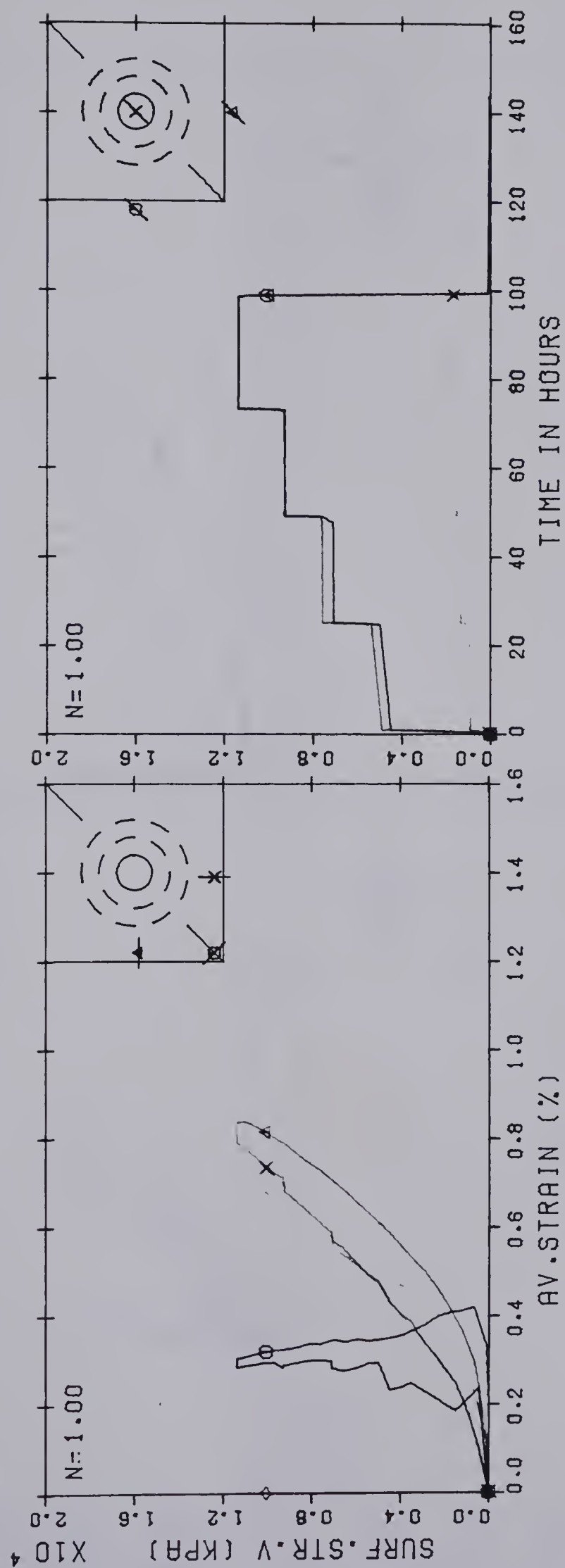
# TEST #MC-4.03 INTACT SAMPLE 1979

51.18



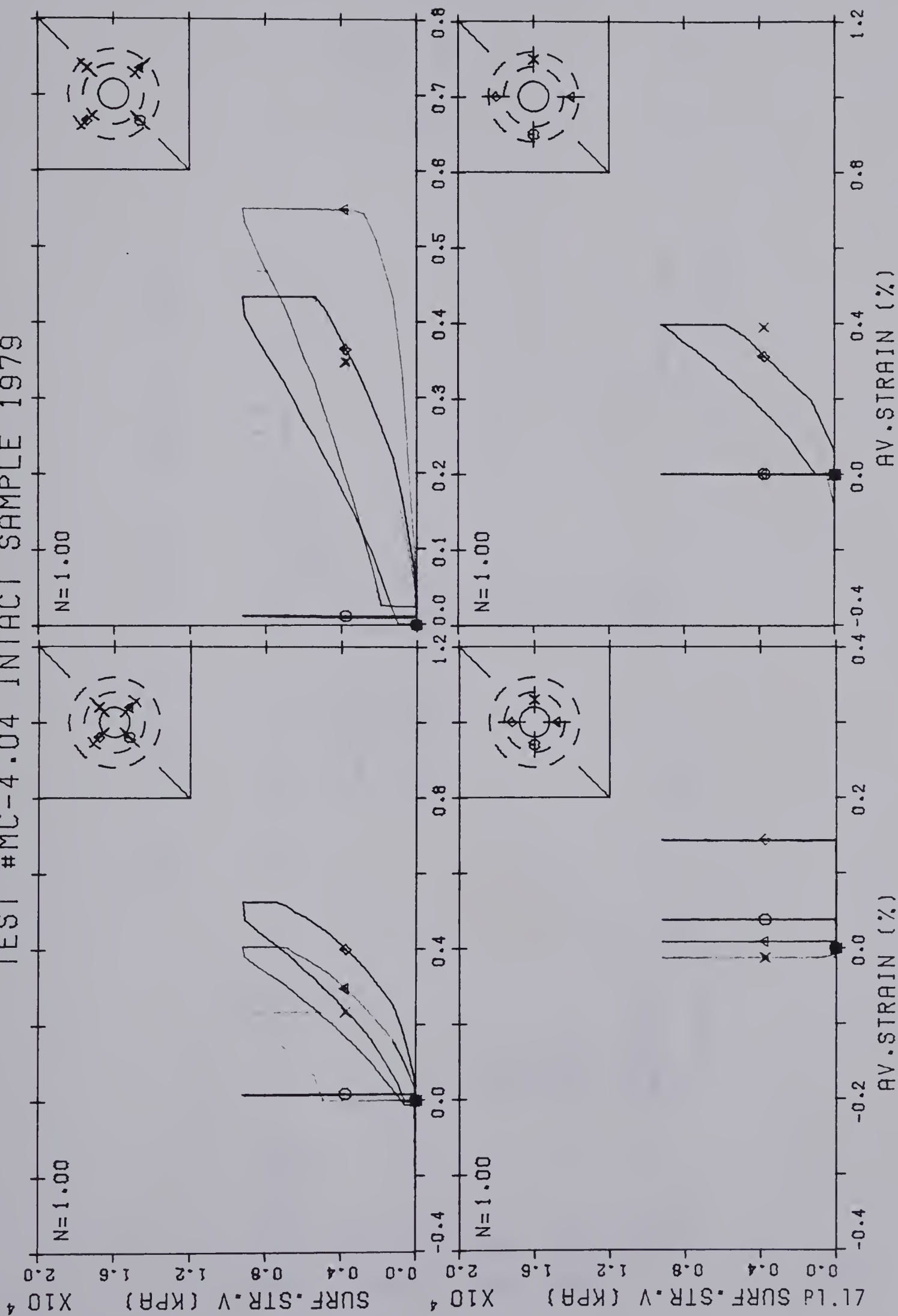


# TEST #MC-4.03 INTACT SAMPLE 1979





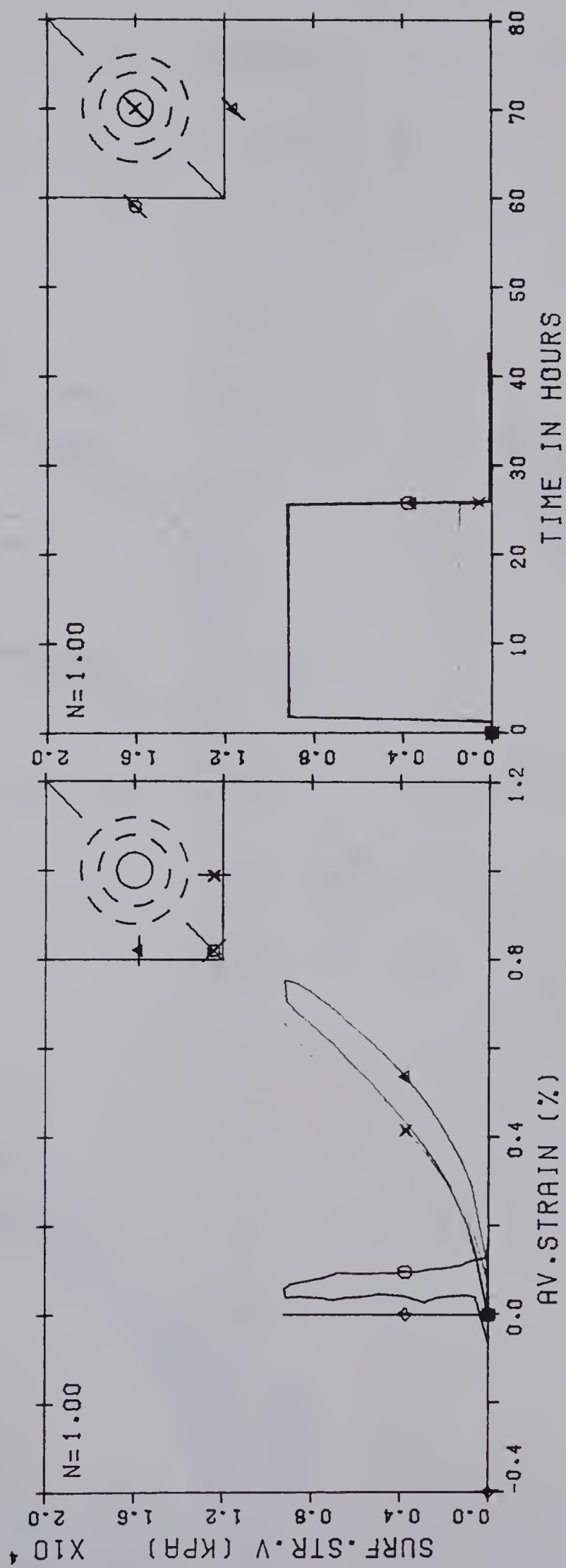
# TEST #MC-4.04 INTACT SAMPLE 1979





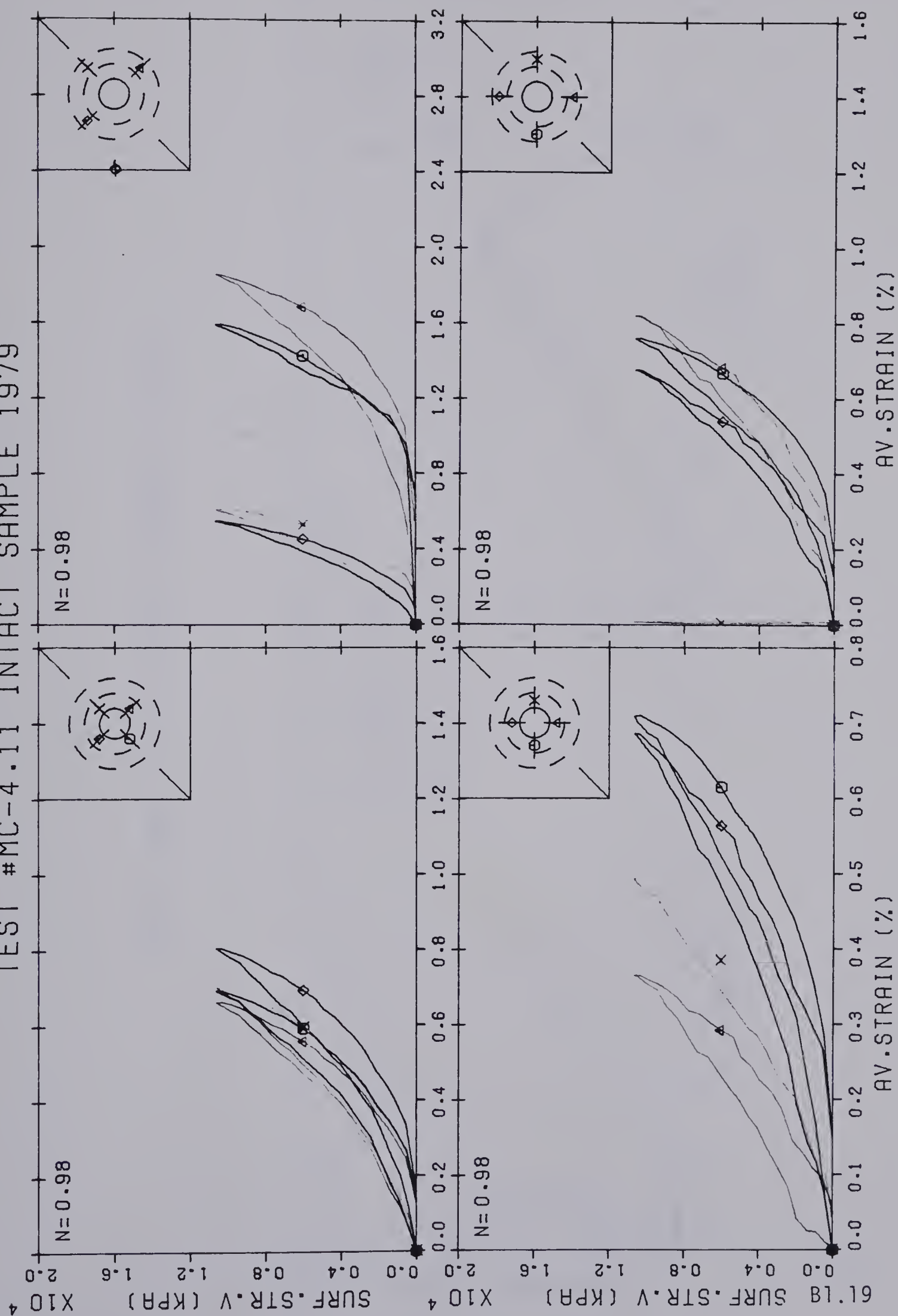


TEST #MC-4.04 INTACT SAMPLE 1979



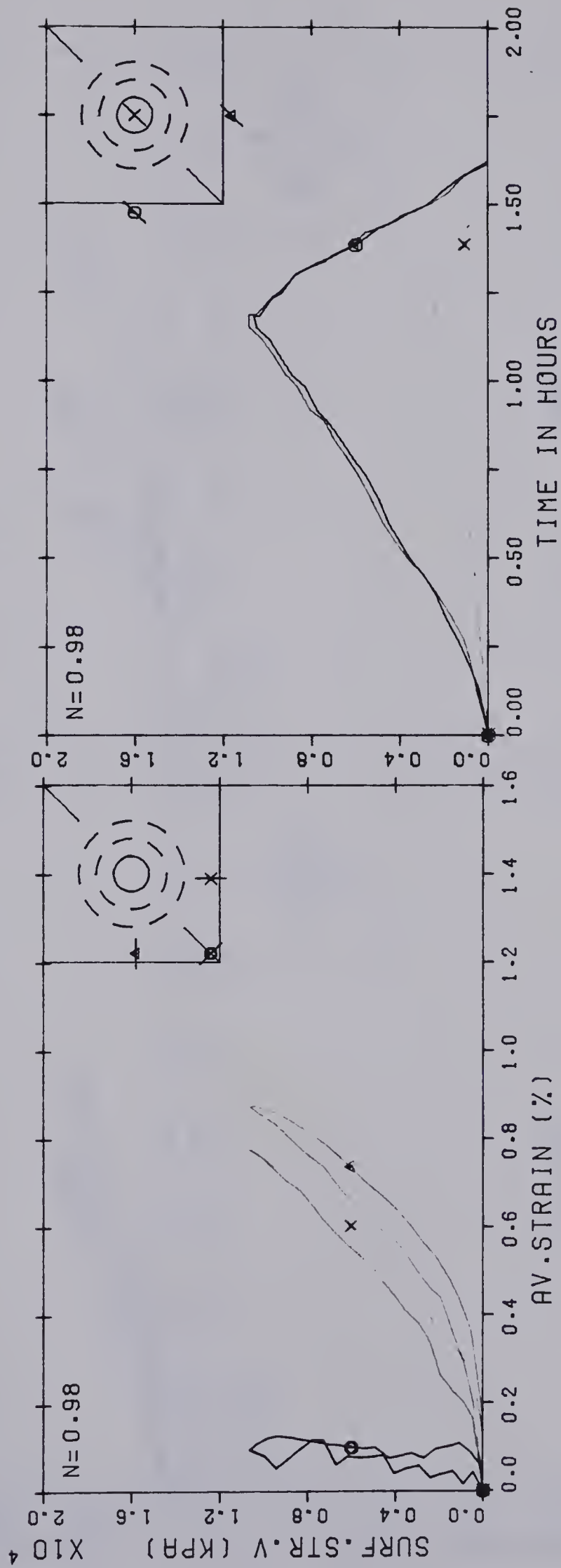


# TEST #MC-4.11 INTACT SAMPLE 1979



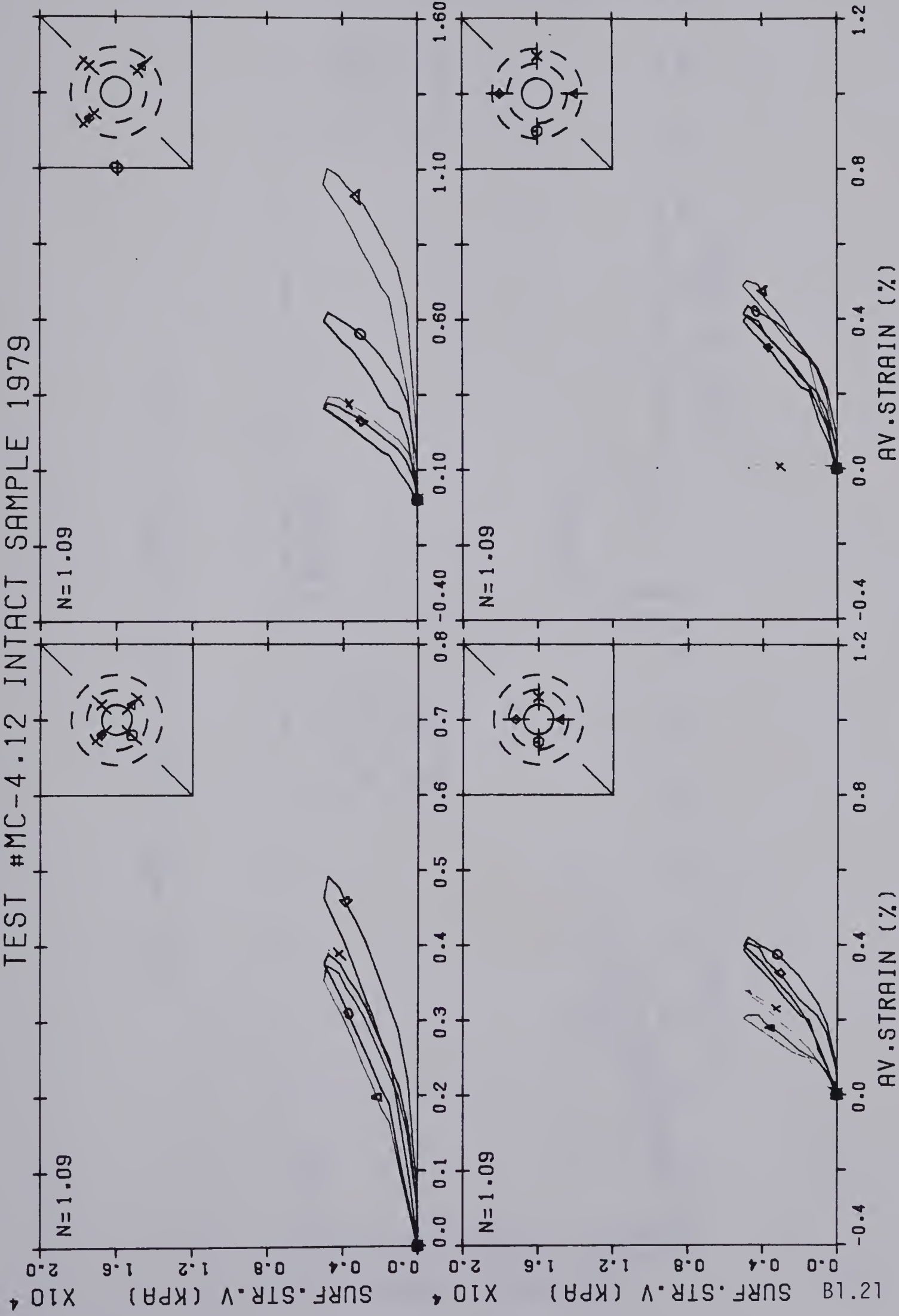


# TEST #MC-4.11 INTACT SAMPLE 1979



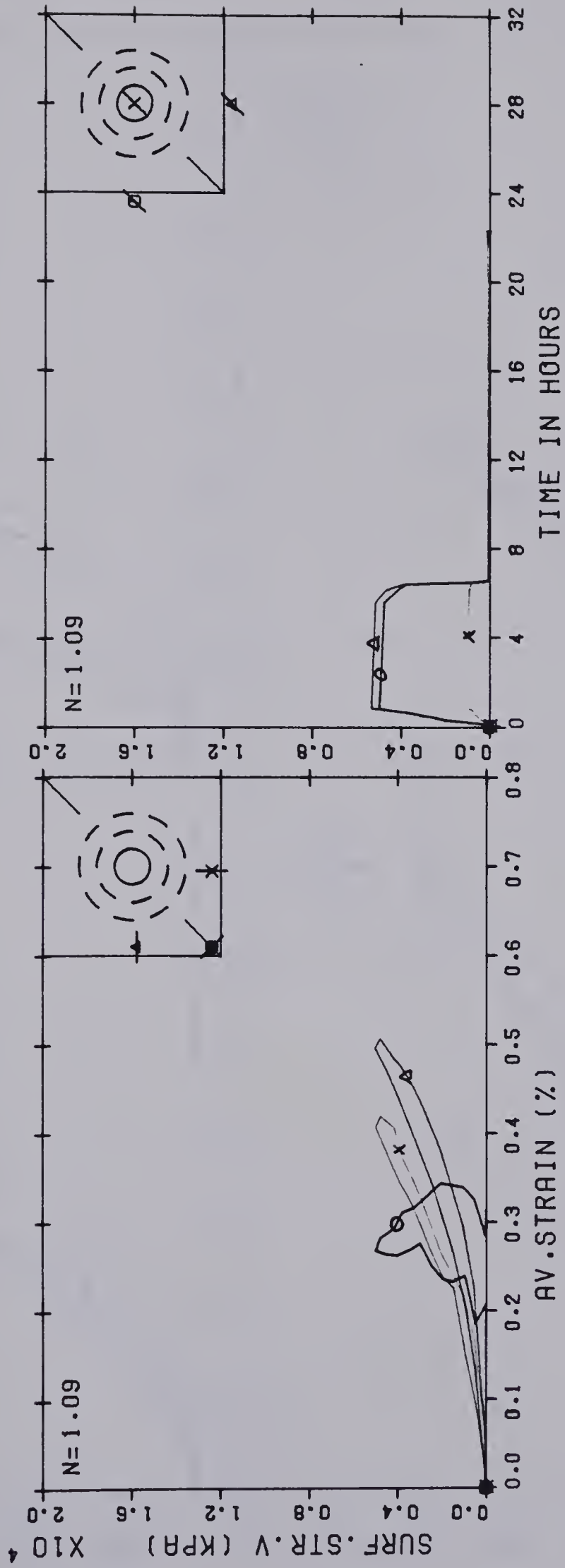






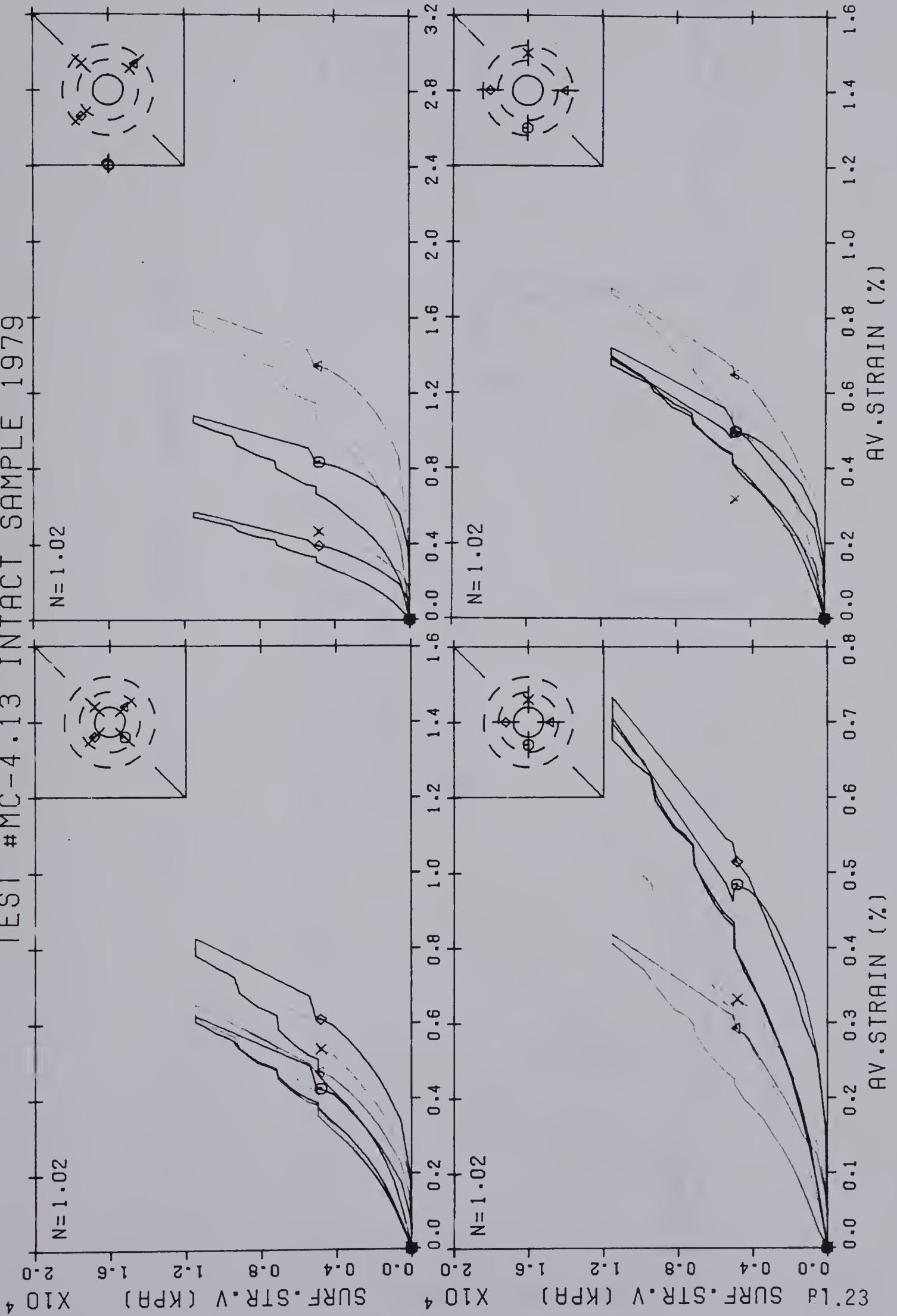


# TEST #MC-4.12 INTACT SAMPLE 1979



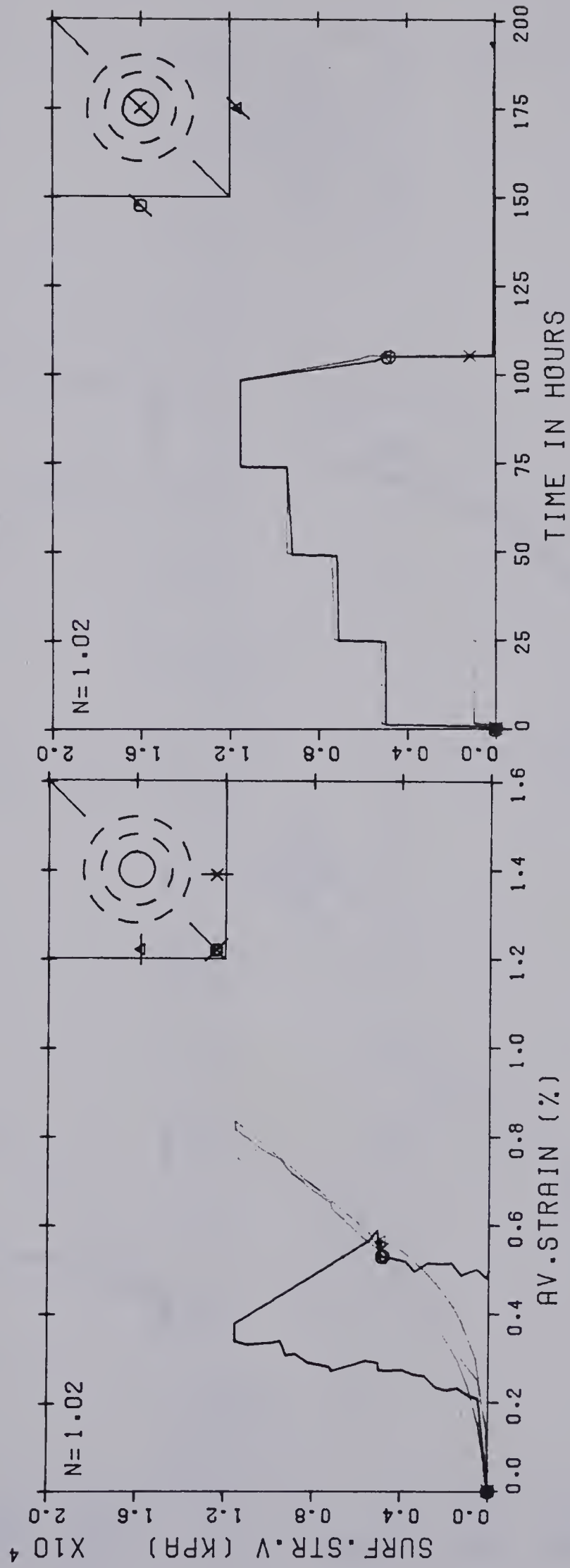


TEST #MC-4.13 INTACT SAMPLE 1979





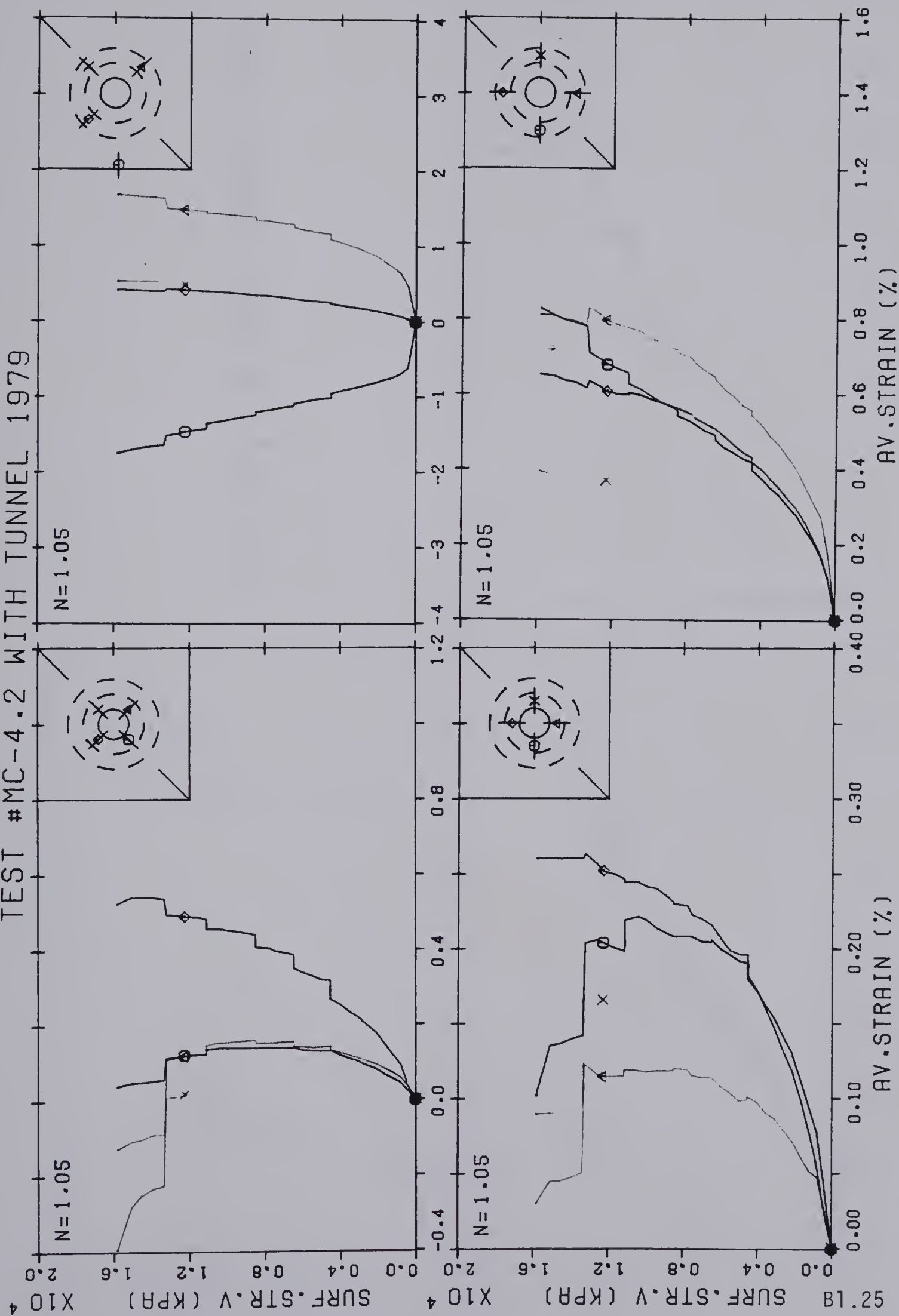
# TEST #MC-4.13 INTACT SAMPLE 1979





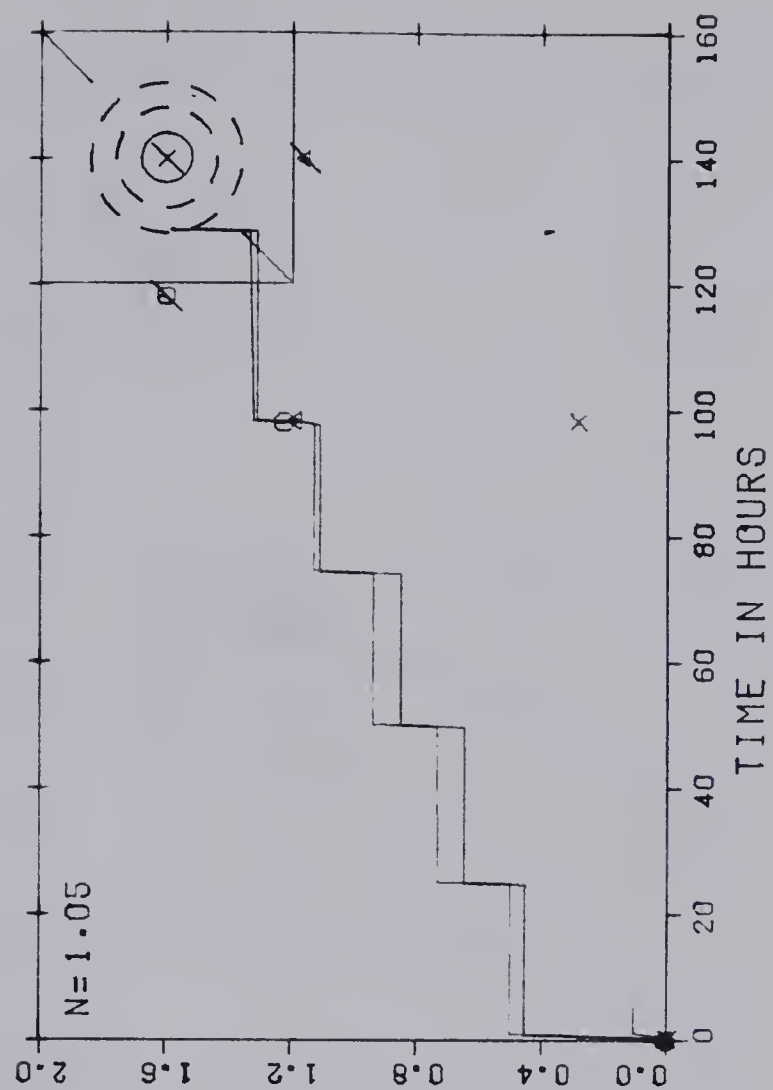
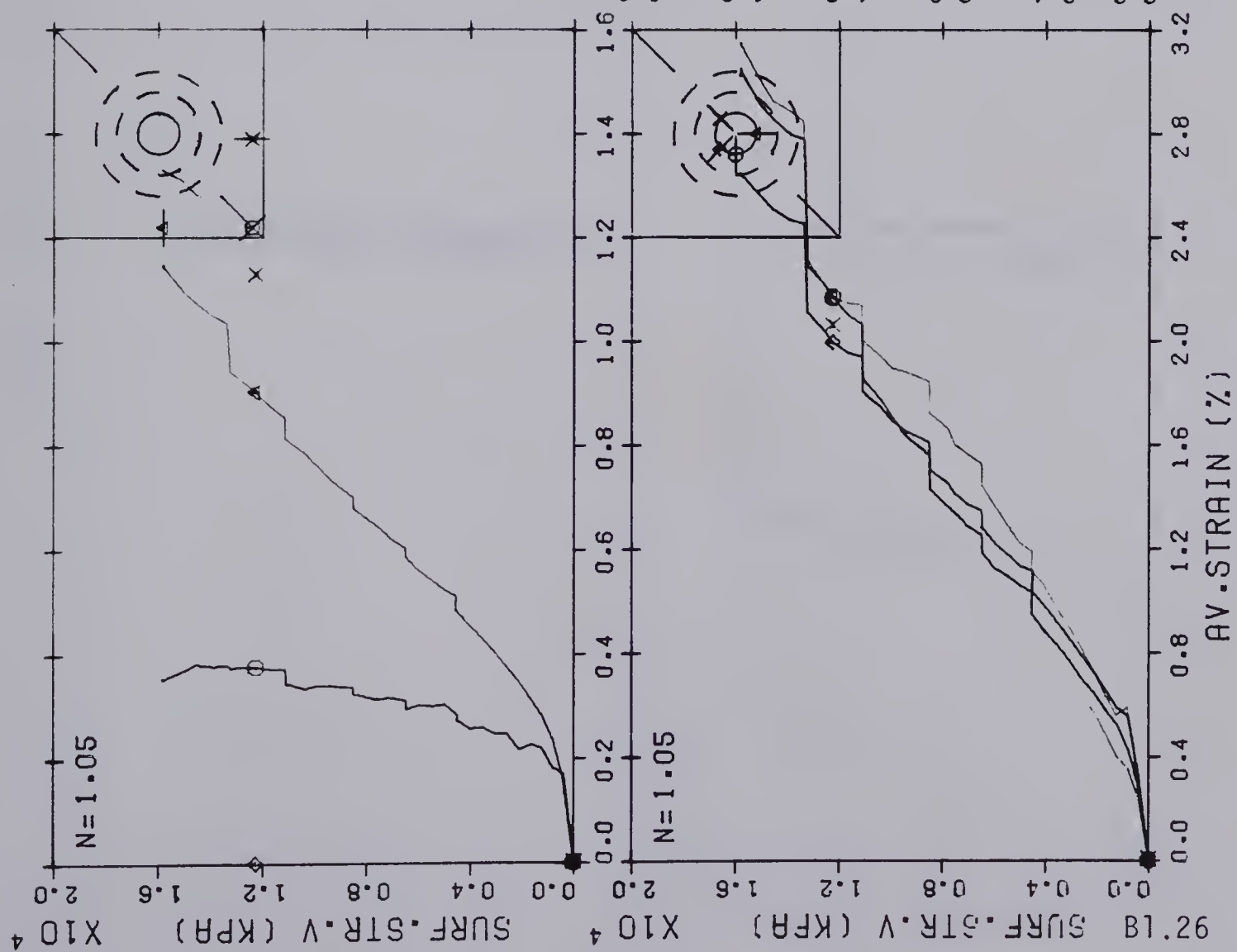


## TEST #MC-4.2 WITH TUNNEL 1979



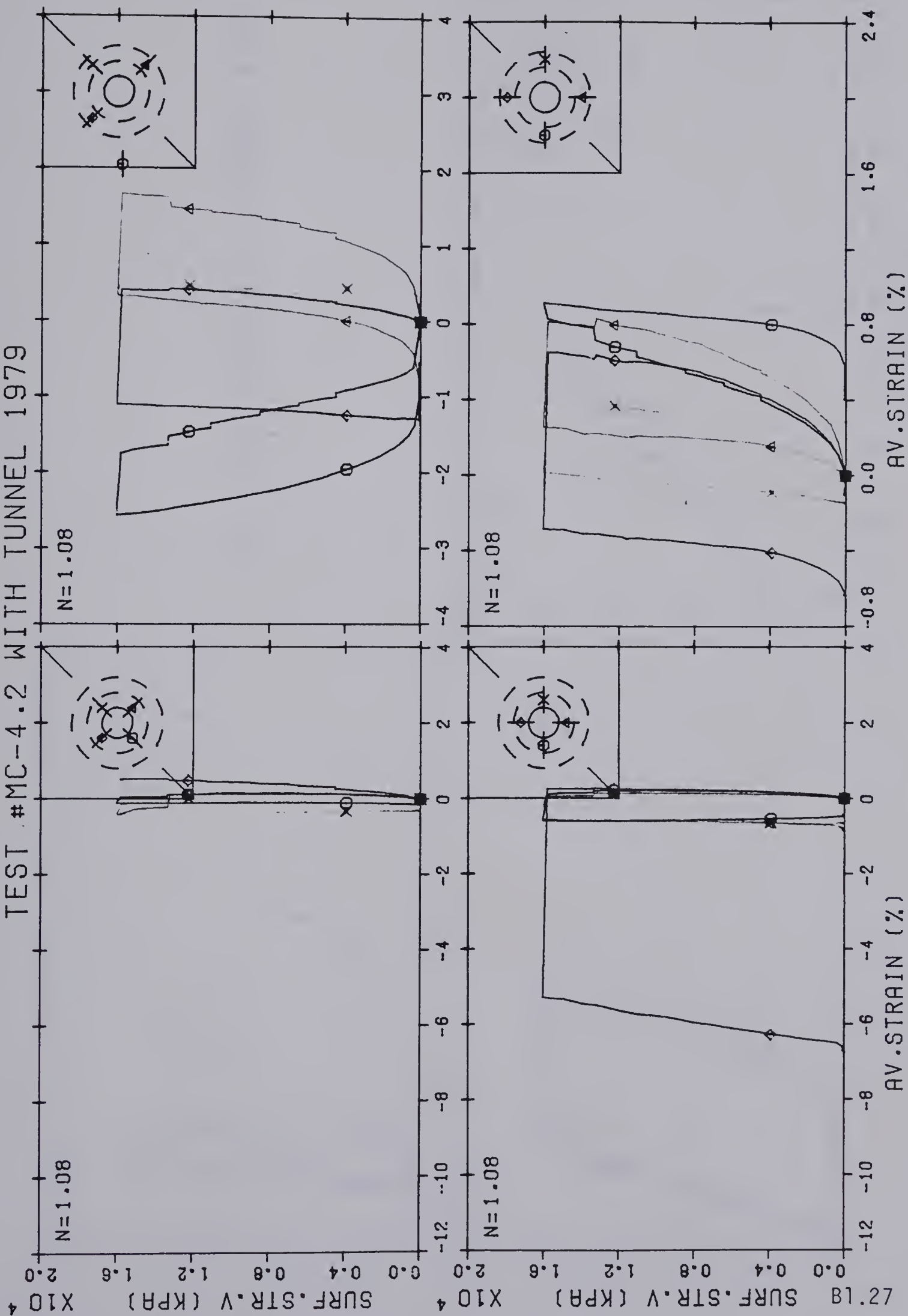


## TEST #MC-4.2 WITH TUNNEL 1979





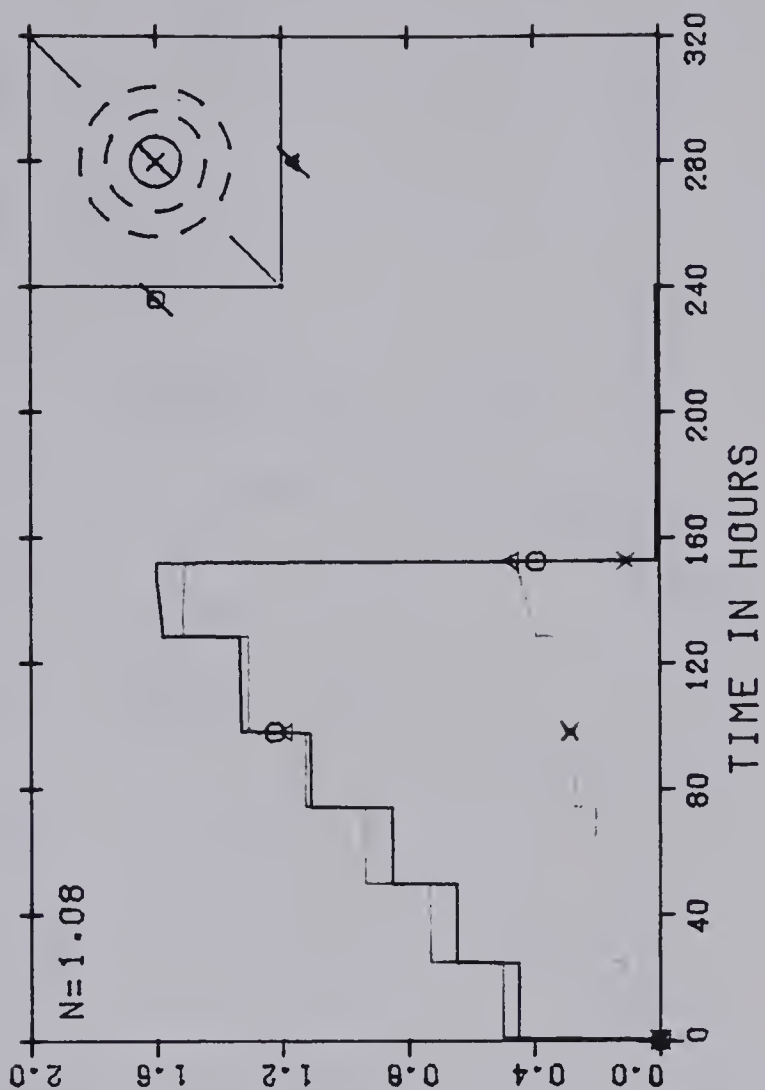
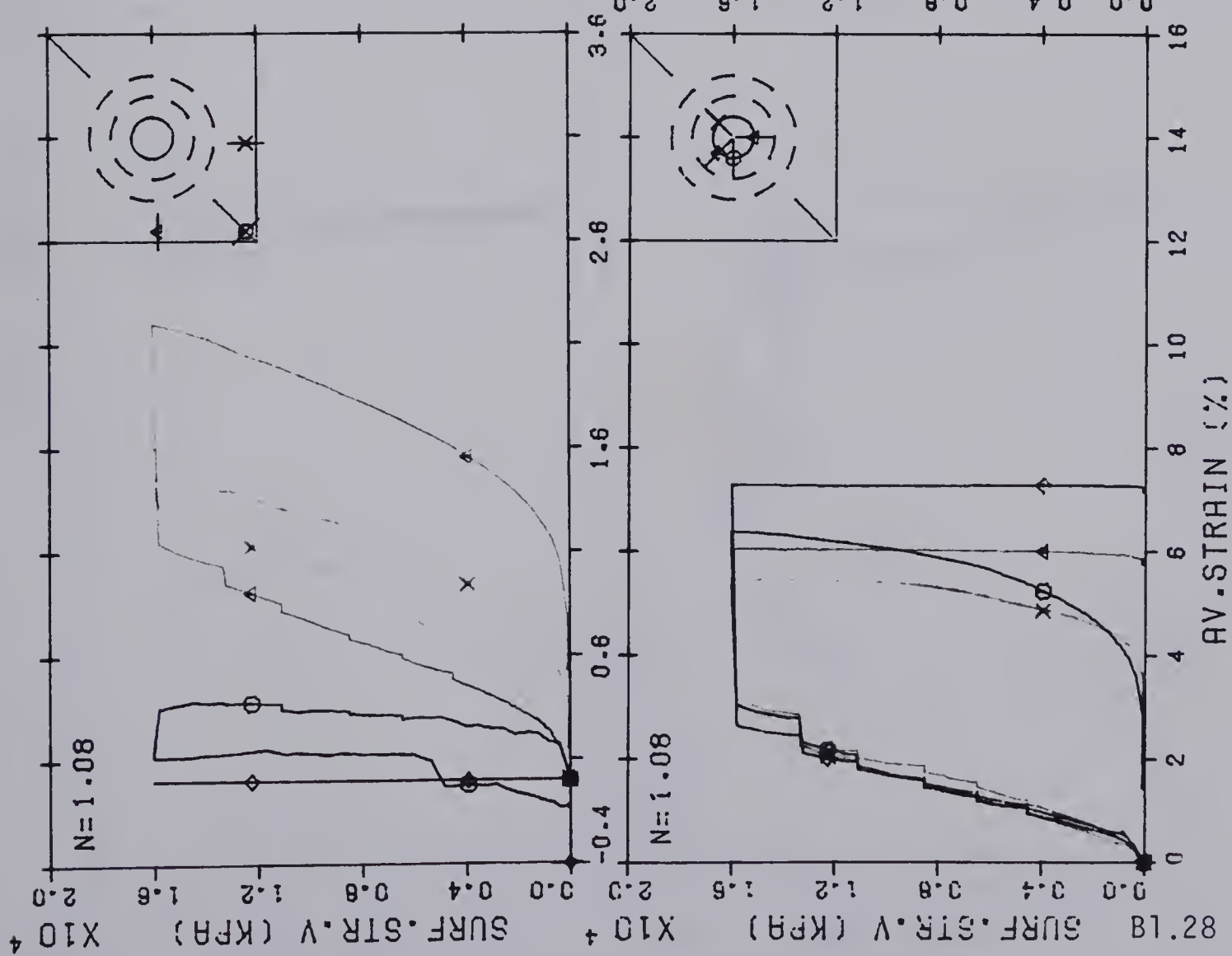
TEST #MC-4.2 WITH TUNNEL 1979





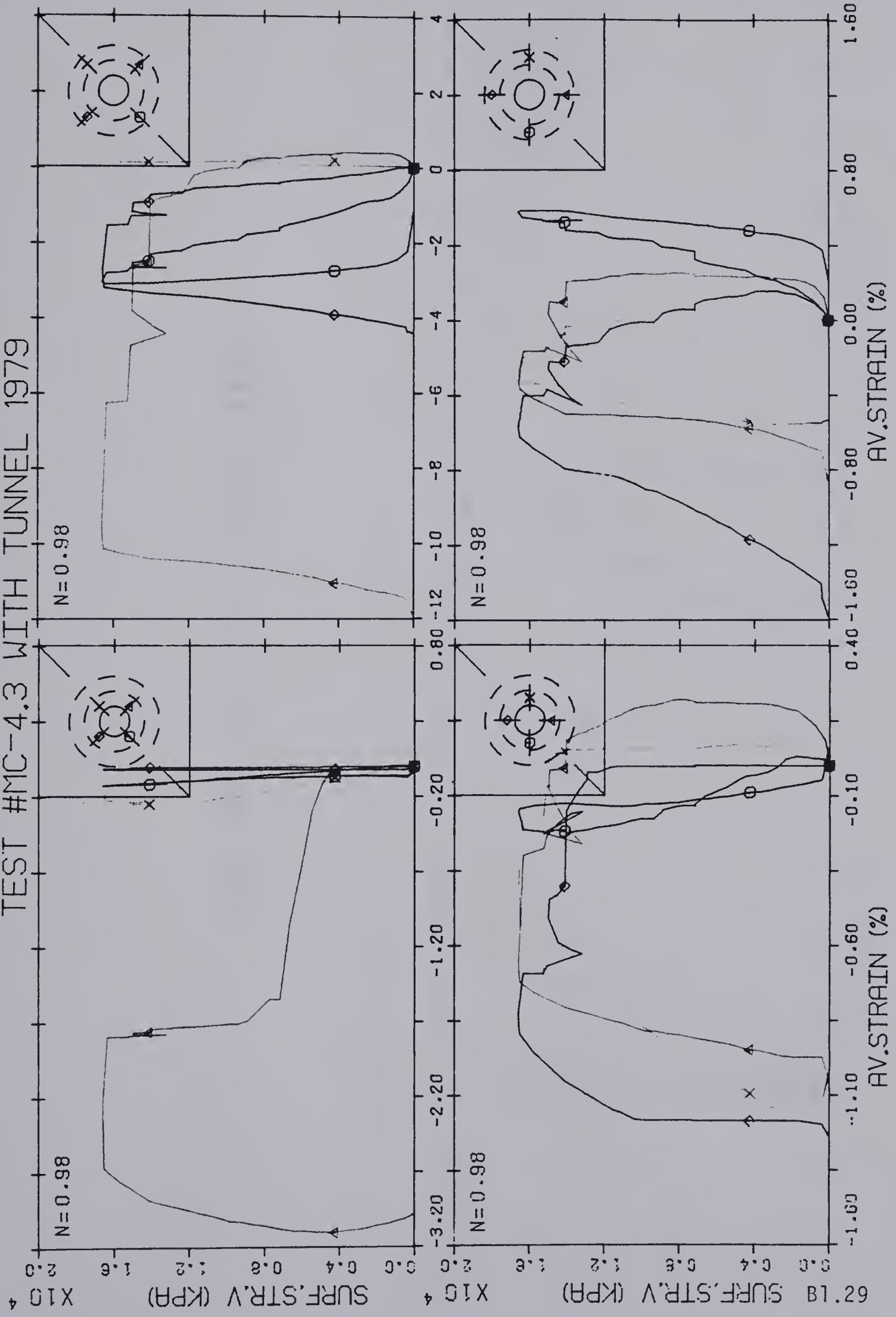


# TEST #MC-4.2 WITH TUNNEL 1979



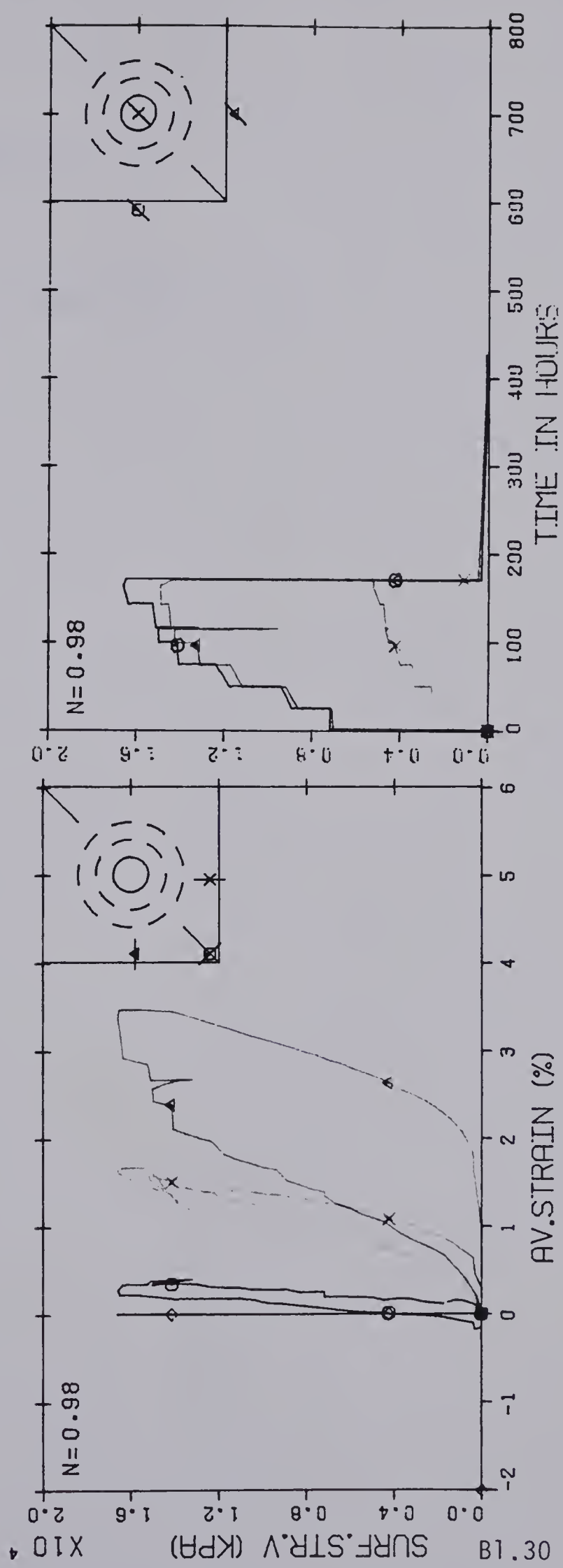


TEST #MC-4.3 WITH TUNNEL 1979





# TEST #MC-4.3 WITH TUNNEL 1979



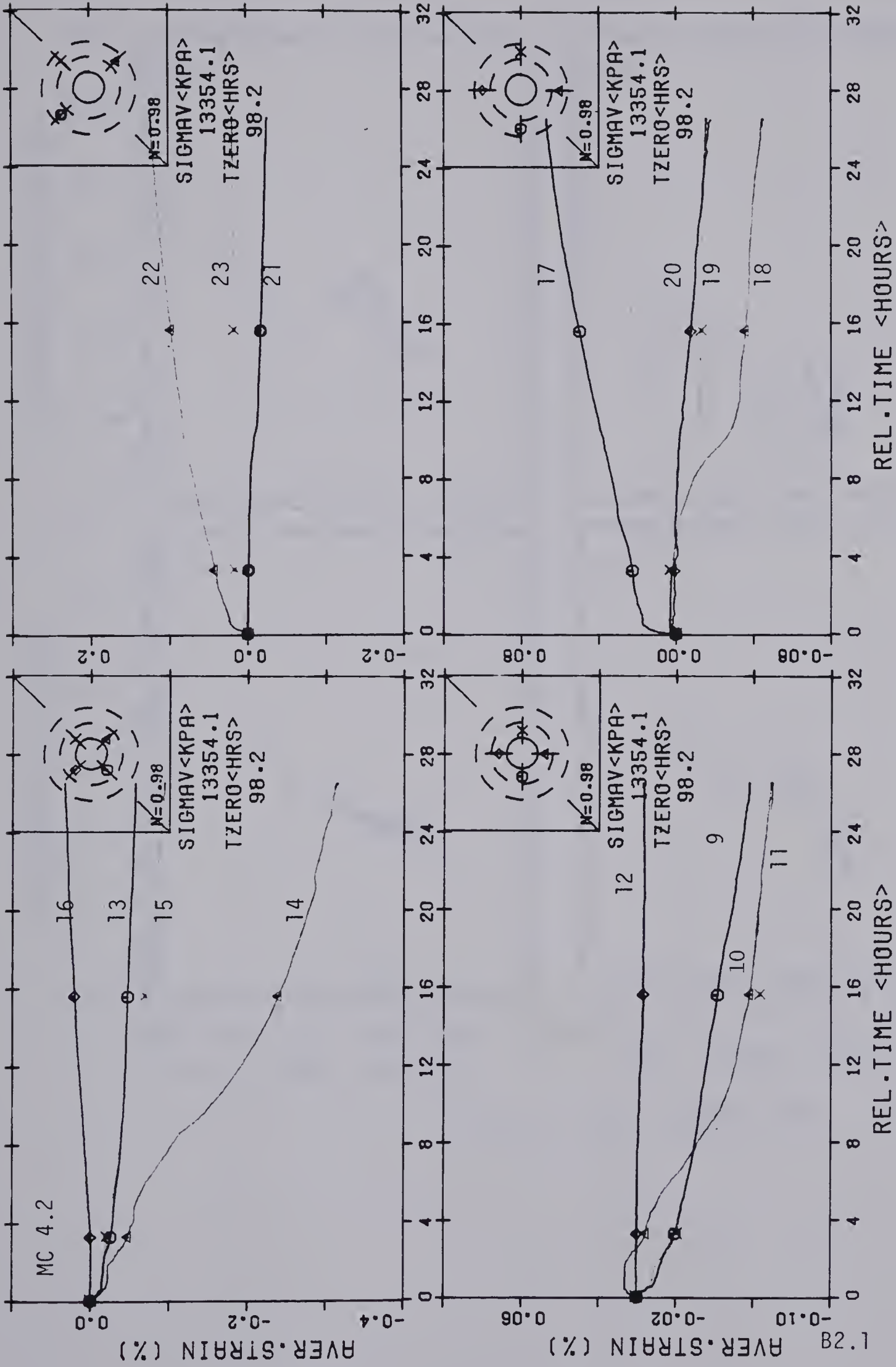


## APPENDIX B2

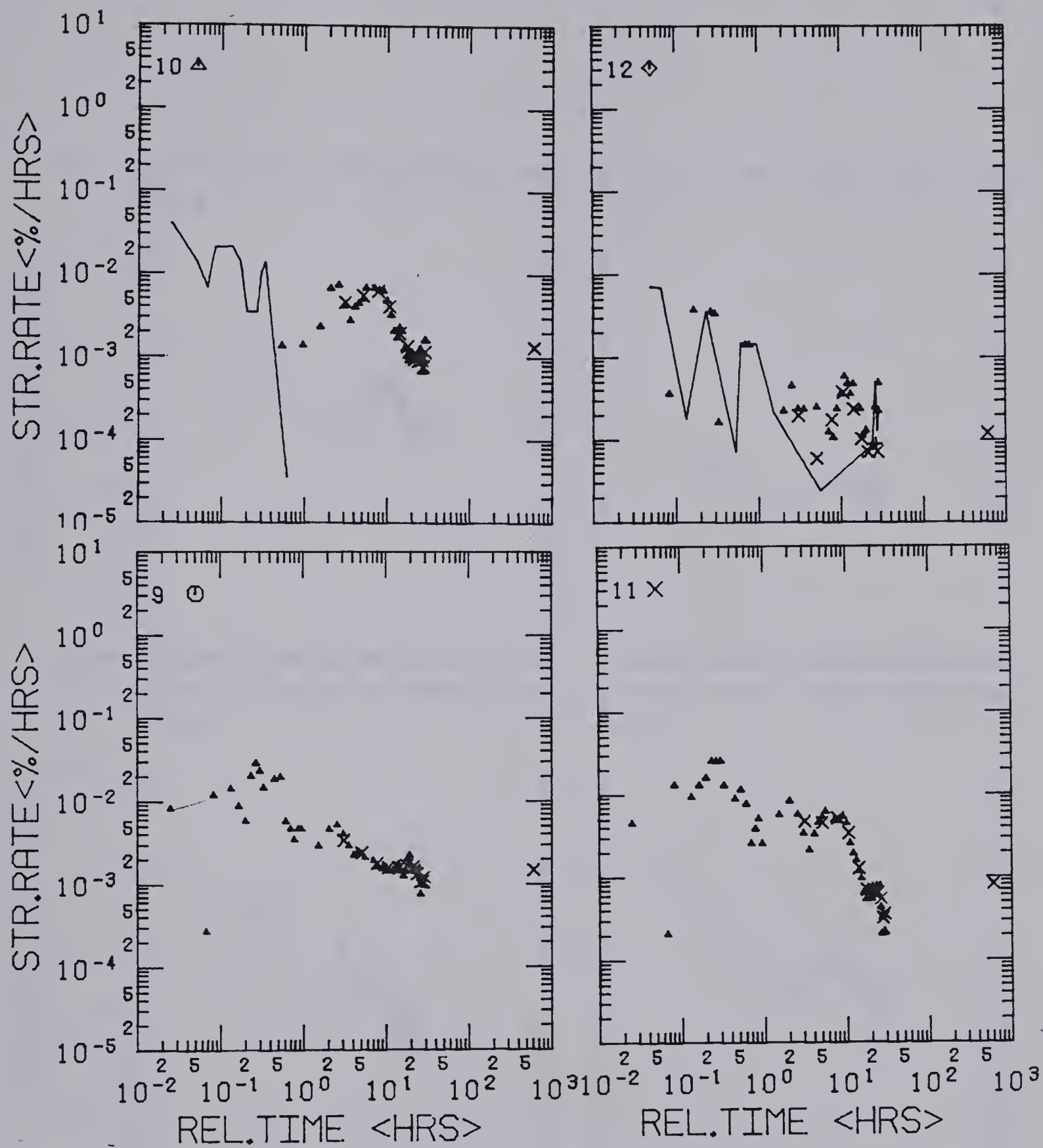
CREEP DATA NEAR RUPTURE (TEST MC.4.2)







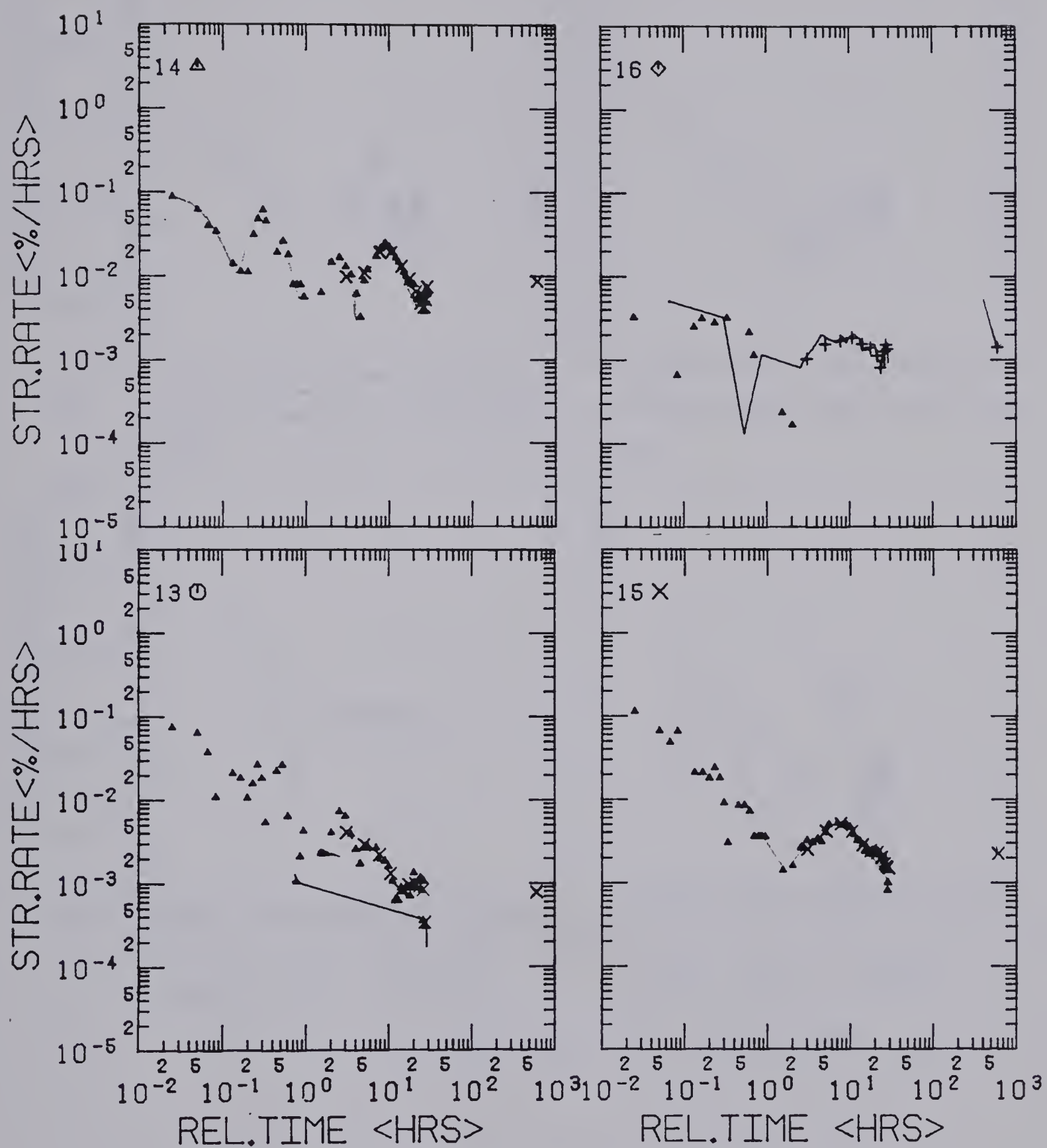




MC 4.2 AT 13000 KPA

B2.2



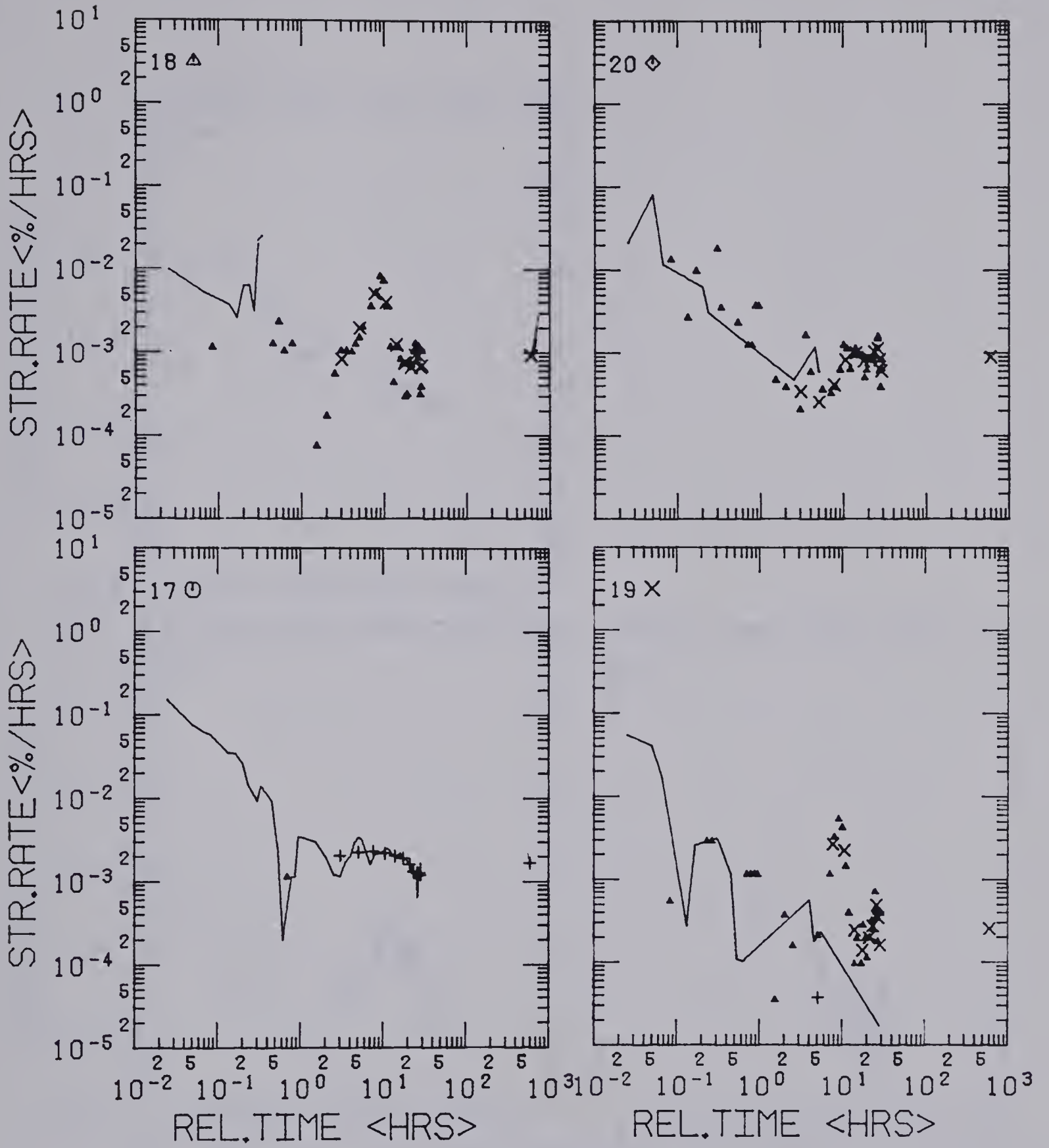


MC 4.2 AT 13000 KPA

B2.3

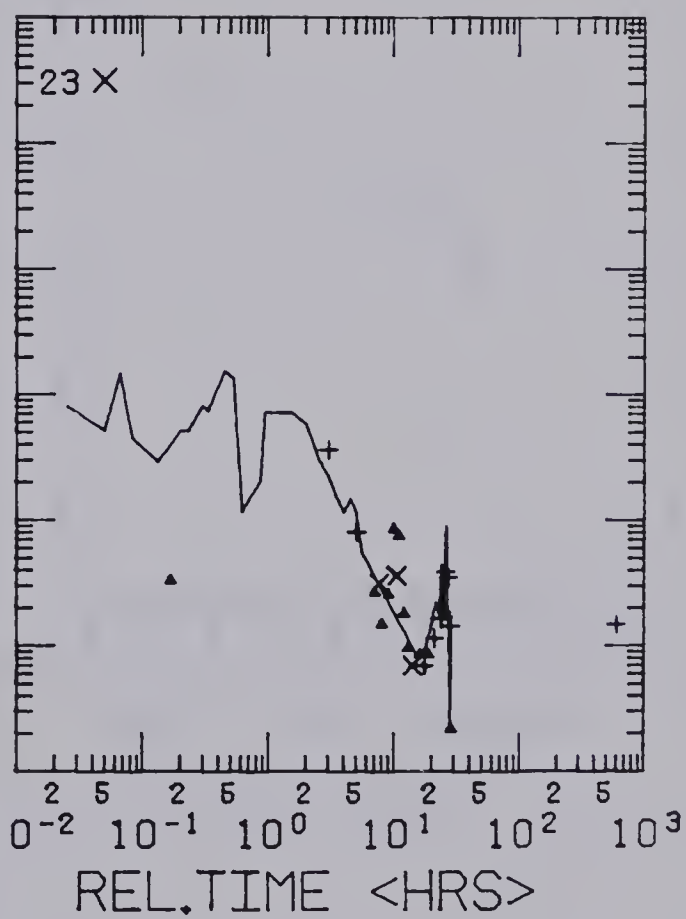
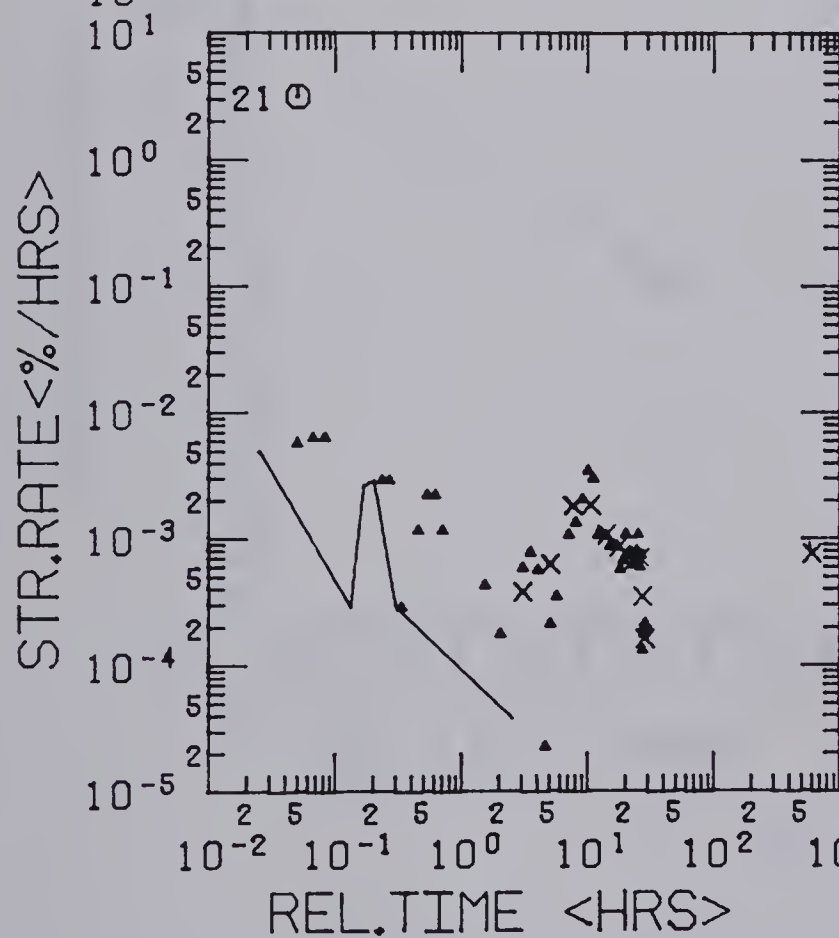
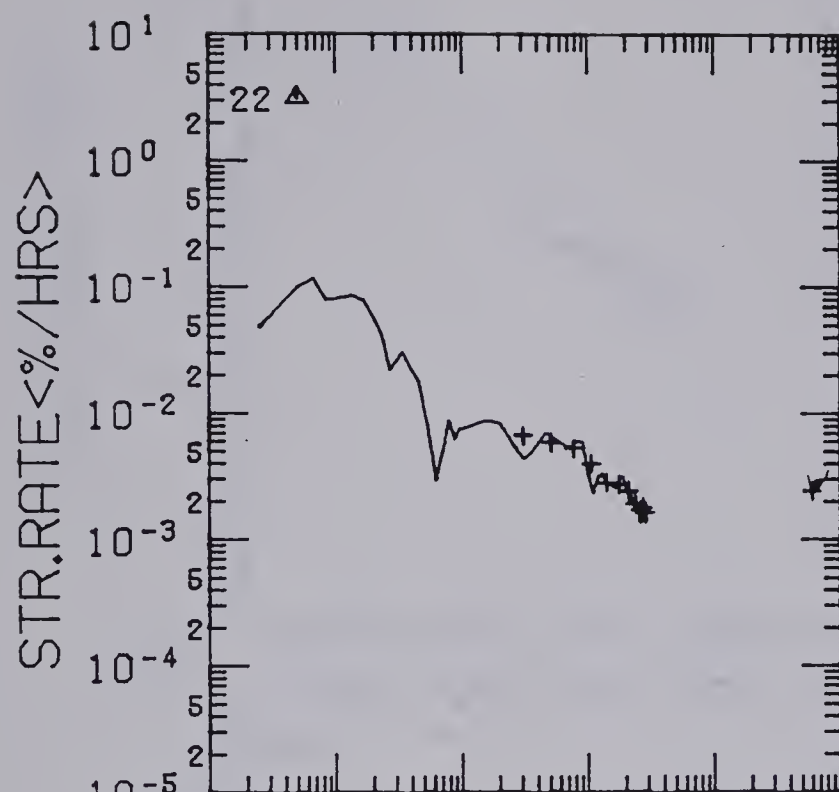






MC 4.2 AT 13000 KPA B2.4

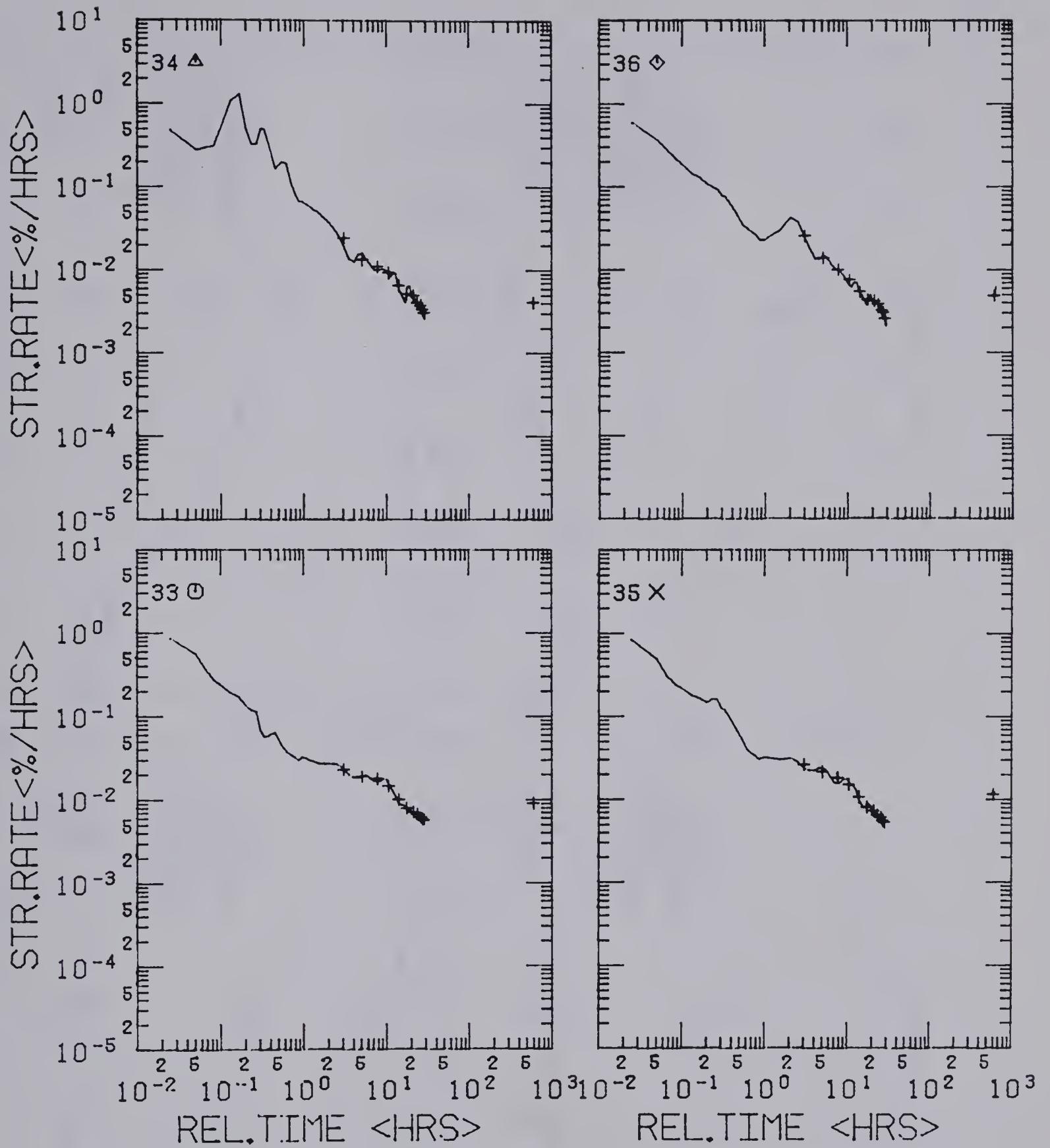




MC 4.2 AT 13000 KPA

B2.5

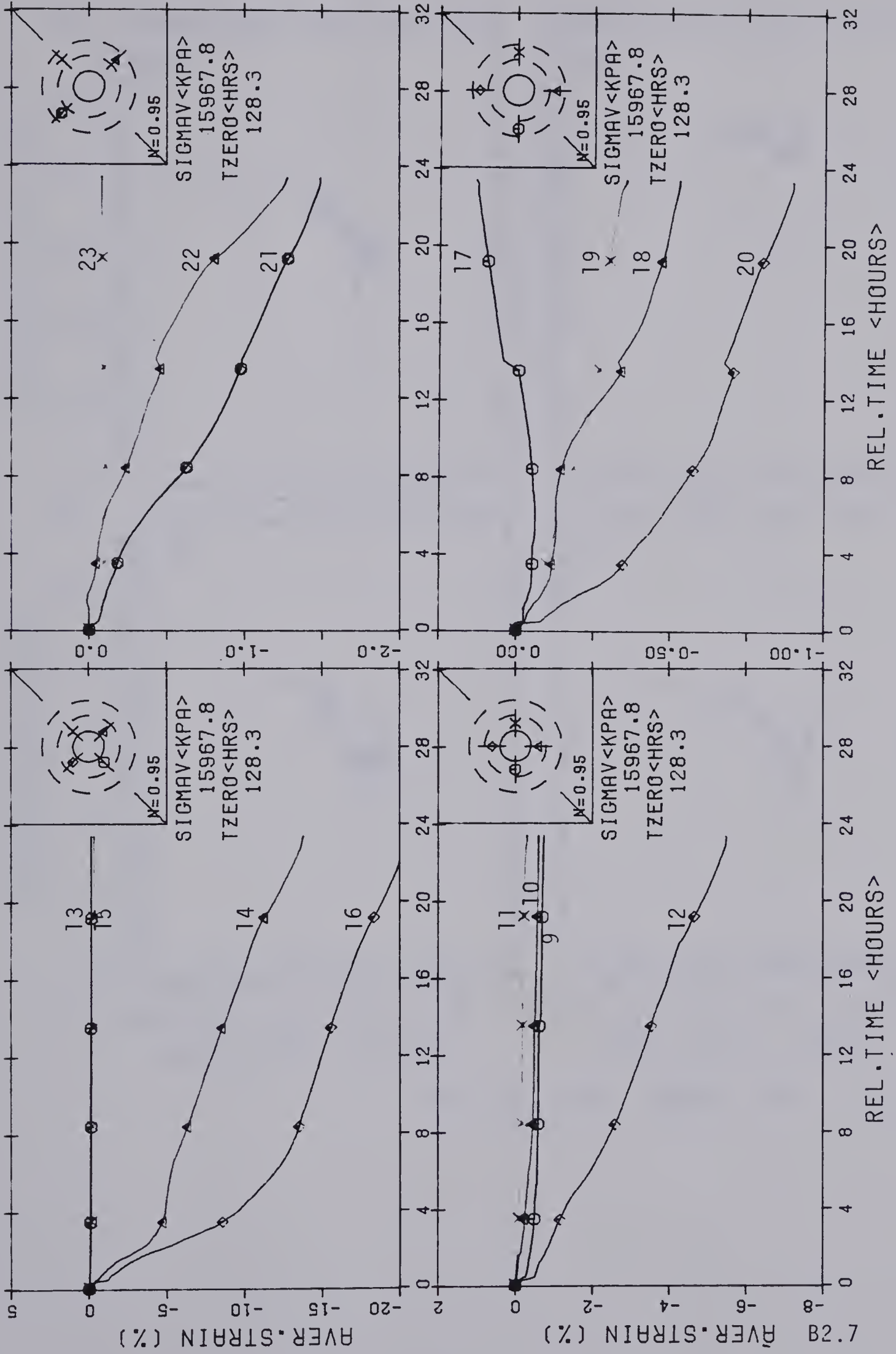




MC 4.2 AT 13000 KPA

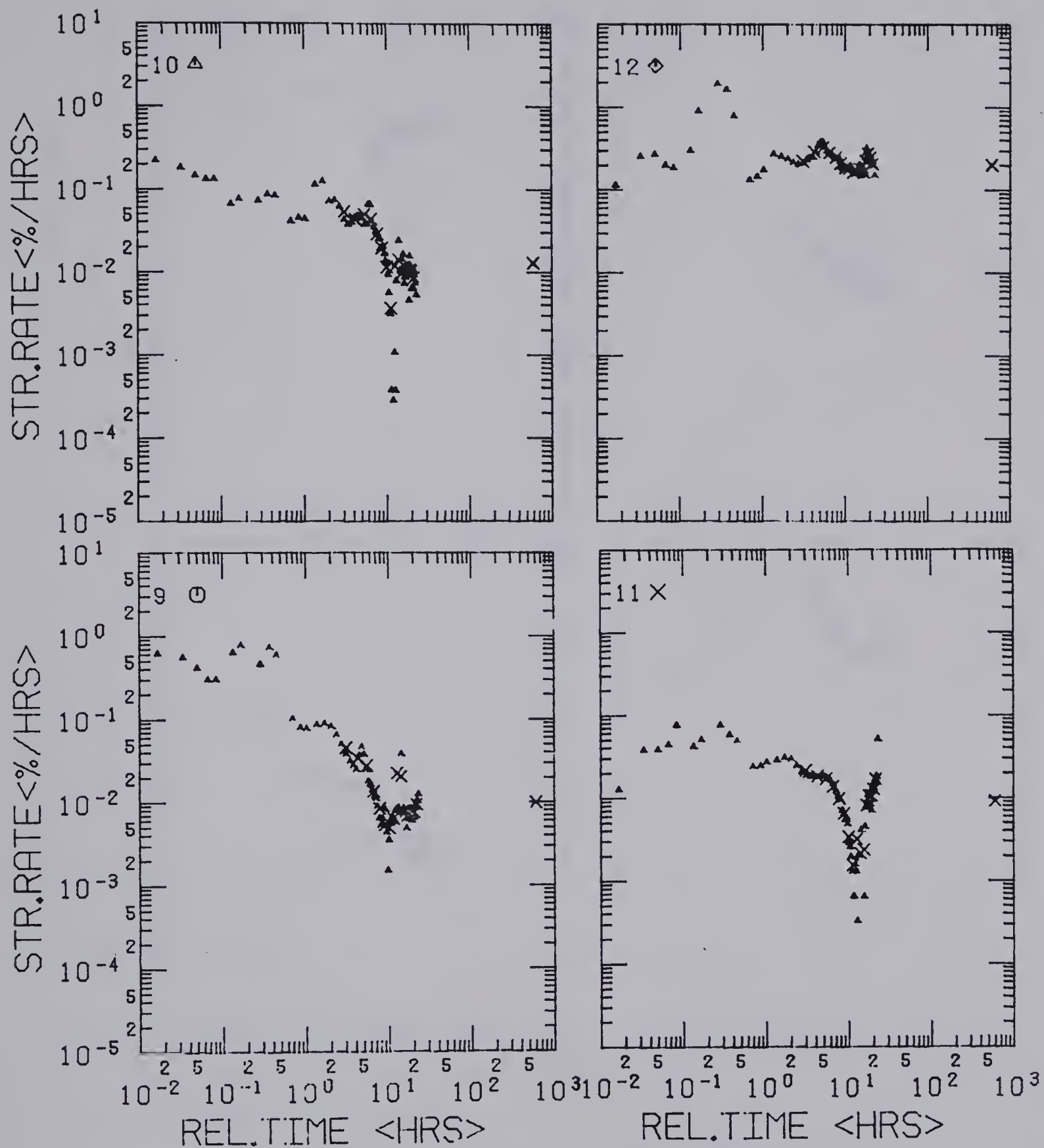
B2.6





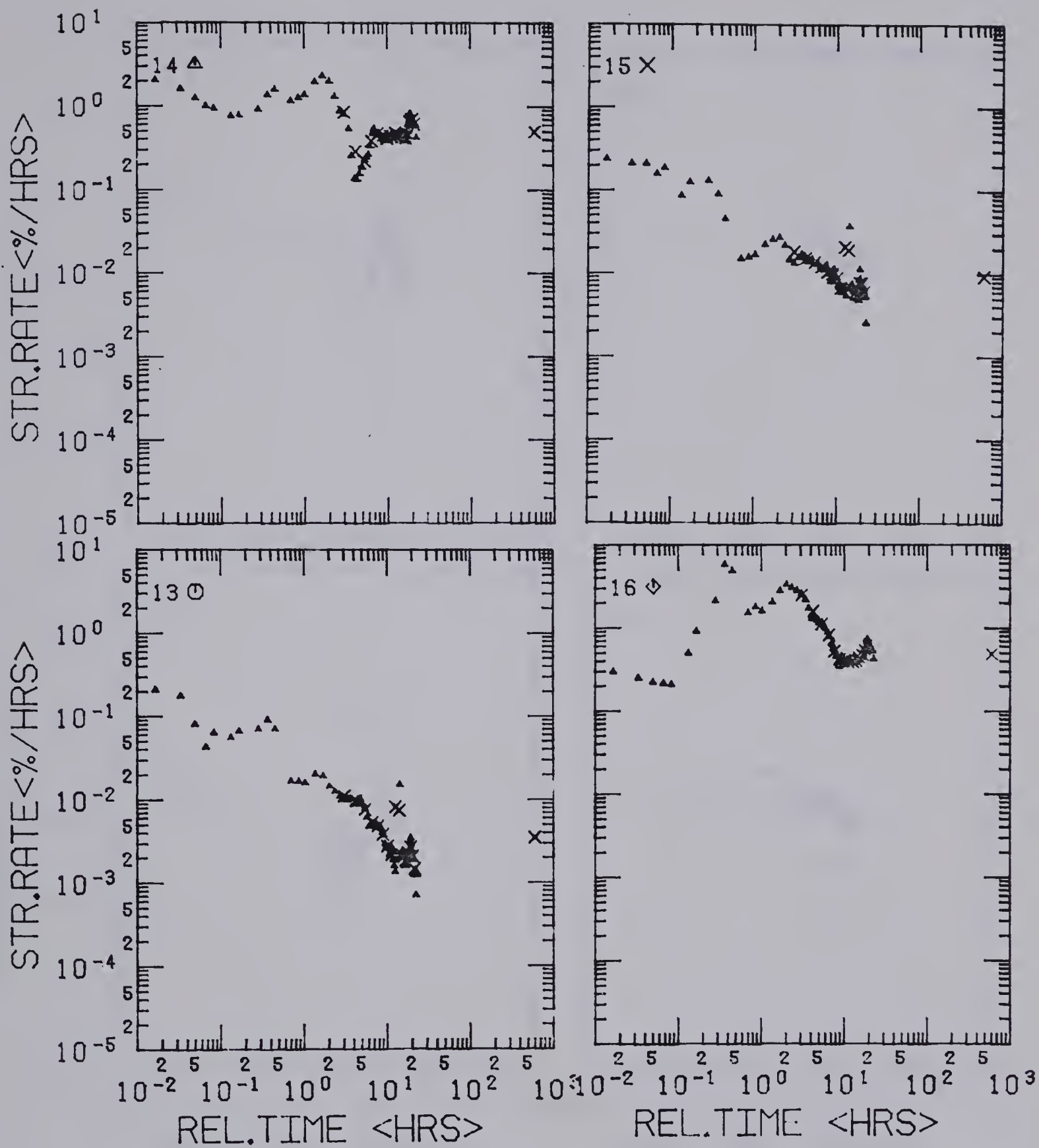






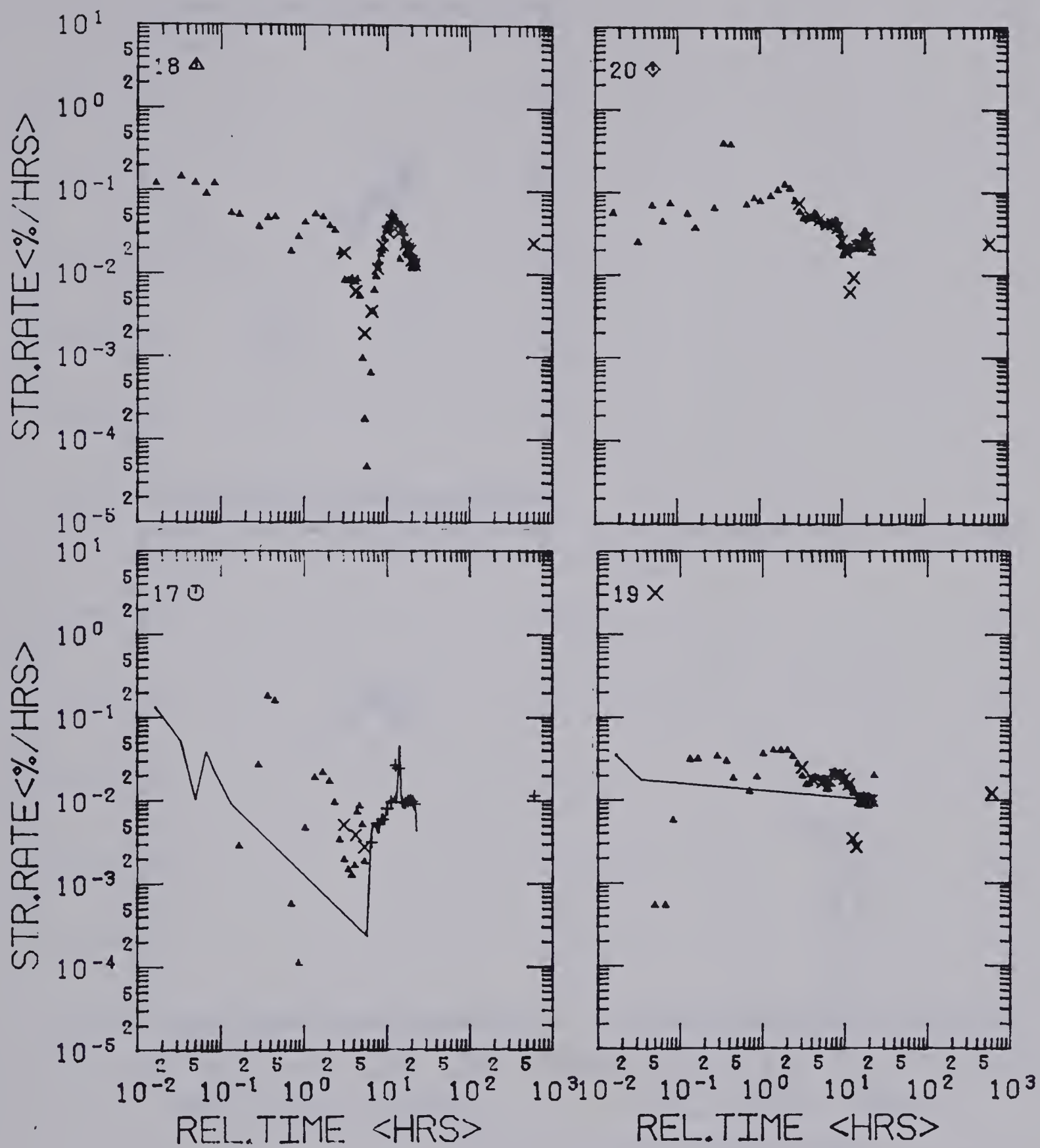
MC 4.2 AT 16000 KPA B2.8





MC 4.2 AT 16000 KPA B2.9



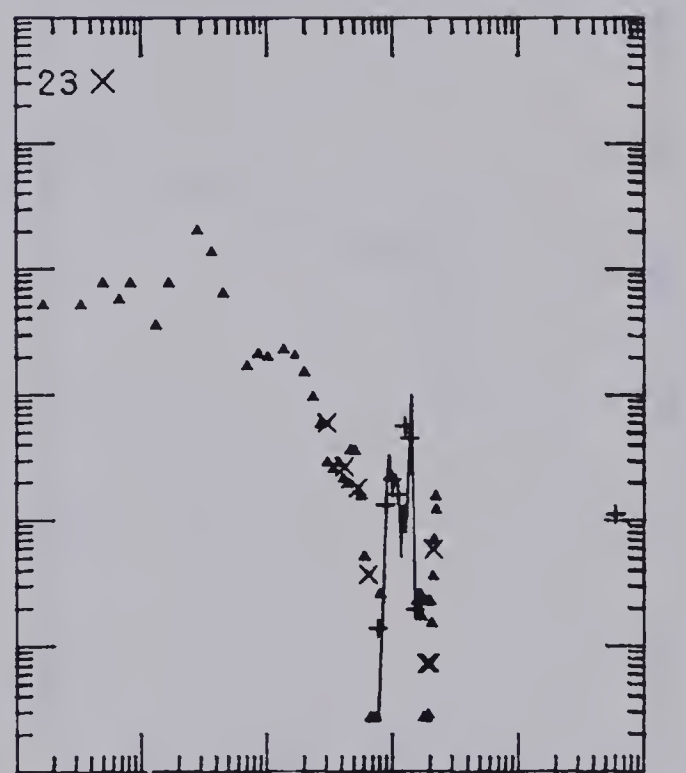
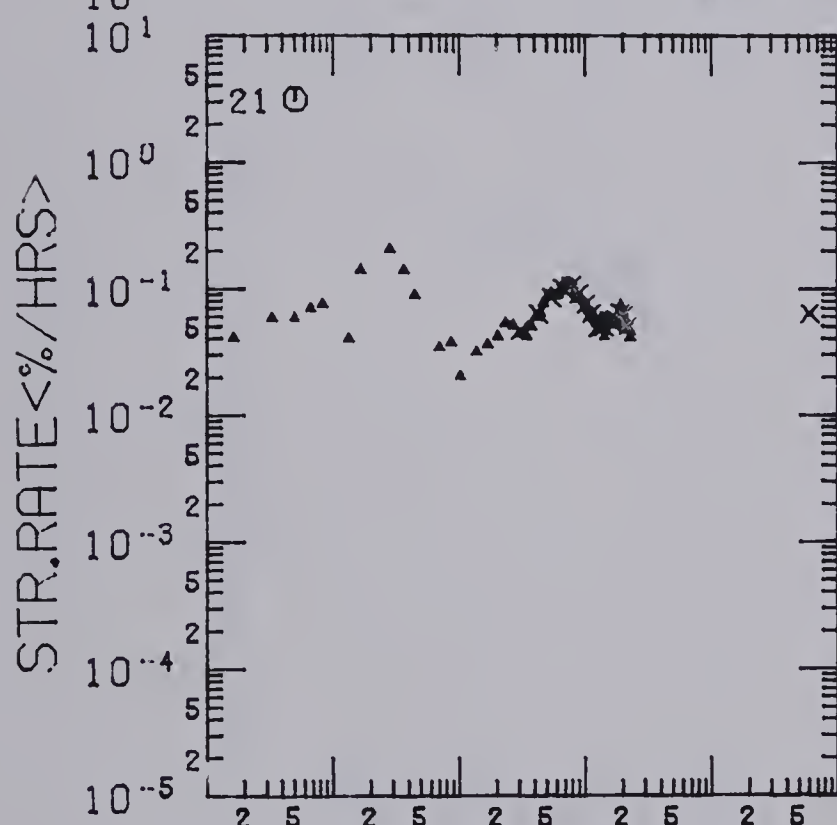
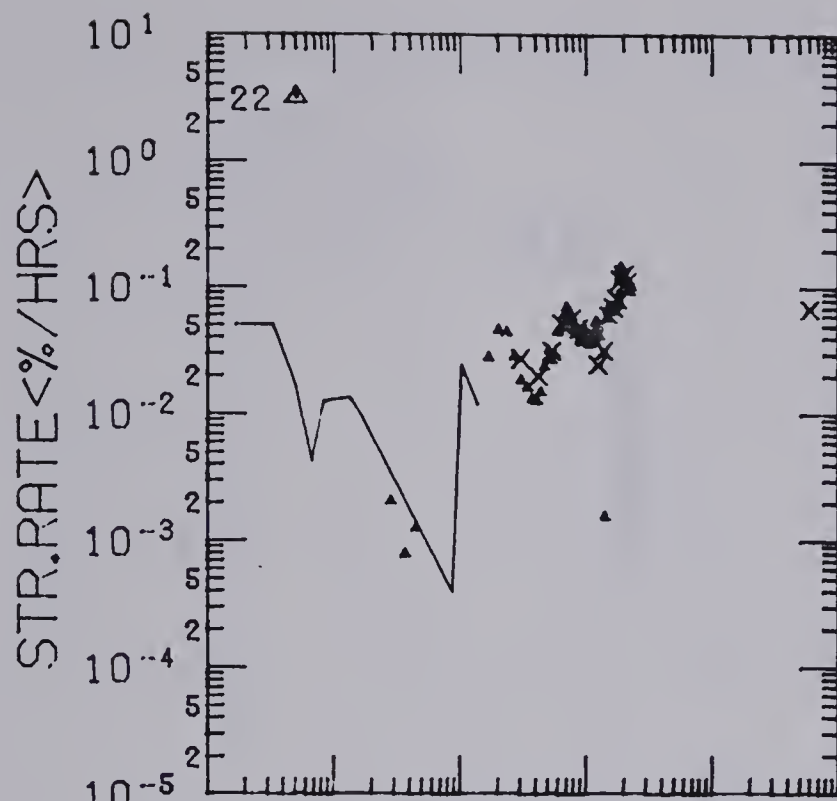


MC 4.2 AT 16000 KPA

B2.10

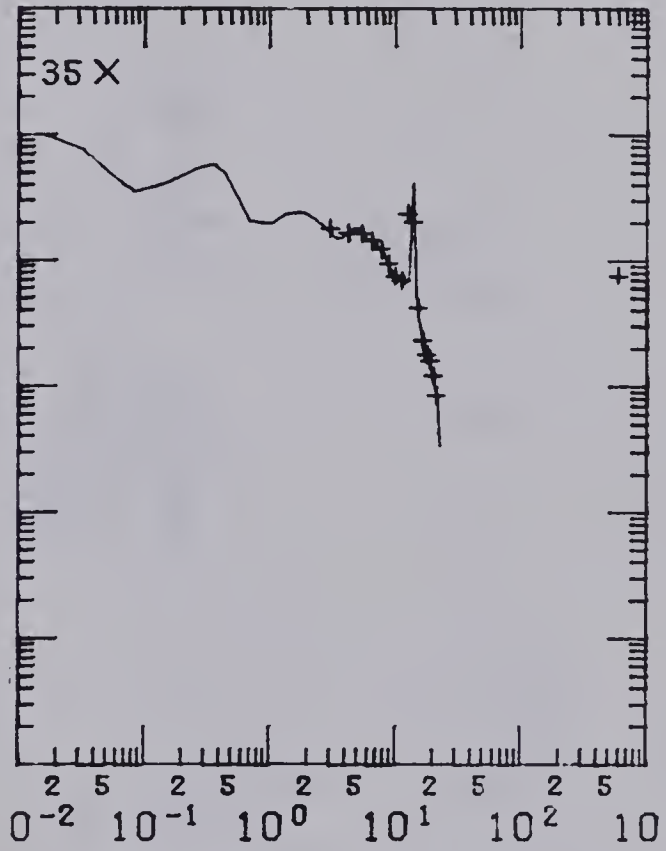
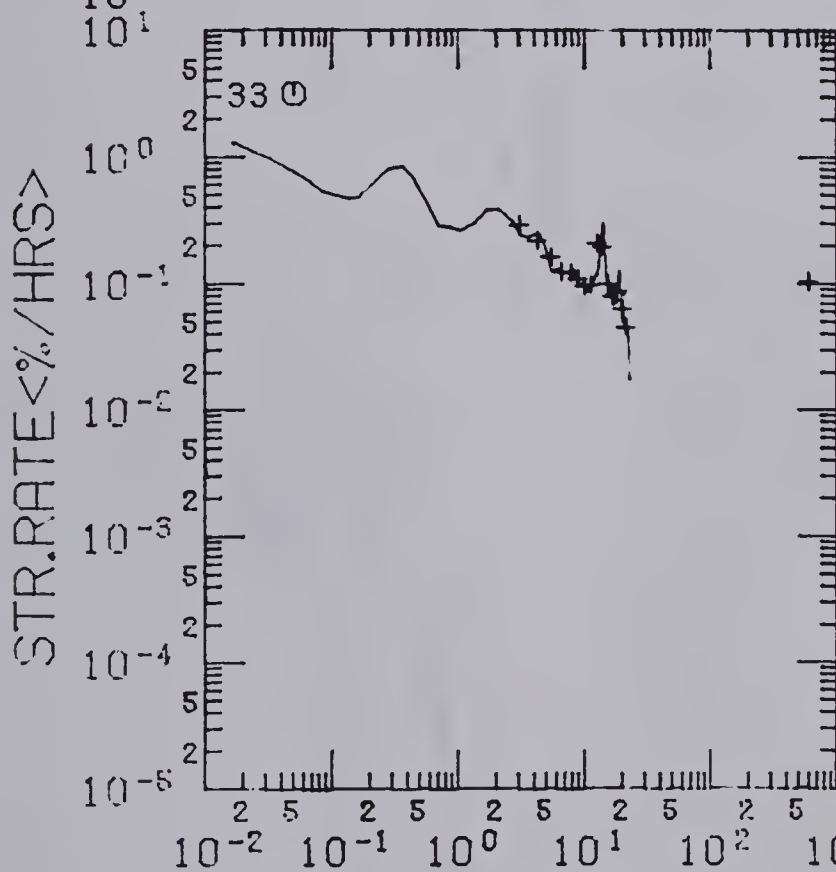
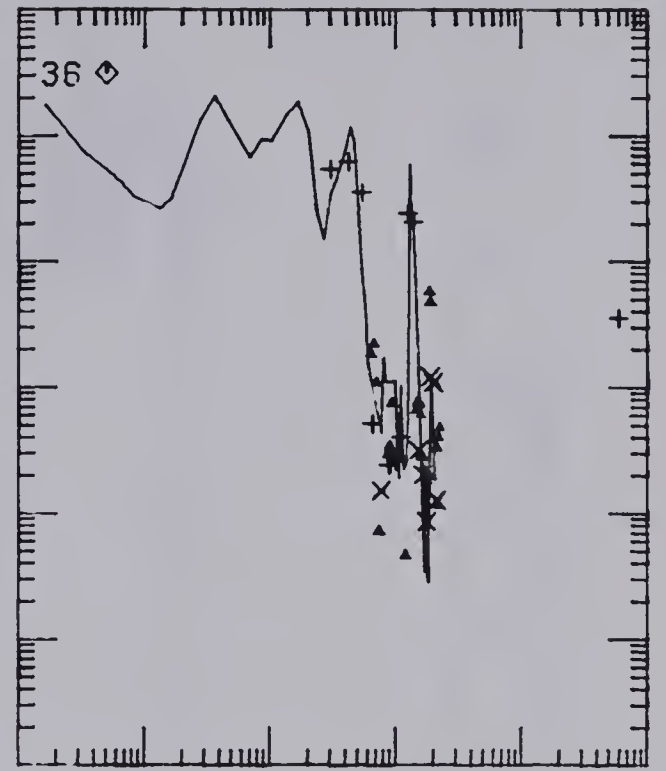
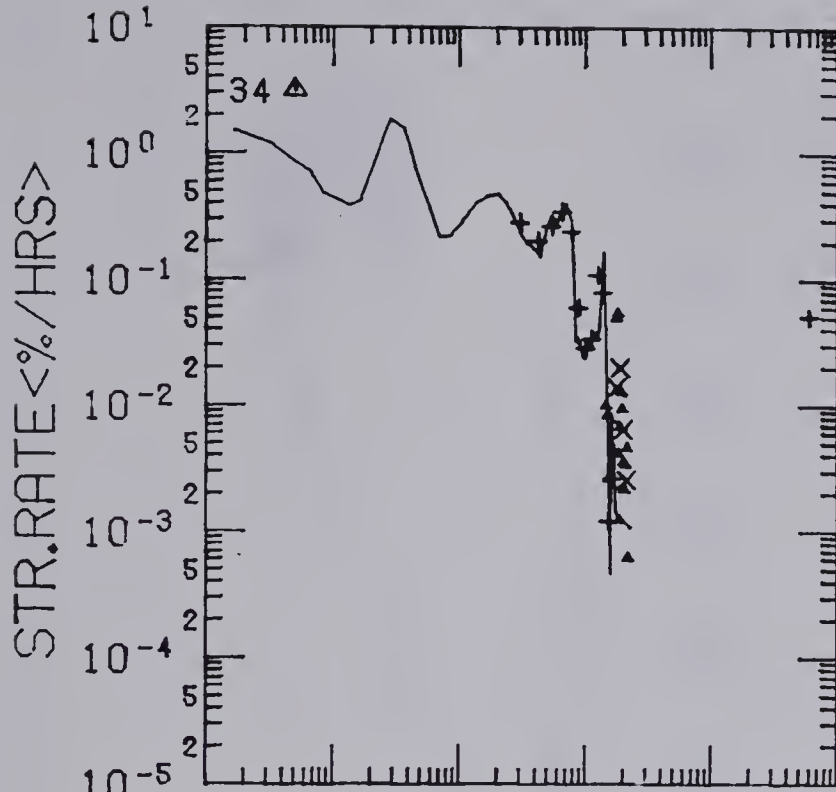






MC 4.2 AT 16000 KPA B2.11



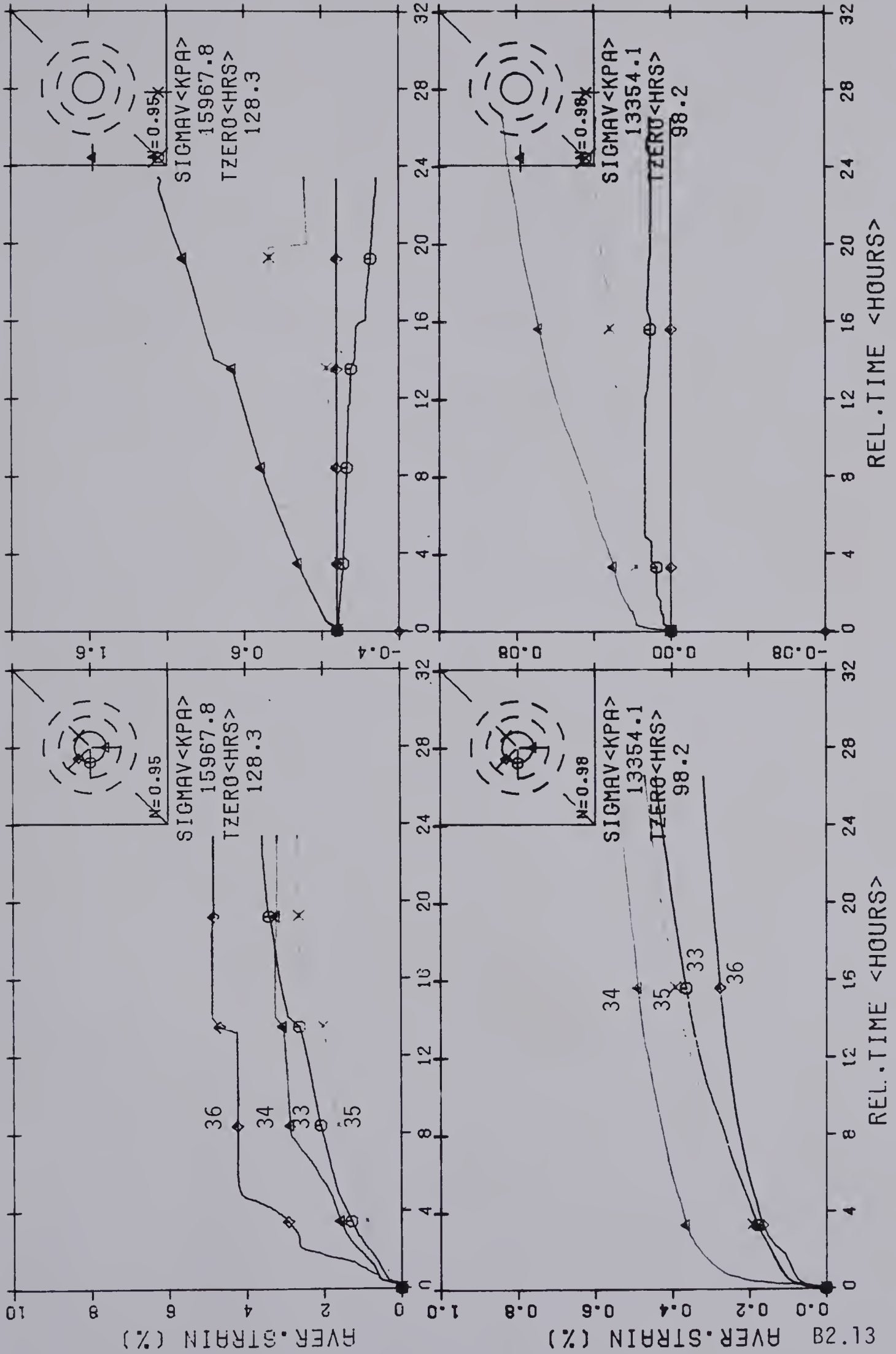


REL.TIME <HRS>

REL.TIME <HRS>

MC 4.2 AT 16000 KPA B2.12











**B30249**